A Hybrid Controller for Stability Robustness, Performance Robustness, and Disturbance Attenuation of a Maglev System

Feng Tian
Marquette University

A HYBRID CONTROLLER FOR STABILITY ROBUSTNESS, PERFORMANCE ROBUSTNESS, AND DISTURBANCE ATTENUATION OF A MAGLEV SYSTEM

by

Feng Tian, B.S., M.S.

A Dissertation submitted to the Faculty of the Graduate School,
Marquette University,
in Partial Fulfillment of the Requirements for
the Degree of Doctor of Philosophy

Milwaukee, Wisconsin

May 2015

ABSTRACT
A HYBRID CONTROLLER FOR STABILITY ROBUSTNESS,
PERFORMANCE ROBUSTNESS, AND DISTURBANCE
ATTENUATION OF A MAGLEV SYSTEM

Feng Tian, B.S., M.S.

Marquette University, 2015

Devices using magnetic levitation (maglev) offer the potential for friction-free, high-speed, and high-precision operation. Applications include frictionless bearings, high-speed ground transportation systems, wafer distribution systems, high-precision positioning stages, and vibration isolation tables. Maglev systems rely on feedback controllers to maintain stable levitation. Designing such feedback controllers is challenging since mathematically the electromagnetic force is nonlinear and there is no local minimum point on the levitating force function. As a result, maglev systems are open-loop unstable. Additionally, maglev systems experience disturbances and system parameter variations (uncertainties) during operation. A successful controller design for maglev system guarantees stability during levitating despite system nonlinearity, and desirable system performance despite disturbances and system uncertainties.

This research investigates five controllers that can achieve stable levitation: PD, PID, lead, model reference control, and LQR/LQG. It proposes an acceleration feedback controller (AFC) design that attenuates disturbance on a maglev system with a PD controller. This research proposes three robust controllers, QFT, H_∞, and QFT/H_∞, followed by a novel AFC-enhanced QFT/H_∞ (AQH) controller. The AQH controller allows system robustness and disturbance attenuation to be achieved in one controller design.

The controller designs are validated through simulations and experiments. In this research, the disturbances are represented by force disturbances on the levitated object, and the system uncertainties are represented by parameter variations. The experiments are conducted on a 1 DOF maglev testbed, with system performance including stability, disturbance rejection, and robustness being evaluated. Experiments show that the tested controllers can maintain stable levitation. Disturbance attenuation is achieved with the AFC. The robust controllers, QFT, H_∞, QFT/H_∞, and AQH successfully guarantee system robustness. In addition, AQH controller provides the maglev system with a disturbance attenuation feature.

The contributions of this research are the design and implementation of the acceleration feedback controller, the QFT/H_∞, and the AQH controller. Disturbance attenuation and system robustness are achieved with these controllers. The controllers developed in this research are applicable to similar maglev systems.

ACKNOWLEDGMENT

Feng Tian, B.S., M.S.

First, I wish to thank my dissertation advisor Professor Mark Nagurka for his assistance and guidance. He has provided me with many opportunities to learn and grow. I thank him for all he has done to help and guide me along the way.

I would like to express my deepest gratitude to my dissertation committee members. I wish to thank Dr. Kevin Craig from whom I learned about acceleration feedback control. I wish to thank Dr. Stolfi from whom I learned about the maglev testbed and magnetic bearings. I also wish to thank Dr. Yaz, Dr. Schimmels, Dr. Park, and Dr. Voglewede for their time in evaluating my research and dissertation.

I wish to thank the Department of Mechanical Engineering and the Graduate School at Marquette University, for the financial support and all the help along the way. I also wish to thank our department office associate Mrs. Annette Wolak, who has been an enormous help to me during my stay at Marquette.

I wish to acknowledge my friends Debbie and Bob Young, who helped with my English writing. I wish to acknowledge my friends Tao Yan, Jinming Sun, Carl and Judy Cheng, Ce Xiong, Shan Ke, Jiangling Wang, and Peng Zhang, who have always been there to help and support me and my family.

Finally, I could not have done anything without the support of my family: my mother and father, my wife, and the joy in our lives, my son Benjamin Tian.

TABLE OF CONTENTS

LIST OF FIGURES

LIST OF TABLES

Chapter 1. Introduction

1.1. Research Background

Magnetic levitation (or maglev) refers to the methodology in which a ferrous object is supported by magnetic forces. This method offers fully contactless support, making it possible to eliminate mechanical friction. It has long been known that friction substantially deteriorates the performance of mechanical systems, especially motion control systems [1-5]. Friction forces between contacting surfaces are the root cause of wear, energy loss, and high temperature in mechanical systems. Friction results from many different physical mechanisms, making it complicated and hard to control. It has been reported that in the U.S. alone, the cost of loss due to imperfect control of friction is more than 500 billion dollars every year [1]. Maglev technology can potentially ameliorate some of these losses.

The idea of using magnetic forces to levitate metallic objects is more than one hundred years old [6]. Early experiments turned out to be unsuccessful due to the lack of understanding of magnetism. In the past century the development of theories of electromagnetism and methods of control engineering converted the idea from science fiction into reality in many modern industrial systems [7-9]. The contactless features of maglev technology made it possible to build friction-free, high-speed, high-precision devices. Maglev technology has applications in frictionless bearings [10-18], high speed ground transportation systems [19-27], wafer distribution (or conveyor) systems [28-31], high-precision positioning stages [32-36], and vibration isolation devices [37-41]. A brief review of each of these applications follows. It will reveal the versatility of maglev technology and the benefits to our modern industrial world. A detailed literature review on

how to design controllers for maglev systems is deferred to Chapter 2.

1.1.1. Maglev Technology Applications

Maglev technology was adopted by the bearing industry about fifty years ago. The goal was to replace contact-based bearing forces with non-contact electromagnetic forces. Frictionless magnetic bearings have replaced traditional mechanical bearings in many areas. They have been implemented in centrifugal blood pumps to avoid contamination of blood inside the pumps [42-47]; because the rotor and the stator do not contact, there is no wear and no debris caused by friction. Magnetic bearings are also used in gas turbine engines [48-51]. The advantages include improved stability and reliability, reduced power loss, better fault tolerance, and greatly extended bearing service life [51]. Other applications of magnetic bearings are seen in machine tools [52-56], energy storing flywheels [57-65], and instruments used in space and physics research [12]. Magnetic bearings allow these systems to operate at high angular velocities (500,000 rpm and above) with improved positioning accuracy [66]. Also, vibration at critical speeds can be greatly reduced because the stiffness and damping of magnetic bearings can be optimized electronically, which is not possible using traditional mechanical bearings.

Another application is found in high-speed ground transportation systems. A maglev train is levitated, guided, and propelled from a guideway using magnetic forces. The first patent on a maglev train was awarded to Kemper of Germany in 1937 [67]. It remained an idea on paper until maglev technology became mature in the 1960s. Maglev trains were developed in the United Kingdom, Germany, and Japan. A successful maglev train is the Transrapid, which is a high speed monorail maglev train developed and refined

in Germany in the late 1960s. It maintained the maglev train speed record for years until superseded by a Japanese maglev train in the 1990s. The first generation of the Transrapid, was an indoor experimental model built in 1969 [68]. The latest version, Transrapid 09, which was released in 2009, can cruise at a speed of 500 km/h and accelerate/decelerate at 1 m/s^2 [69]. In 2002, a version specially designed for the Shanghai Maglev Train, Transrapid SMT, was built and has been operating in Shanghai, China. It was the first high speed maglev train in commercial operation [70]. The Japanese maglev train, JR-Maglev, reached a world speed record of 581 km/h for maglev vehicles on December 2, 2003 [71]. Compared to traditional high speed rail vehicles, maglev trains can achieve higher speeds (the highest commercial operating speed record is 350 km/h, held by China Railway as of July 2011), have lower energy consumption (the energy consumption of maglev trains is less than that of jet aircraft even at the speed of 500 km/h [72]), lower life-cycle costs, and produce less noise and vibration [73].

In semiconductor production lines, a wafer distribution system is a magnetically levitated conveyor system. This system uses a container, which is placed on a levitated stage that moves over a pair of rails to transfer wafers. The support and thrust forces acting on the stage are generated through electromagnets. Wafer distribution systems and maglev trains share some similarities. The major difference between these two is the translational speed: maglev trains can travel at speeds above 100 m/s, whereas wafer distribution systems usually operate at translational speeds of several millimeters per second.

Wafers transported by maglev technology have brought revolutionary changes to the manufacturing industry. The primary benefit is no generation of particles due to contact

wear during the transferring process. This is particularly important to semiconductor manufacturers, who need to control particle contamination in the fabrication process. In 2012, the semiconductor manufacturing industry moved from a 32 nanometer (nm) to a 22 nm specification in making complementary metal-oxide-semiconductor (CMOS) chips, following the International Technology Roadmap for Semiconductors (ITRS). In the production lines, particles larger than 22nm are considered contaminations. Traditional wafer transporting systems use rail carts in delivering the wafer material. Particles are unavoidable due to the friction between the cartwheels and the rail. The current particle control methods in manufacturing encounter difficulties when the particle size is smaller than 25nm. The contactless maglev wafer transporting system generates no particles. Raw material contamination in the transporting process is avoided. In addition, the maglev wafer transporting system eliminates the bulky lubricant system needed in traditional wafer transport, and achieves a higher positioning accuracy. It also reduces system maintenance time as there is no mechanical friction wear. Maglev technology has thus provided a novel solution to contamination control problems in manufacturing [74]. Another driver of this method is cost. It has been reported that the expense of deploying a maglev wafer transporting system is less than that of a robotic system [30], and therefore is attractive in many manufacturing plants.

Early research on the use of maglev technology in a wafer transporting system was reported by Azukizawa *et al.* [75]. In 1989, they discussed a system implemented at Toshiba Corporation for a delivery task in the automated semiconductor fabrication process. The system was developed for an environment that must be kept free from

microscopic dust particles and with noise at a minimal level. In 1992, Aik-siong *et al.* reported a platform in which a wafer holder was levitated using electromagnetic forces [76]. In this research, gas-bearing and maglev transport systems were implemented on the same platform and compared. It was found that both methods resulted in stable levitation. However, only the maglev platform could operate in a vacuum. In 1989, Park *et al.* reported a wafer distribution system for a clean room with maglev technology [30]. They successfully designed and built a compact maglev wafer distributor. Stability and precision requirements were validated experiments. In 2006, Hu and Kim reported a high-precision positioning device for wafer processing [29]. They designed and built a device with all six degrees-of-freedom (DOF) controlled by electromagnetic forces. It was reported that this positioning stage demonstrated a positioning resolution of 20 nm. Compared to conventional positioning systems, this positioning stage has the advantages of faster response time and multi-dimensional positioning capability.

Another application using a high-precision maglev stage in semiconductor manufacturing is photolithography. Similar to wafer transporting, photolithography is a process that requires strict control of dust particles in the manufacturing environment. In traditional designs mechanical friction in positioning the stage generates dust particles and thus reduces the production throughput [77]. Maglev stages generate no dust particles in the positioning process. In addition, the maglev design has a simpler mechanical structure, faster dynamic response, and higher mechanical reliability [78].

Many maglev positioning stages have been reported in the literature. In 1993 Williams *et al.* suggested a linear magnetic bearing stage that controlled a suspended object

in six DOF [79]. The intention was to offer a better solution to the traditional mechanical X-Y wafer positioning stage in photolithography (the advanced stage design methodology is also presented in the same research). In 1998, Kim and Trumper developed a high-precision maglev stage for photolithography [78]. Their maglev stage enabled six DOF motion control. It also realized large planar motions (up to 50 mm by 50 mm) with only one levitated moving part. This design relied on a linear motor to provide contact-free forces in both suspension and translation.

Maglev positioning stages have been implemented on many other systems beyond photolithography. In 2000, Holmes *et al*. reported a magnetically suspended six DOF precision motion control stage for scanned-probe microscopy [80]. The stage utilized four linear motors to move a platen horizontally and vertically. It was reported that horizontal and vertical positioning error was less than 0.6 nm and 2.2 nm, respectively. This device provides a means of measuring submicron-scale features with nanometer-scale accuracy. High-precision magnetic suspension systems were reported by Shan *et al.* in 2002 [34], Owen *et al*. in 2005 [33], Jeon *et al.* in 2006 [32], and Ueda and Ohsaki in 2008 [36]. These studies discussed new control design approaches and state-of-the-art electronic components for a maglev positioning stage. They also indicated that the maglev positioning stage exceeds the traditional positioning stage in accuracy and surmised that it would replace it eventually.

Maglev technology can provide systems with tunable dynamic characteristics. One application that exploits this feature is a maglev vibration isolation table. In 1995, Nagaya and Ishikawa proposed such a system [39]. The system includes an actuator consisting of a

permanent magnet and an electromagnet. The weight of the table is counterbalanced by static magnetic forces from permanent magnets, and vibrations and disturbances are attenuated by electromagnetic forces. In 1996, Watanabe *et al.* discussed a control system for a vibration isolation system [41]. This paper documented a typical controller design approach for non-contact vibration isolation systems. The experimental results showed the designed controller successfully isolated vibration in the vertical direction. In 2003 and 2007, Mizuno *et al*. reported the design of vibration isolation systems combining magnetic suspension with springs [37, 38]. Their design used a magnetic suspension connected in series with a mechanical spring, and resulted in high static stiffness against disturbances acting on the isolation table. With an isolation system composed solely of mechanical springs, it is almost impossible to obtain such characteristics.

In summary, maglev technology has been applied to many real-world systems, bringing unique features and numerous benefits. Maglev devices are typical mechatronic devices. The next section will discuss the concept of "mechatronics" and maglev technology.

1.1.2. Mechatronics and Maglev

Maglev technology has found its applications in various industrial systems. The success of maglev technology is based on its "mechatronics" system design approach. The term "mechatronics" was first proposed in 1969 by a Japanese engineer Tetsuro Mori. It blends together a number of technologies: mechanical engineering, electronic and electrical engineering, computer technology, and control engineering. A mechatronic design requires a rethinking of the whole system in terms of design requirements,

subsystems, available new technologies, and novel control engineering strategies.

Many products are designed using a mechatronics approach. Examples include maglev systems, automatic cameras, and robots on automatic production lines. Craig *et al.* discussed the importance of embedding the mechatronics philosophy into the education of future engineers [81-85]. In their research, several systems (an inverted pendulum system, a ball-on-plate system, and a desktop maglev system) were developed to demonstrate the mechatronics methodology. The design processes of these systems demonstrate how to work across disciplinary boundaries and utilize a blend of technologies to develop novel engineering solutions.

The maglev system discussed by Craig *et al.* includes an electromagnet, a ferrous object, electrical components, and a controller. The system is simple enough for undergraduate students to build in a laboratory environment, and sophisticated enough to provide a platform for advanced controller design. This research investigates multiple novel control design methods and classical approaches using this maglev system.

Although the applications of maglev technology keep growing, it is not likely that magnetic bearings will completely take the place of traditional mechanical bearings in the near future, nor will maglev trains be a substitute for rail trains. In some cases, the costs of implementing maglev systems are more expensive than using traditional mechanical systems. More importantly, in comparison to traditional systems, the system dynamics of maglev systems change drastically when components are magnetically-levitated. There is a need for more research on improving system performance with maglev technology.

Many research studies have been conducted to improve the overall performance of

maglev systems. The goal is to make the system more reliable than its traditional counterpart. From a mechatronics point of view, improvement can be made in each of the subsystems, as well as in the technology that brings them together. Improvements in traditional mechanical or electronic systems require new materials or manufacturing technology. In addition to updating the mechanical or electronic components, systems can be improved by using advanced control algorithms. It is the most convenient way to improve the system. There are many discussions in the literature on various potential improvements [12, 19, 23, 86-90].

Section 2 of this chapter discusses the motivation for this research. Section 3 presents the problem statement. Section 4 summarizes the contributions of this research.

1.2. Motivation

In maglev systems electromagnetic forces are controlled to achieve levitation. The control algorithms determine the stability and system response to disturbances. The control algorithm is designed based on the mathematical model of the physical system ('the plant'). An accurate system model and appropriate control algorithm will significantly improve the system performance.

There are several challenges in the control design process due to the nature of the maglev system. A first challenge is the need to account for system variation in the design. In designing a controller for a maglev system, a traditional approach is to model the plant at a certain 'operating point' and then design the controller for that particular 'operating point'. However, the working loads may vary over a certain range during the system operation. For example, it has been reported that in the compressor industry, manufacturers

need to offer magnetic bearing designs in the 60,000 to 150,000 kg capacity range [91]. Another example is the maglev transportation system operating in Shanghai. The mass of the maglev vehicle is 18,000 kg and can hold up to 60 people, which means the total mass of the vehicle could vary between 18,000 kg (no passengers) and 23,100 kg (all passengers). For a controller designed for a single nominal 'operation point', it is difficult to accommodate the large variation.

A second challenge is the need for the controller to guarantee the system performances under all working conditions. Maglev systems usually work at higher speeds than traditional systems. As an example, typical magnetic bearing systems work at angular speeds above 10,000 rpm (the angular speed of a magnetic bearing is limited by the material strength to overcome the stress due to the centrifugal force), while typical mechanical bearings work at angular speeds below 7,000 rpm. In the maglev train system, the vehicle may operate at a speed of about 500 km/h, almost twice as fast as traditional rail trains. The controllers need to maintain and improve the system performance when operating at high speeds.

A third challenge is the need to deal with disturbances and maintain a constant operating point. There are various disturbances that maglev systems experience during operation. For example, a magnetic bearing may encounter sudden bearing load changes, unbalanced rotor loads, and unmodeled rotor dynamics at high rotational speed [92]. A maglev train has to accommodate payload variations (change in mass distribution of the vehicle), vehicle vibration, changes in terrain features, and air dynamic disturbances (such as wind gusts) [93]. The controllers need to drive abruptly disturbed systems to their

normal working conditions. Also, there are other challenges common to all control system designs, such as how to minimize energy consumption during operation and how to balance performance with control effort. The design challenges call for the study of novel control design strategies to improve the overall performance of maglev systems.

Motivated by the design challenges, this research studies how to improve the performance of maglev systems with novel control design approaches. Particularly, methods to attenuate disturbances and to design robust systems are investigated. Questions addressed in this study include: How are disturbances attenuated in maglev systems through control design? Will system performance change after disturbance attenuation control? What is robustness of a maglev system? Why is the robustness of a maglev system important? Is the robustness of a maglev system related to its controller? How can the robustness of a maglev system be guaranteed during the control design process?

This thesis will explore control designs using both time-domain as well as frequency-domain approaches. System uncertainties that have been neglected in traditional control design methods will be investigated. Control design methods discussed in this research will demonstrate: (1) disturbance attenuation can be achieved in a maglev system without altering its original controller form; (2) robustness of a maglev system can be improved using a proposed control design approach; and (3) a design method to tune the controller to the exact amount of model uncertainties of the control plant to achieve desired system performance. Control design methods discussed in this research can be used for other similar maglev systems, especially when the systems have large parameter uncertainties.

1.3. Problem Statement

Maglev systems are challenging to control because of their nonlinear system dynamics and their open-loop unstable nature. Maglev systems are difficult to model accurately, primarily due to the nature of electromagnetic forces. During operation, maglev systems are subject to various disturbances. Additionally, some maglev systems work in environments where the systems themselves have large variations. Disturbances and system variations plus unmodeled system dynamics can lead to deterioration in performance and even failure in some maglev systems.

In order to deal with model variations, robust control design methods are introduced in the controller design process in this dissertation. Many control design methods are suggested in the literature to deal with the robustness issues. Some of them have been proven to be successful. However, few current control design methods take into consideration the actual physical system uncertainties. Moreover, none of the current control design approaches is able to claim that the designed controller is tuned to the exact amount of uncertainty of the control plant. None of the current design approaches is able to show the trade-off between the system performance, controller complexity, and control effort. In addition to the robustness issue, disturbance attenuation is an important topic in designing controllers for maglev systems. Based on a review of prior literature, there is a research void addressing how to achieve disturbance attenuation in a maglev system without making changes to the existing controllers.

This research develops new control strategies for maglev systems. Specifically, disturbance attenuation and robustness topics are discussed in this dissertation. A

disturbance attenuation control design using acceleration feedback is studied. The objective of using this design method is to make a maglev system as insensitive as possible to disturbances. The designed controller will achieve this goal without changing the original controller form, which is needed to maintain the stability of the maglev system. Acceleration feedback control (AFC) has been reported for use in other systems but, to the author's knowledge, it has never been implemented on a maglev system. This research demonstrates that the acceleration feedback control provides disturbance attenuation in maglev systems.

To address the robustness issue of the maglev system, this dissertation studies two robust control design methods, the Quantitative Feedback Theory (QFT) and the H_∞ methods. Both methods are particularly successful in designing robust controllers [94, 95]. In the designing of a QFT controller, the system uncertainty range and model variation range are represented with a finite set. Then the controllers are derived through classical loop-shaping techniques based on the finite set, highlighting the trade-off among the system performance, controller complexity, and control efforts. In the designing of an H_∞ controller, the control problem is expressed as a mathematical optimization problem, and the controller is derived by solving this optimization. This research presents a QFT controller and a H_∞ controller respectively, and then proposes a design approach to combine these two controllers into a QFT/H_∞ controller. The QFT/H_∞ controller has the advantages of both QFT controller and H_∞ controllers. It is not only designed to guarantee system performance despite uncertainties and variations, but is optimized to minimize the closed loop impact of a perturbation.

In an effort to address the disturbance attenuation and the robustness issue with a single controller, this dissertation proposes a novel AFC-enhanced QFT/H_∞ controller. This AFC-enhanced QFT/H_∞ controller introduces an acceleration feedback loop into the QFT controller configuration. Then the closed loop system is optimized to achieve desirable system stability and robustness using the H_∞ method. The resultant optimized controller guarantees system robustness and achieves disturbance attenuation.

To demonstrate that the proposed AFC-enhanced QFT/H_∞ controller improves the system performance, experiments are conducted to compare the system responses to those with traditional controllers. These traditional controllers include a PID controller, a lead controller, a model-reference controller (MRC), and a LQG controller. The classic PID controller and lead-lag controller are designed with the traditional measurement of system robustness. The MRC is designed to improve the system performance by minimizing the modeling error. The LQG controller is designed by minimizing the quadratic control cost of a linear system disturbed by additive white Gaussian noise. These controllers are designed to address one or two specific questions in disturbance attenuation and system robustness. None of them provides a solution to both issues. Experimental results prove that the system performance is considerably improved with the proposed AFC-enhanced QFT/H_∞ controller.

1.4. Contributions

The first contributions of this research are the development and implementation of the AFC-enhanced QFT/H_∞ control design method for the maglev system. This novel design approach guarantees the system robustness and achieves disturbance attenuation

with a single controller. The second contribution of this research is the implementation of an acceleration feedback loop to achieve disturbance attenuation in a maglev system. Prior to this research, acceleration feedback control was reported to successfully improve motor control, but has never been implemented to attenuated disturbance on a maglev system. The third contribution of this research is the implementation of a QFT/H_∞ controller. Although there are other robust control design methods reported in the literature, none of them provides a design technique based on a quantitative evaluation of system uncertainties.

To give background information on this research, a literature review in Chapter 2 summarizes how the traditional controllers guarantee system robustness and achieve disturbance attenuation. And why the system performance needs to be improved. This research first implements the AFC to attenuation disturbances, and then continues to investigate the QFT and H_∞ robust control design approaches. Similarities and differences between the QFT and H_∞ methods are discussed. A control design approach combining QFT and H_∞ is proposed. The advantage of this combination is twofold: it quantitatively addresses the system uncertainty issue in controller design and it guarantees the system robustness by restricting the magnitude of the disturbance/noise triggered response.

All the controllers are experimentally tested with the same maglev system. This study evaluates the system performance using indices derived from transient response and steady-state of the system. The experimental results validates that the proposed AFC-enhanced QFT/H_∞ controller successfully resolves the robustness and disturbance issues with the maglev system. The robust control design methods discussed in this

research could be applied to other single DOF maglev systems.

Chapter 2. Literature Review

2.1. Introduction

The scope of this research, as stated in Chapter 1, is to improve the performance of a maglev system by achieving system robustness and disturbance attenuation. This chapter reviews the literature relevant to the design of feedback controllers for maglev systems. In particular, this review summarizes how system stability, robustness, and disturbance attenuation are guaranteed in prior control design methods. In Chapter 3 a PD controller will be designed to achieve stable magnetic levitation, and then an AFC will be implemented to attenuate disturbance. In Chapter 4 will begin with designing robust controllers for the maglev system. A QFT and an H_∞ robust controllers will be designed for a maglev system, followed by a discussion on how to combine them into a QFT/H_∞ controller. Then a novel controller to achieve disturbance attenuation and robustness, an AFC-enhanced QFT/H_∞ controller, will be proposed. Chapter 5 will discuss the experimental validation of improvement on the system performance with the proposed controllers.

In Chapter 3, we attempt to answer the following questions: What is the design of a typical maglev system? What is the purpose of using controllers in maglev systems? What control methods have been implemented in maglev systems prior to this research? How do maglev systems perform with these controllers? Specifically, do these control methods deal with robustness in the design process and, if so, how? Is there a need to investigate other control design methods? What are the design approaches discussed in this study?

This chapter is organized as follows: (1) a brief review of the history of maglev is

provided, (2) the configurations of typical maglev systems are introduced, (3) an experimental platform (referred to as the *maglev testbed*) that will be used through this research is described, and (4) the prior art as well as the state-of-the-art of feedback control designs for maglev systems are summarized. Special attention will be given to the system robustness of each of the reviewed control design methods.

2.2. A Brief History of Maglev

A brief history of magnetic levitation provides a context for this dissertation. Although magnetism was first recorded around 545 B.C. [96, 97], there was no record of successful levitation using magnetic forces generated by permanent magnets (static magnetic forces). In 1842, British mathematician Samuel Earnshaw proved mathematically that the stable stationary equilibrium of a point charge could not be maintained solely through its electrostatic interactions with other charges [98]. This was later known as Earnshaw's theorem. Earnshaw's theorem also applies to all the classical inverse-square law forces, including gravitational and magnetic forces. In other words, near the earth's surface, the gravitational force acting on a mass cannot be balanced out by any number of static magnetic forces, no matter how they are arranged.

Earnshaw's theorem does not exclude the possibility of achieving a stable levitated state. Several methods to realize magnetic levitation were found after Earnshaw's theorem was published. Commonly reported methods are: maglev using the gyroscopic effect [99, 100], maglev using diamagnetism [101, 102], maglev using eddy current [103-105], and maglev using feedback control [106-108]. Among these methods, maglev with feedback control is considered to be practical and cost-effective, and has been used in the current

industrial maglev applications. This research, as has been stated previously, will adopt this particular method.

Maglev with feedback control was brought to the public domain with the publication of research work of Holmes, Beams, Woodson and Melcher, and Weaver [10, 11, 18, 108-110]. Early research progress was slow because of the lack of high performance control hardware. With the development of microcontroller in the late 1970s, sophisticated control algorithms could be tested for maglev control. In 1990 Trumper published his doctoral dissertation on the design of a maglev system for precision motion control [35]. He designed a linear controller and implemented it with an 8088/8087 microcontroller. Microcontrollers specialized for digital signal processing (DSP) were introduced to the market in the mid 1980s. They were superior to the general purpose microcontrollers in motion control applications. In 1990 Kinichi *et al.* published a paper on the linear motor drive system for the Japanese maglev vehicle HSST-05 [111]. In 1997 Green published his doctoral dissertation on the robust nonlinear control design of maglev systems [112]. Green's design was implemented on a MX-31 DSP system. A large number of linear and nonlinear controllers have been tested on maglev systems since then.

Today the research trend is to improve maglev system performance with novel control design approaches. However, some questions still remain. Are further improvements in maglev system performance possible with novel control algorithm? Have system dynamics been neglected in the control design process? If yes, how can they be included in design approaches? How does the system performance change after the implementation of novel controllers? Is it possible to simplify the controller complexity

without sacrificing the performance? How can a balance among the system uncertainties, control effort, and controller complexity be achieved?

This research will address these questions and investigate the design of novel controllers. Classical controller designs are also included in this study. They serve as benchmarks to compare the performance of a maglev system with the proposed controllers.

2.3. Configurations of Maglev Bearings and Trains

The configurations of the two most popular maglev systems, magnetic bearings and maglev trains, are introduced in this section. Other maglev systems, such as wafer delivery systems [29-31, 76, 113-115] and precision positioning stages [35, 77, 78, 116-118], share configurations similar to maglev trains and are not discussed. This section begins with a brief review of the history of these two maglev systems.

An early discussion of magnetic levitation devices appeared in an article published by Holmes in 1937 [109]. In this article Holmes described an experimental device in which a vertical ferromagnetic needle was supported by an electromagnetic force. This device levitated a 6 gram rotor and achieved a rotational speed of 7,200 rpm. The controller was built with analog electronic components. It was the first reported device that successfully demonstrated the concept of magnetic levitation. In the same year, a magnetically levitated transportation device appeared in a patent. In 1937, a patent was awarded to Kemper for an overhead suspension railway design [67]. However, due to the technological limitation, this concept was never turned into reality.

From 1942 to 1965, Beams received multiple patents for magnetic bearings and magnetically suspended systems [10, 110, 119, 120]. In 1964, Beams built an apparatus

with a rotor suspended by electromagnetic forces [11]. This was the first known prototype of an axially suspended magnetic bearing. The magnetic bearings were used on ultracentrifuges (with an angular speed of 3.1×10^7 rpm) that separated uranium isotope U-235 from other isotopes.

In 1963, White and Weltin published a paper describing how to construct a tabletop electromagnetic levitator. They built this small device for the purpose of demonstrating the concept of magnetic levitation in physics education [121].

Since the early 1970s, magnetic bearings and maglev trains were developed by several engineering groups and companies. In 1973, Thornton presented an overview of the advantages of maglev trains, including high speed, low noise, less maintenance, and low energy consumption [72]. In 1974, Gutberlet summarized the development of a German maglev train, which included the most advanced maglev technology at that time [122]. Based on the experience gained from operation of the German maglev train, Gotizein *et al*. proposed the "magnetic wheel" concept in 1980, which was applied to maglev trains after its publication [21].

Magnetic bearing characteristics were first analyzed by Schweitzer in 1976; he studied how to utilize magnetic bearings for vibration control [123]. Based on the work of Schweitzer, Studer proposed a "practical magnetic bearing" design in 1977 [16]. This design was regarded as a milestone, because it reduced the size, weight, and complexity of a magnetic bearing to achieve acceptance in flight systems. The controller in this design was built with analog circuits.

In 1979, Habermann suggested a new magnetic bearing design with the opposite

poles of each electromagnet arranged axially [124]. This design turned out to be effective in applications requiring high accuracy. In 1980, Habermann summarized his work on an Actidyne™ active magnetic bearing system in a paper titled "An Active Magnetic Bearing System" [125]. In the paper, Habermann described the principles of the design and operation of the magnetic bearing system, and demonstrated high accuracy of a shaft position (up to 0.01 mm) through experiments.

The working principles of magnetic bearings and maglev trains are similar. The components carrying loads are magnetically supported by electromagnet forces. The magnitudes of the magnetic forces depend on how much current runs through the electromagnets (assuming the magnetic cores are not saturated.) The currents are controlled based on a difference of the measured and desired positions of the levitated loads. The next two sections provide details about the configurations of magnetic bearings and maglev trains.

2.3.1. Magnetic bearings

Magnetic bearings differ from traditional mechanical bearings in that their rotors are suspended by electromagnetic forces. There are two types of magnetic bearings: passive magnetic bearings and active magnetic bearings [12, 126]. The passive magnetic bearing utilizes static magnetic forces plus other means of support to achieve what is called "pseudo-levitation" [127-132]. It has no feedback loop and therefore is not in the scope of this research. The active magnetic bearing, which uses a feedback control loop to realize stable levitation, is addressed in this research.

Figure 2.1: MBC 500 magnetic bearing system [133]

Figure 2.1 shows an MBC 500 magnetic bearing system built by LaunchPoint™ Technologies LLC. The electromagnet assembly inside the active magnetic bearing is visible. The gap sensors and control circuits are built inside the aluminum housing (which cannot be seen in the picture.)

This system has two radial active magnetic bearings (AMB) and two axial passive magnetic bearings (PMB) [133]. Each AMB has four pairs of electromagnets, whose current can be controlled individually. A turbine is built in the magnetic bearing system (which cannot be seen in the picture). The air-turbine drive is capable of driving the shaft to a rotational speed of 10,000 rpm (the speed limitation is preset by the control system for safety, and is not the maximum rotational speed the system can achieve.) Several research projects have studied the system identification, modeling, and control designs of this system [134-138]. The controllers tested for this AMB are usually linear controllers.

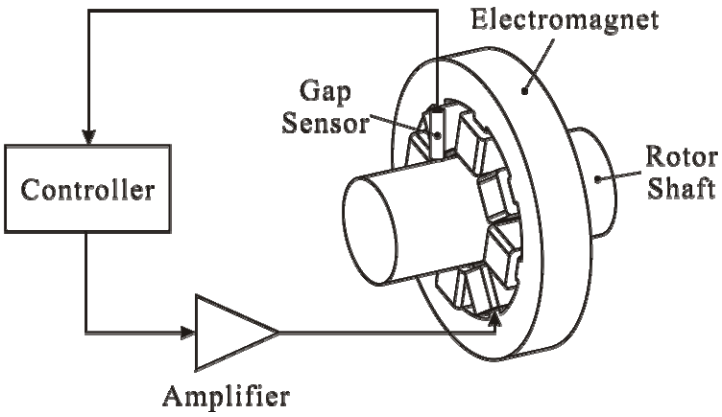

Figure 2.2: Configuration of one AMB electromagnet with a control loop [139]

Figure 2.2 shows the configuration of one group of the electromagnets with a feedback loop to control the current through one electromagnet. The electromagnets are part of one AMB built inside the MBC 500 system. In Figure 2.2, there is a gap distance sensor, which is a Hall effect sensor; it is located near the rotor shaft to measure the position of the shaft (i.e., the gap distance between the shaft and the electromagnet.) There are multiple gap distance sensors in the system. For simplicity, Figure 2.2 shows just one of them.

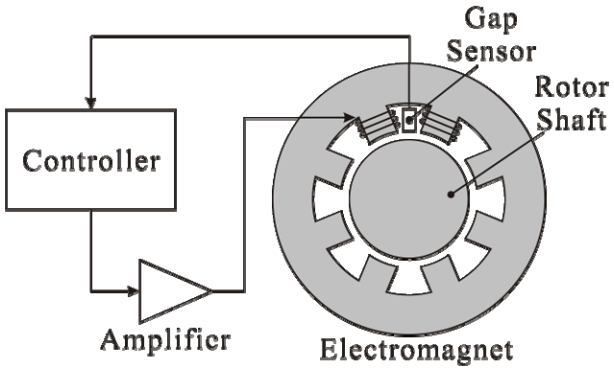

Figure 2.3: Schematic of the electromagnet of AMB [139]

Figure 2.3 shows a schematic of a typical AMB. In this schematic, the gap sensor

measures the gap distance between the rotor shaft and the electromagnets and outputs a position signal. This position signal is sent to the controller, which controls the current through the electromagnets using a power amplifier to generate an electromagnetic force. The electromagnetic force acts on the ferrous rotor shaft and pulls it toward the electromagnets (stator.)

As is seen in Figure 2.3, a typical AMB consists of four major components: a gap sensor, an electromagnet (stator of the AMB), a controller, and a rotor. The distance between the rotor and the stator is measured by a gap sensor, and controlled by a controller. In the next section, the configurations of maglev trains will be discussed. It will be seen that the configurations of magnetic bearings and maglev trains are similar.

2.3.2. Maglev Trains

Maglev trains utilize electromagnetic forces to levitate the train bodies. There are also electromagnets for lateral guidance and propelling, but are not discussed in this research. There are three major types of suspensions used in maglev trains: the Electromagnetic Suspension (EMS) [107, 140-143], the Electrodynamic Suspension (EDS) [144-148], and the Inductrak [149-155]. In EMS, there is one electromagnetic unit that controls the “levitation”. A second electromagnet unit, which includes groups of linear motors built along the guideway, drives the train forward. This research discusses the unit that controls the levitating forces.

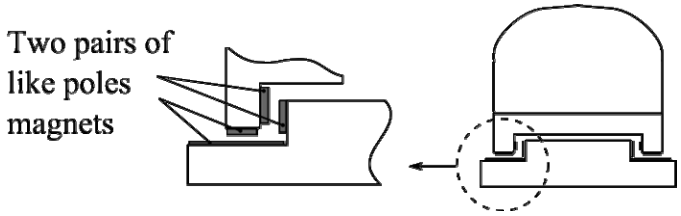

Figure 2.4 Principle of repulsive-type maglev trains [156]

Magnetic force between two magnets is either repulsive or attractive depending on the how their polarities are arranged. Maglev train operations can be divided into two types: repulsive-type and attractive-type based on the levitating magnetic forces. EMS is the attractive-type maglev train; EDS and Inductrak are the repulsive-type. Figure 2.4 shows the principle of repulsive-type maglev trains. The magnets on the trains and those on the guideway are assembled to bring like poles together, generating repelling forces between the train and the guideway. The repelling magnetic forces levitate and guide the train. Control design for repulsive-type maglev trains is not discussed in this research. (The mathematical model is different from that of the experimental testbed.)

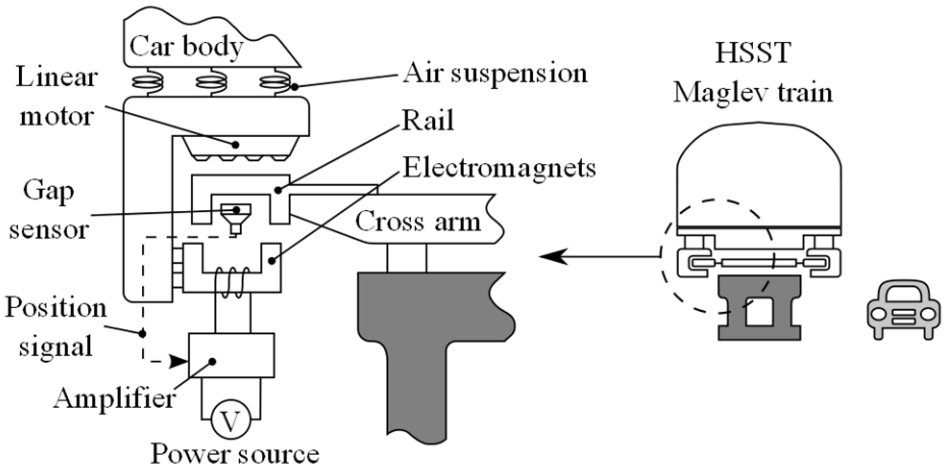

Figure 2.5: Schematic of principle of HSST Maglev train [156]

Figure 2.5 shows a schematic of the principle of the High Speed Surface Transport (HSST) maglev train, which represents the design of a modern attractive-type maglev train [156]. Figure 2.5 also shows the configuration of the attractive-type maglev train in detail. Electromagnets are assembled on the frame underneath the car body and positioned underneath the rail. The rail is made of a ferromagnetic magnetic material. The magnetic forces between the electromagnets and the rail are attractive forces. The car body of the HSST maglev train, which is made of welded aluminum alloy, is levitated when the electromagnets are pulled upward towards the rail. The gap sensor measures the gap distance between the car body and the rail. The position signal from the gap sensor is sent to the control unit, which controls an amplifier that regulates the current delivered to the electromagnets from the power source. The electromagnetic forces vary depending on the amount of current through the electromagnets. Thus, the gap distance is controlled by electromagnetic forces.

The first commercial maglev train was the HSST in Japan, which started its service on the Tobu Kyuryo Line in the northeastern suburbs of Nagoya city in 2005 [157]. Many publications have reported the modeling, analysis, control design, as well as experimental validation of the HSST maglev train [158-164].

In summary, as shown in Figure 2.5, there are four major components in a maglev system: the gap sensor, the maglev train, the rail, and the controller. The position of the maglev train relative to the rail is measured with a gap sensor, and controlled by a controller. The working principle of maglev trains is the same principle as that of magnetic bearings (discussed in the previous section.)

2.3.3. Similarities of Systems

Magnetic bearings and maglev trains have four major hardware components: electromagnets, gap sensor, control unit (including the controller and the amplifier), and levitated load. The control unit controls the electromagnetic forces and thus the position of the levitated load. The behavior of the system is dependent on how the controller reacts to the position signal.

There are several maglev systems sold for educational use. Educational Control Products® makes an educational maglev system, in which rare earth magnets move along a polished glass bar [165]. Feedback Instruments® offers a maglev experimental apparatus, in which a hollow steel sphere is suspended by electromagnetic forces [166]. In 2004 Lundberg suggested a low-cost maglev project kit [167]. In 2013 Awelewa presented a magnetic levitation system for control engineering education [168].

In this research, the maglev testbed was designed by Scott Green [112]. This testbed was chosen for this research because its design is well documented in Green's dissertation. The detailed geometric dimensions and material properties allow an FEA model to be created to simulate the magnetic field and magnetic forces. Additionally, Green has designed and tested multiple controllers with this system, thereby providing references for the control design. In the next section, this maglev system will be described.

2.3.4. Desktop Maglev Testbed

This research utilizes a desktop size testbed to investigate the behavior of a maglev system with controllers designed with different control design approaches. Like the maglev systems discussed above, this maglev testbed consists of four major hardware parts. The

details on how the electromagnet is built and how to derive the electromagnetic force are included in Appendix A.

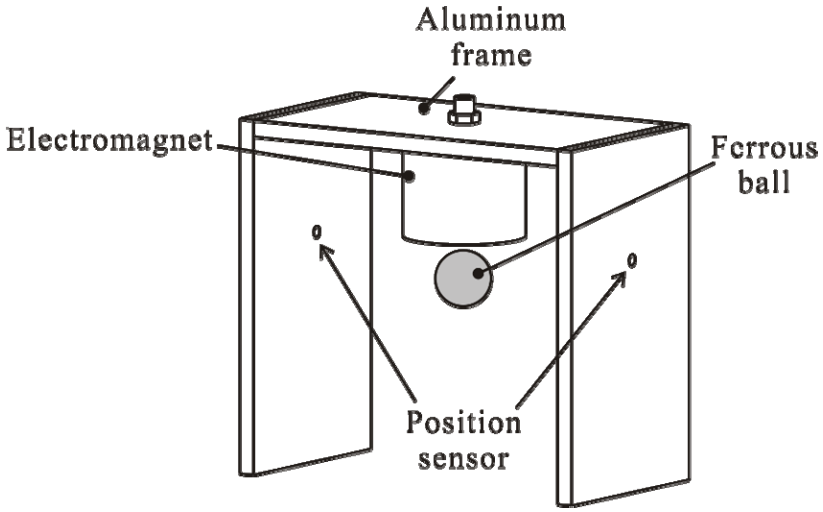

Figure 2.6: Maglev testbed used in this research

Figure 2.6 shows a graphic representation of the maglev testbed used in this research. Research work conducted using the same apparatus has been reported by Green *et al*. in 1997, Craig *et al*. in 1998, Craig in 1998 and in 1999, and Green and Craig in 2001 [81, 83, 169-171]. Several control design ideas have been successfully demonstrated with this testbed [112].

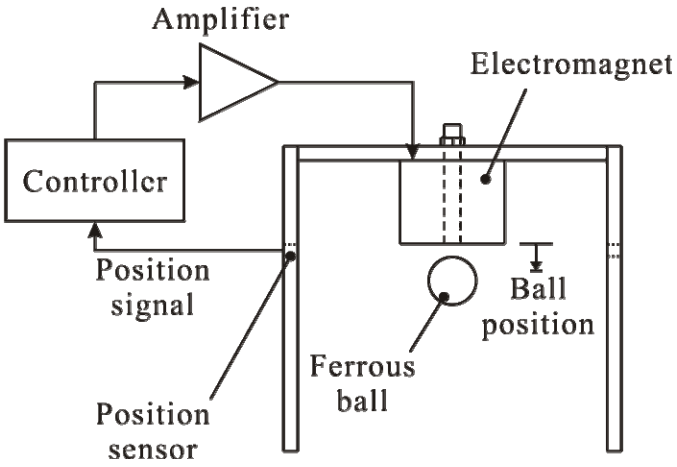

Figure 2.7: Schematic of the maglev testbed

Figure 2.7 shows the front view of the maglev testbed. A single electromagnet is fixed on an aluminum frame. When the current flows, the electromagnet force pulls the ferrous ball up. There is a position sensor (optical sensor) mounted on the frame. It measures the gap distance between the electromagnet and the ferrous ball and outputs a position signal. The signal is sent to the controller that is connected to an amplifier and controls the current through the electromagnet. The electromagnetic force is adjusted to counterbalance the weight of the ball and achieve stable levitation. This research investigates how to design controllers that control the electromagnetic forces to guarantee stable levitation despite external disturbances and system uncertainties.

2.4. Feedback Control Design for the Maglev Systems

This section summarizes the control design methods that are relevant to this research in the literature, and describes how the maglev system stability and system robustness were addressed previously. Literature on AFC will be summarized in Chapter 3, after the discussion of how to achieve a stable levitation. The following two sections review

control design methods that guarantee stable levitation and system robustness, respectively. The discussion motivates why robust controllers are needed, and ultimately, how to design a robust controller.

2.4.1. Linearizing a Nonlinear System

The linear control design methods work with system models described by linear differential equations. If the system equations are nonlinear, a mathematical method is used to transfer them into a form that works with the linear control design approaches. The common method is to linearize the nonlinear system about an operating point. This method approximates the nonlinear system behavior with a linear model derived either analytically or numerically. A controller is then designed for the linearized approximation, assuming the system works in the vicinity of the operating point and the operating range is small enough so that the nonlinearities can be ignored.

The linearization process is described briefly here. The nonlinear system (or plant) model is given by:

$$\begin{aligned} \dot{x} &= f(x(t), u(t)) \\ y &= h(x) \end{aligned} \tag{2.1}$$

where $x \in \mathbb{R}^n$ is the state vector, $u \in \mathbb{R}^p$ is the input vector, and $y \in \mathbb{R}^m$ is the output vector.

To linearize this system, a Taylor series expansion is performed around an operating point (x_0, u_0), where x_0 is the plant state when the input is u_0. Eq. (2.1) becomes:

$$\begin{aligned}\dot{x}_i &= \frac{dx_i}{dt} \\ &\approx f_i(x_0,u_0) + \sum_{j=1}^{m} \left.\frac{\partial f_i(x,u)}{\partial x_j}\right|_{x_0,u_0} \left(x_j - x_{0,j}\right) + \sum_{j=1}^{n} \left.\frac{\partial f_i(x,u)}{\partial x_j}\right|_{x_0,u_0} \left(u_j - u_{0,j}\right) + \dots\end{aligned} \tag{2.2}$$

Eliminating the higher order terms and changing the notation in Eq. (2.2) with

$$\Delta x_j = x_j - x_{0,j},\ \Delta u_j = u_j - u_{0,j}.$$

and

$$\Delta \dot{x}_i = \dot{x}_i - \dot{x}_{0,i} = \dot{x}_i - f_i(x_0,u_0)$$

the expression of the linearized model is given by:

$$\Delta \dot{x}_i = \sum_{j=1}^{m} \left.\frac{\partial f_i(x,u)}{\partial x_j}\right|_{x_0,u_0} \Delta x_j + \sum_{j=1}^{n} \left.\frac{\partial f_i(x,u)}{\partial u_j}\right|_{x_0,u_0} \Delta u_j \tag{2.3}$$

Eq. (2.3) can be rewritten in the standard linear state-space form:

$$\Delta \dot{x} = A \cdot \Delta x + B \cdot \Delta u \tag{2.4}$$

where A and B are the Jacobian matrices:

$$A = \left.\begin{pmatrix} \frac{\partial f_1}{\partial x_1} & \frac{\partial f_1}{\partial x_2} & \dots & \frac{\partial f_1}{\partial x_n} \\ \frac{\partial f_2}{\partial x_1} & \frac{\partial f_2}{\partial x_2} & \dots & \frac{\partial f_2}{\partial x_n} \\ \vdots & \vdots & \ddots & \vdots \\ \frac{\partial f_n}{\partial x_1} & \frac{\partial f_n}{\partial x_2} & \dots & \frac{\partial f_n}{\partial x_n} \end{pmatrix}\right|_{x_0,u_0}$$

and

$$B = \left.\begin{pmatrix} \frac{\partial f_1}{\partial u_1} & \frac{\partial f_1}{\partial u_2} & \dots & \frac{\partial f_1}{\partial u_n} \\ \frac{\partial f_2}{\partial u_1} & \frac{\partial f_2}{\partial u_2} & \dots & \frac{\partial f_2}{\partial u_n} \\ \vdots & \vdots & \ddots & \vdots \\ \frac{\partial f_n}{\partial u_1} & \frac{\partial f_n}{\partial u_2} & \dots & \frac{\partial f_n}{\partial u_n} \end{pmatrix}\right|_{x_0,u_0}$$

2.4.2. Review of the Linear Control Design Methods

Several publications summarized the linear control design techniques tested with maglev systems similar to the desktop testbed before the 1980s, with the controllers implemented using analog electronic components. These publications included the papers published by Jayawant [107, 172], the project report by Wong [173], the book published by Sinha [174], the articles published by Covert [175], Eastham and Hayes [19], Barie and Chiasson [176], and doctoral theses by Trumper [40] and Green [112]. Additionally, Scudiere *et al.*, Williams *et al*., Trumper, and Green discussed digital control designs for maglev systems [177, 178].

In the abovementioned research publications, the maglev systems were modeled as linear systems, i.e., the nonlinear system dynamics were linearized. Classical control design methods were used to design the controllers. Designs with the assistance of graphical tools such as the Bode plot and the Nyquist plot were reported in the literature. PID type controllers, lead-lag type controllers, and a combination of these two types of control (such as a PI controller with lead term, which forms a PI-Lead controller) were tested. Most research prior to the 1980s implemented the controllers using analog electronic components. The design goal was to obtain stable levitation, and these controllers successfully achieved this goal.

In the literature on the linear control design of the maglev system, there is a lack of discussion of disturbance attenuation. Two facts contributed to this: (1) The linear control design methods were aimed to solve the stability problem. The methods do not deal directly with disturbances in the system. (2) With analog electronic components, it is difficult to

implement the acceleration feedback algorithm as an acceleration estimator is needed. This research introduces a DSP board and implements the acceleration feedback algorithm in software. With acceleration feedback control, disturbance attenuation is achieved on the maglev system. In Chapter 3, acceleration feedback is added to the maglev system after a linear controller is designed.

2.4.3. Nonlinear Control Techniques

This literature review of nonlinear control techniques focuses on the nonlinear theories that have been applied to the three specific types of maglev systems: (1) maglev transportation systems (maglev vehicles and wafer transporting systems); (2) magnetic bearing systems; and (3) single DOF experimental systems that are similar to the one shown in Figure 2.6. Table 2.1 identifies nonlinear control techniques that were reviewed in the doctoral dissertation by Green [112]. Green's review focused on adaptive control design approaches, while this review focuses on robust control design methods. There are overlaps in these two reviews since both methods are used to design controllers that account for system uncertainties.

For each method reviewed here, the basic concept of the nonlinear control theory is described, and then research related to the particular theory is presented with applications to maglev systems. Finally, the advantages and disadvantages of each of the nonlinear control design methods are summarized.

2.4.3.1. Relay control/on-off control/bang-bang control

A simple discontinuous nonlinear control element (e.g., on and off) can be used to

force the system to oscillate in a limit cycle around the required operating point. For a nonlinear plant, the controlled system is assumed to be piecewise linear with known switching times. Relay control can be applied to both linear and nonlinear plants. The systems might behave differently for the different modes (on/off) of the controller (e.g., it may present different time constants or process gains).

A common practice for relay control is to apply a modulation technique that manipulates the width of the on/off (pulse) time based on the plant state fed back to the controller. This pulse-width modulation (PWM), or pulse-duration modulation (PDM), technique is a common method to control motors. Its application to maglev systems has been reported in the literature. Hurley *et al*. described a controller design based on a PWM converter in 2004 [179]. Experiments showed that the controller could stabilize a maglev system that was similar to the desktop testbed. Another PWM controller for magnetic bearings was reported by Zhu and Mao in 2005 [180]. In their research, a two-level PWM-based switching power amplifier was utilized for the control design to stabilize a magnetic bearing. Issues such as the static input-output characteristic, frequency response, and current harmonic distortion were also addressed in this research.

The advantages of on-off control include: (1) the controller implementation is very simple, (2) the delay elements in the system can be treated easily, and (3) the controller provides a certain level of robustness despite plant parameter variations.

The disadvantages of this method are: (1) the dynamics of the system are different when the controller is on and when it is off, (2) control signal oscillation is unavoidable, and (3) there is no real steady-state of the system.

2.4.3.2. Feedback linearization

The feedback linearization method transforms the nonlinear system into an equivalent linear system through a change of variables along with a change of the suitable control inputs. By performing this transformation, a stabilized outer-state feedback loop is achieved. Oftentimes, the inner feedback loop acts as a dynamic nonlinear parallel compensation loop. There are two types of feedback linearization: the input-to-state linearization and the input-to-output linearization [181, 182].

1. Input-to-state feedback linearization

Input-to-state feedback linearization finds a control input that renders a linear input-state map between the new input and the state [182]. For example, for the nonlinear system

$$\begin{aligned} \dot{x} &= f(x) + g(x)u \\ y &= h(x), \end{aligned} \tag{2.5}$$

this method finds a state feedback control

$$u = \alpha(x) + \beta(x)v$$

and a change of variables

$$z = T(x)$$

that transforms the original system to

$$\begin{aligned} \dot{z} &= Ax + Bv \\ y &= h(T^{-1}(z)). \end{aligned} \tag{2.6}$$

Table 2.1: Nonlinear control techniques overview by Green [112]

<table>
<tr><td colspan="5">Nonlinear Control Theory</td></tr>
<tr><td colspan="2">Robust Theory</td><td colspan="2">Adaptive Theory</td><td>Stability Theory</td></tr>
<tr><td>Inversion Methods</td><td>Non-inversion Methods</td><td>Direct</td><td>Indirect</td><td rowspan="2">1. Lyapunov direct method
2. Input-output stability theory
3. Phase-plane method
4. Describing-function method
5. Linear techniques:
(Lyapunov indirect method and frequency domain methods)</td></tr>
<tr><td>1. Feedback linearization (input-output linearization and input-state linearization)
2. Time-delay control
3. Variable-structure control (sliding-mode control)
4. Robust-saturation control</td><td>1. Gain scheduling
2. Energy shaping (passivity-based control)</td><td>Adaptive control parameters</td><td>Adaptive plant parameters (adaptive backstepping control)</td></tr>
</table>

The nonlinear system expressed in Eqs. (2.5) is transformed into a linear system expressed in Eqs. (2.6). Then a linear controller can be designed using the updated linear system equations [182].

2. Input-to-output feedback linearization

Input-to-output feedback linearization is the same as the input-to-state method, except the transformation is from the input to the output [183]. Consider the same nonlinear system in Eq. (2.5). Taking the derivative of the output, the system equations become:

$$\dot{y} = \frac{\partial h}{\partial x}\big(f(x) + g(x)u\big) = L_f h(x) + L_g h(x)u \tag{2.7}$$

where

$$L_f h(x) = \frac{\partial h}{\partial x} f(x)$$

is the "Lie derivative" of h along f. If $L_g h(x) = 0$ in Eq. (2.7), then $\dot{y} = L_f h(x)$ is independent of u.

Repeating the differentiation for the second derivative of y,

$$\ddot{y} = \frac{\partial (L_f h)}{\partial x}\big(f + gu\big) = L_f^2 h(x) + L_g L_f h(x)u\,. \tag{2.8}$$

Again, if $L_g L_f h(x)u = 0$ then $\ddot{y} = L_f^2 h(x)$ is independent of u.

The same process is repeated until

$$\begin{cases} 0 = L_g L_f^{i-1} h(x), \ (i = 1, 2, \ldots, p-1) \\ 0 \neq L_g L_f^{p-1} h(x) \end{cases}$$

where u does not appear in the equations of $\dot{y}, \ddot{y}, \ldots, y^{(p-1)}$. Rewriting the p-th order differential equation of y

$$y^{(p)} = L_f^p h(x) + L_g L_f^{p-1} h(x)u \tag{2.9}$$

and letting the control signal be $u = \dfrac{1}{L_g L_f^{p-1}\left(-L_f^p h(x) + v\right)}$, Eq. (2.9) becomes

$$y^{(p)} = v \,. \tag{2.10}$$

Eq. (2.10) shows a linearized form of the nonlinear system. Controllers can then be designed using linear control design techniques [184].

There has been significant research on designing controllers for maglev systems using feedback linearization methods. In 1991 Hung reported a design using feedback linearization control for a maglev system [185]. In this study, the regulation performance was compared to that achieved by linear state feedback. Other issues such as feedback requirements, computational demands, and system robustness were also discussed. The conclusion was that nonlinear control yielded better performance than the linear state feedback approach, especially in the reduction of sensitivity to system parameter changes. It was also noted that the difference in computational demands between the two types of controllers was not significant.

In 1997 Joo and Seo presented a different feedback linearization controller design for a maglev system [143]. In their research, the maglev system was treated as a nonlinear SISO system. A class of nonlinear systems with bounded uncertain parameters was characterized and then transformed into a group of linear interval matrices. Feedback linearization control was proposed for the maglev system. Experiments showed that feedback linearization control of the maglev system provided better performance in comparison to classical state feedback control under small perturbations.

In 2001 Filho and Munaro studied the problem of designing tracking controllers for a maglev system [186]. The nonlinear system was linearized using the input-state feedback linearization technique. They also developed a linear reduced-order observer to estimate

the states because of the structure of the linearization transformation. The tracking control law for the input-state linearization model was developed using integral control based on the estimation obtained by the observer. The derived tracking controller successfully met the design requirements.

In 2001 Yang and Tateishi described a robust control design with feedback linearization [187]. Their design was a backstepping controller based on the nonlinear system model. Parameter uncertainties were also included during the design process. The control design was carried out in two steps. In the first step, a PI controller was designed to stabilize the system. In the second step, an adaptive robust nonlinear controller composed of an adaptive feedback linearization term and a robust nonlinear damping term was designed to attenuate the parameter uncertainty effects. The authors reported that the designed system exhibited excellent position tracking performance with the high-gain feedback issue of the robust controller and the poor transient performance of the adaptive controller overcome by the combination of the adaptive and robust approaches.

In 2002 Lindlau and Knospe applied the feedback linearization method to a magnetic bearing [188]. They designed a feedback linearization controller and then proposed a high-performance controller for the system with feedback linearization and μ-synthesis . Their test results showed the controller designed with μ-synthesis guaranteed the design specification of system robustness.

In 2004 Mizutani *et al*. studied the stabilization and tracking problems of a maglev system [189]. They transferred the nonlinear model of the maglev system into a feedback linearized system. Then a controller was developed using the output regulation theory to

optimize system tracking performance. Additionally, a stabilizing output feedback controller was designed. Experiments proved both controllers achieved the design goals.

In 2005 Chen and Knospe published a paper on feedback linearization for a magnetic bearing system [190]. Their research reported a feedback linearization controller with a filter to compensate for the nonlinearities of the amplifier and measurement instruments in the maglev system. A robust controller using μ-synthesis based on the feedback linearization model was proposed. The compensation filter was essential for the system to achieve stability and the specified performance.

The advantages of the feedback linearization method include: (1) the method is simple and easy to implement, and (2) after the linearization, linear control design methods can be used on the linearized model.

The disadvantages of this method include: (1) the variable change must be invertible, (2) the derived model might be sensitive to parameter changes, and (3) all the state variables must be available or otherwise observers are needed. Usually nonlinear observers are needed to estimate the states, which increases the complexity of calculation.

2.4.3.3. Lyapunov redesign

The Lyapunov redesign method exploits the Lyapunov function for the synthesis of nonlinear control systems. To design a controller, first a Lyapunov function V needs to be defined for the closed-loop system, then a control law is designed which makes the derivative $\dot{V}$ negative for the required domain of attraction (for all possible initial conditions, disturbances, and uncertainties). The derived control law is usually a nonlinear

state feedback law.

To describe the method, consider a nonlinear system which is affine (linear) in the input, i.e.,

$$\dot{x} = f(x) + g(x)u \tag{2.11}$$

with $f(0) = 0$.

The Laypunov candidate function, V, can be found by letting

$$V : \mathbb{R}^n \to \mathbb{R}$$

be a continuous scalar function (which means the Lyapunov function V is a mapping from $\mathbb{R}^n$ to $\mathbb{R}$). If V satisfies the locally positive-definite function conditions, i.e.,

$$V(0) = 0;$$
$$V(x) > 0, \ \forall x \in U \setminus \{0\}$$

with $U \setminus \{0\}$ standing for the neighborhood around, but not including the point x=0, it is one of the Lyapunov candidate functions.

Choosing one $V(x)$ Lyapunov candidate function set as the Lyapunov function for the system, a stabilizing feedback control law, $u(x)$, can be written using Sontag's formula [191, 192]

$$u(x) = \begin{cases} \dfrac{-\dfrac{\partial V}{\partial x} f + \sqrt{\left(\dfrac{\partial V}{\partial x} f\right)^2 + \left(\dfrac{\partial V}{\partial x} g\right)^4}}{\left(\dfrac{\partial V}{\partial x} g\right)} & \text{for } \dfrac{\partial V}{\partial x} g \neq 0 \\ 0 & \text{for } \dfrac{\partial V}{\partial x} g = 0 \end{cases} \tag{2.12}$$

Due to the difficulty in finding a Lyapunov function for the system, this method is often used with other control design methods (especially the nonlinear approaches which need to find stability conditions) to derive a feasible controller. There are several such designs

reported in the literature.

In 1994 Blanchini and Carabelli presented a study of a design technique for the robust stabilization of a maglev system with a Lyapunov function [193]. The nonlinear maglev system was linearized and treated as a linear system with time-varying uncertain parameters. A polyhedral Lyapunov function (polyhedral Lyapunov functions have been discussed by Polanski [194]) was constructed and a linear variable structure stabilizing controller was derived. Stable levitation was thus achieved.

In 2006 Chiang *et al*. used an integral variable-structure grey (‘grey’ meaning the system is partly known) control for a maglev system for position tracking [195]. The stability of the system was proved by the Lyapunov function and a sliding mode control was derived. This design utilized a mathematically simple but computationally efficient grey compensator for the integral variable structure controller to reduce the chattering and steady-state error. It was shown that the performance of the system depended on the magnitude of the uncertainties and disturbances. Chattering and steady-state error may exist if either one of them exceeded their estimated values.

In 2010 Lin and Chen proposed an intelligent integral backstepping sliding model control for the position control of a maglev system [196]. Their design used backstepping sliding model control with integral action to track the reference trajectory. Then the switching function of the sliding mode control was discarded and the requirement for the needed bounds was relaxed. The controller was then implemented using a MIMO recurrent neural network estimator. The Lyapunov stability theorem was used to train the parameters of the recurrent neural network and finally adaptive learning algorithms were derived.

Experiments demonstrated the validity of the control by tracking periodic sinusoidal trajectory signals.

The advantages of this method are: (1) the stability of the nonlinear system can be guaranteed, and (2) the robustness of the system can be balanced against the performance by the choice of the Lyapunov function.

The disadvantages of this method are: (1) it might be difficult to find a Lyapunov function, and (2) all the state variables need to be measurable, otherwise nonlinear observers are needed to estimate the states.

2.4.3.4. Backstepping

The backstepping method is based on a Lyapunov function and is a stepwise control design approach. The design of a first-order subsystem is performed first. Then an additional set (which is referred to as the upper system) is considered and the design for the second-order system is performed for incremental orders until the whole system is controlled.

The backstepping procedure can be applied as follows to a system of the form

$$\begin{cases} \dot{x} = f_x(x) + g_x(x) z_1 \\ \dot{z}_1 = f_1(x, z_1) + g_1(x, z_1) u_1 \end{cases} \tag{2.13}$$

where $x = [x_1, x_2, \ldots, x_n]^T$, $f_x(x)$ and $g_x(x)$ are function of x, $z1$ and $u1$ are scalars for all x and $z1$, $f_1(x, z_1)$ and $g_1(x, z_1)$ are functions of x and $z1$ with $g_1(x, z_1) \neq 0$.

It is assumed that a control input is known for which the Lyapunov function proves the stability of the upper system. A new control input is introduced together with the variable substitution:

$$u_1(x,z_1)=\frac{u_{a1}-f_1(x,z_1)}{g_1(x,z_1)} \tag{2.14}$$

which is possible as long as $g_1 \neq 0$. The system becomes

$$\begin{cases} \dot{x}=f_x(x)+g_x(x)z_1 \\ \dot{z}_1=f_1(x,z_1)+g_1(x,z_1)\cdot\underbrace{\dfrac{u_{a1}-f_1(x,z_1)}{g_1(x,z_1)}}_{u_1(x,z_1)}=u_{a1} \end{cases} \tag{2.15}$$

and then the input is designed according to the law

$$u_{a1}(x,z_1)=-\frac{\partial V_x}{\partial x}g_x(x)-k_1(z_1-u_x(x))+\frac{\partial u_x}{\partial x}(f_x(x)+g_x(x)z_1) \tag{2.16}$$

with gain $k_1>0$. So the final feedback-stabilizing control law is:

$$u_1(x,z_1)=\frac{\overbrace{-\frac{\partial V_x}{\partial x}g_x(x)-k_1(z_1-u_x(x))+\frac{\partial u_x}{\partial x}(f_x(x)+g_x(x)z_1)}^{u_{a1}(x,z_1)}-f_1(x,z_1)}{g_1(x,z_1)}.$$

This input stabilizes the system since the new Lyapunov function

$$V_1(x,z_1)=V_x(x)+\frac{1}{2}(z_1-u_x(x))^2$$

proves stability of the system with the design of $u_{a1}(x,z_1)$ and $u_1(x,z_1)$ above.

The backstepping control design method utilizes the Lyapunov function to guarantee the stability of the nonlinear system. It is possible to combine the method with other nonlinear control methods to design the controllers. In the literature, control design with backstepping and control design with adaptive backstepping have been reported as described below.

In 1996 De Queiroz and Dawson developed a backstepping nonlinear controller for a full-order electromechanical system with a magnetic bearing [197]. Simulation proved that the controller guaranteed the stability of the magnetic bearing and achieved global

exponential position tracking. However, it also required the measurement of the rotor position, velocity, and stator current. In 1996 Long *et al*. described a backstepping adaptive controller to deal with magnetic bearing static load changes and unbalance [92]. Simulation studies showed that the performance of the system was satisfactory; no experimental results were presented.

In 2000 Pranayanuntana and Riewruja presented a backstepping nonlinear controller to guarantee the position tracking of a maglev system [198]. This research suggested using two inputs, the position and the second derivative of the position, to generate a piecewise continuous control law and guarantee the asymptotic stability of the system.

In 2007 Lin *et al*. proposed an intelligent adaptive backstepping controller using a recurrent neural network to control the position of a maglev apparatus [199]. Uncertainties were also taken into consideration when designing the controller. A dynamic model was first derived, and then an adaptive backstepping approach was proposed. Further, a recurrent neural network estimator was adopted to deal with the uncertainties. Experimental results showed improved transient performance and system robustness during tracking of periodic trajectories.

In 2010 Wai and Chuang reported a backstepping particle-swarm-optimization controller for a maglev transportation system [200]. The goal was to design an on-line particle-swarm-optimization control method to deal with the control transformation and the chattering effect in the system. Experiments proved the effectiveness of the proposed controller.

The advantages of using the backstepping method are: (1) since this method takes a recursive method to derive the controller, if the dimension of the system increases the same controller can be extended accordingly, and (2) the stability of the system is guaranteed using the Lyapunov function.

The disadvantages associated with this method are: (1) finding the Lyapunov function might be difficult, and (2) all the state variables need to be measured, or otherwise nonlinear observers are needed.

2.4.3.5. Sliding-model control (SMC)

SMC is a nonlinear control technique that solves the system uncertainty issues. It was derived from variable structure control (VSC), a form of discontinuous nonlinear control that changes the dynamics of a nonlinear system using a switching controller. The stability issue of SMC is addressed using the Lyapunov approach. The modeling uncertainties are dealt with by the application of the alternating control signals. Details about this technique as well as the theoretical and practical developments of SMC and VSC have been summarized by Emelyanov and Utkin in their publications from the 1970s to the 1990s [201-206].

Here a brief description of the method is given. The method divides the control into phases in time. In a reaching phase the *n*-th order system is first driven by a stabilizing control law (which could be derived using the Lyapunov function) to a stable manifold of order $n-1$. In the sliding phase the system "slides" along the manifold towards equilibrium. The overall control law switches between several controllers, depending upon

the process. Figure 2.8 shows a chattering in the system when it is driven to "slide" along the manifold (sliding surface) until equilibrium is reached [207].

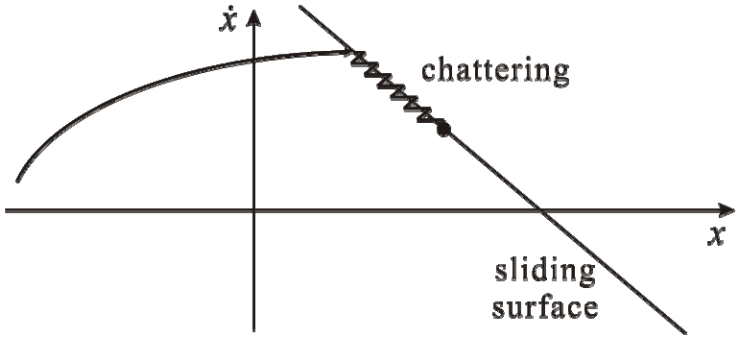

Figure 2.8: Chattering in sliding mode control [207]

In 1992 an SMC controller for a maglev system was reported by Cho *et al*. [208]. In this research, an experiment was conducted to compare a sliding mode controller with a classical controller. During the sliding mode control design, trade-offs were made among system robustness, uncertainties, disturbances, and performance. The sliding mode controller had a better system response in terms of stability and command following.

In 2001 El-Hajjaji and Ouladsine proposed a different SMC controller for a maglev system [209]. In their work, they used an experimentally validated model to design an SMC controller. The controller was synthesized based on the differential geometry of the model. Experiments showed that the proposed controller successfully achieved stable levitation.

In 2004 Al-Muthairi and Zribi designed an SMC for a maglev system [210]. Simulation results showed the effectiveness of their proposed controller; there were no experimental results. Another SMC controller design was reported by Tsai *et al*. in 2004 [211]. They designed an SMC controller for the axial motion of a rotor in a magnetic

bearing. Their research differed from others in that they reported an embedded prefilter in the control loop to provide integral action. The steady-state error of positioning was thus eliminated. Their SMC controller provided better stability compared to a conventional PI controller.

In 2007 Alvarez-Sanchez *et al*. reported a sliding mode control design for a maglev system with 3 DOFs [212]. A SMC controller was proposed to regulate the levitation position and stabilize the rotational movements. Experimental validation of the controller was also included. In 2008 Chen *et al*. reported an adaptive sliding mode controller [117]. The maglev system they studied included a permanent magnet and an electromagnet. The permanent magnet brought larger nonlinearity into the system. They reported that the designed controller gave a satisfactory system performance in both simulations and experiments.

The advantages of the SMC design methods include: (1) it deals with both time-varying and physical system nonlinearities, (2) classical control such as PID control or lead-lag control can be combined in designing the overall control law, and (3) the system uncertainties are dealt with by a "switching and sliding" process and therefore system robustness can be achieved.

The disadvantages associated with this method include: (1) the system must be single-input, (2) there is control law "switching" during operation, which changes the system dynamics, and (3) chattering is unavoidable.

2.4.3.6. Gain Scheduling (open-loop adaptive scheme)

The idea of gain scheduling control is to design a group of linear controllers, with each providing satisfactory system performance around one particular operating point. Together the group of controllers guarantees the system performance over a large range of operating conditions. To enable the transition among the controllers, one or more observers (scheduling variables) are designed to monitor the state of the system (disturbances, controller outputs, process outputs, state variables or reference signals) and activate the corresponding linear controller. Mathematically, the linear controllers are parameterized as a function of the gain scheduler.

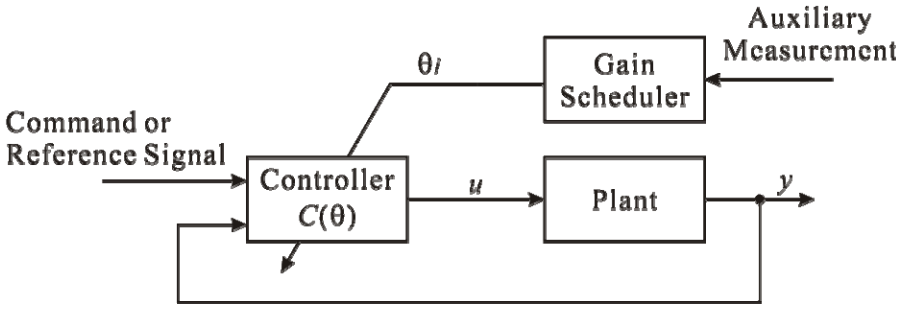

Figure 2.9: Gain scheduling block diagram [213]

Figure 2.9 shows a block diagram of a system with gain scheduling control. The auxiliary measurement is the measurement (or observer state) of the scheduling variables. A group of linear controllers $C(\theta)$ is controlled by the gain scheduler according to the auxiliary measurement.

Several gain scheduling control designs have been reported in the literature. In 1977 research on gain-scheduling control for a magnetic bearing was reported by Knospe and Yang [214]. In their research, the magnetic bearing was modeled as a nonlinear system.

The nonlinearity was then formulated as a quasi linear-parameter-varying system (quasi-LPV) by linearizing the quadratic terms in system equations and the control input saturation nonlinearities. The controller was then designed based on the quasi-LPV model. It was reported that this design was able to stabilize the magnetic bearing and reduce the bias current and hence the energy loss.

In 2001 Betschon and Knospe described a gain-scheduling approach with adaptive vibration control for a magnetic bearing [215]. In their design, the gain matrix was synthesized based on the operating speed of the magnetic bearing. It was shown that a significant current reduction was achieved over a wide range of operating speeds.

The advantage of using the gain scheduling control design method is that linear techniques can be used in the design process without introducing complicated nonlinear techniques.

The disadvantages of this method are: (1) the designed system is piece-wise linear, meaning transitions between operating points could lead to additional nonlinear system behavior, (2) it might be difficult to find a function between the controllers and the scheduling variables, and (3) the stability and robustness of the system change over the operating range.

2.4.3.7. Adaptive Control

Adaptive control is another control design method that can solve the system uncertainty issues. This method provides a controller design that is adjustable along with a mechanism to adjust the parameters [216]. It was developed based on the concept of

parameter estimation. The origin of the adaptive control can be traced back to the early 1950s for the design of autopilots for high-performance aircraft [216]. In the 1960s, the introduction of the state-space method and the stability theory contributed to the development of the adaptive control technique. Later, Bellman introduced the method of dynamic programming, which also helped in the understanding of the adaptive processes [217]. A major contribution was made by Tsypkin in the 1970s, who showed that a common framework could be used to describe adaptive control and many schemes for learning [218-220].

In the early 1980s, research work on the stability of adaptive systems led to the idea of merging robust control and system identification with adaptive control. The research in the late 1980s and early 1990s gave new insights into both control design methods and finally these two methods were developed to solve different control problems. In 1991, Unbehauen explained the concept of adaptive control in his "Review and Future of Adaptive Control Systems" as [221]:

"In adaptive control the controller settings are automatically adjusted in order to achieve better process operation over a wide range of conditions. The controller adaptation is necessary either for poorly understood processes or to compensate for unanticipated parameter changes of the process due to environmental conditions or unpredictable operating point changes. Thus adaptive control provides possibilities to control processes with uncertainties, as e.g. nonlinearities and time-varying parameters."

Table 2.2 Comparison of adaptive control and robust control

Control methods differences	Adaptive Control	Robust Control
Control design methods for time-varying systems or system with parameter uncertainties?	Yes	Yes
Need information about bounds of the uncertainties or time-varying parameters before the design process?	No	Yes
Will the control law change during the operation?	Yes	No

Table 2.2 highlights the differences between the adaptive control and robust control methods. Although both of these methods can be used to design controllers for systems with large uncertainties, their approaches and results are different.

An adaptive controller adjusts its parameters continuously (hence the name "adaptive") to accommodate relatively slow changes in the process dynamics and disturbances. There are two possible methods to realize this parameter adaptation: applying it through the feedback loop or the feedforward loop (which, strictly speaking, is not a feedback control design).

There are two classes of adaptive controllers: those based on direct methods and those based on indirect methods. For the direct methods, controller parameters are adjusted directly according to the data measured during closed-loop operations (e.g., closed-loop model reference adaptive control). For the indirect methods, the model parameters are first determined online by recursive parameter estimations and then the control parameters are derived from the model parameter estimations (e.g., self-tuning regulator). Therefore, the

indirect method can be viewed as a repetitive sequence of model identification and controller redesign and update.

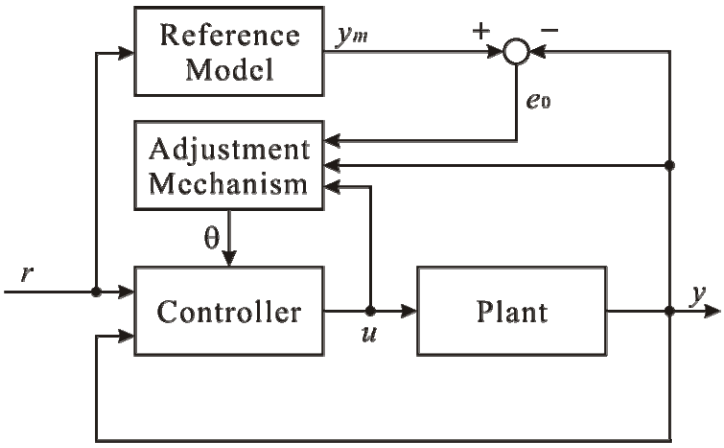

Figure 2.10: Adaptive control block diagram [216]

Figure 2.10 shows the block diagram of a system with an adaptive controller, where r is the reference signal, θ is the adjustment parameter, u the controller output, y_m is the reference model output, y is the plant output, and e_0 is the difference between the reference model output and plant output. The adaptive controller included in Figure 2.10 uses the indirect method to derive the control parameters. The reference model provides the model parameter estimations. The estimations are then fed into the adjustment mechanism, which determines the control parameters for the controller. The whole process is recursive and the controller is updated/re-designed continuously.

There are several adaptive control designs for maglev systems reported in the literature. Green, in his doctoral dissertation in 1997, discussed the application of an adaptive backstepping control (ABC) for a desktop maglev system [112]. He concluded that the maglev system with a controller derived from a nonlinear design approach of ABC

exhibited better system robustness than linear controllers and feedback linearization controllers.

In 2001 Yang and Tateishi proposed an adaptive roust nonlinear controller for a similar maglev system [187]. Their controller took a feedback linearization approach [222]. In 2008 Yang *et al*. proposed an adaptive robust controller for a maglev system [223]. The controller they proposed was designed to solve the tracking problems of the system. They concluded that the derived adaptive control law reduced the position tracking error and guaranteed the system performance during the parameter transient.

In 2012 Huang *et al*. proposed an adaptive controller design for a maglev system [224]. They tried to use this control design to accommodate the internal time-varying uncertainties and external disturbances in the maglev system. Their experiment included a comparison between conventional PID control and adaptive control, and the results showed that the adaptive controller allowed the system to deal with larger uncertainties and disturbances.

The advantages of using the adaptive control method are: (1) the controller may have a large operating range through the "adaptive" process, (2) since the controller is updated/re-designed continuously the system is capable of accommodating parameter variation and model uncertainties fairly well.

The disadvantages of the adaptive control method are: (1) it includes a complicated parameter estimation process, (2) there are multiple feedback loops in the system and the adaptation loop updates itself only if there is a change in the control loop, (3) the model parameter estimation may need a nonlinear state observer, which introduces nonlinearity

into the system, and (4) the stability of the system may change during the control parameter updating/re-designing process.

2.4.3.8. Neural network control (NNC)

A novel nonlinear control design method developed based on the adaptive control approach is neural network control proposed by Werbos in 1989 [225] and Narendra in 1990 [226]. A neural network is a system whose model is based on the structure of biological nervous systems. It provides a nonlinear mapping from an input space $\mathbb{R}^n$ into an output space $\mathbb{R}^m$ [227]. In neural network control (NNC) there is a nonlinear function of several input and output variables with a parameter identification procedure called "training". NNC is composed of many similar elements (called *neurons* or *nodes*) performing the nonlinear operations. The input of one element is connected to the output of other elements, and the strengths of the interconnections are denoted by parameters called *weights*. The weights are adjusted based on the control task and the feedback information. Typically, the neurons are organized in layers (inputs of neurons of one layer are outputs of neurons from another layer).

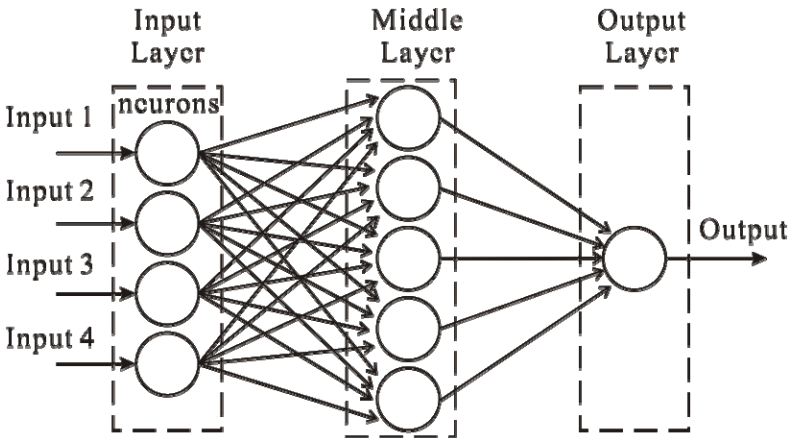

Figure 2.11: Neural network scheme [228]

Figure 2.11 shows a scheme of a three layer neural network with four inputs and one output. Generally, a two-layer NNC has sufficient generality for closed-loop control [227]. The choice of the operation implemented in the neuron, such as the threshold, number of layers, and number of neurons per layer are the main design parameters. Because of its flexibility and adaptability, the application of NNC in the control of nonlinear systems is increasing.

NNC for maglev systems usually incorporates other design approaches to improve the performance of the system. A paper discussing a maglev device for modeling and controls education, especially for testing NNC, was published by Shiakilas *et al*. in 2004 [229]. The system modeling and controller tuning were conducted on a hardware-in-loop maglev system. The author reported that it was an excellent demonstration of the NNC design.

In 2008 Aliasghary published a paper on the design of an SMC for the maglev system using Radial Basis Function Neural Networks [230]. The purpose of introducing SMC was to eliminate the need for the Jacobian matrix of the system, which is needed by

the adaptive neural network to adjust the NNC. This research provided simulation results without experimental validation.

In 2008 Aliasghary published another paper on NNC and a feedback error learning (FEL) approach for maglev system control design [231]. The FEL was introduced to work with the NNC to guarantee the stability of the system. Simulation studies showed that the NNC with FEL was more effective than PID control. Again, no experimental results were given.

In 2010 Yasser *et al*. proposed a control design method based on simple adaptive control (SAC) using neural networks to reduce the offset error for a SISO maglev system. In this research, the authors proposed an algorithm on using the output of both SAC and NNC as the control input. NNC compensates the output error during the linearization of the nonlinear system dynamics. SAC performs a model matching for the linear system with unknown structures to provide a linear reference model. The author reported that the positioning error was reduced by using this method. Both simulation and experimental results were given to validate the control design.

The advantages of using NNC are: (1) The control design process does not need a precise model; it could rely on the output data of the system. (2) Since the parameter variations and model uncertainties are dealt with by the adjustment of the controller, nonlinearities of the system can be accommodated.

The disadvantages of NNC are: (1) There are many parameter changes needed before the final controller can be derived. (2) The structure and size of the controller affect the final system performance. (3) Once the NNC is “trained”, it works within the vicinity of

the particular system states. If the states change, the NNC needs to be updated. (4) The stability of the system is not guaranteed.

2.5. Summary

In this chapter, the operation of magnetic bearings and maglev trains are explained, followed by an introduction of the maglev testbed that is used in this research. Several specific control design approaches, which are closely related to the control design methods studied in this research, are reviewed, followed by summaries of the advantages and disadvantages of each approach.

By reviewing the control design methods reported in the literature, the following conclusions can be drawn:

1. Linear control design methods have been tested extensively on maglev systems, and can guarantee their stability. Linear controllers have simple mathematical forms and are easy to implement. However, there is a lack of discussion of how to improve the system performance, especially in terms of disturbance attenuation.
2. Linear control design methods are based on linear system equations. However, the system equations for the maglev system involve nonlinear terms, and the typical approaches neglected the nonlinearities. Although this allows the use of a linear controller to achieve stability, system robustness cannot be guaranteed.
3. In the literature, many nonlinear control design approaches have been proposed and tested with maglev systems. However, there are performance issues or design difficulties with nonlinear controllers. Some of the nonlinear control methods, such as relay control, do not provide satisfactory system stability; some of them, such as

feedback linearization control, Lyapunov redesign, and backstepping control, need complicated stability functions; some of them, such as the gain scheduling method, SMC, and adaptive control, involve control parameter changes, which lead to changes in the system dynamics, and do not guarantee stability.

These conclusions lead to the proposal of a novel method, AFC-enhanced QFT/H_∞ control design method, to improve system performance of maglev systems. The AFC-enhanced QFT/H_∞ method, which is a blend of AFC, QFT and H_∞ design methods, will provide a controller that attenuates disturbance and guarantee system robustness. The AFC adds one feedback loop to manipulate the second order term in system transfer function, and thus achieves disturbance attenuation. The QFT/H_∞ controller guarantees stability and system robustness. Compared to the Lyapunov function based design approaches, the QFT/H_∞ method does not need a stability function — the controller is designed to the system is operating in the stability region in the existence of system parameter variation. The parameter uncertainty range is treated as a finite set. There is no controller gain rescheduling during the operation, which makes it easier to control internal stability. The variations in the system plant are accommodated by a single controller. In addition, the H_∞ norm optimization process helps to minimize the impact of perturbations.

Chapter 3 first presents the details of how to design a controller for maglev system stability with the linearized system model. Then an acceleration feedback controller is designed based on a stable maglev system. Disturbance attenuation with the acceleration feedback is proved to be feasible by comparing the input-to-output transfer functions.

Robust controller designs are discussed in Chapter 4, where QFT, H_∞, and QFT/H_∞ control design methods are investigated. Finally, the AFC-enhanced QFT/H_∞ controller is proposed. They are compared with classical control methods to illustrate how the system robustness is improved.

Chapter 3. Linear Controller Design

3.1. Chapter Outline

Chapter 3 first presents the design of a PD controller to stabilize the maglev system, and then an AFC controller is designed to achieve disturbance attenuation. Designs of PID, lead, MRC, and LQG controllers are also discussed in this chapter.

A typical controller design exercise includes six steps: (1) describing the system, (2) defining desirable system performance characteristics, (3) modeling the system, (4) designing the controllers, (5) choosing/building the control hardware, and (6) simulating and experimental validating. The maglev system has been described in Chapter 2. This chapter discusses about the control design goal (in terms of system performance), the system model, and the designs of controllers. Simulation results will be presented in this chapter. Control hardware and experiments are discussed in Chapter 5.

The workflow of the designing process is illustrated by the flowchart in Figure 3.1. This flowchart is originated from Fireland [232] and Yaniv [233] but has been modified (with system identification using experimental data skipped) to reflect the work in this research.

This chapter is organized as follows: Section 3.2 presents the maglev system block diagram. Section 3.3 discusses the designs of a PD controller and an AFC. Section 3.4 discusses a PID controller design. Section 3.5 discusses a lead controller design. Section 3.6 discusses a MRC design. Section 3.7 discusses a LQG controller design.

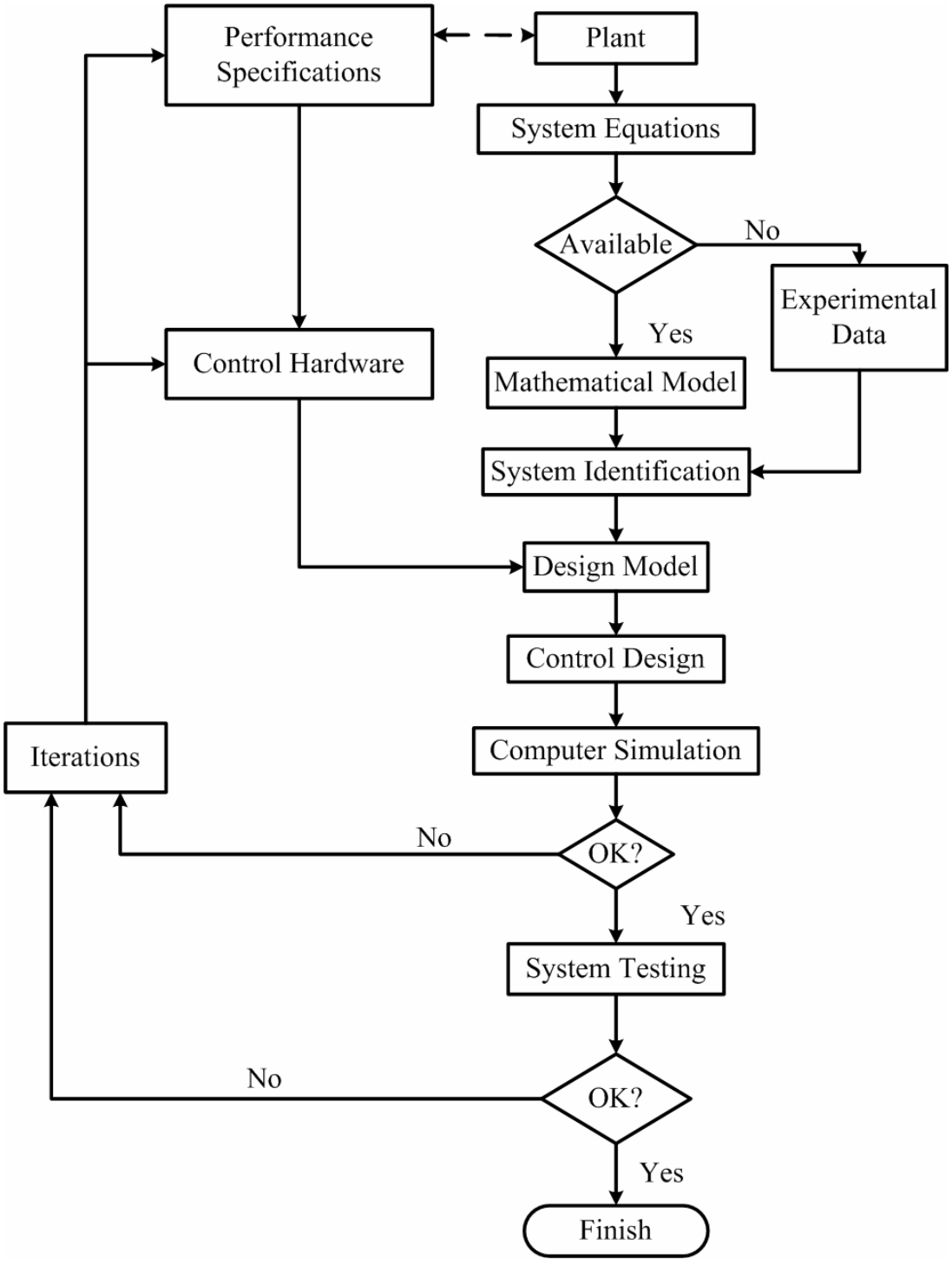

Figure 3.1 Feedback controller design flowchart

3.2. Maglev System Transfer Functions

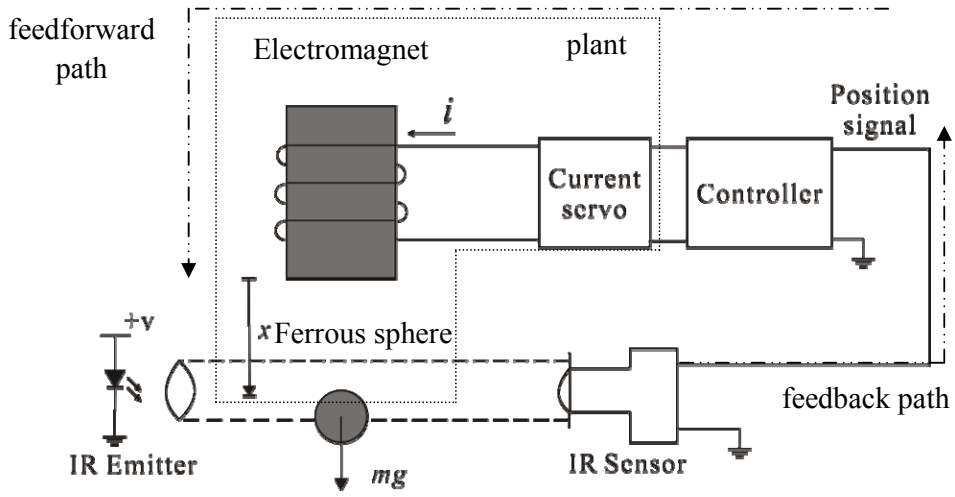

Figure 3.2 Maglev system configuration

Figure 3.2 shows the closed-loop control configuration of the maglev system. As shown in the figure, the plant includes an electromagnet, a ferrous sphere, a current servo, and some analog components. The sensor is an infrared emitter and detector pair.

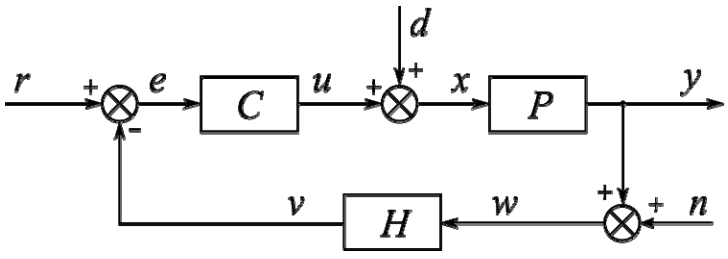

Figure 3.3 Block diagram of the maglev system

Assuming the maglev system is a linear system (which will be discussed in detail in Section 4), the block diagram of the system can be created, as shown in Figure 3.3. In the block diagram, the output of the plant, *P*, is the gap distance, *x*, between the levitated ball and the electromagnet. The input to the plant, *u*, is the current through the electromagnet; *u*

is also the output of the controller. The disturbance is denoted by *d*, and the reference position command by *r*. The controller *C* is responsible for (1) maintaining a desirable plant output y for a regulator problem and tracking the reference command r for a servomechanism problem (both will be explained later), (2) reducing the plant output *y* due to the disturbance *d,* and (3) attenuating the variation of *y* if the plant deviates from the nominal mathematical model P. In the sensor-measuring process, *H,* the plant output *y* is measured and fed back to the controller *C*. There may be another signal, the noise *n*, which is not correlated to any of the signals in the system, added to the plant output. Assuming *r*, *d*, and *n* are three unrelated inputs with *u*, *y*, and *v* being controller, plant, and sensor outputs, respectively, there are nine transfer functions from $\begin{bmatrix} r & d & n \end{bmatrix}^{\mathrm{T}}$ to $\begin{bmatrix} u & y & v \end{bmatrix}^{\mathrm{T}}$:

$$\begin{bmatrix} u \\ y \\ v \end{bmatrix} = \begin{bmatrix} \dfrac{C}{1+PHC} & -\dfrac{PHC}{1+PHC} & -\dfrac{CH}{1+CHP} \\ \dfrac{CP}{1+CPH} & -\dfrac{P}{1+PHC} & -\dfrac{HCP}{1+HCP} \\ \dfrac{CPH}{1+CPH} & -\dfrac{PH}{1+PHC} & -\dfrac{H}{1+HCP} \end{bmatrix} \begin{bmatrix} r \\ d \\ n \end{bmatrix} \tag{3.1}$$

This research studies the system behavior with certain inputs. The transfer function from the system input to system output, $\dfrac{y}{r} = \dfrac{CP}{1+CPH}$, is of primary interest.

Based on the desired output, control systems are divided into two types. One is a process control (or regulator) system. In a regulator system the controlled variables are driven to stay as close as possible to a constant desired value, despite disturbances. The second type is a servomechanism system. In a servomechanism system, the controlled variables are made to follow a time-varying input as closely as possible [234].

Based on their applications, maglev systems belong to either regulator or servomechanism systems. For example, a magnetic bearing is a regulator system since the

position of the levitated bearing shaft is desired to stay (regulated) at a fixed position. In comparison, a maglev positioning stage is a servomechanism system since it follows the position command during operation. Controllers for a regulator system tend to keep the controlled variable constant. They are designed to be insensitive to disturbances (which can be regarded as another input signal, as shown in Eq. (3.1).) Controllers for a servomechanism system make the controlled variable follow the input signal. They are designed to be sensitive to the smallest variations of the reference signal. Both regulator and servomechanism designs are addressed in this thesis. This chapter discusses how to design controllers to maintain stable maglev systems, which are typical regulator system design cases. Chapter 4 discusses how to design robust controllers, which belong to servomechanism cases.

3.3. Feedback Control Designs for System Stability

Previous discussion has stated a maglev system is open loop unstable. In this section, the mathematical model of the maglev system is first derived, followed by a discussion of why the open loop system is unstable. Then a PD controller is designed to achieve a stable maglev system. Based on the stable maglev system, an AFC is designed.

3.3.1. Mathematical model of the electromagnetic force

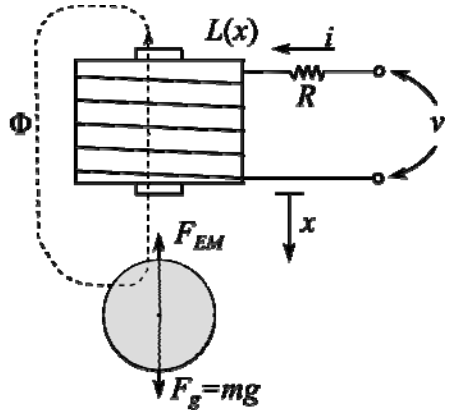

Figure 3.4 Electromagnet and the ferrous sphere

Figure 3.4 shows a figure of the ferrous sphere and the electromagnet in the maglev system, where Φ is the magnet flux, $L(x)$ is the inductance of the electromagnet, i is the current through the electromagnet, R is the resistance of the electromagnet, v is the voltage across the electromagnet, x is the gap distance between the ball and the electromagnet, and F_g is the force of gravity. The positive direction of x points downwards, i.e., when the ball moves away from the electromagnet. The electromagnetic force F_{EM} acting on the ball can be calculated given electromagnet inductance $L(x)$, current i, and gap distance x using the equation [235]:

$$F_{EM}(x) = \frac{1}{2} i(x)^2 \frac{dL(x)}{dx} \tag{3.2}$$

Woodson and Melcher suggested that for a configuration like the one shown in Figure 3.4, the electromagnet inductance is approximated by equation [108]:

$$L(x) = L_1 + \frac{L_0}{1 + x/a} \tag{3.3}$$

where a is a constant (with units of displacement) determined by the physical parameters of

the electromagnet. In Eq. (3.3), L_1 is the inductance of the electromagnet with no ferrous ball, and L_0 is the incremental of inductance the electromagnet due to the ferrous ball being positioned at the end of the electromagnet.

Since the permeability of the electromagnetic core is three orders of magnitude larger than that of air, L_0 is significantly larger than L_1, and Eq. (3.3) can be simplified as:

$$L(x) = \frac{L_0}{1 + x/a} \tag{3.4}$$

In Eq. (3.4) the gap distance x is divided by constant a and the quotient $\frac{x}{a}$ can be viewed as a normalized gap distance. It allows the performance of the controller to be compared in terms of the gap distance using a dimensionless value.

In Appendix B, a finite element analysis (FEA) is presented, showing that the electromagnetic force equation in Eq. (3.2) is a reasonable engineering approximation when $x \leq 6$ mm. Therefore, the control designs in this research are based on the electromagnetic force calculated using Eq. (3.2).

3.3.2. Modeling the system using Newtonian dynamics

In the following discussion, the mathematical model for the maglev system is derived. The maglev plant in Figure 3.4 includes two parts: the electromagnetic circuit and the mechanical component, i.e., the levitated ball. The modeling process starts with the electronics. Using Kirchhoff's voltage law and Ohm's law, the voltage across the electromagnet is:

$$v = Ri + \dot{p}_e \tag{3.5}$$

where $p_e = L(x)i$ is the magnetic flux.

For the mechanical part of the plant, the governing equation is derived using Newton's second law of motion. Choosing the bottom of the electromagnet as the origin of the reference frame, and assuming the positive direction is down, the force balance on the ferrous ball is:

$$m\ddot{x} = mg - F_{EM} \tag{3.6}$$

where F_{EM} is the electromagnetic force generated by the electromagnet. The system equations become:

$$\left.\begin{aligned} v &= Ri + \dot{p}_e \\ m\ddot{x} &= mg - \frac{1}{2}\dot{L}(x)i^2 \end{aligned}\right\} \tag{3.7}$$

The first derivative of $L(x)$ with respect to x is

$$\dot{L}(x) = -\frac{aL_0}{(a+x)^2} \tag{3.8}$$

The negative sign in Eq. (3.8) indicates that the first derivative of $L(x)$ decreases as x increases. Since the positive direction is chosen to be pointing downwards, Eqs. (3.7) use the absolute value of $\dot{L}(x)$.

The system equations can be simplified by assuming that the electromagnet inductance remains constant despite the change of gap distance x. This results in the simplified form of the system equations,

$$\left.\begin{aligned} Ri + L\dot{i} &= v \\ m\ddot{x} &= mg - \frac{1}{2}K_1\left(\frac{i}{K_2 + x}\right)^2 \end{aligned}\right\} \tag{3.9}$$

where K_1 and K_2 are determined by the physical parameters of the electromagnet. Previously, it was pointed out that the gap distance x can be normalized to a constant a to evaluate the system response with different control designs. However, the system equations

in (3.9) with two constant K_1 and K_2 make it easier to identify the modeling uncertainty. Hence, this system model is preferable when it comes to robust control design.

Eqs. (3.9) give the *voltage control form* of the maglev system equations, in which the input is the voltage v supplied to the electromagnet and the output is the gap distance x. From Eqs. (3.9), it is found that the voltage v appears only in the first equation. The electronic part of the maglev system is an *RL* circuit, which can be viewed as a low-pass filter. It transfers the voltage signal *v* into current *i*. Comparing the two equations in Eq. (3.9), it is found the current *i* is the only independent variable if *x* is assumed to be a dependent variable. Hence, it is possible to consider making *i* the control signal and modeling the system in a simpler fashion.

Since the response time of the electronic part is more than 100 times smaller than that of the mechanical part, the first equation can be neglected by assuming that the electromagnet current i can be controlled directly. Hence, it results in the *current control form* of the maglev plant:

$$m\ddot{x} = mg - \frac{1}{2}K_1\left(\frac{i}{K_2 + x}\right)^2 \tag{3.10}$$

where the input is the electromagnet current i and the output is the gap distance x.

All the parameters in Eq.(3.10) can be measured experimentally. Table 3.1 shows a group of experimentally measured values for the parameters. The experiment to measure the system parameters is described in Appendix C.

Table 3.1 Measured maglev system parameters

System Parameter	Experimental Measurement
m	$(16.1 \pm 0.05) \times 10^{-3}$ kg
x_0	$(4.5 \pm 0.2) \times 10^{-3}$ m
$\dot{x}_0$	0 m/s
R	$31.08 \pm 0.005\ \Omega$
L	0.16 ± 0.005 H
i_0	0.345 ± 0.0005 A
K_1	$3.9 \times 10^{-5}\ \frac{\mathrm{N} \times \mathrm{m}^2}{\mathrm{A}^2}$
K_2	0.8×10^{-3} m

3.3.3. Transfer function and state-space representation model

Eq. (3.10) represents the maglev system model in nonlinear differential equation form. To start the linear controller design process, a linear model is developed first. To linearize the model, it is necessary to define an operating point [236]. In this research, the operating point is chosen to be a position where the gap distance between the ball and the electromagnet equals x_0 (where the following conditions are satisfied: $i=i_{eq}$, $x_{gap}=x_0$, and $\dot{x}_{gap} = 0$). The Taylor series of equation (3.10) is given as follows (neglecting higher order terms):

$$m\ddot{x}_{gap} = mg - \frac{1}{2}K_1\left(\frac{i_{eq}}{K_2 + x_0}\right)^2 + K_1\left(\frac{2i_{eq}^2}{(K_2 + x_0)^3}\right)\delta x_{gap} - K_1\left(\frac{2i_{eq}}{(K_2 + x_0)^2}\right)\delta i_{eq} \quad (3.11)$$

At the operating point, when the system reaches its equilibrium state, the following condition is satisfied:

$$mg = \frac{1}{2}K_1\left(\frac{i_{eq}}{K_2 + x_0}\right)^2 \quad (3.12)$$

Therefore, equation (3.10) becomes:

$$m\ddot{x}_{gap} = K_1\left(\frac{2i_{eq}^2}{(K_2 + x_0)^3}\right)\delta x_{gap} - K_1\left(\frac{2i_{eq}}{(K_2 + x_0)^2}\right)\delta i_{eq} \quad (3.13)$$

Dividing both sides of equation (3.13) by m and letting $k_x = \frac{K_1}{m}\left(\frac{2i_{eq}^2}{(K_2 + x_0)^3}\right)$ and $k_i = \frac{K_1}{m}\left(\frac{2i_{eq}}{(K_2 + x_0)^2}\right)$, the equation of motion for the maglev system at a gap distance x_0 is written as:

$$\ddot{x} = -k_i i + k_x x \quad (3.14)$$

In Eq. (3.14) there is only one input, the control current *i*. Eq. (3.14) is referred to as the governing equation for the maglev system with current control.

Using Eq. (3.14), the transfer function of the maglev plant can be derived. Taking the Laplace transform on both sides of Eq. (3.14),

$$s^2 X(s) = -k_i I(s) + k_x X(s) \quad (3.15)$$

where $X(s)$ and $I(s)$ are the gap distance and current in the frequency domain, respectively. Rearranging Eq. (3.15), the transfer function of the maglev plant becomes

$$\frac{X(s)}{I(\mathrm{s})} = \frac{-k_i}{s^2 - k_x} \quad (3.16)$$

Eq. (3.16) is the transfer function of the maglev plant with current control.

To obtain the state-space representation of the maglev plant, the state variables need to be defined. In Eq. (3.14) there is one variable x and one input i. The left side of the equation is the second order derivative of x. With the state variables chosen to be $x = [x,\ \dot{x}]^{\mathrm{T}}$ and the output being x, the state-space representation of the plant is written as:

$$\left.\begin{aligned} \begin{bmatrix} \dot{x} \\ \ddot{x} \end{bmatrix} &= \begin{bmatrix} 0 & 1 \\ k_x & 0 \end{bmatrix} \begin{bmatrix} x \\ \dot{x} \end{bmatrix} + \begin{bmatrix} 0 \\ -k_i \end{bmatrix} i \\ [x] &= [1 \quad 0] \begin{bmatrix} x \\ \dot{x} \end{bmatrix} + [0] i \end{aligned}\right\} \tag{3.17}$$

Eq. (3.17) shows a linearized state space model of the maglev plant with the current as the control input.

The voltage control form of the maglev plant includes the governing equation of the *RL* circuit. Combining the governing equation of the circuit in Eq. (3.18)

$$Ri + L\dot{i} = v \tag{3.18}$$

and Eq. (3.14), the linearized system equations are written as:

$$\begin{cases} \ddot{x} = -k_i i + k_x x \\ \dot{i} = -\dfrac{R}{L} i + \dfrac{1}{L} v \end{cases} \tag{3.19}$$

In a similar fashion, the transfer function of the plant is obtained by taking the Laplace transfer function on both sides of Eqs. (3.19),

$$\left.\begin{aligned} s^2 X(s) &= -k_i I(s) + k_x X(s) \\ sI(s) &= -\frac{R}{L} I(s) + \frac{1}{L} V(s) \end{aligned}\right\} \tag{3.20}$$

Collecting common terms, the above equations become:

$$\left.\begin{aligned} \frac{X(s)}{I(s)} &= \frac{-k_i}{s^2 - k_x} \\ \frac{I(s)}{V(s)} &= \frac{\frac{1}{L}}{s + \frac{R}{L}} \end{aligned}\right\} \tag{3.21}$$

Multiplying the two equations in Eqs. (3.21), the transfer function of the plant becomes

$$\frac{X(s)}{V(s)} = \frac{-\frac{k_i}{L}}{\left(s + \frac{R}{L}\right)\left(s^2 - k_x\right)} \tag{3.22}$$

Since the voltage control form includes the *RL* circuit governing equation, there is one additional state variable in the state-space representation of the maglev plant (now the input is the voltage *v* and current *i* is a secondary variable). Therefore, there are three state variables in the system equation. Choosing the state variables to be $x = \left[x,\ \dot{x},\ i\right]^{\mathrm{T}}$, the state-space representation of the plant can be written as

$$\left.\begin{aligned} \begin{bmatrix} \dot{x} \\ \ddot{x} \\ \dot{i} \end{bmatrix} &= \begin{bmatrix} 0 & 1 & 0 \\ k_x & 0 & -k_i \\ 0 & 0 & -\frac{R}{L} \end{bmatrix} \begin{bmatrix} x \\ \dot{x} \\ i \end{bmatrix} + \begin{bmatrix} 0 \\ 0 \\ \frac{1}{L} \end{bmatrix} \begin{bmatrix} v \end{bmatrix} \\ \begin{bmatrix} x \end{bmatrix} &= \begin{bmatrix} 1 & 0 & 0 \end{bmatrix} \begin{bmatrix} x \\ \dot{x} \\ i \end{bmatrix} + \begin{bmatrix} 0 \end{bmatrix} \begin{bmatrix} v \end{bmatrix} \end{aligned}\right\} \tag{3.23}$$

There are four observations when comparing Eq. (3.16) to (3.22): (1) Eq. (3.16) shows a transfer function of a second-order system, but there is no first order term in the characteristic equation. It indicates that there is no generalized *damping* in the system. This agrees with what has been discovered in the previous section that "*there is a lack of effective coupling between the electrical and mechanical subsystems.*" (2) The

characteristic equation of Eq. (3.22) has three poles. One single pole results from the *RL* circuit and a pair of conjugate poles results from the electromagnetic force and ferrous ball mass. Since the electronic system responds much faster (hence "the faster pole") than the mechanical system, the *RL* circuit pole is located further away from the origin (which will be discussed later.) (3) The electromagnetic force generates a conjugate pair in the solution of the characteristic equation. Since there is no generalized damping term in this second order system, the generalized stiffness and the generalized mass terms produce a pair of conjugate poles. One of the two is in the RHP, which means the system response increases without bound when subject to even a small input. Therefore, the system is open-loop unstable (how to evaluate the stability and why stability is important will be discussed later.) This explains why a maglev system cannot be controlled using an open-loop control configuration. (4) The unstable pole is caused by the mechanical subsystem of the system, specifically, the lack of damping in the subsystem. The mechanical subsystem is included in both voltage control and current control models.

3.3.4. Property of the maglev system

3.3.4.1. Stability of the Maglev System

This section explains why the maglev system is open-loop unstable by examining both current control and voltage control models. Taking the transfer function of the current control model from Eq. (3.16), and substituting values from Table 3.1 into the equation, the maglev system plant (in units of $\frac{\mathrm{m}}{\mathrm{A}}$) is given by:

$$\frac{X(s)}{I(s)} = \frac{-56.82}{s^2 - 66.03^2} \tag{3.24}$$

The state matrix A in the state-space representation Eq. (3.17) is:

$$A = \begin{bmatrix} 0 & 1 \\ k_i & 0 \end{bmatrix} = \begin{bmatrix} 0 & 1 \\ 66.03^2 & 0 \end{bmatrix} \tag{3.25}$$

The roots of the characteristic polynomial in Eq. (3.24) are $r_{1,2} = \pm 66.03$. These are the eigenvalues of matrix A: $\lambda_{1,2} = \pm 66.03$. The values of the roots equal the values of the eigenvalues. There is a real pole in the RHP (at 66.03), which means the maglev plant has one unstable mode.

In a similar fashion, the roots and eigenvalues of the voltage control model can be calculated. The transfer function (in units of $\frac{\text{m}}{\text{V}}$) is calculated as follows:

$$\frac{X(s)}{V(s)} = \frac{-355.13}{(s+187.5)(s^2 - 66.03^2)} \tag{3.26}$$

The A matrix is:

$$A = \begin{bmatrix} 0 & 1 & 0 \\ k_x & 0 & -k_i \\ 0 & 0 & -R/L \end{bmatrix} = \begin{bmatrix} 0 & 1 & 0 \\ 66.03^2 & 0 & -56.82 \\ 0 & 0 & -187.5 \end{bmatrix} \tag{3.27}$$

The roots of the characteristic polynomial in Eq. (3.26) are $r_1 = -187.5$, and $r_{2,3} = \pm 66.03$. These match the eigenvalues of the A matrix in Eq. (3.27): $\lambda_1 = -187.5$, and $\lambda_{2,3} = \pm 66.03$. Both system models give the same system dynamics.

Comparing the roots and eigenvalues found from the two system models, it is found that: (1) the unstable mode of the maglev plant is captured by both models, and thus the controller design for stability can use either of these two models; and (2) there is one pole whose absolute value is three times larger than the other two poles in the voltage control model. This pole is a result of introducing the *RL* circuit into the system model. Because the dynamics of this pole decays much faster that the other two, it can be neglected, which

results in the current control model.

3.3.4.2. Internal Stability

The previous section discussed the system stability based on the input and output signals. However, a control design should not only guarantee the stability of the input-to-output transfer function, but also the other signals inside the system. In the general feedback system structure shown in Figure 3.3, there are three signals *e*, *x*, and *w* that were input into the controller *C*, plant *P*, and sensor *H*, respectively. It is also desired that these signals are bounded during system operation. This section discusses how to determine if a controller design can achieve this goal, which is known as *internal stability* [237].

Before discussing how to evaluate a control design through internal stability, the definition of well-posedness [237] is introduced.

Definition 1. The feedback system shown in Figure 3.3 is said to be well-posed if all nine closed-loop transfer functions from the input signals to the output signals exist.

Well-posedness can be determined by the following theorem.

Theorem 1. The system is well-posed iff the 3×3 matrix

$$\begin{bmatrix} 1 & 0 & H(s) \\ -G_c(s) & 1 & 0 \\ 0 & -G(s) & 1 \end{bmatrix} \tag{3.28}$$

is nonsingular, i.e., the determinant of the matrix $1+G_c(s)G(s)H(s)$ does not equal zero.

Definition 2. The system shown in Figure 3.3 is said to be internally stable if all nine closed-loop transfer functions from the inputs to the internal signals are stable.

The nine transfer functions can be written as:

$$\begin{bmatrix} x_1 \\ x_2 \\ x_3 \end{bmatrix} = \frac{1}{1+G_c(s)G(s)H(s)} \begin{bmatrix} 1 & -G(s)H(s) & -H(s) \\ G_c(s) & 1 & -G_c(s)H(s) \\ G_c(s)G(s) & G(s) & 1 \end{bmatrix} \begin{bmatrix} r \\ d \\ n \end{bmatrix} \quad (3.29)$$

Theorem 2. The system is internally stable iff the following two conditions are satisfied:

1. The transfer function $1+G_c(s)G(s)H(s)$ has no zeros on $\mathrm{Re}(s)>0$;

2. There is no zero-pole cancellation in $G_c(s)G(s)H(s)$ on $\mathrm{Re}(s)>0$.

In the following sections, a PD controller will be designed for the maglev system. The internal stability of the systems will be checked to evaluate the designs.

3.3.5. PD controller design

This design uses the transfer function (in units of $\frac{\mathrm{m}}{\mathrm{A}}$) in Eq. (3.24):

$$\frac{X(s)}{I(s)} = \frac{-56.82}{s^2 - 66.03^2}.$$

As has been discussed, there is one pole in the RHP, which indicates this plant is unstable. Although the simplest solution is to use pole-zero cancellation to stabilize the system, this is impractical. In 1970, Ramaswami and Ramar proved that if the plant has a pole in the RHP, pole-zero cancellation will not guarantee the system stability [238]. Practically, it is impossible to achieve perfect pole-zero cancellation. Every plant bears some level of uncertainties. The cancellation is only achieved with the nominal model. If there is a mismatch between the plant and the model, the cancellation fails and the system becomes unstable.

As the first step to initiate a control design process, the design goals are identified. Typical design goals involve achieving certain time-domain response and frequency domain characteristics. This design starts with a group of design goals in both time-domain

and frequency domain, including the peak overshoot, settling time, steady-state error, gain margin, and phase margin.

For a time-domain response, the peak overshoot should be controlled within a relatively small range because the linearized magnetic force model is valid around a chosen point. Also, it is desired to drive the levitated ball back to equilibrium within a reasonable amount of time. In addition, the maximum steady-state error is chosen to be 5% since below 5% of the maximum plant operation range the sensor noise becomes dominant with this particular testbed. Hence the design goals are chosen as follows: peak overshoot $M_P \le 15\%$, 5% settling time $t_s \le 3\,\text{s}$, and steady-state error $e \le 5\%$. For a frequency domain response, it is desired to have certain amount of system robustness despite the system parameter change. This research chooses a gain margin $\text{GM} \ge 4.5$ dB and a phase margin $\text{PM} \ge 50$ degree as the design goals.

With the selected time-domain design goal, the equivalent frequency-domain design goals can be calculated.

$$\zeta = \frac{\left|\ln M_p\right|}{\sqrt{\pi^2 + \left(\ln M_p\right)^2}} = \frac{\left|\ln(0.05)\right|}{\sqrt{\pi^2 + \left[\ln(0.05)\right]^2}} = 0.69$$

The damping ratio $\zeta = 0.69$, and natural frequency is chosen to be $\omega_n = 100$ rad/s to avoid the 66.03 rad/s pole of the plant. Therefore, the 5% settling time with the chosen parameters is approximately

$$t_s = \frac{3}{\zeta\omega_n} = \frac{3}{0.69 \times 100} = 0.043\,\text{s}$$

which satisfies the design goal.

The desired dominant poles of the system are calculated to be:

$$\lambda_{1,2} = -\zeta\omega_n \pm j\omega_n\sqrt{1-\zeta^2} = -69 \pm 69j \tag{3.30}$$

The dominant poles can be plotted in the complex plane to show their relative positions to the plant poles. The graph will also assist to establish the trigonometric equations to solve the controller zero(s) and pole(s).

1. PD gains calculation

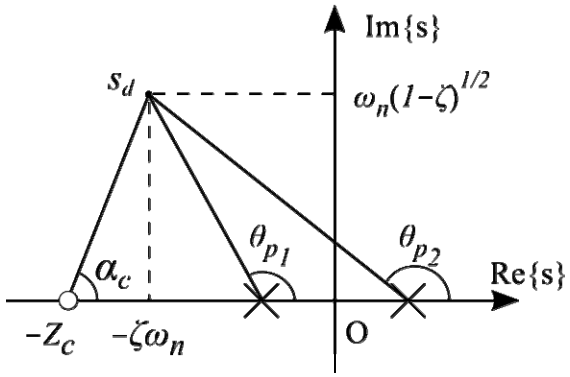

Figure 3.5 Zero location of a PD controller

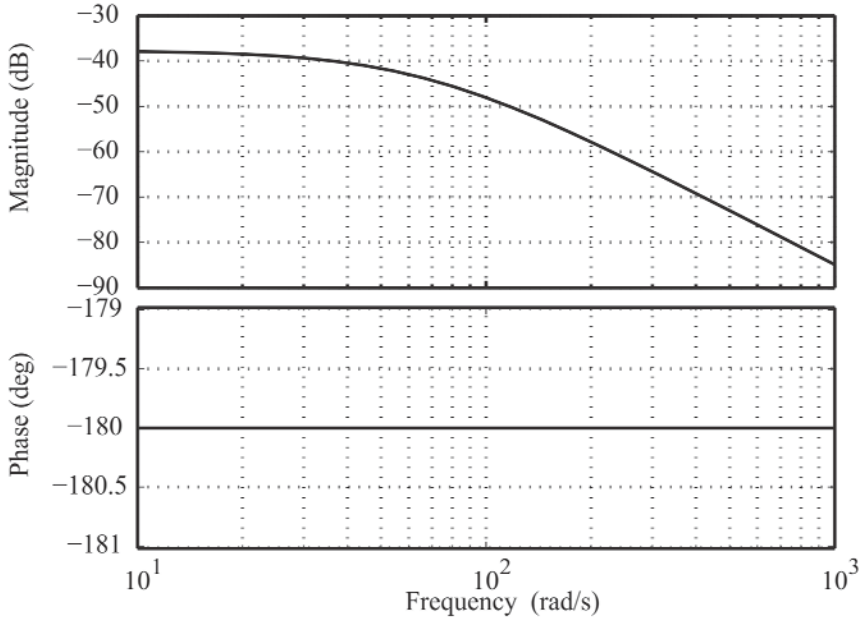

Figure 3.6 Maglev plant open loop Bode plot

Figure 3.5 shows one of the desired poles s_d in the complex plane. Figure 3.6 shows an open loop Bode plot of the maglev plant. In the Bode plot, the phase angle is -180 degree over the whole frequency domain, indicating an unstable plant. The controller needs to provide enough phase lead to achieve the desired phase margin of 50 degree. The phase angle can be estimated before the controller is designed. Suppose the phase angle of the plant model is $\phi_1(\omega_c)$ at the expected crossover frequency $\omega = \omega_c$, the phase angle of the controller at ω_c should be $\phi_c(\omega_c) = \gamma - 180^\circ - \phi_1(\omega_c)$, where γ is the expected phase margin of the closed-loop system. For this design, $\phi_c(\omega_c) = 50^\circ$. The magnitude of the plant model at ω_c, which is denoted by $A(\omega_c)$, can be calculated as:

$$A(\omega_c) = \left| G_c(\omega_c)\,\mathrm{G}(\omega_c) \right| \tag{3.31}$$

which will be calculated after the controller is designed.

Assuming the controller is a PD type controller, there is one zero z_c on the negative real axis. The trigonometric relationship between the desired poles and the controller zero is plotted in Figure 3.5. The required phase contribution of a PD regulator can be found with the phase contributions of the two plant poles,

$$\theta_{p_1} = \pi - \tan^{-1}\left(\frac{69}{69 - 66.03}\right) = 1.61 \text{ rad/s} \tag{3.32}$$

$$\theta_{p_2} = \pi - \tan^{-1}\left(\frac{69}{69 + 66.03}\right) = 2.67 \text{ rad/s} \tag{3.33}$$

and the triangle relationship

$$\angle\left(s_d + z_c\right) = \pi + 1.61 + 2.67 = 7.42 \text{ rad/s} \tag{3.34}$$

Then the magnitude of a PD controller zero z_c can be found from the trigonometry equation:

$$\frac{69}{\left(|z_c|-69\right)} = \tan 7.42 \tag{3.35}$$

and $|z_c|$ is solved,

$$|z_c| = 69 + \frac{69}{\tan 7.42} = 101 \tag{3.36}$$

The abovementioned process only solved for the controller zero. The controller gain is not identified in the complex plane. Therefore at this point, the PD controller is known to take the following form:

$$G_c(s) = K\left(s+101\right) \tag{3.37}$$

where K is the gain value that needs to be solved using the pre-defined steady-state error.

The desired steady-state error is less than 5%. Using the equation

$$e_{ss} = \lim_{s\to 0} \frac{1}{1+G_c G} \tag{3.38}$$

the controller gain is found to be $K \geq 5.2$ .Therefore, one possible PD type controller is

$$G_c(s) = 6s + 606. \tag{3.39}$$

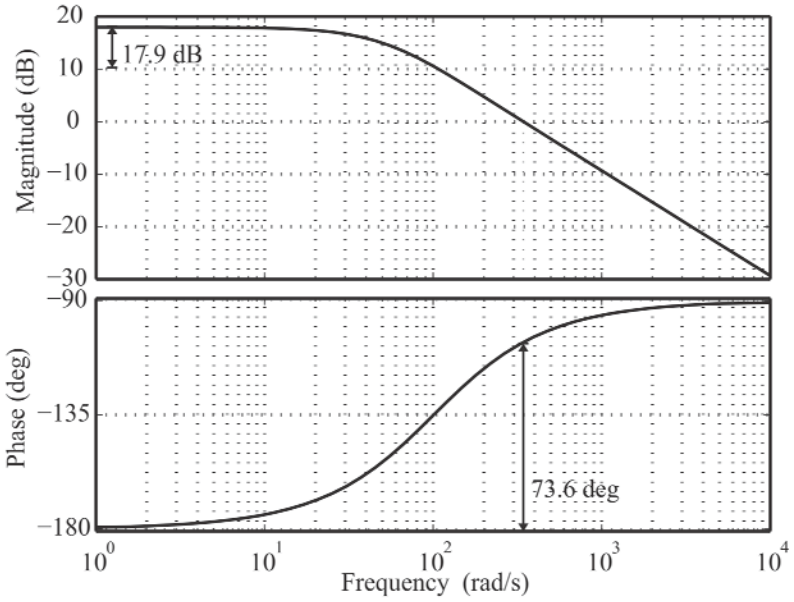

Figure 3.7 Bode plot of the maglev plant with a PD controller

Figure 3.7 shows a Bode plot of the maglev plant with the PD controller. The gain margin of the system is 17.9 dB at the phase crossover frequency of 1 rad/s. The phase margin is 73.6 degree at the gain crossover frequency of 343 rad/s. Comparing Figure 3.7 with Figure 3.6, it is found this controller increases the loop gain and provides a 73.6 degree of phase lead, which makes the system stable.

2. Internal stability check

The internal stability is checked by calculating the poles of the following transfer function,

$$1+G_c(s)G(s)H(\mathrm{s})=1+(6s+606)\times\frac{56.82}{s^2-66.03^2}=\frac{s^2+6s-3\mathrm{E}4}{s^2-66.03^2} \qquad (3.40)$$

There is no zero on $\mathrm{Re}(s)>0$ and no zero-pole cancellation in $G_c(s)G(s)H(s)$ on $\mathrm{Re}(s)>0$. Therefore, this system is internally stable.

3.3.6. AFC design

This section proposes an AFC design approach that attenuates disturbances in the maglev system. The maglev system has been stabilized with a PD controller. This design takes the stable system, and adds the AFC to achieve the design goals.

Methods to attenuate disturbances and improve the performance of maglev systems have been reported, but they are different from the approach discussed in this section. In 2002 Shan and Menq reported two disturbance-rejection algorithms — internal model-based control and sliding mode control — that improved the dynamic stiffness of a magnetic suspension stage [239]. In both simulation and experiments the dynamic stiffness of the system was increased. Fang, Feemster, and Dawson (2003) reported a position regulation control strategy developed for a maglev system operating in the presence of a bounded, nonlinear, periodic disturbance [240]. They included simulation results, but no experimental data was reported. Another position regulation control strategy, reported by the same authors in 2006, required that the disturbance be bounded and the period of the disturbance be known. She, Xin, and Tomio described a technique called equivalent-input-disturbance estimation [241]. The controller, designed using H_∞ control theory, generated an input signal based on the information from a state observer. The input signal cancelled the effect of the disturbance. They provided simulation results without experimental verification.

Previous research efforts show that different control strategies can be used to increase the overall performance of a maglev system. This research investigates an approach that attenuates disturbances while not changing the system response to a

reference signal. Acceleration feedback has been studied by previous researchers and proved to be effective in improving system performance in disturbance rejection [242]. However, prior work has not discussed the implementation of acceleration feedback on maglev systems. This research shows that acceleration feedback can be used on a maglev system to attenuate disturbance. Both analytical and experimental evaluations of the acceleration feedback technique are presented.

The acceleration control type servo system was proposed as a novel design paradigm of servo systems by Hori [243, 244], and was further developed as a hybrid control method for the position and mechanical impedance of robot actuators [245]. Experiments demonstrated the effectiveness of both systems in disturbance suppression.

In 1992 Schmidt and Lorenz demonstrated the principle, design, and implementation of acceleration feedback control to improve the performance of DC servo drives. In their research, the acceleration signal was estimated using an acceleration observer, scaled, and fed back to the controller. The feedback loop adds “electronic” inertia to the system [242]. It allows systems to achieve substantially higher overall stiffness without requiring higher bandwidths of the velocity and position loops.

For a maglev system, it is important to note that acceleration feedback control alone does not guarantee stability. For that, the system needs a position regulator. The acceleration feedback provides the equivalent effect of an “electronic” inertia for the system. It increases the effective inertia of the levitated object for disturbance rejection purposes.

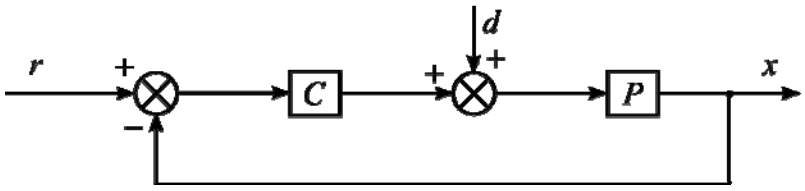

Figure 3.8 Block diagram of a system subject to disturbance *d*

Figure 3.8 shows a block diagram of a feedback control system subject to a disturbance d. This design uses the previously discussed maglev system with a PD controller, so C represents the transfer function of a PD controller.

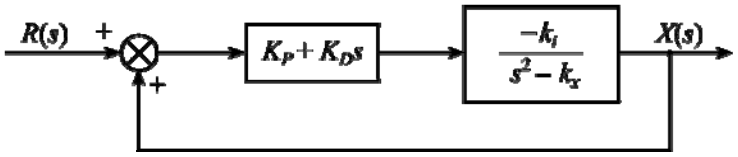

Figure 3.9 Maglev system with a PD controller

Figure 3.9 shows a block diagram of the maglev system with a PD controller. The PD controller serves the purpose of a position regulator. If the levitated ball moves away from the designed operating point, the controller adjusts the current passing through the electromagnet which provides a restoring force to reduce the position error. It is similar to adding a mechanical spring (which generates the "static stiffness") to the system.

For the open-loop maglev system, there is no restoring force to correct the position error. Therefore, the static stiffness is zero. For a maglev system with a PD controller, the stiffness is provided solely by the controller. This type of stiffness is sometimes referred to as "active stiffness." (Active stiffness is added by the stiffness terms resulting from the controller gains.)

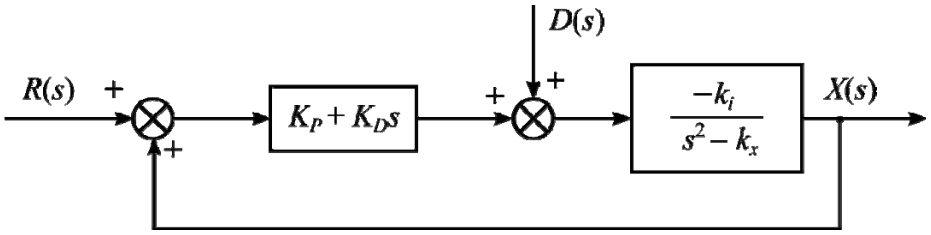

Figure 3.10 Maglev system subject to a disturbance D

Figure 3.10 shows the block diagram of such a system with a disturbance D. The transfer function between the disturbance D and the output position X for this system is

$$\frac{X(s)}{D(s)} = \frac{-k_i}{s^2 + k_i K_d s + k_i K_p - k_x} \tag{3.41}$$

Eq. (3.41) shows that the frequency response is shaped by the active controller gain K_d and K_p. The position regulator is used to achieve a stable levitation as well as reduce the response of the system to disturbances. In order to increase the stiffness of the system, a larger controller gain is needed.

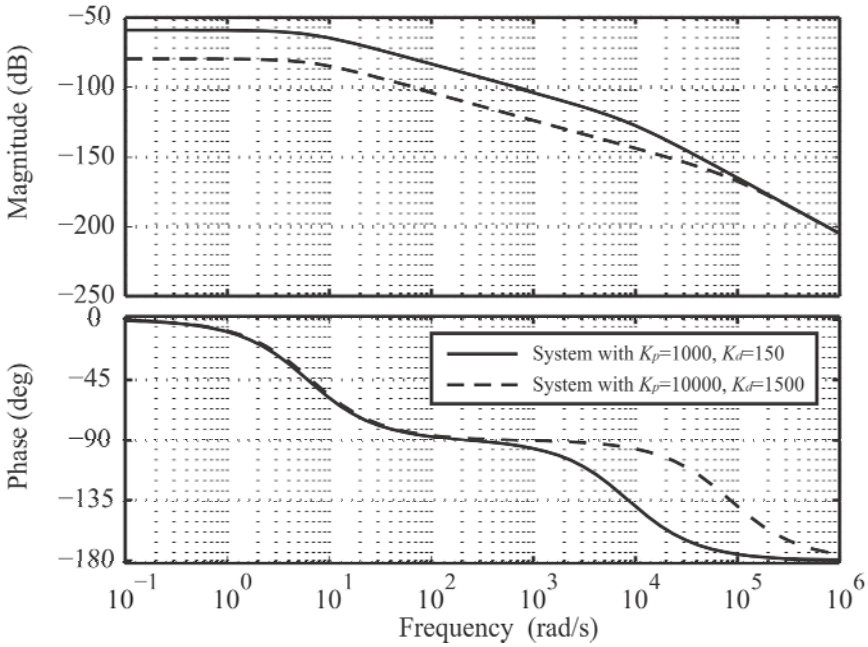

Figure 3.11 Bode plots of a maglev system with different controller gains

Figure 3.11 shows the Bode plots of the same maglev systems with different P and D controller gains. The Bode plots show that higher controller gains help to attenuate the system response to the disturbance. However, for a maglev system, increasing the controller gains may result in larger oscillations in the system response and make the system unstable.

The conclusion is that in order to increase the stiffness, the controller gains need to be increased, but only certain gain values will maintain the stability of the system. To raise the dynamic stiffness curve without changing the controller gains requires the use of acceleration feedback. In the following discussion, this research shows how to configure AFC into the maglev system.

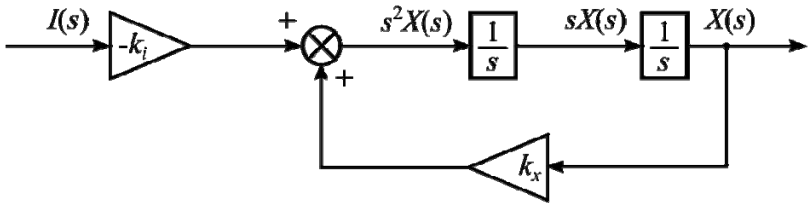

Figure 3.12 Block diagram of the open-loop maglev plant

Figure 3.12 shows a block diagram of the open-loop maglev system. The system transfer function, as discussed before, is $\frac{X(s)}{I(s)} = \frac{-k_i}{s^2 - k_x}$ where the input is the control current and the output is the ball position.

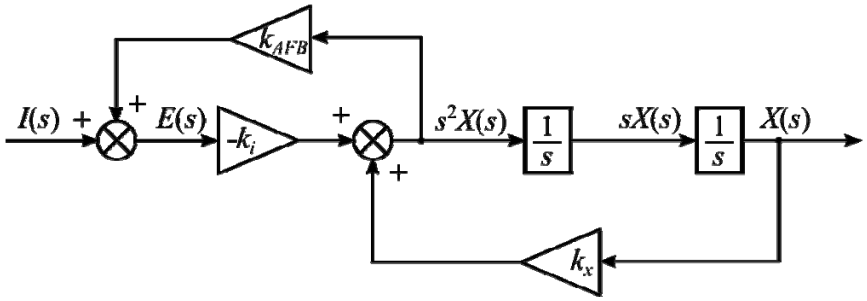

Figure 3.13 Block diagram of the maglev plant with acceleration feedback

Figure 3.13 shows a block diagram of the maglev plant with an acceleration feedback loop. Here the acceleration signal is assumed to be available. It can be calculated using Eq. (3.14). Details about acceleration estimation and acceleration feedback loop implementation are discussed in Chapter 5. By adding this acceleration feedback loop, the error signal *e* becomes

$$e = i + k_{AFB}\ddot{x} \tag{3.42}$$

The acceleration signal $\ddot{x}$ now becomes

$$\ddot{x} = -k_i e + k_x x \tag{3.43}$$

Substituting Eq. (3.43) into Eq. (3.42), the acceleration signal can be written as

$$\ddot{x} = -k_i(i + k_{AFB}\ddot{x}) + k_x x \tag{3.44}$$

Taking the Laplace transform of both sides of Eq. (3.44) and rearranging the terms, the open-loop transfer function of a maglev system with an acceleration feedback loop is written as:

$$\frac{X(s)}{I(s)} = \frac{-k_i}{(1 + k_i k_{AFB})s^2 - k_x} \tag{3.45}$$

where the input is the control current and the output is the gap distance.

In order to ensure the transfer function between the reference single R and output X remains the same, the PD position control gains must be scaled by a factor of $(1 + k_i k_{AFB})$.

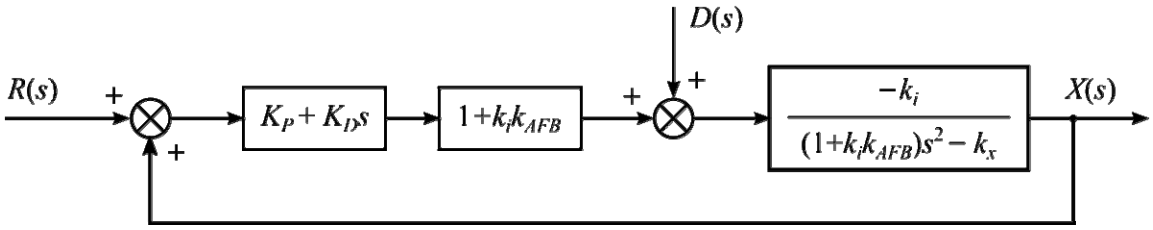

Figure 3.14 System with a PD controller and an acceleration feedback loop

Figure 3.14 shows a block diagram of the closed-loop maglev system with both a PD controller and an acceleration feedback loop. The transfer function between the disturbance D and the displacement X now becomes:

$$\frac{X(s)}{D(s)} = \frac{-k_i}{(1 + k_i k_{AFB})s^2 + [k_i(1 + k_i k_{AFB})K_d]s + [k_i(1 + k_i k_{AFB})K_p - k_x]} \tag{3.46}$$

The effect of adding acceleration feedback is the same as adding inertia — the so-called "electronic" inertia. The electronic inertia makes the disturbance seem like it is driving a

larger mass. The resulting effect on the dynamic stiffness is shown in Figure 3.20. (The phase shift does not change and is omitted here.)

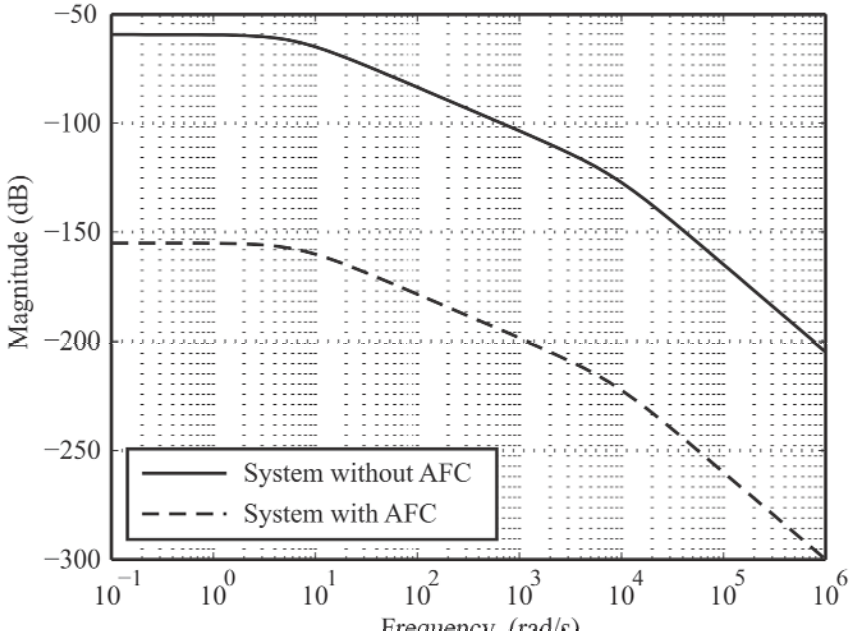

Figure 3.15 Bode magnitude plot of system with and without acceleration feedback

The acceleration feedback has caused the dynamic magnitude response curve to shift down, which means the stiffness of the system has increased. The concept can be understood better by considering the dynamic stiffness change of the system, which is the inverse of the transfer function between the disturbance and the system output. For a system without acceleration feedback, the dynamic stiffness is

$$\frac{D(s)}{X(s)} = \frac{s^2 + k_i K_d s + k_i K_p - k_x}{-k_i} \tag{3.47}$$

For a system with acceleration feedback, the dynamic stiffness is

$$\frac{D(s)}{X(s)} = \frac{(1 + k_i k_{AFB})s^2 + [k_i(1 + k_i k_{AFB})K_d]s + [k_i(1 + k_i k_{AFB})K_p - k_x]}{-k_i} \tag{3.48}$$

The denominators of Eqs. (3.47) and (3.48) are the same and the numerators are the characteristic equations of the systems. Choosing an appropriate acceleration feedback gain k_{AFB}, the gains for the double derivative term, derivative term, and constant term can be made larger in Eq. (3.48) than those in Eq. (3.47). The factor "$1+k_i k_{AFB}$" makes the mass seem to be "$k_i k_{AFB}$" more than its actual value. This additional part is the "electronic" inertia added to the system. In addition, the "electronic" damping coefficient $k_i K_d$ is increased by "$k_i k_{AFB}$". The equivalent spring constant is also increased, meaning more "effort" in the disturbance D is needed to achieve the same X. Thus introducing an acceleration feedback loop has the effect of increasing the effective mass, damping, and stiffness of the system.

The AFC design discussed in this section is based on the linearized system transfer function. Disturbance attenuation is achieved by manipulating the gain of an acceleration feedback loop. Using a Bode plot, the AFC gain and the attenuated disturbance are visualized, which helps determine the appropriate AFC gain value. In practice, the acceleration signal is estimated using a state observer. It requires less effort to generate the control effort and therefore is more effective. This AFC is not designed for any particular disturbance. Later in this chapter, a LQG controller is designed to attenuate a specific noise signal, the Additive white Gaussian noise (AWGN).

3.3.7. PID type controller design

This section discusses the design of a PID controller to achieve a stable maglev system. This research propsed a PID controller design using the Neimark D-partition method [246-248]. This method ensures the desired gain and phase margins are achieved.

The gain crossover frequency of this design is 700 Hz (4398 rad/s). Appendix DAppendix C explains why the 700 Hz crossover frequency is chosen for this particular system.

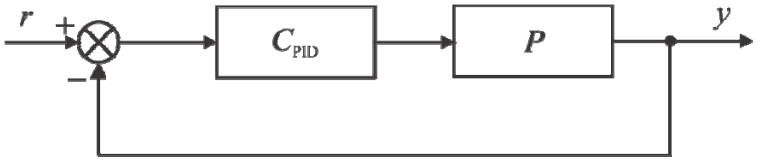

Figure 3.16 PID controller configuration

Figure 3.16 shows the block diagram of the plant with a PID type control. To simplify the design process, it is assumed that the configuration has unity feedback. An appropriate group of P, I, and D gains needs to be find to stabilize the system. However, the derivative gain of the PID controller cannot be zero, which is discussed below.

If the derivative gain $k_D = 0$, the controller is a PI type. The transfer function of a PI type controller $C_{PI}(s)$ is:

$$C_{PI}(s) = k_P + \frac{k_I}{s} = \frac{k_P s + k_I}{s} \tag{3.49}$$

The transfer function for the feedback system becomes:

$$\frac{Y(s)}{R(s)} = \frac{C_{PI}P}{1 + C_{PI}P} = -\frac{k_i(k_P s + k_I)}{s^3 + (k_i k_P - k_x)s + k_i k_I} \tag{3.50}$$

The characteristic polynomial of Eq. (3.50) is a cubic polynomial. The discriminant of a cubic function $ax^3 + bx^2 + cx + d = 0$ is

$$\Delta = 18abcd - 4b^3 d + b^2 c^2 - 4ac^3 - 27a^2 d^2 \tag{3.51}$$

Using Δ, the roots of the cubic function can be found as:

$$x_k = -\frac{1}{3a}\left(b + u_k C + \frac{\Delta_0}{u_k C}\right),\ k \in \{1,2,3\} \tag{3.52}$$

with $u_1 = 1$, $u_2 = \frac{-1+i\sqrt{3}}{2}$, and $u_3 = \frac{-1-i\sqrt{3}}{2}$. C and Δ_0 are calculated using

$$C = \sqrt[3]{\frac{\Delta_1 + \sqrt{\Delta_1^2 - 4\Delta_0^3}}{2}} \tag{3.53}$$

and

$$\begin{aligned} \Delta_0 &= b^2 - 3ac \\ \Delta_1 &= 2b^3 - 9abc + 27a^2 b \end{aligned} \tag{3.54}$$

To avoid excessive math, the details of calculating the three roots $x_{1,2,3}$ are skipped. The conclusion is given directly without proof, that is, $\forall (k_P, k_I) \in [0, \infty)$, $\exists \mathrm{Re}(x_k) > 0, k \in \{1,2,3\}$. Hence a PI type controller will not stabilize a maglev system.

A PD controller was successfully designed to stabilize the system in previous section. The system transfer function is examed to see why stability can be achieved. The transfer function of a PD type controller is:

$$C_{PD}(s) = k_P + k_D s \tag{3.55}$$

The transfer function for the feedback system becomes:

$$\frac{Y(s)}{R(s)} = \frac{C_{PD}P}{1 + C_{PD}P} = -\frac{k_i(k_P + k_D s)}{s^2 + k_i k_D s - k_x + k_i k_P} \tag{3.56}$$

Using the discriminant $\Delta = b^2 - 4ac$ for the quadratic equation $ax^2 + bx + c = 0$, the solution to the characteristic polynomial can be found:

$$x_{1,2} = \frac{-b \pm \sqrt{\Delta}}{2a} \tag{3.57}$$

Again, the mathematical details are skipped here and the conclusion is given without proof: $\exists (k_P, k_D) \in [0, \infty)$, which makes $\mathrm{Re}(x_i) < 0,\ i \in \{1,2\}$. The Routh-Hurwitz stability criterion [249, 250] can be used to find the range of the PD gains (k_P and k_D values.) The characteristic polynomial is

$$D(s) = s^2 + k_i k_D s - k_x + k_i k_P \tag{3.58}$$

and the coefficient table can be calculated using values in Eq. (3.58),

Table 3.2 Coefficient table of the characteristic polynomial

1	$k_i k_P - k_x$
$k_i k_D$	0
$k_i k_P - k_x$	

The Routh-Hurwitz stability criterion states that the number of sign changes in the first column will be the number of non-negative poles. Therefore, it is desired to keep the sign of the first column the same. Since the first element is 1, it follows that if two conditions, $k_i k_D > 0$ and $k_i k_P - k_x > 0$, are satisfied, a stable output will be achieved. Solving these two inequalities gives:

$$\begin{aligned} &k_i k_D > 0 \Rightarrow k_D > 0 \\ &k_i k_P - k_x > 0 \Rightarrow k_P > \frac{k_x}{k_i} = 76.73 \end{aligned} \tag{3.59}$$

Eq. (3.59) gives the ranges of k_i and k_d values. A PD controller formed by values chosen from these ranges will achieve stable levitation. This result can also be verified using a Nyqusit plot.

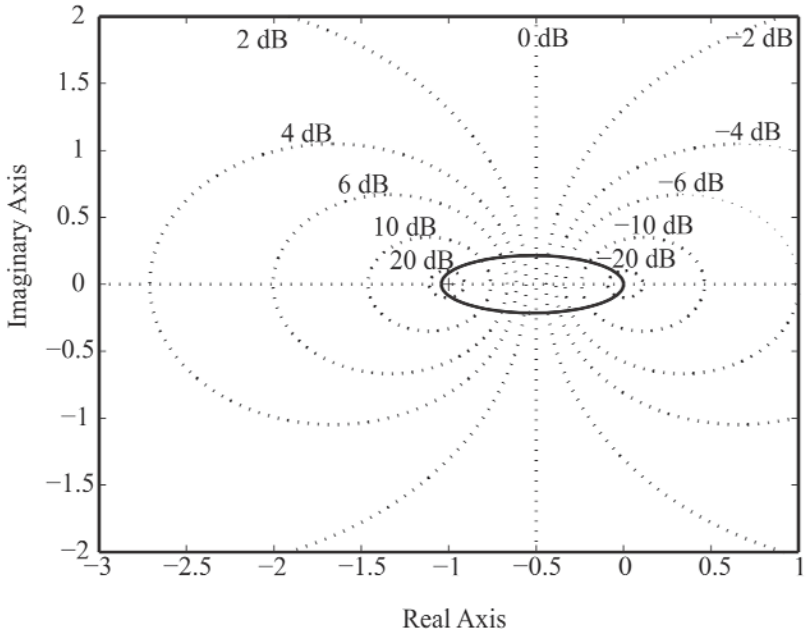

Figure 3.17 Nyquist plot of the maglev system with a PD controller

Figure 3.17 shows a Nyquist plot of the maglev system with a PD controller with $k_P = 56$, and $k_D = 0.5$. The Nyquist curve encircles the point $-1 + j0$. Since the plant has one pole in the RHP, the maglev system is found to be stable using Nyquist stability criterion [251]. However, a PD type controller cannot eliminate the steady-state error [252]. A non-zero k_I is needed to guarantee zero steady-state error, which means the controller needs to have non-zero P, I, and D gains.

The Neimark D-partition method starts with a general form PID controller transfer function. Assuming that the gains of the PID controller are non-zero, its transfer function is written as:

$$G_c(s) = k_P + \frac{k_I}{s} + k_D s \tag{3.60}$$

The plant transfer function can be written in the following form:

$$G_P(s) = \frac{\text{num}(s)}{\text{den}(s)} \tag{3.61}$$

where num(s) stands for the numerator polynomial of the transfer function $G_P(s)$ and den(s) stands for the denominator of $G_P(s)$. Then the feedforward loop transfer function becomes:

$$1 + G_c(s)G_P(s) = 0 \tag{3.62}$$

Substituting Eqs. (3.60) and (3.61) into Eq. (3.62),

$$k_P + \frac{k_I}{s} + k_D s = -\frac{\text{den}(s)}{\text{num}(s)} \tag{3.63}$$

Replacing s with $j\omega$ in Eq. (3.63), the real part and imaginary part can be written as:

$$k_P = \text{Re}\left(-\frac{\text{den}(j\omega)}{\text{num}(j\omega)}\right) \tag{3.64}$$

and

$$-\frac{k_I}{\omega} j + k_D \omega j = \text{Im}\left(-\frac{\text{den}(j\omega)}{\text{num}(j\omega)}\right) \tag{3.65}$$

If the independent variable $\omega \in (0, \infty)$, it is possible to solve the frequency dependent vector of complex numbers and plot them in the complex plane to create a D-curve for parameter k_P. In a similar fashion, the imaginary part in Eq. (3.65) can be used to create k_I and k_D.

In order to guarantee the phase margin, a phase shift is added to the original system. Suppose ω is the desired phase shift. Multiplying the plant transfer function by $e^{j\omega}$ to shift its phase curve, the feedforward loop transfer function becomes:

$$1 + G_c(s)G(s)e^{-j\omega} = 0 \tag{3.66}$$

Then Eqs. (3.64) and (3.65) can be written as:

$$k_P = \mathrm{Re}\left(-\frac{\mathrm{den}(j\omega)}{\mathrm{num}(j\omega)e^{-j\omega}} \right) \tag{3.67}$$

and

$$-\frac{k_I}{\omega} j + k_D \omega j = \mathrm{Im}\left(-\frac{\mathrm{den}(j\omega)}{\mathrm{num}(j\omega)e^{-j\omega}} \right) \tag{3.68}$$

With Eqs. (3.67) and (3.68), the controller parameters are selected directly from the D-curves.

Finally, the PID type controller gains are calculated from the following equation:

$$G_c(s) = \left(k_1 + k_D s\right)\left(k_2 + \frac{k_I}{s}\right) = k_1 k_2 + k_D k_I + \frac{k_1 k_I}{s} + k_D k_I s \tag{3.69}$$

The updated PID gains are listed as below:

$$\tilde{k}_P = k_1 k_2 + k_D k_I \tag{3.70}$$

$$\tilde{k}_I = k_1 k_I \tag{3.71}$$

$$\tilde{k}_D = k_D k_I \tag{3.72}$$

In this study, the frequency range is chosen to be $\omega \in [0, \infty)$. To start the control design, assume that k_I is 0. Using Eqs. (3.64) and (3.65), the P and D gain values that guarantee the stability of the maglev system can be calculated. Using Eqs. (3.67) and (3.68), the P and D gain values that guarantee both stability and phase margin can be calculated.

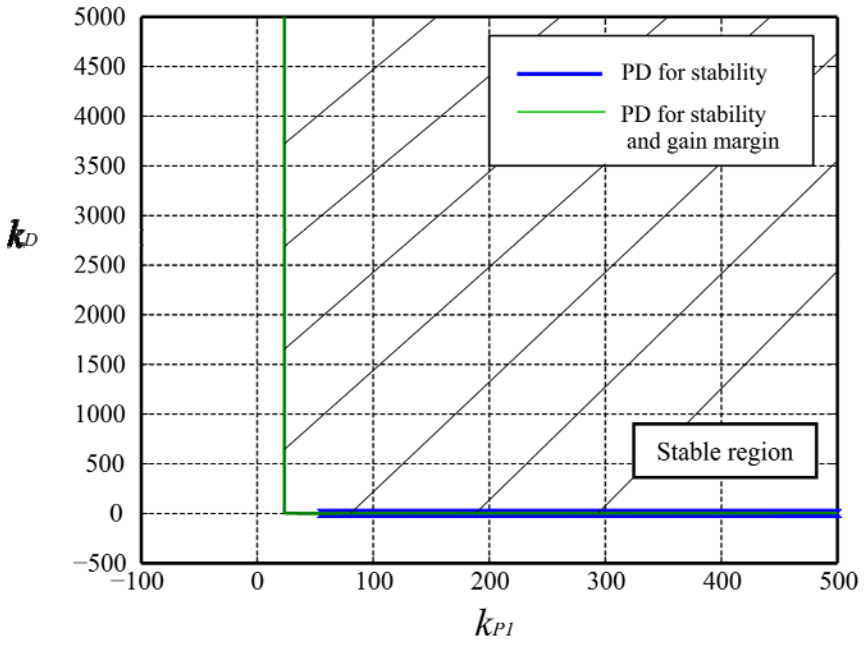

Figure 3.18 D-curves of PD controller calculation

Figure 3.18 shows the D-curves of P gain values versus D gain values. The figure shows that the 50 degree phase margin requirement can be met once the system stability is achieved. In other words, if the PD controller gains satisfy Eq. (3.59), stable magnetic levitation with at least 50 degree of phase margin is achieved. This study chooses a P gain $k_{p1} = 300$ and a D gain $k_D = 15$.

The next step assumes that D gain is 0. Then Eqs. (3.64) and (3.65) are used to derive the P and I gain values that stabilize the system. Once again, Eqs. (3.67) and (3.68) are used to calculate the gain values that stabilize the system and guarantee a 50 degrees phase margin.

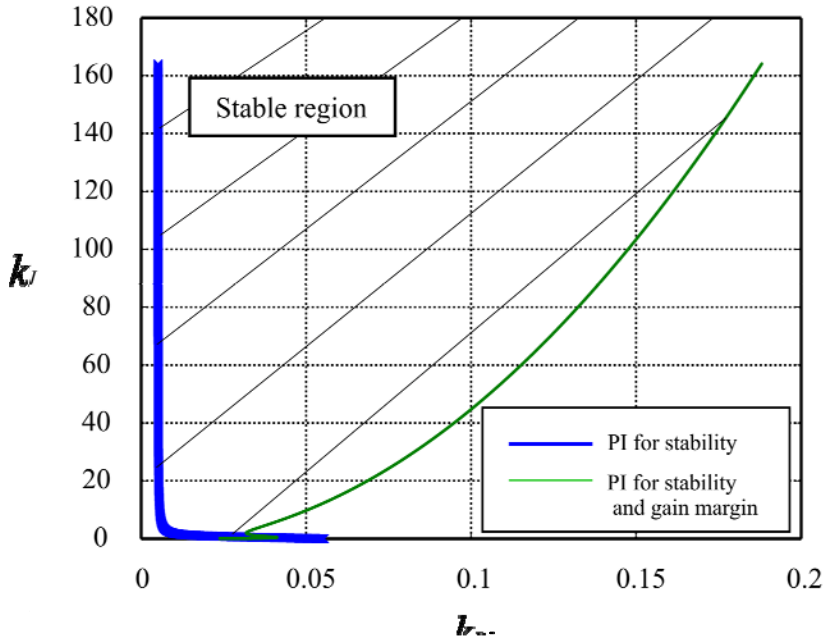

Figure 3.19 D-curves of PI controller calculation

With these values, the D-curves plotted in Figure 3.19 can be found showing P and I values that meet the 50 degree gain margin design goal. This study chooses the gain values as: $k_{p2} = 0.2$ and $k_I = 17.29$. The PID controller is thus calculated using Eq. (3.69) to be:

$$G_c(s) = 284.5 + \frac{4511}{s} + 5.3s \tag{3.73}$$

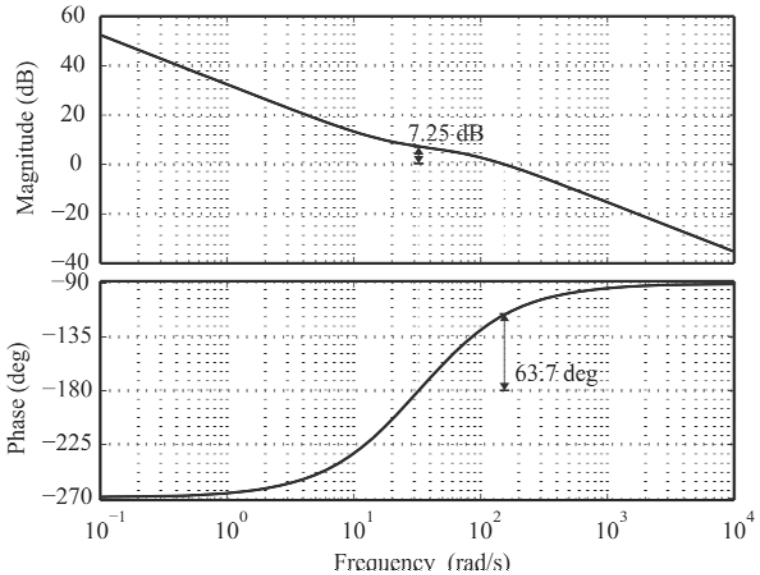

Figure 3.20 Bode plot of the maglev plant with a PID controller

Figure 3.20 shows a Bode plot of the maglev plant with the PID controller. It is seen that this design meets all the design goals. The gain margin of the system is 7.25 dB at the phase crossover frequency at 32.5 rad/s. The phase margin is 63.7 degree at the gain crossover frequency at 154 rad/s. Comparing Figure 3.6 with Figure 3.20, it is found this controller increases the loop gain and provides a 63.7 degree of phase lead, which makes the system stable.

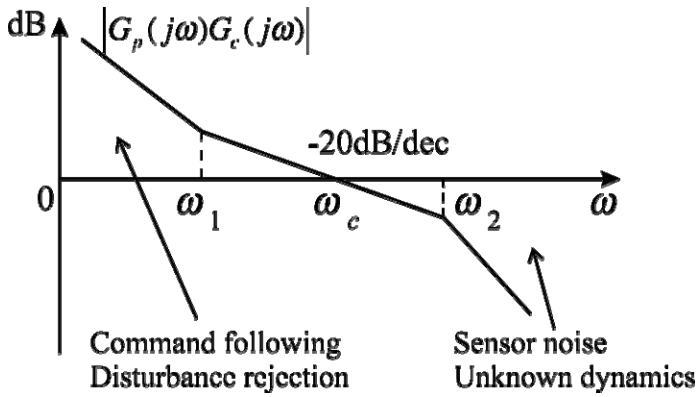

Figure 3.21 Ideal loop-shaping

In addition, there is a -20 dB/decade roll-off near on the Bode magnitude plot near the phase crossover frequency, whic satisfies the loop-shaping requirements. An ideal loop-shaping curve is shown in Figure 3.21. The frequency response curve of a system with a PID controller resembles the ideal curve. More about loop-shaping will be discussed in Chapter 4 where controllers are designed for system robustness.

3.3.8. Lead controller design

The lead-lag controller is designed in a similar way as the PD controller. A lead-lag controller differs from a PD controller in its transfer function denominator. The general transfer function form of a lead-lag controller is:

$$G_c(s) = \frac{K_c(s+z_{c1})(s+z_{c2})}{(s+p_{c1})(s+p_{c2})} \tag{3.74}$$

with $z_{c1} \le p_{c1}$, $z_{c2} \ge p_{c2}$.

Figure 3.6 has shown the Bode plot of the open-loop maglev plant. In order to meet the design goal of crossover frequency around 700 Hz, the controller needs to have a lead term to shift the magnitude curve up.

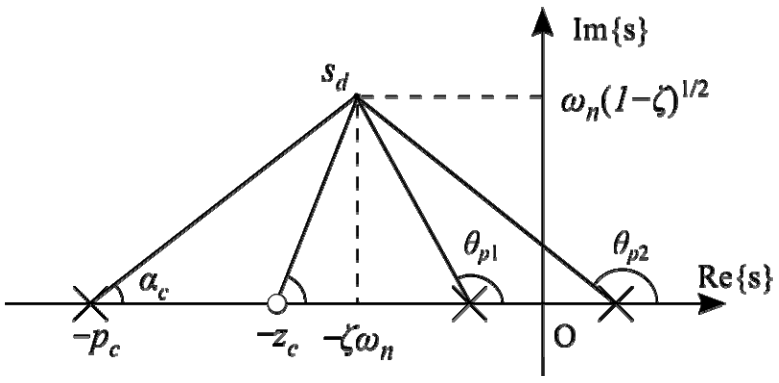

Figure 3.22 Pole and zero locations of a lead-lag type controller

Figure 3.22 shows a plot illustrating the relative position of the system and controller poles and zeros. The angle contribution by a controller which ensures the desired pole s_d belongs to the root locus of desired system is obtained from

$$\angle G_c(s_d) = \pi - \angle G(s_d) \tag{3.75}$$

which gives

$$\theta_c = \angle(s_d + z_c) - \angle(s_d + p_c) = \pi - \sum_{i=1}^{m} \angle(s_d + z_i) + \sum_{i=1}^{n} \angle(s_d + p_i) \tag{3.76}$$

It indicates that the lead controller needs to provide 7.42 rad of phase contribution to the system, i.e., $\theta_c = 7.42$ rad. Using the trigonometric relationship in Figure 3.22, it is found

$$\frac{|p_c| - |z_c|}{69} = \tan 7.42$$

and the relationship between the controller pole and zero can be written as

$$|p_c| = 69 \times \tan 7.42 + |z_c|$$

To simplify the calculation, assume that the distance between zero and $\zeta\omega_n$ is the same as that between the pole and $\zeta\omega_n$. Then a lead controller is derived with a zero at 46.2 rad/s, and pole at 197 rad/s. Therefore the controller transfer function is:

$$G_c = \frac{s + 46.2}{s + 197} \tag{3.77}$$

Again, the controller gain needs to be calculated. Let K_p be the desired static position error constant. K_p can be written as:

$$K_p = \lim_{s \to 0} G_c(s) G(s) \tag{3.78}$$

The controller gain can be calculated using Eq. (3.38) and the result is

$$K > 1.6\text{E}3$$

The final lead controller is written as:

$$G_c = \frac{1.6\text{E}3(s+46.2)}{s+197} \tag{3.79}$$

Comparing transfer function of the lead controller to that of the PD controller, it is found that the lead controller has a relatively larger gain value, and therefore, it may introduce oscillation in the system response. The lead controller has a pole in the controller transfer function, which has the same effect of including a low-pass filter in the feedforward loop. This pole helps to attenuate the high frequency noise. It has also been observed that the PD type controller does not provide performance robustness (does not guarantee zero steady-state error) while the lead controller does because of its pole.

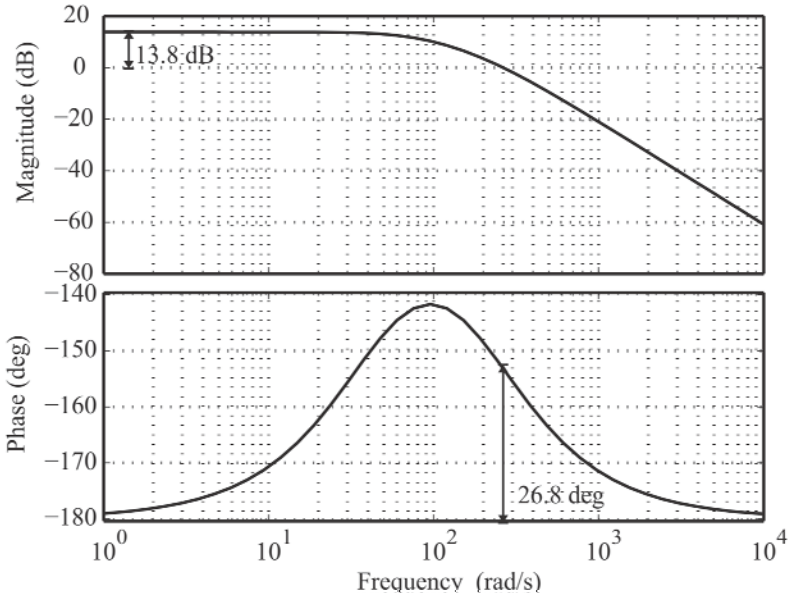

Figure 3.23 Bode plot of the maglev plant with a PID controller

Figure 3.23 shows a Bode plot of the maglev plant with a lead controller. The gain margin of the system is 13.8 dB at the phase crossover frequency at 0 rad/s. The phase margin is 26.8 degree at the gain crossover frequency at 264 rad/s. Comparing Figure 3.6 with Figure 3.23, it is found this controller increases the loop gain and provides 26.8 degree

of phase lead.

The closed-loop system with the PD and lead controllers are type 0 systems, which means the steady-state errors are finite values when tracking a step input signal, but are infinite values when tracking ramp and parabolic inputs. Therefore, when comparing the performance of the closed-loop systems with PD and lead controllers, the reference signal should be a step position change.

3.3.9. Model-reference control design

The previous sections presented design techniques of linear, time-invariant controllers. In reality, all physical plants have a certain amount of nonlinearity. For example, in this research the maglev plant is nonlinear because of the nature of the electromagnetic force. For the maglev system, as the ball moves towards the electromagnet from the equilibrium point, the electromagnetic force exhibits a quadratic increase. This nonlinearity leads to unsatisfactory performance or even failure of linear controllers when the system moves away from equilibrium. This research discusses how to use the model-reference control (MRC) technique to improve the performance of the maglev system near its equilibrium.

In order to design a MRC system, one mathematical representation of the physical plant is chosen as the "reference." This mathematical model is selected so that a desired output is obtained with a given input. The model is chosen to be as simple as possible, and efficient enough to be implemented. To build the MRC system, the output of the model and that of the plant are compared and the differences (error signal e) are used to generate the control signals. Compared to the structurally gain-fixed PID controller, the MRC

parameters are continuously adjusted according to the error signal (hence in some literature it is also referred to as model-reference adaptive control), so it is capable of handling larger plant parameter variations.

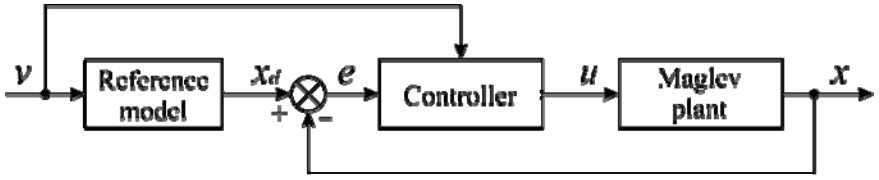

Figure 3.24 MRC system configuration

Figure 3.24 shows the configuration of an MRC system. The reference model is used to generate a desired output to the reference signal. There is a set of acceptable controller parameters. The parameters chosen to form the controller are determined by an internal adjustment mechanism, based on both the reference signal v and the error e. Multiple mathematical methods have been reported to assist with developing the adjustment mechanism; MIT rules [253-257], Lyapunov theory [182, 258-261], and the theory of augmented error [216, 262-265] are the most commonly discussed methods in the literature. In this research, the Lyapunov method is used to determine adjustment mechanism and ultimately determines the stability of the designed system [253, 266-269]. The detailed design process is discussed below.

The design of a MRC control starts with a continuous-time system model. The maglev plant can be written in the following state-space form:

$$\dot{x} = f\left(x,u,t\right) \tag{3.80}$$

where $x \in \mathbb{R}^m$ is the state vector, $u \in \mathbb{R}^m$ is the control vector and $f : \mathbb{R}^m \mapsto \mathbb{R}^m$ is a

vector-valued function.

The design goal is to derive a controller that continuously outputs a signal to force the plant states to track the model states. For the maglev system, although the plant is open-loop unstable, a controller can be designed to make the state variables track those of a stable model and thus obtain a stable system.

To derive the control law, the reference system is written as:

$$\dot{x}_d = Ax_d + Bv \tag{3.81}$$

where $x_d \in \mathbb{R}^m$ is the state vector of the reference model, v is the input vector, $A \in \mathbb{R}^{m\times m}$ is the constant state matrix, and $B \in \mathbb{R}^m$ is the constant input matrix. In order to achieve asymptotic stability at the equilibrium state, the eigenvalues of A are chosen to have negative real parts.

The error vector e between the reference system and the plant output is given by

$$e = x_d - x \tag{3.82}$$

The design goal is to reduce the error vector to zero using control signal u. The error function can be obtained by substituting Eqs. (3.80) and (3.81) into Eq. (3.82),

$$\begin{aligned} \dot{e} &= \dot{x}_d - \dot{x} \\ &= Ax_d + Bv - f\left(x,u,t\right) \\ &= Ae + Ax - f\left(x,u,t\right) + Bv \end{aligned} \tag{3.83}$$

Eq. (3.83) is the differential equation of the error vector.

A Lyapunov function is chosen to be

$$V(e) = e^{\mathrm{T}}Pe \tag{3.84}$$

where P is a positive-definite real symmetric matrix. Then the derivative of $V(e)$ can be calculated:

$$\dot{V}(e) = e^{\mathrm{T}}\left(A^{\mathrm{T}}P + PA\right)e + 2M \tag{3.85}$$

where

$$M = e^{\mathrm{T}}P\left[Ax - f\left(x,u,t\right) + Bv\right]. \tag{3.86}$$

By identifying the matrices A and B from Eq. (3.81) and choosing the matrix Q to be

$$Q = \begin{bmatrix} q_{11} & 0 \\ 0 & q_{22} \end{bmatrix} = \text{positive definite}, \tag{3.87}$$

$\dot{V}(e)$ can be expressed as

$$\dot{V}(e) = -(q_{11}e_1^2 + q_{22}e_2^2) + 2M \tag{3.88}$$

where $M = \begin{bmatrix} e_1 & e_2 \end{bmatrix}\begin{bmatrix} p_{11} & p_{12} \\ p_{12} & p_{22} \end{bmatrix}\left\{\begin{bmatrix} 0 & 1 \\ -\omega_n^2 & -2\zeta\omega_n \end{bmatrix}\begin{bmatrix} x_1 \\ x_2 \end{bmatrix} - \begin{bmatrix} 0 & 1 \\ -b & -a(t)x_2 \end{bmatrix}\begin{bmatrix} x_1 \\ x_2 \end{bmatrix} - \begin{bmatrix} 0 \\ u \end{bmatrix} + \begin{bmatrix} 0 \\ \omega_n^2 v \end{bmatrix}\right\}$.

Carrying out the multiplication, the equation for *M* is given as follows:

$$M = \left(e_1p_{12} + e_2p_{22}\right)\left[-\left(\omega_n^2 - b\right)x_1 - 2\zeta\omega_n x_2 + a(t)x_2^2 + \omega_n^2 v - u\right] \tag{3.89}$$

Now the control effort u can be chosen to be

$$u = -\left(\omega_n^2 - b\right)x_1 - 2\zeta\omega_n x_2 + \omega_n^2 v + a_m x_2^2 \text{sign}(e_1p_{12} + e_2p_{22}) \tag{3.90}$$

where

$$a_m = \max\left|a(t)\right| \tag{3.91}$$

Then it follows that

$$M = \left(e_1p_{12} + e_2p_{22}\right)\left[a(t) - a_m \,\text{sign}(e_1p_{12} + e_2p_{22})\right]x_2^2 \tag{3.92}$$

is non-positive.

With the control function *u* in Eq. (3.90), the equilibrium state $e = 0$ is locally asymptotically stable. Thus, Eq. (3.90) defines a nonlinear control law that will guarantee an asymptotically stable operating point.

The *P* matrix in Eq. (3.84) can be solved using the Riccati Equation

$$A^T P + PA = -Q \tag{3.93}$$

which can be written as:

$$\begin{bmatrix} 0 & -\omega_n^2 \\ 1 & -2\zeta\omega_n \end{bmatrix}\begin{bmatrix} p_{11} & p_{12} \\ p_{21} & p_{22} \end{bmatrix}+\begin{bmatrix} p_{11} & p_{12} \\ p_{21} & p_{22} \end{bmatrix}\begin{bmatrix} 0 & 1 \\ -\omega_n^2 & -2\zeta\omega_n \end{bmatrix}=-\begin{bmatrix} q_{11} & q_{12} \\ q_{21} & q_{22} \end{bmatrix} \tag{3.94}$$

where $q_{12} = q_{21} = 0$ and ζ and ω_n are the damping ratio and natural frequency, respectively, of the chosen reference model. Eq. (3.94) results in four equations:

$$\left(p_{21} + p_{12}\right)\omega_n^2 = q_{11} \tag{3.95}$$

$$\left(p_{12} + p_{21}\right) - 4\zeta\omega_n p_{22} = -q_{22} \tag{3.96}$$

$$p_{11} - 2\zeta\omega_n p_{21} - \omega_n^2 p_{22} = q_{21} \tag{3.97}$$

$$-\omega_n^2 p_{22} + p_{11} - 2\zeta\omega_n p_{12} = q_{12} \tag{3.98}$$

In Eqs. (3.95) through (3.98), q_{12} and q_{21} equal zero, and q_{11} and q_{12} are random numbers that make *Q* positive-definite. Therefore, there are four unknowns p_{11}, p_{12}, p_{21}, and p_{22}, which can be solved using Eqs. (3.95) through (3.98).

In order to minimize oscillation, this research chooses $\zeta = 0.69$ and $\omega_n = 100\,\text{Hz}$ as the damping ratio and natural frequency of the reference model [342]. *Q* is chosen to be

$$Q = \begin{bmatrix} 1 & 0 \\ 0 & -1 \end{bmatrix}.$$

P can be solved as

$$P = \begin{bmatrix} 0.47 & 0.101 \\ 0.101 & 1.11 \end{bmatrix}.$$

A closed-loop system can be built with the derived parameters.

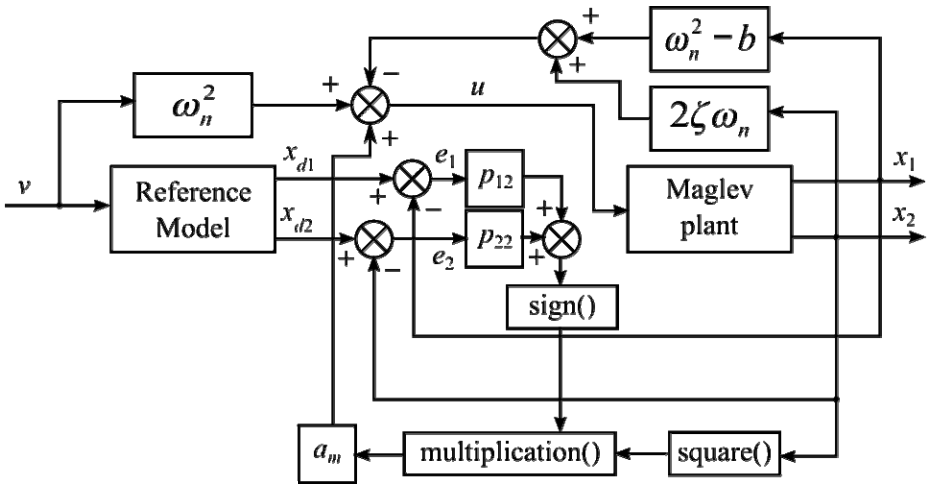

Figure 3.25 Block diagram of the maglev system with an MRC controller

Figure 3.25 shows the block diagram of a maglev system with an MRC controller. This system is more complicated compared to the previous designs. There are two algebraic functions, multiplication and square, one logic function, and one sign function in the closed-loop system. These functions require controller hardware that can handle these numeric and logic operations. The implementation of this controller will be discussed in Chapter 5.

3.4. Optimal control design

This section discusses the design of a linear-quadratic-gaussian (LQG) controller. The LQG controller and the H_∞ controller discussed in Chapter 5 are optimal controllers. The goal of optimal control is to find a controller that provides the best possible performance with respect to certain criteria. This discussion focuses on studying the optimal control theory originated from the work of Pontryagin [270-274]. It was field-tested in the Apollo Program (1963–1972), where NASA designed controllers that optimized fuel consumption when the Lunar Module descended from the lunar orbit on the

Moon, and was brought back to the orbit to rendezvous with the Command Module [275-280].

3.4.1. LQR regulator

This discussion starts with a control design to derive a regulator that achieves stable levitation using a Linear Quadratic Regulator (LQR) approach. As a second design, a LQR/LQG controller is developed to attenuate Gaussian noise. This design assumes the maglev sysem is a linearized system.

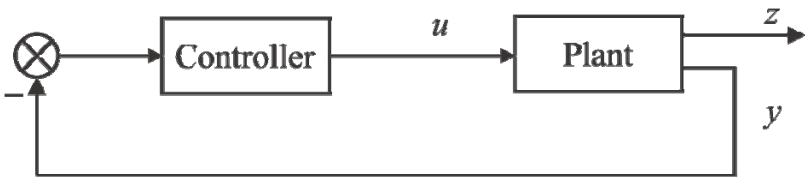

Figure 3.26 System configuration of LQR problem

As discussed in previous sections, a regulator type controller regulates the system output to a constant value. There is no reference signal in the system. Figure 3.26 shows the configuration of the system, in which $u \in \mathbb{R}^m$, $z \in \mathbb{R}^l$, and $y \in \mathbb{R}^k$. In the state-space representation model, not all the state variables are available (the velocity of the ball is not available). Therefore, the system equations are written as:

$$\begin{aligned} \dot{x} &= Ax + Bu \\ y &= Cx \\ z &= Gx + Hu \end{aligned} \tag{3.99}$$

in which $x \in \mathbb{R}^n$. The output $y(t)$ corresponds to the signal that can be measured directly and therefore is available for control. The controlled output, $z(t)$, corresponds to the signal that needs to be regulated. In this research, it is the position of the levitated ball. The goal is

to return it to the equilibrium position when disturbed.

The first step is to define the design goal. An optimal control design defines its goal in the form of an optimality criterion. It usually is a function of the state and control variables. This function is also referred to as the *cost functional* (performance index functional) [281-283]. The design process is to solve a set of differential equations to derive the control variable paths that minimize the cost functional. In this study, the maglev system model is an SISO system. Generally, for an SISO system, the cost functional includes both the input and output. This research uses the cost functional:

$$J = \int_0^\infty \|z(t)\|^2 + \rho \|u(t)\|^2 \, dt \tag{3.100}$$

where $\rho > 0$ is the weight of $\|u(t)\|^2$. The term

$$\int_0^\infty \|z(t)\|^2 \, dt \tag{3.101}$$

is the energy of the controlled output and the term

$$\int_0^\infty \|u(\mathrm{t})\|^2 dt \tag{3.102}$$

is the energy of the control signal. The goal of the LQR regulator design is to find a controller whose transfer matrix makes the sum of these two energies as small as possible (with different weight values.)

With this cost functional, J, an LQR regulator can be developed to achieve stable levitation. In order to solve the differential equations to derive the controller, this study assumes that all the state variables are measureable and available for control. Later an observer is designed to provide state estimation for those state variables that are not available.

This research uses the linearized maglev system model and derives a linear optimal

controller. An optimal controller satisfying the optimal criteria in Eq. (3.100) is a matrix gain in the form of:

$$u = -Kx \tag{3.103}$$

where $K \in \mathbb{R}^{m \times n}$ is the optimal feedback gain matrix. Lewis *et al.* [284] have discussed different approaches to calculate matrix K. The control design problem discussed here is the *Initial Condition Problem* discussed in [284]. K is chosen to be

$$K = \left(H'QH + \rho R\right)^{-1}\left(B'P + H'QG\right) \tag{3.104}$$

in which $Q \in \mathbb{R}^{l \times l}$ is a symmetric positive-definite matrix, and P is the unique positive-definite solution to the following Algebraic Riccati Equation (ARE):

$$A'P + PA + G'QG - \left(PB + G'QH\right)\left(H'QH + \rho R\right)^{-1}\left(B'P + H'QG\right) = 0 \tag{3.105}$$

With a feedback control signal u, a closed-loop system is built with the following state-space form:

$$\dot{x} = \left(A - BK\right)x \tag{3.106}$$

By properly selecting K, the eigenvalues of matrix $A - BK$ will have negative real parts. This K matrix, which is the LQR controller, makes the closed-loop system asymptotically stable. However, because this controller is derived assuming that all state variables are available, there are two conditions that need to be satisfied:

1. The original system in Eq. (3.99) is controllable;
2. The system in Eq. (3.99) is observable when y is ignored and z is assumed to be the only output.

Condition 1 can be verified by calculating the system controllability matrix. Since in this study, the maglev plant is SISO, condition 2 can be verified by calculating the

system observability matrix. The maglev system controllability and observability matrices are calculated to test if the closed-loop system is asymptotically stable. The transformation matrix T_c defined by

$$T_c = \left[B, AB, \ldots, A^{n-1}B \right] \tag{3.107}$$

is referred to as the controllability matrix. Using Eq. (3.17) and the parameter values in Table 3.1, the controllability matrix is calculated to be:

$$T_c = \begin{bmatrix} 0 & -56.82 \\ -56.82 & 0 \end{bmatrix}$$

The rank of T_c, also known as the controllability index of the system, is 2. It indicates there are 2 controllable states in the system. In other words, the maglev system is fully controllable.

The transformation matrix T_o defined by

$$T_o = \begin{bmatrix} C \\ CA \\ \vdots \\ CA^{n-1} \end{bmatrix} \tag{3.108}$$

is the observability matrix. The observability matrix for the maglev system is

$$T_o = \begin{bmatrix} 1 & 0 \\ 0 & 1 \end{bmatrix}$$

The rank of matrix T_o, also known as the observability index, equals 2. It indicates that there are 2 observable states in the system. For this case, the system is fully observable.

Since the state variables are observable and controllable, matrix K makes the closed-loop system asymptotically stable no matter whether the system is open loop stable or not. In other words, with an LQR controller matrix K, a stable magnetic levitation can be achieved. For this study, the plant is open-loop unstable. The following calculation

checks if there exists an analytical solution of matrix K.

Assuming the feedback gain matrix is:

$$K = \begin{bmatrix} k_1 & k_2 \end{bmatrix} \tag{3.109}$$

and using Eq. (3.17), the closed-loop system Eq. (3.106) can be written as

$$A - BK = \begin{bmatrix} 0 & 1 \\ 66.03^2 & 0 \end{bmatrix} - \begin{bmatrix} 0 \\ -56.82 \end{bmatrix} \begin{bmatrix} k_1 & k_2 \end{bmatrix} = \begin{bmatrix} 0 & 1 \\ 4360 + 56.82k_1 & 56.82k_2 \end{bmatrix} \tag{3.110}$$

Hence, the characteristic equation becomes

$$\left| sI - A + BK \right| = \begin{bmatrix} s & -1 \\ -(4360 + 56.82k_1) & s - 56.82k_2 \end{bmatrix} \tag{3.111}$$

The closed-loop poles are at:

$$s_{1,2} = \frac{1}{2}\left[56.82k_2 \pm \sqrt{(-56.82k_2)^2 + 4(56.82k_1 + 4360)} \right] \tag{3.112}$$

By properly choosing k_1 and k_2, the closed-loop poles s_1 and s_2 can be allocated as desired. To obtain the optimal controller, matrix K is solved using Eq. (3.104). This study chooses the following Q matrix:

$$Q = \begin{bmatrix} 1 & 0 \\ 0 & 2 \end{bmatrix}$$

which means the weight of the velocity is twice as much as that of the position, and $\rho = 1$, which means the control effort efficiency is not as important as how fast the system becomes stable. In other words, it is desired to achieve a faster response even if the steady-state error is large, regardless of how much control effort is required. Solving Eqs. (3.104) and (3.105), matrix P is found to be:

$$P = \begin{bmatrix} 17.67 & 0.014 \\ 0.014 & 0.0044 \end{bmatrix},$$

and the optimal state-feedback controller is found to be:

$$K = \begin{bmatrix} 119.56 & 22.42 \end{bmatrix}.$$

The designed K matrix is equivalent to a PD controller with a k_P equal to 119.56, and a k_D equal to 22.42. These gain values satisfy the minimum gain requirements in Eq. (3.59). Gain k_D is relatively large compared to the other PD controllers designed previously (Eqs. (3.73) and (3.39)). This can be explained by the weight factors chosen in matrix Q .

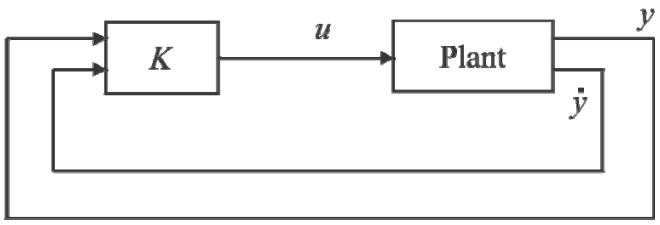

Figure 3.27 Maglev system with an LQR controller *K*

Figure 3.27 shows a block diagram of the system with the designed LQR controller *K*. This controller is designed assuming that all the state variables (the position and velocity of the levitated object) are available. With the maglev testbed used in this research, the velocity of the object is not available. In the next section, an observer is designed to estimate the unavailable state variable for the controller to be implemented in hardware.

3.4.2. Optimal state estimation

Previous discussion formulated an LQR optimal state feedback control law of

$$u(t) = -Kx(t) \tag{3.113}$$

which requires that all the state variables are available. This section discusses how to design a state estimator so the unavailable state variables are mathematically calculated using the available states and the system model.

The state estimator design starts by assuming the process state $x(t)$ in Eq. (3.113) can be substituted by an estimation $\hat{x}(t)$, i.e.,

$$u(t) = -K\hat{x}(t) \tag{3.114}$$

instead of Eq. (3.113), where $\hat{x}(t)$ denotes an estimate of the process state $x(t)$. This estimation, $\hat{x}(t)$, can be constructed by replicating the process dynamics in Eq. (3.99)

$$\dot{\hat{x}} = A\hat{x} + Bu\,. \tag{3.115}$$

Defining the state estimator error *e* to be $e = x - \hat{x}$, its derivative is

$$\dot{e} = \dot{x} - \dot{\hat{x}} \tag{3.116}$$

Substituting Eqs. (3.99) and (3.115) into Eq. (3.116), the derivative of the state estimator error *e* becomes

$$\dot{e} = Ax - A\hat{x} = Ae\,. \tag{3.117}$$

Three conclusions can be made with Eq. (3.117):

1. If matrix A is asymptotically stable the error e converges to zero.

2. Whether the error *e* converges or not does not depend on the input signal u.

3. If $e = 0$, $\hat{x}$ converges to x as $t \to \infty$. In other words, $\hat{x}$ is a good estimation of x as $t \to \infty$.

For the maglev system discussed in this research, the state matrix A is not stable (as shown in Eq. (3.25)). Therefore, e becomes unbounded as $t \to \infty$, i.e., the difference between $\hat{x}$ and x becomes larger as $t \to \infty$. To avoid unbounded growth of *e*, a classic solution is to include a correction term $L(y - \hat{y})$, and then the system equations become:

$$\begin{aligned} \dot{\hat{x}} &= A\hat{x} + Bu + L\left(y - \hat{y}\right) \\ \hat{y} &= C\hat{x} \end{aligned} \tag{3.118}$$

where $\hat{y}$ is an estimator of y and $L \in \mathbb{R}^{n \times k}$ is the correction matrix that needs to be

determined.

The correction term $L(y-\hat{y})$ only takes effect when $\hat{x}$ deviates from x. When $\hat{x}$ is equal to (or very close) to x, $\hat{y}$ equals (or is very close) to y, and hence $L(y-\hat{y})$ becomes (or is close to) zero. This means the correction term drives the error *e* to zero. It can be explained by re-writing the estimation error *e* using Eqs. (3.115) and (3.118) as

$$\dot{e} = Ax - A\hat{x} - L(Cx - C\hat{x}) = (A - LC)e \tag{3.119}$$

Eq. (3.119) indicates that e converges to zero if matrix $A-LC$ is asymptotically stable. Generally, a matrix L can be selected so that $A-LC$ is asymptotically stable despite an unstable state matrix A. The sufficient and necessary conditions for the existence of matrix *L* have been discussed by Zhou *et al.* [285].

With the correction term, the system equation in Eq. (3.118) can be re-write as:

$$\dot{\hat{x}} = (A - LC)\hat{x} + Bu + Ly \tag{3.120}$$

and is referred to as a full-order observer plant. The term full-order refers to the fact that the order of the estimated state $\hat{x}$ is equal to that of the plant state x. Eq. (3.120) shows that the full-order observers have two inputs: the control signal u and the measured output y, and a single output the state estimate x.

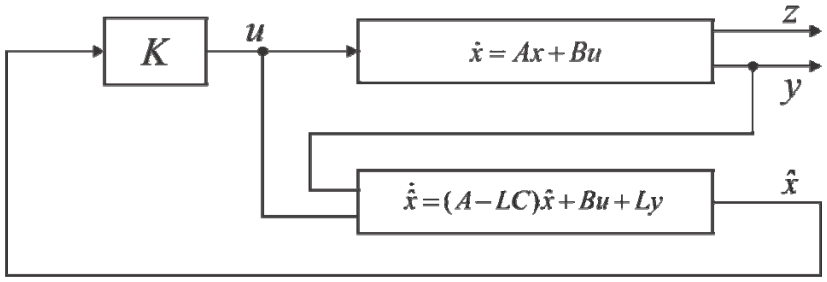

Figure 3.28 LQR feedback control system

Figure 3.28 shows a closed-loop system with a full-order observer. There are two matrices that guarantee the stability of the system, i.e., $A-BK$ and $A-LC$. Matrix $A-LC$ ensures the estimated states reflect the physical plant state. Based on the state estimation, matrix $A-BK$ ensures the system stability. Therefore, it is desired to place the poles of $A-LC$ further to the left in the LHP than the poles of $A-BK$ to achieve fast observer dynamics.

3.4.3. LQG estimation

Previous sections discussed how to develop LQR controllers to achieve stable magnetic levitation. This section and the following section discuss how to use control design methods to attenuate disturbances in the system. In this section, a Linear-Quadratic-Gaussian (LQG) controller is designed. The LQG controller is designed for an uncertain linear system which (1) is disturbed and has an additive white Gaussian noise, (2) does not have complete state information (i.e., not all the state variables are measured and available for feedback), and (3) has a control law subject to quadratic costs.

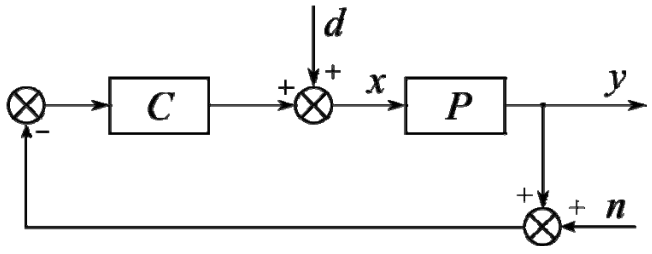

Figure 3.29 A plant subject to disturbance and noise

Figure 3.29 shows a block diagram of a plant subject to disturbance *d* and noise *n*. To facilitate the design process with a state-space system model, an equivalent block

diagram is generated.

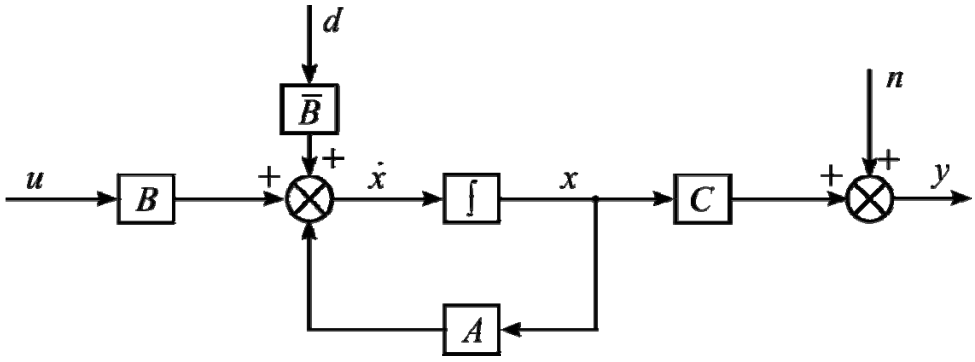

Figure 3.30 State-space model of a plant subject to disturbance and noise

Figure 3.30 shows a system, in its state-space representation form, subject to disturbance and noise. Suppose a LQR regulator has been designed for the system. From the discussion in the previous section, it is known that any choice of L in Eq. (3.118) for which $A-LC$ is asymptotically stable will make $\hat{x}$ converge to x, as long as the process dynamics are given by Eq. (3.99).

For a system shown in Figure 3.30, the output y is affected by measurement noise n and the process dynamics are affected by disturbance d. A more complete model for the process is re-written to include both n and d, i.e.,

$$\begin{aligned} \dot{x} &= Ax + Bu + \bar{B}d \\ y &= Cx + n \end{aligned} \tag{3.121}$$

Now the estimation error dynamics in Eq. (3.117) need to be updated to reflect the change in Eq. (3.121), which leads to:

$$\begin{aligned} \dot{e} &= Ax + \bar{B}d - A\hat{x} - L(Cx + n - C\hat{x}) \\ &= (A - LC)e + \bar{B}d - Ln \end{aligned} \tag{3.122}$$

Because of n and d, the estimation error might not converge to zero. This is especially

true for the open-loop unstable maglev system. Therefore, it is desired to attenuate the error e by appropriately choosing the feedback gain matrix L. This motivates the Linear-Quadratic-Gaussian (LQG) estimation problem.

The design goal is thus redefined for this LQG estimation problem. In this design, it is intended to find a matrix gain to minimize the asymptotic expectation of the estimation error e, which can be expressed as a cost function:

$$\overline{J} = \lim_{t\to\infty} \mathrm{E}\left[\left\| e(t) \right\|^2 \right] \tag{3.123}$$

In this design, the disturbance $d(t)$ and the noise signal $n(t)$, assumed uncorrelated to each other, are modeled as zero-mean additive white Gaussian noises (AWGN) [286-290]. The term white noise indicates these noise signals are random with constant power spectral density across the frequency band. Gaussian means each noise has a normal distribution in the time-domain. AWGN is a model of the general form of noise that control systems experience in real-world applications.

As noted at the beginning of this section, the LQR/LQG design process uses the state-space representation of the system, which relies on matrix algebra to derive the controller. Therefore, signals $d(t)$ and $n(t)$ are transformed to their power spectrum matrix forms to facilitate the controller design. The transformation is illustrated using the noise signal $n(t)$ as an example. Being a zero-mean white noise, the signal $n(t)$ has an autocorrelation of the form:

$$R_n(t_1, t_2) = \mathrm{E}\left[n(t_1) n'(t_1) \right] = Q_N \delta(t_1 - t_2). \tag{3.124}$$

It is also wide sense stationary since its mean is time-invariant and it autocorrelation $R(t_1, t_2)$ depends only on the difference of $\tau := t_1 - t_2$. From this it follows that the power

spectrum of $n(t)$ is frequency-dependent and can be calculated using the Fourier transformation of the autocorrelation function:

$$S_n(\omega) = \int_{-\infty}^{+\infty} R(\tau) e^{-j\omega\tau} d\tau = Q_N \tag{3.125}$$

In a similar fashion, the power spectrum of $d(t)$ can also be derived. Henceforth, $d(t)$ and $n(t)$ are substituted by their power spectrum matrices in the control design:

$$S_d(\omega) = Q_N,\ S_n(\omega) = R_N,\ \text{for } \forall \omega. \tag{3.126}$$

With the noise in the output signal y, using Eq. (3.122), the optimal LQG estimator gain can be calculated using:

$$L = PC^{\mathrm{T}} R_N^{-1} \tag{3.127}$$

with matrix P being the unique positive-definite solution to the following ARE:

$$AP + PA^{\mathrm{T}} + \bar{B} Q_N \bar{B}^{\mathrm{T}} - PC^{\mathrm{T}} R_N^{-1} CP = 0 \tag{3.128}$$

The optimal gain L, if implemented in system (3.120), represents a Kalman-Bucy filter [291-294].

To illustrate the design process, it is assumed that R_N is white noise with

$$R_N = \begin{bmatrix} 0.3 & 0.1 \\ 0.1 & 0.3 \end{bmatrix},$$

Let

$$\bar{B} = \begin{bmatrix} 0.01 \\ 0 \end{bmatrix}$$

represent a case in which a small disturbance is injected into the position signal, and

$$Q_N = \begin{bmatrix} 0.1 & 0 \\ 0 & 0.1 \end{bmatrix}$$

represent the power spectrum of the disturbance. Matrix L can be obtained by solving Eqs. (3.127) and (3.128):

$$L = \begin{bmatrix} 165.4 \\ 9.1E3 \end{bmatrix}.$$

Thus, the gain in the velocity feedback loop has a large value. It indicates that for this open-loop unstable system, with the disturbance is injected into the position channel, the observer needs a large velocity gain to guarantee an accurate estimation of the state variables.

Matrix L is found assuming that all the state variables are available. Therefore, to ensure that the system is asymptotically stable, it requires the following two conditions:

1. The system states in Eq. (3.121) are observable, which means the state variables are available for the calculation of matrix L.
2. The system in Eq. (3.121) is controllable when the reference signal u is ignored and the disturbance d is regarded as the sole input. This condition guarantees the possibility of attenuating the disturbance signal.

With these two conditions satisfied, the estimator gain L is determined by the magnitudes of Q_N and R_N. If R_N is small (compared to Q_N), the measurement noise n is small so the optimal estimator interprets a deviation of $\hat{y}$ from y as an indication that the estimate is inaccurate and needs to be corrected. This leads to a large matrix L and hence fast $A - LC$ poles. On the other hand, if R_N is large (compared to Q_N), the measurement noise n is large, and the optimal estimator is barely reacts to the deviation of $\hat{y}$ from y. This generally leads to smaller matrix L and slow $A - LC$ poles.

In practice, not all the state variables of the maglev plant are available, and therefore an observer is needed. The problem becomes designing an output-feedback controller for the system:

$$\begin{aligned} \dot{x} &= Ax + Bu \\ y &= Cx \\ z &= Gx + Hu \end{aligned} \tag{3.129}$$

The designed state-feedback controller is:

$$u = -Kx \tag{3.130}$$

Previous discussion showed how to design an LQR controller and suggested an LQG state-estimator in the form of:

$$\dot{\hat{x}} = \left(A - LC\right)\hat{x} + Bu + Ly \tag{3.131}$$

Therefore, it is possible to obtain an output-feedback controller using the estimated state in Eq. (3.131). Substituting Eq. (3.130) into (3.131) the following output-feedback controller is derived:

$$\dot{\hat{x}} = \left(A - LC - BK\right)\hat{x} + Ly \tag{3.132}$$

and the control signal becomes

$$u = -K\hat{x}\,. \tag{3.133}$$

The negative feedback transfer matrix can be calculated using:

$$C(s) = K(sI - A + LC + BK)^{-1}L\,. \tag{3.134}$$

With the state estimator, a LQG/LQR output feedback control system can be built:

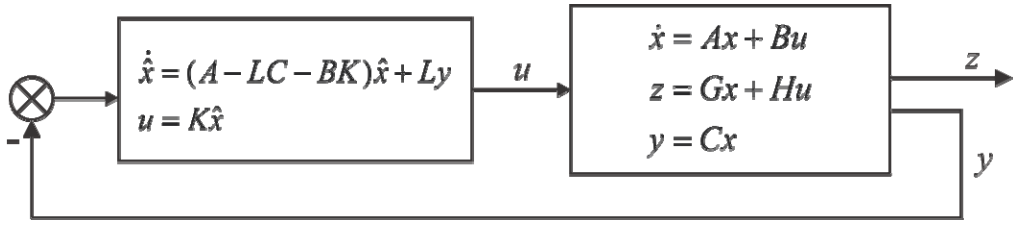

Figure 3.31 LQR/LQG feedback control

Figure 3.31 shows the block diagram of a closed-loop system with an LQR/LQG

controller. Since a state estimator is used in the system, it is important to ensure that the closed-loop system is stable. To address the stability issue, all the equations that define the closed-loop system are listed as follows for investigation:

$$\left.\begin{aligned} \dot{x} &= Ax + Bu \\ y &= Cx \\ \dot{\hat{x}} &= (A - LC)\hat{x} + By + Ly \\ u &= -K\hat{x} \end{aligned}\right\} \tag{3.135}$$

To check the stability of the system, it is possible to consider the dynamics of the estimation error $e = x - \hat{x}$ instead of the state estimate $\hat{x}$. If $e = 0$, $x = \hat{x}$, and the estimator is an accurate replication of state x. To this effect $\hat{x}$ is replaced by $x - e$ in Eq. (3.135), which yields:

$$\left.\begin{aligned} \dot{x} &= Ax + Bu \\ &= (A - BK)x + BKe \\ y &= Cx \\ \dot{e} &= (A - LC)e \\ u &= -K(x - e) \end{aligned}\right\} \tag{3.136}$$

From Eq.(3.136), the system equation can be written in matrix notation by choosing $\begin{bmatrix} x \\ e \end{bmatrix}$ as state variables, which leads to the following state-space model:

$$\begin{aligned} \begin{bmatrix} \dot{x} \\ \dot{e} \end{bmatrix} &= \begin{bmatrix} A - BK & BK \\ 0 & A - LC \end{bmatrix} \begin{bmatrix} x \\ e \end{bmatrix} \\ y &= \begin{bmatrix} C & 0 \end{bmatrix} \begin{bmatrix} x \\ e \end{bmatrix} \end{aligned} \tag{3.137}$$

In Eq.(3.137), matrix $\begin{bmatrix} A - BK & BK \\ 0 & A - LC \end{bmatrix}$ is triangular. The *separation principle* [295-298] says that the eigenvalues of the matrix are given by the eigenvalues of the state-feedback regulator dynamics $A - BK$ together with those of the state-estimator dynamics $A - LC$. If both matrices $A - BK$ and $A - LC$ are asymptotically stable, so is

the closed-loop system in Eq. (3.137).

3.5.Chapter Summary

This chapter discussed controller design methods that guarantee stable magnetic levitation and disturbance attenuation. As a general first step in control design, the mathematical model of the plant is derived. Based on the model, controllers are designed.

With the derived model, multiple controllers are designed using different methods. This research discusses the classical linear control design method, the nonlinear model-reference control design, and the optimal control design method. Stable levitation can be achieved using these design approaches. The issue of how to improve the system performance is also investigated.

Two methods to attenuate disturbances are discussed in this chapter. The first one is a novel AFC. This chapter presents an AFC designed based on a system with a PD controller. Disturbance is attenuated by manipulating the loop gain in the system. The second is a LQG method. The LQG controller is designed to attenuate Gaussian noise.

This chapter also discusses control designs to satisfy the time-domain (transient response) and frequency-domain (gain and phase margins) requirements. All the control designs discussed in this chapter are based on a nominal system model. In the next chapter, robust controller design is discussed. It is intended to address the system robustness issue when the modeling uncertainty exists.

Chapter 4. Control Design for Robustness

4.1. Chapter outline

Chapter 4 discusses robust controller design and reviews how the robustness issue is addressed with the controllers discussed in Chapter 3. In this chapter three robust controller design using QFT, H_∞, and a novel QFT/H_∞ approach are studied. In addition, this chapter proposes a design technique that combines the AFC and QFT/H_∞ controllers to obtain an AFC-enhanced QFT/H_∞ controller.

This chapter focuses on the discussion of robust controller design. The design methods discussed in this chapter, the QFT and the H_∞ methods, take different approaches to guarantee system robustness. Each of them has its distinct merits. Based on QFT and H_∞ controllers, the research suggests a combined QFT/H_∞ controller, which takes advantage of both and addresses the robustness issue from a new perspective. In an effort to provide disturbance attenuation, this research further proposes a novel design to embed the AFC into the system with QFT/H_∞. Experiments are designed to verify both the disturbance attenuation feature and system robustness are achieved with the proposed AFC-enhanced QFT/H_∞ controller. Experimental results are presented in Chapter 5.

This chapter is organized as follows: Section 4.2 provides a brief review of the background information of robust control. Section 4.3 discusses robustness of systems with controllers designed in Chapter 3. Section 4.4 discusses QFT controller design. Section 4.5 discusses H_∞ controller design. Section 4.5 proposes a novel QFT/H_∞ controller design. Section 4.6 discusses how to embed an AFC into a QFT/H_∞ to derive an AFC-enhanced QFT/H_∞ controller. Finally, Section 4.7 summarizes the key finding of this chapter.

4.2. Background Information

The system robustness issue can be understood by reviewing the controller design processes in Chapter 3. For all the classical linear controllers discussed, the synthesis processes are based on a nominal model of the plant. However, in applications the model always bears a certain amount of difference from the physical system. Many factors can contribute to this inaccuracy, such as an over-simplified model, a physical plant change during operation, ignored high-frequency dynamics, noise, and disturbance. The differences between the mathematical model and physical plant raise questions about the effectiveness of the designed controller, as Barmish and Jury [299] pointed out: "*If we used an inexact mathematical model to derive the controller, will the system perform satisfactorily?*"

A successful control design should be capable of maintaining system stability and performance despite uncertainties associated with system dynamics and/or working environments. Multiple design approaches have been proposed to deal with the uncertainty issue. Chapter 2 summarized the controllers designed to accommodate maglev system uncertainties. From a practical point of view, there are two categories of robust control design approaches reported for maglev systems: adaptive control, which is based on continuous identification of the plant and adjusting the controller accordingly [300], and robust control, which ensures preservation of certain properties of the control loop despite system uncertainties [301, 302]. In industrial applications, robust control has some advantages over adaptive control because (1) it is capable of dealing with both deterministic and stochastic models; (2) it can be designed using both time-domain and

frequency-domain methods; and (3) robust controllers for SISO systems can be expanded to MIMO systems without much modification.

There are three principal issues that need to be addressed when it comes to robust controller design [303]: the robust stability analysis, robustness margin, and robust synthesis. Robust stability analysis checks the stability of the designed closed-loop system with the uncertain plant and designed controller. Robust margin analysis finds the maximal uncertainty bounds that guarantee the performance specifications. And robust synthesis is the process of determining the controller parameters/forms to ensure the closed-loop system robustness. This chapter discusses how QFT and H_∞ design approaches address these three issues.

Before starting the robust controller design, this chapter briefly summarizes what uncertainties exist in the system models. Generally, there are two classical approaches to determine the linear-time-invariant (LTI) model of a physical plant. The first is an analysis method based on physical laws. This approach derives the system equations in the ordinary differential equation form, determines the appropriate form of the time-delay, and reduces the high order set of ordinary differential equations when necessary. The purely mathematical procedure of model simplification is an approximation [304-306]. In any approximation, it is unavoidable that some characteristics of the physical system are ignored. Therefore, the mathematical model is only a partially correct representation of the system.

The second approach to determine the model is generally referred to as “system identification.” It determines the mathematical model from experimentally measured

output of the system with particular system inputs. However, it is impossible to reproduce all of the inputs the system will experience during operation. Although robust identification methods [307-309] with classical parameter identification [310-313] have been reported and improved, it is still not possible to experimentally measure the system response to every possible signal over the entire frequency spectrum. In other words, no matter how the mathematical model of the system is derived, there are always uncertainties.

There are two types of model uncertainties. One is referred to as parametric (or structured) uncertainty, occurring when the actual plant parameters are unknown. Another is the nonparametric (or unstructured) uncertainty, which represents the ignored system dynamics, nonlinearities, and model variations [314]. Both parametric and nonparametric uncertainties can be expressed in two forms — the additive form and the multiplicative form. In most cases, both forms are present and their combination leads to mixed uncertainty [315-317].

Since uncertainties in the system are unavoidable, a controller should be designed to accommodate them. As a conventional approach, the robust control design methods assume the physical system to be an LTI model plus certain uncertainties. With this assumption, many control design methods have been proposed. They can be divided into two categories: the algebraic approach and the engineering approach. The algebraic approaches rely heavily on using mathematical tools to perform robust stability analysis on systems with parameter uncertainties [299, 301, 317, 318]. Advanced theorems have been proposed to test the robust stability with interval polynomials. For example, Kharitonov [319], Chapella and Bhattacharyya [320], and Barlett *et al.* [321] proposed different

mathematical methods to evaluate the robust stability of systems in differential equation form.

The engineering approaches, on the other hand, rely on the tools and techniques developed in classic control theory. The robust stability analysis uses the terms such as gain and phase margins. Mathematically, the stability of a closed-loop system depends on the norm of the open-loop transfer function. Robust margins are evaluated using the sensitivity and complementary sensitivity functions. Robust synthesis uses either the "loop shaping technique" [322] or the conventional parameter-based tuning methods. The loop shaping technique is discussed later in this chapter. Some of the conventional tuning methods have been proven successful in robust controller design, such as the standard Ziegler-Nichols method [323-325], Cohen-Coon method, Chien-Hrones-Reswick method, and Naslin method [326-329]. Discussion on these tuning methods is outside the scope of this thesis.

The control design methods discussed in this study use the engineering approaches. Sensitivity and complimentary sensitivity functions are used as references in guiding and evaluating the controller design. In particular, in designing a QFT controller, gain margin, phase margin, sensitivity function and complimentary sensitivity function are all transferred into "bounds" on the Nichols Chart. Then the controller transfer function is derived through a loop shaping process. In designing an H_∞ controller, a group of weight functions are selected based on the design goals. The weight functions are used in solving the controller, and they guarantee the frequency response of the designed system meet the requirements of sensitivity and complimentary sensitivity functions.

In the following section, the robustness of the maglev system with controllers

developed in Chapter 3 is discussed. The system robust stability is evaluated using gain and phase margins. They will be compared to the maglev system with QFT, H_∞, and QFT/H_∞ controllers, which not only guarantee the phase and gain margins, but also the sensitivity and complimentary sensitivity requirements.

4.3. Robustness of Linear Controllers

This section discusses the robustness of the controllers designed in Chapter 3. Three types of linear controllers – PID, lead, and LQR controllers – are investigated in this section. The MRC is an adaptive controller, and it has a logic function in the controller transfer function which makes it impossible to calculate the conventional gain and phase margin values. The robustness of the MRC controller is typically evaluated using different methods [330, 331] and is not discussed here.

4.3.1. PD, PID, and Lead Controller Robustness

For PD, PID, and lead controllers, the system robustness is evaluated using gain and phase margins. A gain margin quantitatively determines the magnitude of loop gain change a system can accommodate before losing stability. The phase margin quantifies the amount of phase lag that can be increased before the closed-loop system goes unstable.

Table 4.1 lists the gain and phase margins of the maglev system with PD, PID, and lead controllers. Three conclusions can be made from this table. (1) The maglev system is stable with these three controllers since the open-loop systems all have certain gain and phase margins. (2) The desired gain and phase margins are achieved except for the phase margin of the system with a lead controller. The pole in the transfer function causes the

decrease in phase margin. Future tuning is needed to increase the phase margin to a desirable value. (3) The Bode magnitude curve of the maglev system with a PID controller resembles the ideal curve, indicating the system with a PID controller has better system performance over the frequency spectrum.

Table 4.1 Gain and phase margins of maglev system with PD, PID, and Lead controllers

Controller	Controller transfer function	Gain Margin (dB)	Phase crossover frequency (rad/s)	Phase Margin (degree)	Gain crossover frequency (rad/s)
PD	$606+6s$	17.9	0	73.6	343
PID	$319.7+\frac{5187}{s}+3.017s$	7.25	32.5	63.7	154
Lead	$\frac{1.6\text{E}3(s+46.2)}{s+197}$	13.8	0	26.8	264

4.3.2. LQR Control Robustness

In this section, the robustness of a LQR controller is discussed. The robustness of the LQR differs from the PD, PID, and lead controllers in that it assumes all the states of the maglev plant are available. However, if a state observer is used to estimate the state variables, the gain margin is lost. This section also discusses how to recover the loop-gain for an LQR/LQG controller with an observer.

4.3.2.1. Robustness of LQR without an observer

Although an LQR controller may not be designed specifically for robustness, the closed-loop system is inherently robust with respect to process uncertainty [285].

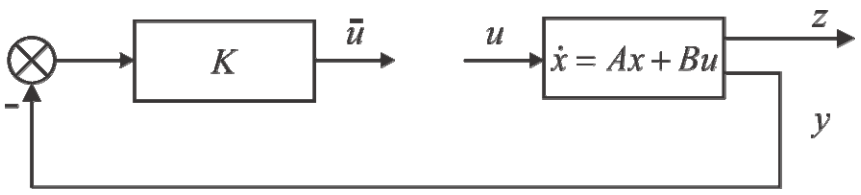

Figure 4.1 Open loop gain of system with an LQR controller

This study uses a system that has been discussed in Chapter 3 and shown in Figure 3.26, in which

$$\left.\begin{aligned} \dot{x} &= Ax + Bu \\ y &= Cx \\ z &= Gx + Hu \end{aligned}\right\} \tag{4.1}$$

is a general linear system, and K represents the matrix form of an already-designed LQR controller. If the system is open loop at the controller signal line, u becomes the system input and $\bar{u}$ the controller output. The open-loop transfer matrix from u to $\bar{u}$ is derived using the block diagram shown in Figure 4.1. The state-space model of the system in Figure 4.1 is given by:

$$\left.\begin{aligned} \dot{x} &= Ax + Bu \\ \bar{u} &= -Kx \end{aligned}\right\} \tag{4.2}$$

Using Eq. (4.2), the open-loop negative feedback transfer matrix of the system can be written as:

$$G_o = K\left(sI - A\right)^{-1} B \tag{4.3}$$

In this research, the plant is a SISO system, for which G_o becomes a scalar transfer function. *Kalman's Inequality* can be derived based on Eq. (4.3):

Kalman's Inequality [302]: When $H^T G = 0$, the Nyquist plot of $G_o(j\omega)$ does not enter a circle of radius one around -1, i.e.,

$$\left|1 + G_o(j\omega)\right| \geq 1, \text{ for } \forall\, \omega \in \mathbb{R}. \tag{4.4}$$

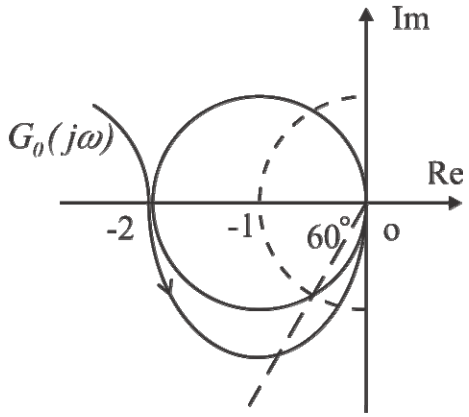

Figure 4.2 Nyquist plot of an LQR controller

Figure 4.2 shows a plot of Kalman's Inequality in the complex plane. The graph shows some interesting features of the system with a LQR controller:

(1) Increasing the feedforward loop gain: If the feedforward loop gain is multiplied by a constant k ($k > 1$), the Nyquist curve expands radially and hence the number of encirclements does not change. This indicates a positive gain margin of ∞.

(2) Decreasing the feedforward loop gain: If the system loop gain is multiplied by a constant k $(1 > k > 0.5)$, this Nyquist curve contracts radially but the number of encirclements still does not change. This indicates a negative gain margin of $20\log_{10}(0.5) = -6$ dB.

(3) Phase margin: If the loop phase increases by $\theta \in [-60, 60]$ degrees, this Nyquist curve rotates by θ but the number of encirclements does not change. This indicates a phase margin of ± 60 degrees.

If the loop is closed with a certain amount of loop gain uncertainty, a multiplicative uncertainty can be added to represent the loop gain uncertainties.

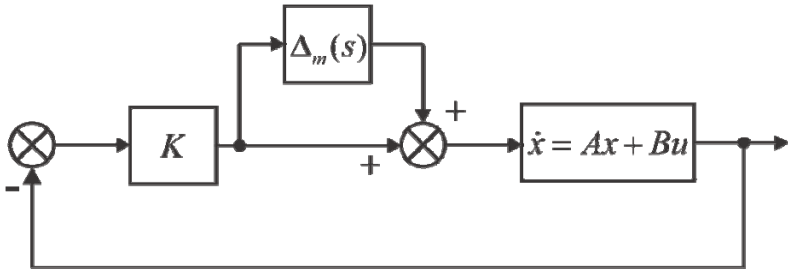

Figure 4.3 System with multiplicative uncertainty

Figure 4.3 shows a block diagram where a multiplicative uncertainty is added into the loop gain to represent the uncertainty associated with the system. The following discussion explains why the system is robust with the LQR controller.

Using Kalman's Inequality, the following inequality can be written:

$$\left|\frac{G_o(j\omega)}{1+G_o(j\omega)}\right| \le 2 \tag{4.5}$$

If the maximum norm of the uncertainty block is written as $\Delta_m(j\omega)$, the closed-loop system in Figure 4.3 remains stable as long as

$$\left|\frac{G_o(j\omega)}{1+G_o(j\omega)}\right| < \frac{1}{l_m(\omega)} \tag{4.6}$$

Comparing Eq. (4.5) and Eq. (4.6), the following bound can be derived:

$$\left|\frac{G_o(j\omega)}{1+G_o(j\omega)}\right| \le 2 < \frac{1}{l_m(\omega)} \tag{4.7}$$

A conclusion can be drawn from Eq. (4.7): *an LQR controller guarantees robust stability with respect to any multiplicative uncertainty with magnitude smaller than* $\frac{1}{2}$. Since generally multiplicative uncertainty is much larger than additive uncertainty, a LQR controller can accommodate additive uncertainty with a magnitude less than $\frac{1}{2}$, or even larger. In other words, the LQR controller derived in Chapter 3 can provide at least -6 dB of gain margin.

4.3.2.2. Loop-gain recovery

Section 3.3.1 has shown that the LQR controllers, with state-feedback, can provide desirable robustness properties. In order to achieve better system robustness, the open-loop gain can be shaped by an appropriate choice of the LQR weight parameter ρ in Eq. (3.140) and the variables in the controlled output z in Eq. (3.138).

As has been discussed, the LQR controller robustness is only guaranteed when all the state variables are available. If an observer is introduced to form an LQR/LQG controller, the feedback controller is not the *K* matrix shown in Figure 4.3. Thus, the gain margin of -6 dB is lost. Fortunately, it turns out that the LQR open-loop gain can be recovered to some extent for the LQG/LQR controller. The technique to recover the open-loop gain is referred to as *loop-gain recovery*.

In the following discussion, the loop-gain of the maglev system with an LQR/LQG controller is recovered partially. Since the maglev plant is a SISO system, and its transfer function does not contain any zero in the RHP, the disturbance gain matrix $\overline{B}$ in Eq. (3.161) can be chosen (or tuned) to be the same as the input gain matrix *B*:

$$\overline{B} = B \tag{4.8}$$

Then for a number $\sigma > 0$

$$R_N = \sigma \tag{4.9}$$

the open-loop gain of the output feedback LQR/LQG controller converges to the open-loop gain of the state-feedback LQR controller over a range of frequencies $[0, \omega_{\max}]$, i.e.,

$$C(j\omega)P(j\omega) \xrightarrow{\sigma \to 0} K(j\omega I - 1)^{-1} B, \ \forall \omega \in [0, \omega_{\max}] \tag{4.10}$$

In general, the larger $\omega_{\max}$ is, the smaller σ is needed to have the gains to match.

In this design, $\omega_{\max} = 1$ kHz. By choosing $\sigma = 0.2$, -3 dB of gain margin can be

recovered for the LQR/LQG controller. However, in order to achieve the loop-gain recovery gain, R_N is chosen to equal σ even if it is not an accurate description of the noise statics. It means the estimator is no longer optimized to reflect the actual noise.

The value of σ cannot be smaller than what is needed to recover the loop-gain. Although small values of σ can recover the loop-gain to -20 dB/decade, it does not prevent the loop-gain from decreasing as frequency increases. It has been suggested by Hespanha [332] that σ should be made just large enough to recover the loop gain to right above or at the crossover frequency. In this study, the maglev system is designed to have a 700 Hz crossover frequency; it turns out that $\sigma = 0.25$ makes the loop gain recover about -4.5 dB near the crossover frequency.

4.4. QFT Controller Design for the Maglev System

The previous section discussed system robustness with the controllers designed in Chapter 3. Two parameters, gain and phase margins, were used to quantify the system robustness to unstructured gain and phase variations in the feedback loop. However, the input-to-output gain of a nominally-stable uncertain system model will generally degrade for specific values of its uncertain element. Moreover, the maximum possible degradation increases as the uncertain elements are allowed to further deviate from their nominal values. In other words, a closed-loop system with guaranteed gain and phase margin is robustly stable (stability robustness), but it may not deliver a robust performance (performance robustness). More discussion on the difference between stability robustness and performance robustness can be found in Bernstein and Haddad, Doyle *et al*., and Skogestad and Poslehwaite [333-335]. In this research a QFT and an H_∞ controller are designed to

guarantee performance robustness. A novel method is proposed to derive a robust controller based on QFT and H_∞ controllers. This section discusses the design of a QFT controller.

4.4.1. System performance robustness

A maglev system, regardless of the control methodology used, must:

1. provide a reliable levitation during the operation of the maglev system,
2. offer robustness to model uncertainties and external disturbances, and
3. give repeatable, predictable performance for a variety of possible loading and working environment conditions.

Beside the system stability issue, the control design challenge for a maglev system is twofold: system performance robustness needs to be achieved (meaning to maintain the same or similar response characters despite system uncertainties) and the external disturbance needs to be attenuated.

A variety of methods have been proposed to deal with these two challenges. Yang *et al*. [336] reported the design of a robust output feedback nonlinear controller to achieve excellent output-tracking performance. In their research, a disturbance observer was introduced to suppress the effects of uncertainties by exploiting the cascade features of a backstepping design. A high-gain observer was included to estimate the immeasurable state of the system.

Vagia [337] reported a robust PID controller coupled with a feedforward compensator. In this research, the system was linearized at multiple operating points, and the feedforward compensator was utilized to provide nominal bias voltage. The PID

controller had multiple gains associated with multiple operating points. Shan [338] presented two disturbance rejection algorithms to improve the dynamics stiffness of a magnetic suspension stage. Shan suggested using an internal model principle-based control together with a frequency estimator based on adaptive-notch filtering to reject narrow-band disturbances with unknown frequencies.

Satoh *et al*. [339] proposed a Lyapunov function based robust nonlinear adaptive controller. The controller consisted of a pre-feedback compensator with an adaptive control mechanism and a robust stabilizing controller. Green [112] studied adaptive backstepping control (ABC) and feedback linearization control (FLC) for a single DOF maglev system. Green concluded that ABC control was superior to FLC in terms of system robustness. These researchers focused on designing systems to meet the classical measurement of robustness, i.e., gain margin and phase margin.

Although a controller can be designed to meet the gain and phase margin specifications, it might fail to guarantee a reasonable bound on the sensitivity [340]. In other words, even if the controller is designed successfully for robust stability, it may not be able to guarantee robust performance.

In order to address this issue, this section presents a control design approach based on QFT for maglev systems. This method addresses the performance robustness issue (with the bounds on the sensitivity function being guaranteed) despite the system uncertainties. QFT is a robust control design method attributed to Horowitz [341]. It was developed to design controllers for systems with model uncertainties and/or parameter variations that satisfy gain margin specifications and bounds on the sensitivity. The QFT design method

gives a variety of choices on the form of the final controller through its loop-shaping procedure.

In this study, a QFT controller is designed using the method proposed by Yaniv and Nagurka [340]. Yaniv and Nagurka proved that controllers can be designed to guarantee the gain and phase margin specifications and the sensitivity constraints for a set of plants. In this research a set of plants are used to represent the system uncertainties. To utilize the methods by Yaniv and Nagurka, the SISO maglev system is modeled using the transfer function form, plus the uncertainties associated with the model.

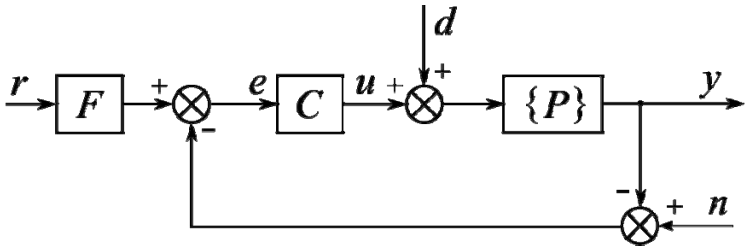

Figure 4.4 System block diagram of a system with QFT control

Figure 4.4 shows a system block diagram of a 2 DOF control architecture, which is the system configuration for the QFT controller design. In the block diagram, $\{P\}$ represents a set of plants, i.e., the original plant with uncertainties, F and C are the pre-filter and controller, respectively, that need to be designed, r is the reference signal, e is the error, u is the controller output, y is the system output, and d and n are disturbance and noise, respectively. Since this control scheme has two unknown transfer functions F and C to be determined, it is referred to as 2 DOF control scheme.

Table 4.2 Displacement and current gain constants

System Parameter	Calculated	Experimental Measurement
k_i	$56.82\frac{\text{m}}{\text{A-s}^2}$	$74.11\frac{\text{m}}{\text{A-s}^2}$
k_x	$4359.96\ \frac{\text{m}}{\text{s}^3}$	$5941.62\ \frac{\text{m}}{\text{s}^3}$

The system equations were derived in Eq. (3.16). The values of the system parameters, m, R, L, K_1, and K_2, were measured experimentally and are listed in Table 3.1. The values of two constants k_i and k_x in Eq. (3.16) can either be calculated using the parameters in Table 3.1 (using Eq. (3.13)) or measured experimentally. Table 4.2. shows two groups of k_i and k_x values, when $x_0 = 4.5$ mm and $i_0 = 0.345$ A. The difference between the calculated and directly measured k_i and k_x values is approximatly 30%. In this research, the direct measured values have larger instrument error because of the unreliable reading of the strain gauge in the experiment setup. Therefore, the calculated k_i and k_x values are used in controller design.

Many control designs in the literature assumed that k_i and k_x are constants. This assumption is incorrect if either the gap distance or the levitated load is changed. To demonstrate the variations of the values of k_i and k_x, five balls with masses equal to 8 gram, 12 gram, 16 gram, 20 gram, and 24 gram are levitated at gap distances of 3.5 mm, 4.5 mm, and 55 mm, then values of k_i and k_x are calculated for each case.

Table 4.3 shows the maglev plant transfer functions calculated with different masses at different gap distances. It is found that the values of k_i and k_x vary within two sets of values:

$$k_i \in \left[41.57,\ 96.24\right]\ \frac{\text{m}}{\text{A-s}^2} \tag{4.11}$$

and

$$k_x \in \left[3.57\times10^3,\ 5.61\times10^3\right]\ \frac{\text{m}}{\text{s}^3} \tag{4.12}$$

If the maglev system is designed to operate at a gap distance $x_0 = 4.5$ mm, the measured values are $k_i = 56.82\ \text{m}/\text{A-s}^2$ and $k_x = 4.36\times10^3\ \text{m}/\text{s}^3$. Comparing the values in Eq. (4.11) to those in Eq. (4.12), it is found that the value of k_i has 69.4% uncertainty and the value of k_x has 28.7% uncertainty. Therefore, the designs assuming constant k_i and k_x values missed a large part of system uncertainty.

The controllers proposed in this chapter are designed to accommodate the uncertainties and variations in the control plant. In other words, the designed controller should guarantee: (1) stability, which means the maglev system is able to levitate objects with different masses, and (2) robustness, which means the maglev system is able to maintain constant responses despite the model uncertainties and load changes (in this case, any change in the levitated mass *m*).

Table 4.3 System models variations as gap distance and m change

$P(s)$	m = 8 g	m = 12 g	m = 16 g	m = 20 g	m = 24 g
x_0 = 3.5 mm	$\frac{-96.24}{s^2 - 74.87^2}$	$\frac{-76.13}{s^2 - 74.87^2}$	$\frac{-65.93}{s^2 - 74.87^2}$	$\frac{-58.97}{s^2 - 74.87^2}$	$\frac{-53.83}{s^2 - 74.87^2}$
x_0 = 4.5 mm	$\frac{-80.42}{s^2 - 66.03^2}$	$\frac{-65.66}{s^2 - 66.03^2}$	$\frac{-56.86}{s^2 - 66.03^2}$	$\frac{-50.86}{s^2 - 66.03^2}$	$\frac{-46.43}{s^2 - 66.03^2}$
x_0 = 5.5 mm	$\frac{-72.01}{s^2 - 59.73^2}$	$\frac{-58.79}{s^2 - 59.73^2}$	$\frac{-50.92}{s^2 - 59.73^2}$	$\frac{-45.54}{s^2 - 59.73^2}$	$\frac{-41.57}{s^2 - 59.73^2}$

4.4.2. QFT Control Design

This section details the design of a QFT controller for the maglev system. The parameter variations are shown in Eqs. (4.11) and (4.12). The nominal plant is chosen as the model when gap distance $x_0 = 4.5$ mm (where, $k_i = 56.82\ \mathrm{m/A\text{-}s^2}$ and $k_x = 4.36\times10^3\ \mathrm{m/s^3}$). To derive an effective controller for this particular maglev system, the system performance specifications are chosen based on the linear control designs in Chapter 3 and suggestions in references [112, 342]. The stability margins and tracking specifications are listed below.

1. Stability margins: gain margin is at least 4.5dB, phase margin is at least 50 degrees.
2. Tracking specifications: 90% rise time $t_r \in [0.01,\ 0.5]$ seconds, overshoot $M_P \le 15\%$, and steady-state error $e_{ss} \le 5\%$.

To begin the QFT control design, the templates for the control plant must be calculated. Templates, as stated in reference [233], are "… *the set of all complex numbers for a given set of transfer functions, evaluated at a given frequency*…" The plant templates were determined by plotting the frequency response of the plant with the maximum and minimum uncertain values and then finding the boundaries of the responses.

The templates are built with the plants that cover the range of parameter uncertainties. In this research the maximum and minimum values of k_i and k_x are chosen to form the corners of the templates. With different combinations, the template corner transfer functions are:

$$G_1 = \frac{-96.24}{s^2 - 74.87^2} \tag{4.13}$$

$$G_2 = \frac{-53.83}{s^2 - 74.87^2} \tag{4.14}$$

$$G_3 = \frac{-41.57}{s^2 - 59.73^2} \tag{4.15}$$

$$G_4 = \frac{-72.01}{s^2 - 59.73^2} \tag{4.16}$$

Green [112] indicated that this maglev system was designed to operate at control signal frequencies less than 15Hz. However, research on the apparatus found that the infrared sensor noise had a natural frequency of 22Hz [343]. To avoid resonance of the sensor noise, the highest control signal frequency is limited to 10Hz, which is 62.8 rad/s. Five frequencies are used in this design: $\omega = 0.1$, 0.5, 3, 15, and 60 rad/s. With the four chosen corner transfer functions and five frequencies, the templates can be calculated and plotted.

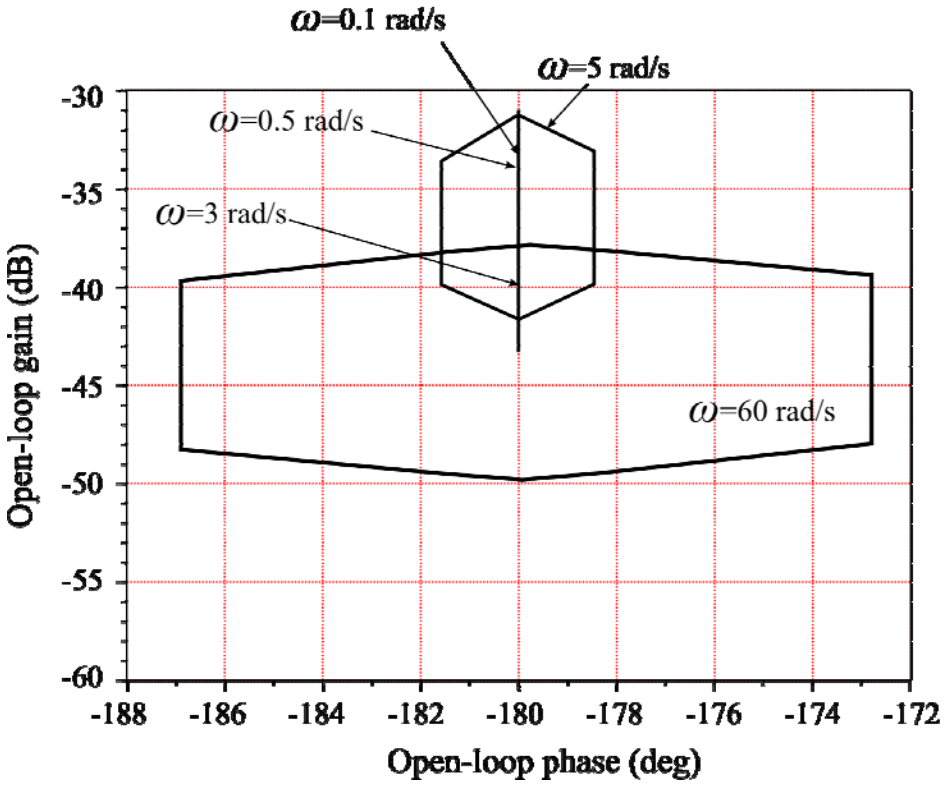

Figure 4.5 Plant templates for the QFT design

Figure 4.5 shows the templates of the maglev system in an open-loop gain vs. phase plot. The model uncertainties at the chosen frequencies have been included by the plant templates. The next step is to design for the command following ability, or "tracking," of the system. It guarantees that the system response to the command signal be the same despite system changes (such as a change in the operating point). The tracking models are determined using specifications discussed at the beginning of this section, with 90% rise time between 0.1 and 0.5 seconds and overshoot less than 20%. Using these criteria, the transfer functions for the upper bound T_{lb} and lower bound T_{ub} are calculated to be:

$$T_{lb} = \frac{4\text{E}4}{s^2 + 296s + 4\text{E}4} \tag{4.17}$$

and

$$T_{ub} = \frac{1.4\text{E}4}{s^2 + 156s + 1.4\text{E}6}. \tag{4.18}$$

The bounds need to be reshaped to relax the constraints on the higher frequencies. It helps in the design of the pre-filter since the relaxed constraints allow simpler pre-filter forms. To reshape the bounds, zeros and poles are added into the upper bound and the lower bound transfer functions, respectively. The reshaping process usually changes the response curve at higher frequencies. Based on the design goals, the reshaped bounds are updated to be:

$$T_{lb} = \frac{8\,\text{E}\,3}{(s^2 + 255.4s + 1\text{E}\,4)} \tag{4.19}$$

and

$$T_{ub} = \frac{750(s + 1000)}{(s^2 + 2.4\,\text{E}\,3s + 6.4\text{E}5)} \tag{4.20}$$

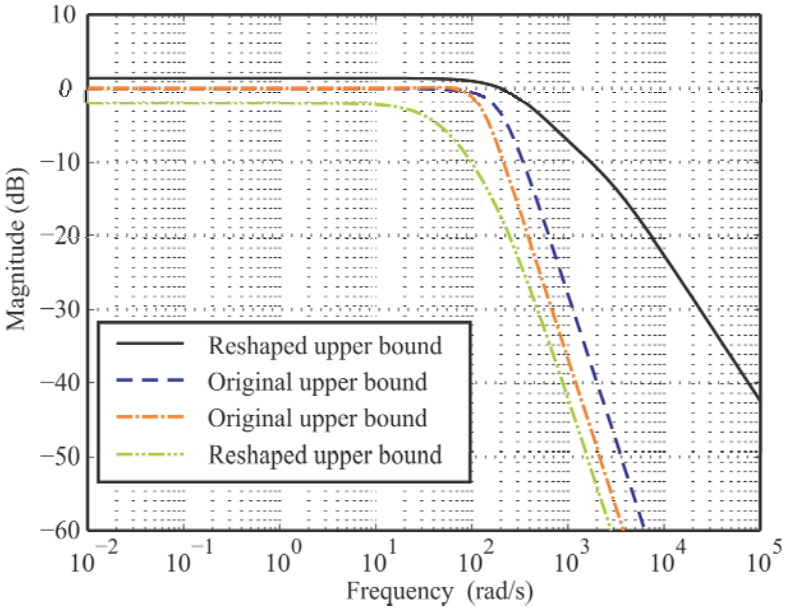

Figure 4.6 Bode magnitude plot of bounds

Figure 4.6 shows the Bode magnitude plot for the original model bounds and the "reshaped" model bounds. The tracking requirement has covered the disturbance rejection since disturbance can be treated as system changes in the maglev system. Hence, the disturbance rejection design is included.

The stability margin is determined based on the desired gain margin and phase margin for all plants in the set $\{P\}$. As shown in [233] the stability margin can be calculated using:

$$\mathrm{GM} = 20\log\left(1+\frac{1}{\mathrm{SM}}\right) \tag{4.21}$$

and

$$\mathrm{PM} = 180 - \cos^{-1}\left(\frac{0.1}{\mathrm{SM}^2} - 1\right) \tag{4.22}$$

The bounds and stability margins for the chosen frequencies are plotted on a Nichols chart for each frequency value using the MATLAB® QFT toolbox, as is shown in

Figure 4.7.

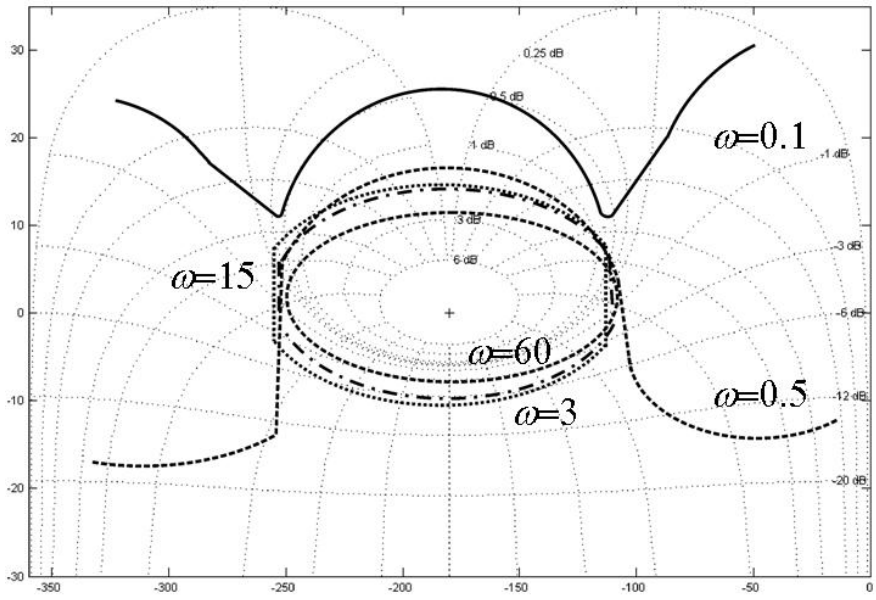

Figure 4.7 Design bounds on the Nichols chart

Using these bounds, the nominal loop transfer function L_0 should pass below and to the right of the oval bounds (stability bounds) and should lie above the line bounds (tracking bounds) at the specific frequencies [233]. To meet these requirements, poles and zeros are combined to shift L_0 on the Nichols Chart. One controller that ensures that the loop transfer function meets the specifications is found to be:

$$C(s) = \frac{251.2\left(\frac{s}{100}+1\right)\left(\frac{s}{115}+1\right)}{\left(\frac{s}{590}+1\right)\left(\frac{s}{97}+1\right)} \tag{4.23}$$

Controller $C(s)$ in Eq. (4.23) guarantees the system steady-state response meets the stability robust specifications. However, it does not ensure the frequency response curves stay between the bounds. Figure 4.8 shows a Bode magnitude plot of the bounds and

feedforward loop transfer functions. The frequency responses are outside of the bounds.

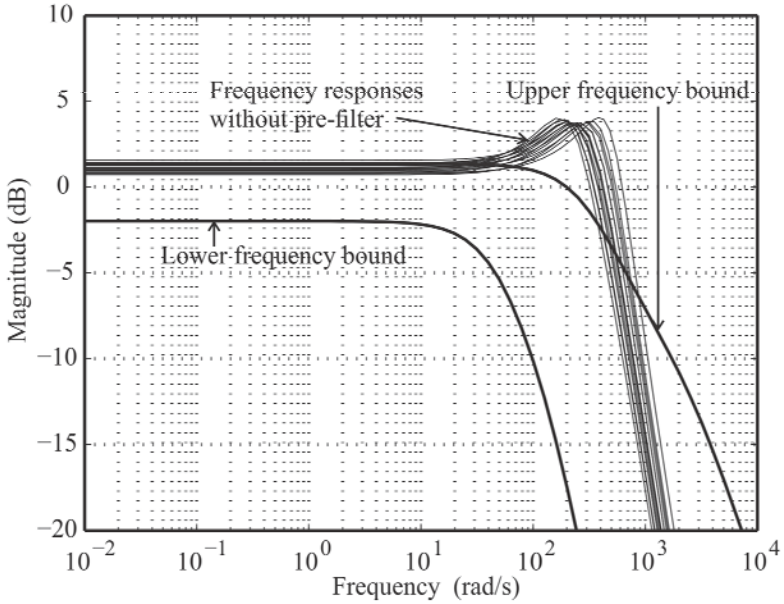

Figure 4.8 Frequency responses without pre-filter

In order to guarantee the transient response of the system also meets the design requirements, a pre-filter is needed. The pre-filter shapes the loop transfer function on the Bode magnitude plot by adding poles and zeros to the system transfer function. Once the response curves are inside the region between the upper and lower bounds, the transient response requirements are met. Using the traditional loop shaping technique, the pre-filter is found to be:

$$F(s) = \frac{9\mathrm{E}(-3)\left(\frac{s}{90}+1\right)}{\left(\frac{s}{50}+1\right)\left(\frac{s}{500}+1\right)} \tag{4.24}$$

Figure 4.9 shows the Bode magnitude plot of the maglev system with a QFT controller. The plot shows that the design goals in frequency domain have been achieved.

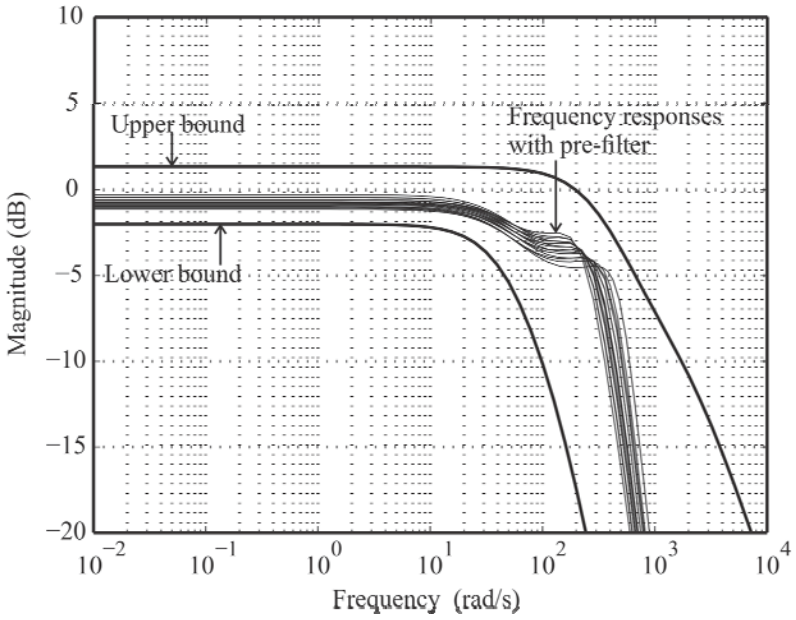

Figure 4.9 Frequency responses with pre-filter

With the derived pre-filter and the controller in Eqs. (4.24) and (4.23), respectively, a set of closed-loop systems can be built to represent different uncertainty states. Simulations of the whole uncertainty set are used to check if the system responses stay inside the predefined bounds in time-domain. If they do, the design is a success; otherwise, the controller and pre-filter transfer function need to be derived again.

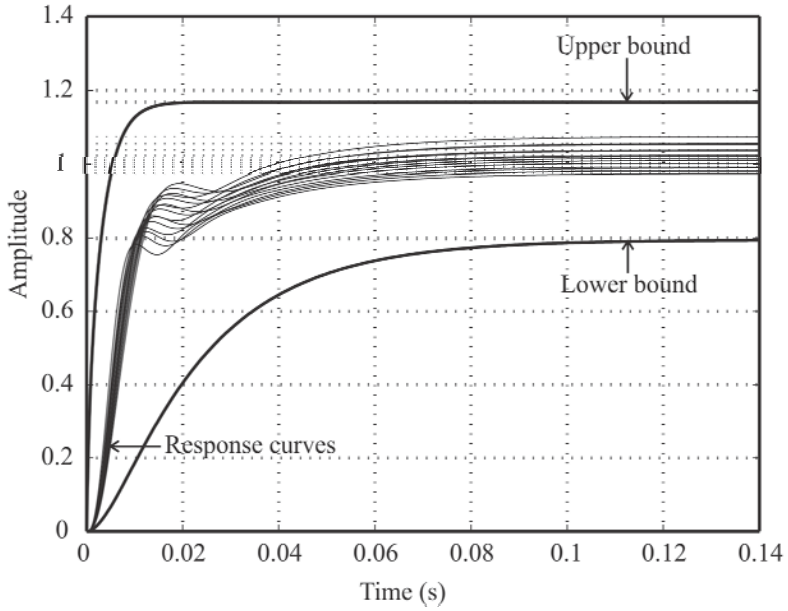

Figure 4.10 Step response of the closed-loop maglev system with uncertainties

To validate the system response with the derived controller and pre-filter, the step input response curves of a set of uncertain plants are plotted in Figure 4.10. It is shown that the system has met all the design specifications. In other words, this design successfully addresses the system uncertainty issue as well as the disturbance attenuation issue. The experiment validation of this design is postponed to Chapter 5.

4.5. H_∞ Controller Design for the Maglev System

4.5.1. H_∞ Control Design Introduction

In the previous section, robust control design using the QFT method has been discussed. With a 2 DOF control scheme, the designed controller has been able to deal with system uncertainty as well as attenuate disturbances. In this section, another robust/optimal control method, the H_∞ control design method, is designed for the same maglev plant. A comparison between these two methods is made at the end of this section, and a new

control design approach is proposed based on these two design methods.

H_∞ control is a novel robust control design approach introduced by Zames in the 1970s [344-346]. H_∞ control includes a variety of control schemes. To facilitate the system robustness issue, this study focuses on one particular H_∞ scheme with the name "mixed-sensitivity approach." Controller synthesis is formulated as a closed-loop transfer function shaping problem, mainly on the sensitivity function *S*, complementary sensitivity *T*, or their combination such as *CS*, where *C* is the resulting stabilizing controller. The combinations of different transfer functions lead to the name "mixed-sensitivity." Although this discussion is based on the SISO maglev system, it can be expanded to MIMO system cases.

4.5.2. H_∞ Design Problem Formulation

This design uses the linearized maglev system transfer function model to derive the controller. To illustrate this method, the system configuration shown in Figure 4.11 is assumed.

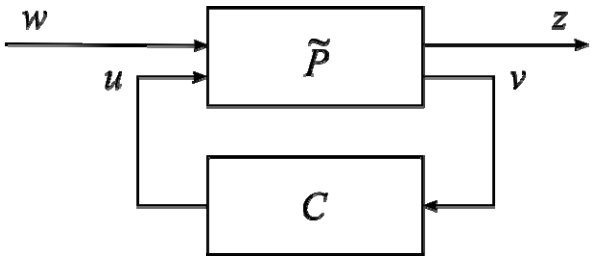

Figure 4.11 Generalized $H\infty$ control configuration

Figure 4.11 shows a block diagram of a generalized $H\infty$ control system. It consists of a generalized plant $\tilde{P}$, which is connected to a stabilizing controller *C*. The data in $\tilde{P}$

contain the plant information and all the weight functions, *C* is the controller that needs to be synthesized, *w* and *u* are exogenous input and control variables, respectively, *z* is an exogenous output that needs to be minimized, and *v* is the measured output that is fed back to the controller. Inside the feedback system, the signal *v* and *u* normally correspond to the input and the output of the controller. The signals *w* and *z* will be selected when solving the control problem.

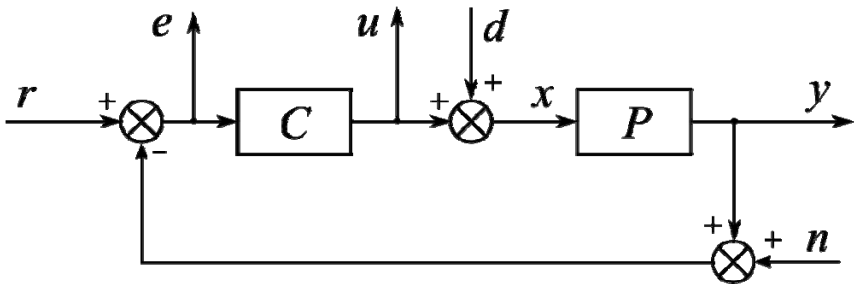

Figure 4.12 Feedback system signal definitions

In order to demonstrate how the controller is designed, a typical feedback system is introduced. In Figure 4.12, *r* is the reference signal, *d* is the disturbance, *n* is the noise, *e* is the error signal, *P* is the plant, and *u* and *y* are controller input and output, respectively. Figure 4.12 shows a system block diagram with three inputs: *r*, *d*, and *n*, and three outputs: *e*, *u*, and *y*. The input and output terminals and the block diagram elements can be rearranged in a way so that the transfer function from the input signal to the output signal can be easily derived.

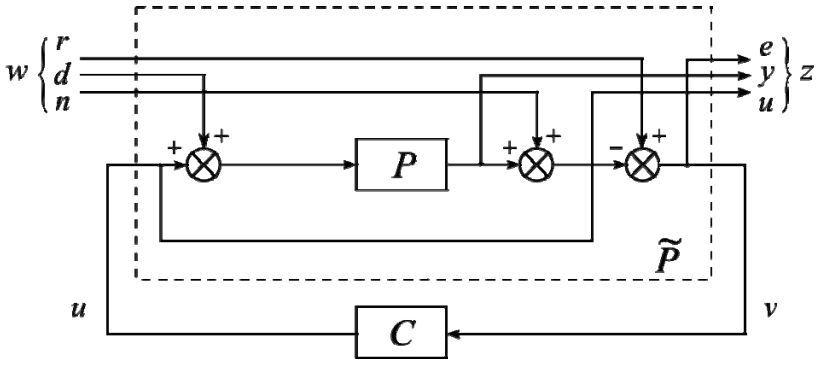

Figure 4.13 Rearranged block diagram of the feedback system

Figure 4.13 shows the rearranged block diagram of the system. Choosing

$$w = \begin{bmatrix} r \\ d \\ n \end{bmatrix},$$

and

$$z = \begin{bmatrix} e \\ y \\ u \end{bmatrix},$$

and assuming plant P and the three summers are one single plant, the system model of Figure 4.13 can be transferred into that of Figure 4.11. Figure 4.13 is more user-friendly for the controller design discussion; the rest of this study uses the block diagram in Figure 4.13. In the following discussion, noise n is assumed to be zero. As with other control designs, the first step of an H_∞ controller design is defining the design goals. There are two distinct goals, which will be discussed in next two sections.

4.5.2.1. H_∞ Control design for Disturbance Attenuation:

To attenuate disturbance, it is assumed that the exogenous input is a disturbance signal d (with reference signal $r = 0$). Normally the disturbance signal has a low frequency

spectrum [347]. Low frequency signals can be attenuated if the gain of the sensitivity function S is made small in the low frequency range. A performance weighting function w_1 can be selected to cast S into the desired shape. In other words, a stabilizing controller is synthesized to minimize $\|w_1 S\|$. This goal alone is impractical because there is no bandwidth limitation for the closed-loop system. The solution is to impose another weighting function w_2 on a suitable transfer function, for example *CS*. So the goal of this mixed-sensitivity S/CS problem is to find a stabilizing controller that minimizes:

$$\left\| \begin{bmatrix} w_1 S \\ w_2 CS \end{bmatrix} \right\|_\infty \tag{4.25}$$

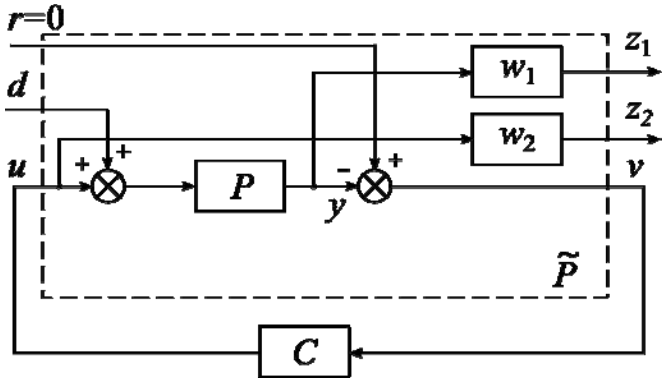

Figure 4.14 Generalized plant configuration for disturbance attenuation

With this setup, a generalized plant can be formed as shown in Figure 4.14. With properly chosen weighting functions w_1 and w_2, the output of P due to d can be minimized.

4.5.2.2. H_∞ Control design for Tracking:

Tracking a reference command is another control system design goal. Being able to follow a reference signal is critically important in some maglev applications. For example,

in designing a maglev position stage, it is desired to obtain a system that is able to follow the position signal closely and quickly. The system should be able to minimize the error between the reference signal r and the plant output y.

Some of the reference signals change rapidly; others change slowly. In order to accommodate the different reference signals, the system is usually designed for the signal that changes fastest. Therefore, it is desired that the gain of S be made small in the low frequency range. Thus, for SISO feedback systems the performance requirements for disturbance attenuation and tracking are similar, i.e., to minimize $\|w_1 S\|$, in which w_1 is a performance weighting function. The closed-loop system bandwidth also needs to be limited to avoid high frequency noise amplification. In order to derive a similar mathematical model as the disturbance attenuation case, the tracking performance design cast another weight w_2 on T. The resulting stabilizing controller is to minimize

$$\left\| \begin{bmatrix} w_1 S \\ w_2 T \end{bmatrix} \right\|_\infty \tag{4.26}$$

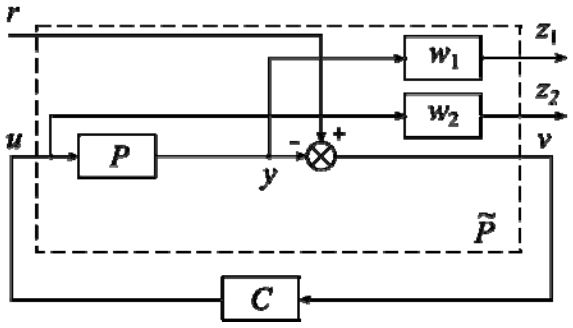

Figure 4.15 Generalized plant configuration for tracking problem

Figure 4.15 shows the configuration of a generalized plant for the tracking problem. Since both the sensitivity and complimentary sensitivity functions appear in the infinity

norm, this setup is also referred to as S/T mixed-sensitivity problem. Now that the system has been configured, the next step is to select the appropriate weighting functions.

4.5.2.3. Performance Weight Function Selection

In the previous section, the performance weight functions w_1 and w_2 have been used to shape the transfer functions of S, T, and their combinations. This section discusses how the performance weight functions are selected.

For the performance requirement discussed in the previous sections, the minimization of $\|w_1 S\|_\infty < 1$ is equivalent to $S(j\omega) < \frac{1}{|w_1(j\omega)|}, \forall \omega$. In other words, it is desired that the sensitivity gain $|S|$ lie below the reciprocal of the weighting function w_1 on the entire frequency spectrum. The gain $\frac{1}{w_1}$ can be plotted to verify that the sensitivity gain meets the desired requirements.

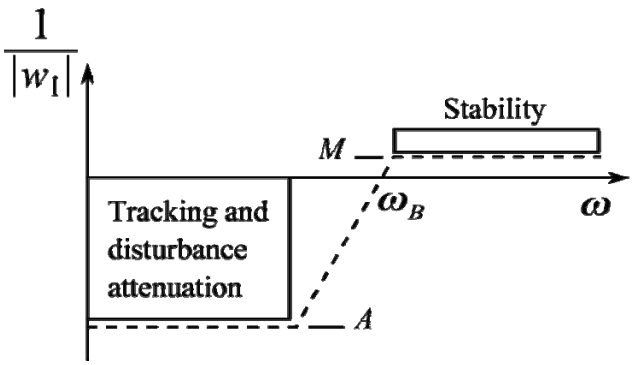

Figure 4.16 Design criteria for the performance weight reciprocal

Figure 4.16 shows a plot of the design criteria for the performance weight reciprocal. Three parameters related to the system performance are discussed in this research. As shown in Figure 4.16, these parameters are: A, the minimum steady-state

tracking error; ω_B, the minimum bandwidth (where $\frac{1}{|w_1|}$ crosses $\frac{\sqrt{2}}{2}$); and M, the maximum peak magnitude of S. Figure 4.16 shows A and M values that stay below the tracking and disturbance attenuation and stability region, respectively. With the abovementioned criteria, a weighting function can be selected as

$$w_1(s) = \frac{\frac{s}{M} + \omega_B}{s + \omega_B A}. \tag{4.27}$$

It is also recommended that an n^{th} order weight function be used for $w_1(s)$ if a larger slope in the low-frequency region is desired [335], i.e.,

$$w_1(s) = \frac{\left(\frac{s}{\sqrt[n]{M}} + \omega_B\right)^n}{\left(s + \omega_B \sqrt[n]{A}\right)^n} \tag{4.28}$$

The second weighting function, w_2, is chosen to constrain the bandwidth. It can be chosen such that the gain of $\frac{1}{w_2}$ forces a roll-off at a desired frequency. In this study, w_2 is selected to have a -20 dB/decade roll-off around the crossover frequency of about 700 Hz.

4.5.3. H_∞ Controller Design for the Maglev System

The maglev system is designed as a tracking problem using S/T mixed-sensitivity H_∞ synthesis. The goal is to synthesis a stabilizing controller that yields good tracking performance. Like the other control design cases, the design goals are chosen before beginning the controller design:

1. Normalized tracking error is less than 0.01 degree at all frequencies below 0.1 Hz;

2. Closed-loop bandwidth is within 1 kHz;

3. Gain margin is at least 4.5 dB, phase margin is at least 45 degrees.

The first step of the design is to choose a system model. This design uses the same model as the QFT design, i.e., the transfer function in Eq. (3.24). The parameter uncertainties have been defined in Eqs. (4.11) and (4.12). As a second step, the weight functions are selected. Using the above specifications, this study uses the following weighting functions:

$$w_1 = \frac{0.5s + 100}{s + 0.2} \tag{4.29}$$

and

$$w_2 = \frac{\frac{s}{500} + 2}{\frac{s}{300} + 1} \tag{4.30}$$

The reciprocals of Eqs. (4.29) and (4.30) can be plotted on a Bode magnitude graph.

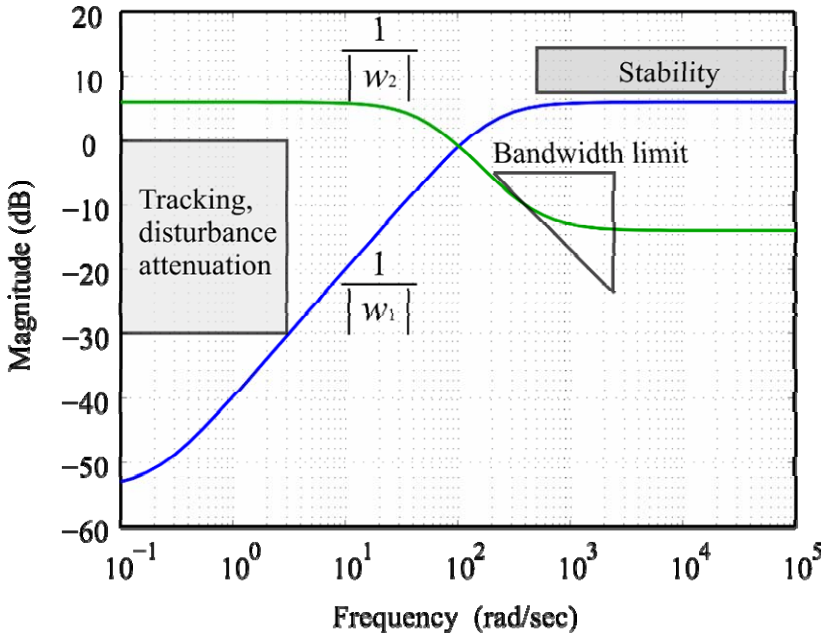

Figure 4.17 Bode magnitude plot of the weight function reciprocals

Figure 4.17 shows a Bode plot of the weight function reciprocals. The design goals

are plotted as constraint areas on the same plot. The chosen weight functions satisfy the design specifications.

The third step in this design is to form a generalized plant so the analytic form of the controller can be solved. To facilitate the controller solving process, this research constructs the generalized plant in a 4-block formulation [348-351]. Then the Glover-Doyle algorithm [352, 353] is used to solve for the H_∞ controller. With the maglev plant model and chosen weight functions w_1 and w_2, the generalized plant is constructed as follows:

$$\begin{bmatrix} \dot{x}_P \\ \dot{x}_{w_1} \\ \dot{x}_{w_2} \end{bmatrix} = \begin{bmatrix} A_P & 0 & 0 \\ -B_{w_1}C_P & A_{w_1} & 0 \\ B_{w_2}C_P & 0 & A_{w_2} \end{bmatrix} \begin{bmatrix} x_P \\ x_{w_1} \\ x_{w_2} \end{bmatrix} + \begin{bmatrix} 0 & B_P \\ B_{w_1} & 0 \\ 0 & 0 \end{bmatrix} \begin{bmatrix} r \\ u \end{bmatrix}$$
$$\begin{bmatrix} z_1 \\ z_2 \\ v \end{bmatrix} = \begin{bmatrix} -D_{w_1}C_P & C_{w_1} & 0 \\ D_{w_2}C_P & 0 & C_{w_2} \\ -C_P & 0 & 0 \end{bmatrix} \begin{bmatrix} x_P \\ x_{w_1} \\ x_{w_2} \end{bmatrix} + \begin{bmatrix} D_{w_1} & 0 \\ 0 & 0 \\ 1 & 0 \end{bmatrix} \begin{bmatrix} r \\ u \end{bmatrix} \tag{4.31}$$

The fourth step is to synthesize the controller using Eq. (4.31). The solution to this design is derived by simultaneously solving two Ricatti equations, one for the controller and one for the observer.

It is assumed that the control law

$$u = -K_c\hat{x} \tag{4.32}$$

guarantees the system performance, where $\hat{x}$ is the observer state. The state estimator equation is given by

$$\dot{\hat{x}} = A_P x - B_{w_1}C_P\hat{w} + B_{w_2}C_P u + Z_\infty K_e(y - \hat{y}) \tag{4.33}$$

where

$$\hat{w} = \gamma^{-2}\left(B_{w_1}C_P\right)^{\mathrm{T}} X_\infty \hat{x} \tag{4.34}$$

and

$$\hat{y} = \gamma^{-2} A_{w_1} \left(B_{w_1} C_P \right)^{\mathrm{T}} X_\infty \hat{x} \tag{4.35}$$

The controller gain K_c can be solved using the LQG design method discussed previously, and the estimator gain becomes $Z_\infty K_e$ with

$$K_c = \tilde{D}_{12} \left(\left(B_{w_2} C_P \right)^{\mathrm{T}} X_\infty + A_{w_1}^{\mathrm{T}} C_P \right) \tag{4.36}$$

in which $\tilde{D}_{12} = \left(A_{w_1}^{\mathrm{T}} A_{w_1} \right)^{-1}$, and

$$K_e = \left(Y_\infty B_{w_1}^{\mathrm{T}} - B_{w_1} C_P A_{w_2}^{\mathrm{T}} \right) \tilde{D}_{21} \tag{4.37}$$

in which $\tilde{D}_{21} = \left(A_{w_2}^{\mathrm{T}} A_{w_2} \right)^{-1}$. In addition,

$$Z_\infty = \left(I - \gamma^{-2} Y_\infty X_\infty \right)^{-1} \tag{4.38}$$

The terms X_∞ and Y_∞ are the solutions to the controller and estimator Ricatti equations, respectively:

$$X_\infty = \mathrm{Ric} \begin{bmatrix} A_P - B_{w_2} \tilde{D}_{12} \tilde{D}_{12}^{\mathrm{T}} C_{w_1} & -\gamma^{-2} B_{w_1} B_{w_1}^{\mathrm{T}} - B_{w_2} \tilde{D}_{12} B_{w_2}^{\mathrm{T}} \\ -\tilde{C}_{w_1}^{\mathrm{T}} \tilde{C}_{w_1} & -\left(A_P - B_{w_2} \tilde{D}_{12} \tilde{D}_{12}^{\mathrm{T}} C_{w_1} \right) \end{bmatrix} \tag{4.39}$$

and

$$Y_\infty = \mathrm{Ric} \begin{bmatrix} \left(A_P - B_{w_1} \tilde{D}_{21} \tilde{D}_{21}^{\mathrm{T}} C_{w_2} \right)^{\mathrm{T}} & -\gamma^{-2} C_{w_1}^{\mathrm{T}} C_{w_1} - C_{w_2}^{\mathrm{T}} \tilde{D}_{21} C_{w_2} \\ -\tilde{B}_{w_1} \tilde{B}_{w_1}^{\mathrm{T}} & -\left(A_P - B_{w_1} \tilde{D}_{21}^{\mathrm{T}} \tilde{D}_{21} C_{w_2} \right) \end{bmatrix} \tag{4.40}$$

Eqs. (4.33) through (4.40) are solved with MATLAB® robust control design toolbox routines. The H_∞ controller is solved to be (in its state-space form):

$$\left.\begin{aligned} \dot{x}_c &= \begin{bmatrix} -130 & 1 & 0 & -110 \\ -71\mathrm{E}3 & -36\mathrm{E}1 & 83\mathrm{E}4 & 16\mathrm{E}4 \\ 0 & 0 & -2.1\mathrm{E}-2 & 0 \\ 30 & 0 & 0 & -10\mathrm{E}2 \end{bmatrix} x_c + \begin{bmatrix} -140 \\ 31\mathrm{E}3 \\ 10 \\ -4.4 \end{bmatrix} y \\ u &= \begin{bmatrix} 84\mathrm{E}1 & 4.6 & -10\mathrm{E}3 & -21\mathrm{E}2 \end{bmatrix} x_c + \begin{bmatrix} -50\mathrm{E}1 \end{bmatrix} y \end{aligned}\right\} \tag{4.41}$$

The stability and performance check for this design will be discussed in the next section.

4.5.4. Stability and Performance Check

For a quick check of the H_∞ control design, the follow three steps are taken:

1. Closed-loop system is stable.

The closed loop stability is checked by calculating the eigenvalues of the closed-loop system. The eigenvalues for this design are:

$$\lambda = \begin{bmatrix} -993.01 \\ -115.36 + 225.61i \\ -115.36 - 225.61i \\ -137.78 \\ -82.88 \\ -50.78 \end{bmatrix} \tag{4.42}$$

Since all the eigenvalues have negative real parts, this closed-loop maglev system is asymptotically stable.

2. Frequency response meets performance specifications.

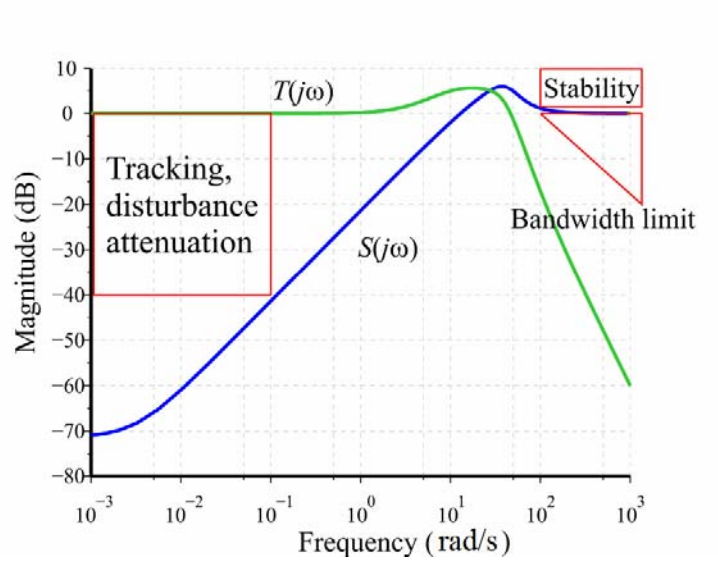

Figure 4.18 Bode magnitude plot of sensitivity and complimentary sensitivity functions

The frequency response of the system is checked by plotting the S and T

transfer functions on the Bode plot. Figure 4.18 shows a Bode magnitude plot of the sensitivity and complimentary sensitivity functions for this design. The plot shows that all the design goals on the frequency domain are met with the designed H_∞ controller.

3. Time-domain response is satisfactory

A time-domain check is postponed to Chapter 5, where the results of simulation studies and experiments are reported.

4.6. QFT/H_∞ Controller Design for the Maglev System

4.6.1. Background information of QFT/H_∞ control design

Previous sections discussed two robust design techniques: QFT and H_∞ methods. These methods take two different approaches to derive robust controllers. There were discussions in the control engineering community about the advantages and disadvantages of these two methods. For example, Doyle intended to prove that the QFT theory is unjustified by providing several counterexamples [354]. Yaniv and Horowitz replied to Doyle's criticisms and explained in detail why QFT is more efficient than other LTI controllers [355].

Sidi proposed a novel design method that combines the QFT and H_∞ methods, called the QFT/ H_∞ design approach [356-361]. This method takes the 2DOF control design architecture and uses the uncertainty template from the QFT method along with the weighting functions from the H_∞ method. It has all the advantages of both methods.

4.6.2. Comparing QFT and H_∞ methods

Since the QFT/H_∞ method is based on QFT and H_∞, it is necessary to compare these two methods to find out how they can be merged into a single design process. This discussion first summarizes the difference between these two methods. The major difference between the methods is that the H_∞ technique does not specify the acceptable closed-loop tracking input/output tolerance on the system response for all plant conditions in the set of $\{P\}$. Therefore, the controller is not tuned for all possible plant models.

The two methods also share some similarities:

(1) The QFT method specifies the desired output according to the bounds on the Bode plot, and uses the Nichols chart to derive the controller transfer function. On the other hand, the H_∞ method specifies the weighting functions to guarantee the magnitude of the output signal H_∞ norm, and derives the controller transfer function based on the weighting functions.

(2) The QFT method uses plant templates on the Nichols chart to quantitatively determine the uncertainties of the system. The H_∞ method calculates the maximum gain changes of the plant at all frequencies, and derives the limiting weighting function. However, only using the maximum gain changes of the plant may lead to over-design.

(3) The maximum peaking in $\left|T\left(j\omega\right)\right|$ and $\left|S\left(j\omega\right)\right|$, β and γ, is used by the QFT technique, which manipulates the plant templates and guarantees they do not cross the standard closed-loop specification contours of β and γ in either the Nichols chart or inverted Nichols chart. The same effect is achieved by the H_∞ method by

defining the weighting function of $\frac{1}{w_1(j\omega)}$ and $\frac{1}{w_2(j\omega)}$ to have maximum peaking resembling β and γ, respectively.

(4) With the H_∞ technique, the sensor noise is minimized by specifying $w_2(s)$. With the QFT method, the sensor noise is minimized by manipulating the nominal open-loop transfer function $L(j\omega)$ in the Nichols chart. The noise gain at the high frequency range is minimized while the tracking sensitivity bound, which is also frequency-dependent, is satisfied.

(5) Both the QFT and H_∞ methods can provide multiple analytic controller forms. The QFT controller is derived using the loop shaping technique, with the plant uncertainty and input-output sensitivity specified, and a trade-off between system performance and controller complexity. The boundaries of $L(j\omega)$ can be derived from the Nichols chart. The H_∞ controller is designed by solving the two Riccati equations in Eqs. (4.39) and (4.40) simultaneously. If different weighting functions are chosen, different H_∞ controllers are derived. The design process is a trade-off between the controller complexity and the weighting functions while the system performance is guaranteed.

(6) Finally, the system architecture of these two design approaches are different: the QFT controller uses a second DOF with a pre-filter F(s) in the system, whereas the H_∞ controller uses a 1DOF architecture.

In summary, the QFT and H_∞ methods both solve the robustness problem using system performance specifications. QFT emphasizes the quantitative system variation and minimizes the change in response due to system uncertainties with two control blocks. H_∞

embeds the analytical weighting function in solving the Riccati equations and mathematically minimizes the norm of undesirable signals.

4.6.3. QFT/H_∞ Control Design

This study adopts an approach that combines the QFT and H_∞ methods. In order to facilitate using both QFT and H_∞ methods, the system configuration is updated to form a 2DOF control system, as shown in Figure 4.4.

The design process is divided into three stages: (1) identifying the system model and uncertainties, along with the frequency range for frequency-domain analysis, (2) calculating the tracking input-output sensitivity specifications, i.e., the acceptable changes in $\left|T\left(j\omega\right)\right|$, and then designing for robust system performance using the H_∞ norm optimization, and (3) shaping the closed-loop gain into the tracking bounds (i.e. maximum and minimum of $\left|T\left(j\omega\right)\right|$) using the pre-filter $F\left(s\right)$.

In the second stage, the tracking input-output sensitivity (robust performance) specifications are calculated and thus the sensitivity weighting function can be determined. This study provides a brief discussion on how the sensitivity function, input-output sensitivity specification, and model uncertainties are related to each other.

The original definition of the sensitivity function $S(s)$ is given by Bode [362] as

$$S_P^T = \frac{\dfrac{\partial T}{T}}{\dfrac{\partial P}{P}} = \frac{d\ln(T)}{d\ln(P)} = \frac{1}{1+G(s)P(s)} = \frac{1}{1+L(s)} \tag{4.43}$$

Bode explained Eq. (4.43) as "*The variation in the final gain characteristic in dB, per dB changes in the gain of P, is reduced by feedback in the ratio of* $1+L(s)$." In other words,

the sensitivity function $S(s)$ evaluates how the change in plant P affects the closed-loop system output, and it is determined by loop gain $L(s)$.

Eq. (4.43) includes two partial differential terms, making it difficult to calculate S_P^T. As an alternative, Horowitz and Sidi [360, 361] suggested that Eq. (4.43) can be replaced by

$$\left|S(j\omega)\right| = \frac{\max\left(\Delta\left|T(j\omega)\right|\right)}{\max\left(\Delta\left|P(j\omega)\right|\right)} \tag{4.44}$$

in which $\max\left(\Delta\left|T(j\omega)\right|\right)$ is the maximum acceptable change between the system performance bounds, and $\max\left(\Delta\left|P(j\omega)\right|\right)$ is the maximum change in the plant gain (i.e., the maximum uncertainty.)

In the following discussion, a QFT/H_∞ controller is designed following the seven steps suggested by Sidi [360]:

1. Determine a nominal plant.

This study uses the maglev plant defined in Eq. (3.51) with the parameter changes in Eqs. (4.11) and (4.12).

2. Determine the design goals.

This study uses the design goals defined in Section 4.2. The time-domain specifications have been transferred into their frequency domain equivalences in Eqs. (4.17) and (4.18).

3. Find the weight function for robust stability.

In this design, the frequency vector is chosen to be

$$\omega_{QFT} = \left[0.1,\ 0.5,\ 1,\ 5\ ,10,\ 50,\ 100,\ 200,\ 500,\ 1000\right]\ \text{rad/s}, \tag{4.45}$$

to cover a broader operation range. The acceptable sensitivity function value at each

frequency is calculated using Eq. (4.44) and listed in Table 4.4.

Table 4.4 Calculate the sensitivity values over the frequency spectrum

ω_{QFT} (rad/s)	0.1	0.5	1	5	10	50	100	200	500	1000
$\Delta\lvert T\rvert$ (dB)	4.11	4.11	4.11	4.37	5.95	10.84	19.35	25.06	30.51	40.48
$\Delta\lvert P\rvert$ (dB)	6.43	6.43	6.45	6.81	7.22	16.45	25.50	30.95	41.20	55.45
$\lvert S\rvert$ (dB)	2.32	2.32	2.34	2.44	1.27	5.61	6.15	5.89	10.69	14.97

By plotting the $\lvert S\rvert$ values on a Bode plot, the sensitivity function can be determined by the loop shaping technique.

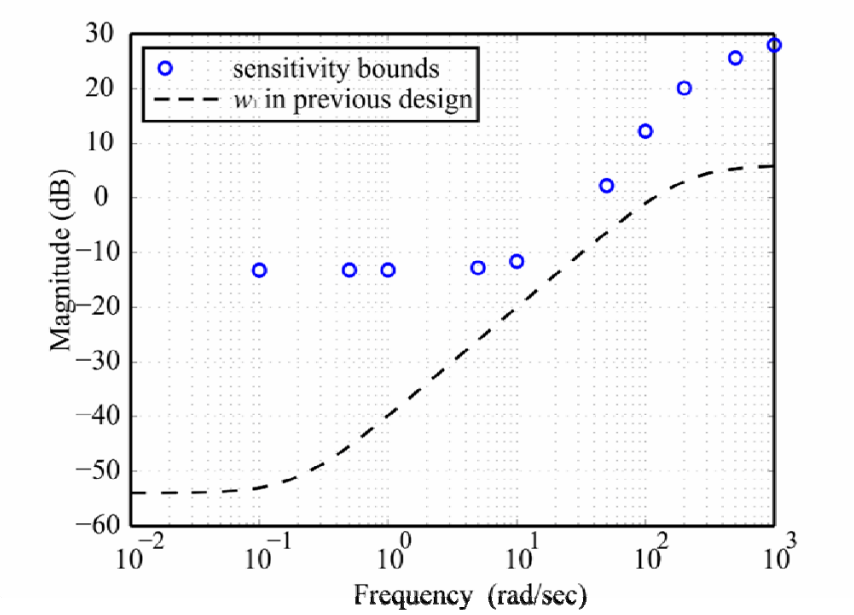

Figure 4.19 Sensitivity bounds and the *w*1 in previous design

Figure 4.19 shows a plot of the desirable sensitivity function values from Table 4.4, along with the weighting function w_1 used in Section 5, the H_∞ control design. The w_1 provide too much attenuation in both low and high frequency ranges. This study uses the

loop shaping technique to find a new w_1 weighting function.

4. Find a new sensitivity weight functions based on the sensitivity values.

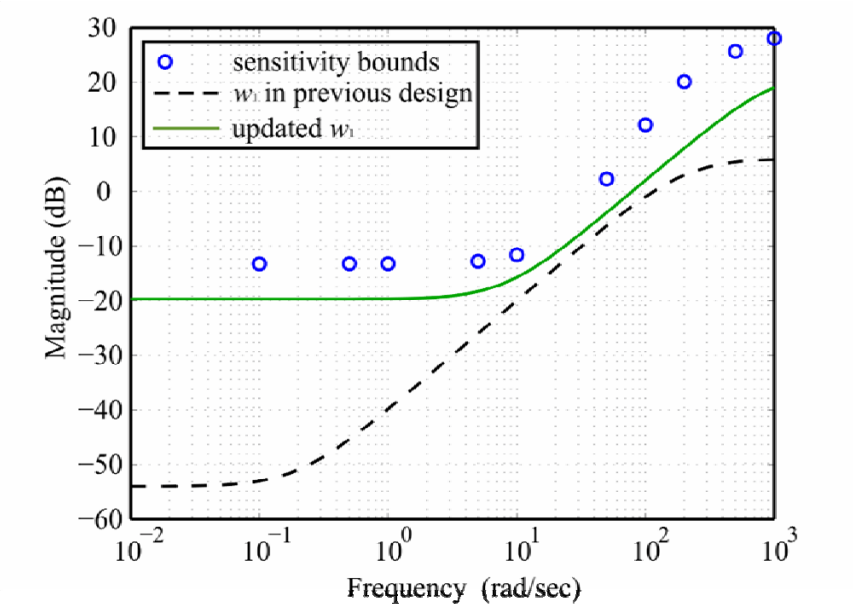

Figure 4.20 Update the $w1$ function for $H\infty$ norm calculation

Figure 4.20 shows a plot of the updated weighting function $\tilde{w}_1$ along with the original w_1 and the sensitivity function values. The transfer function for the updated weighting function is:

$$\tilde{w}_1 = \frac{1.5s + 100}{19 + 155} \tag{4.46}$$

5. Solve the H_∞ norm optimization.

In this design, w_2 uses the same transfer function as in Eq. (4.30), since w_2 is proved to be appropriate in Figure 4.17. With $\tilde{w}_1$ and w_2, the H_∞ controller can be solved using Eqs. (4.33) through (4.40). The solved H_∞ controller is:

$$\left.\begin{aligned}\dot{x}_{1c} &= \begin{bmatrix} -130 & 1 & 0 & -110 \\ -52\text{E}2 & -45 & -82\text{E}5 & 14\text{E}4 \\ 0 & 0 & -10\text{E}2 & 0 \\ 30 & 0 & 0 & -10\text{E}2 \end{bmatrix} x_{1c} + \begin{bmatrix} -130 \\ 96\text{E}4 \\ 110 \\ -4.4 \end{bmatrix} y \\ u &= \begin{bmatrix} 12 & 0.59 & 11\text{E}4 & -19\text{E}2 \end{bmatrix} x_{1c} + \begin{bmatrix} -13\text{E}3 \end{bmatrix} y \end{aligned}\right\} \tag{4.47}$$

Comparing the two H_∞ controllers in Eqs. (4.41) and (4.47), it is found that the controller in Eq. (4.47) has smaller feedback gains in the plant state feedback loop. This is due to the change in the weighting function. Figure 4.20 shows that w_1 has been shifted up in the Bode magnitude graph to derive $\tilde{w}_1$, which means the constraints on the weighting function are relaxed. Therefore, the feedback loop gains can be reduced.

6. Use the derived H_∞ controller to evaluate the closed loop system.

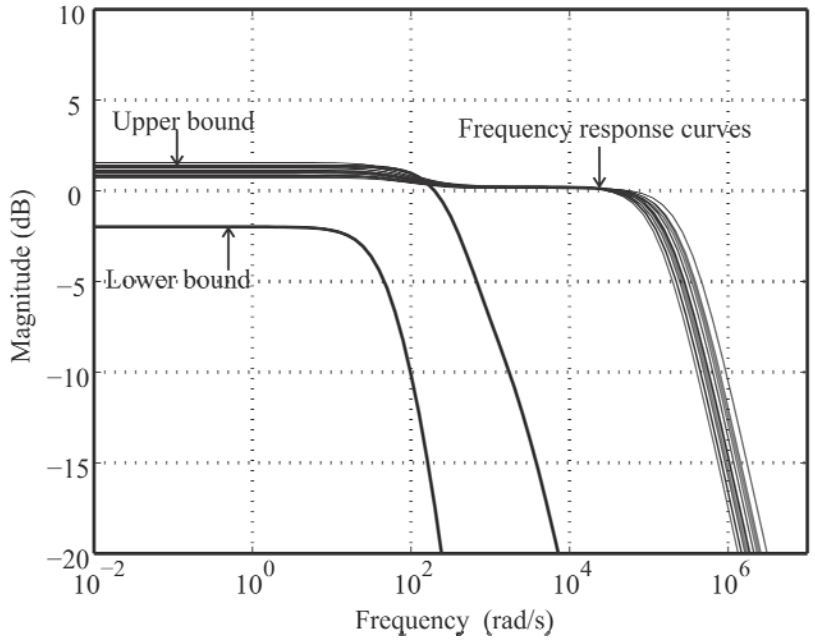

Figure 4.21 Response of the uncertain systems along with the bounds

With the derived H_∞ controller, the system response is evaluated with the extremes in the plant transfer function variations. If the system response is between the

specified upper and lower bound, there is no need for a prefilter. If not, a prefilter needs to be designed to shift the system response into the acceptable region. If the system response variation exceeds the difference between the upper and lower bounds, the weighting function needs to be reconsidered.

Figure 4.21 shows a plot of the responses of the uncertain system, along with the desirable upper and lower bounds. It indicates that system responses need to be shifted in between the lower and upper bounds. Therefore, for this design, a prefilter is necessary.

7. Use the loop shaping technique to design a pre-filter.

The prefilter design process has been discussed in Section 4.2. One of the pre-filters that can shift all the curves between the bounds takes the following form

$$F(s)=\frac{(9.5\,\mathrm{E}-2)\left(\frac{s}{70}+1\right)}{\left(\frac{s}{45}+1\right)\left(\frac{s}{605}+1\right)} \tag{4.48}$$

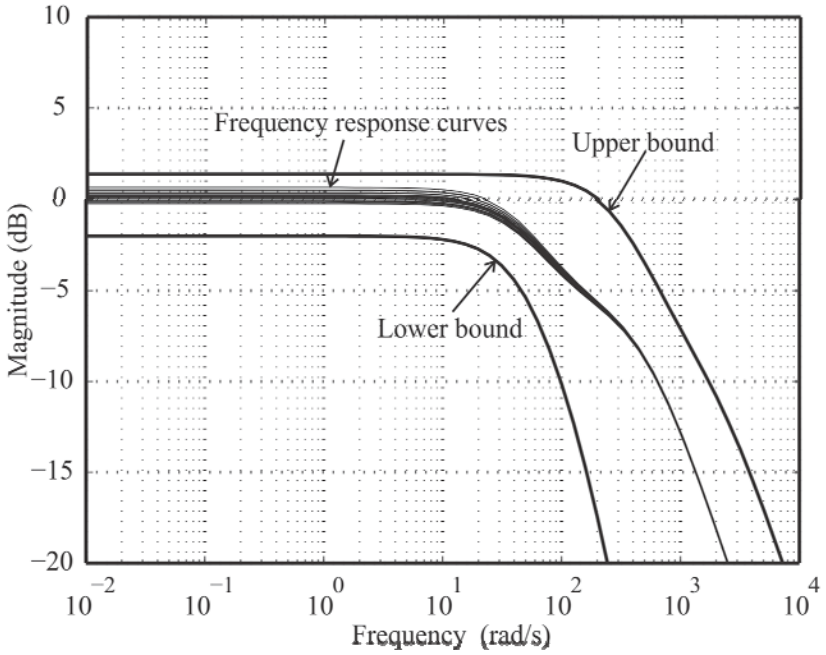

Figure 4.22 Closed-loop system response with a prefilter

Figure 4.22 shows a plot of the closed-loop system with the prefilter in Eq. (4.48). The plot shows that the frequency responses of the closed-loop systems are inside the bounds. Therefore the design goals have been achieved.

4.6.4. Evaluation of the Closed Loop System Performance

Finally, the closed loop system is checked to see if all the design goals are met.

1. System stability:

The closed loop system stability is checked by calculating the eigenvalues of the closed-loop system. The eigenvalues for this design are:

$$\lambda = \begin{bmatrix} -1000 \\ -502.34 + 861.86i \\ -502.34 - 861.86i \\ -40.25 \\ -66.99 + 1.71i \\ -66.99 - 1.71i \end{bmatrix} \tag{4.49}$$

All the eigenvalues have negative real parts. Therefore, the closed loop maglev system with the QFT/ H_∞ controller is asymptotically stable.

2. Frequency-domain response

Since the QFT/ H_∞ controller is designed according to the frequency-domain specifications, its frequency-domain response automatically satisfies all the design requirements.

3. Time-domain response.

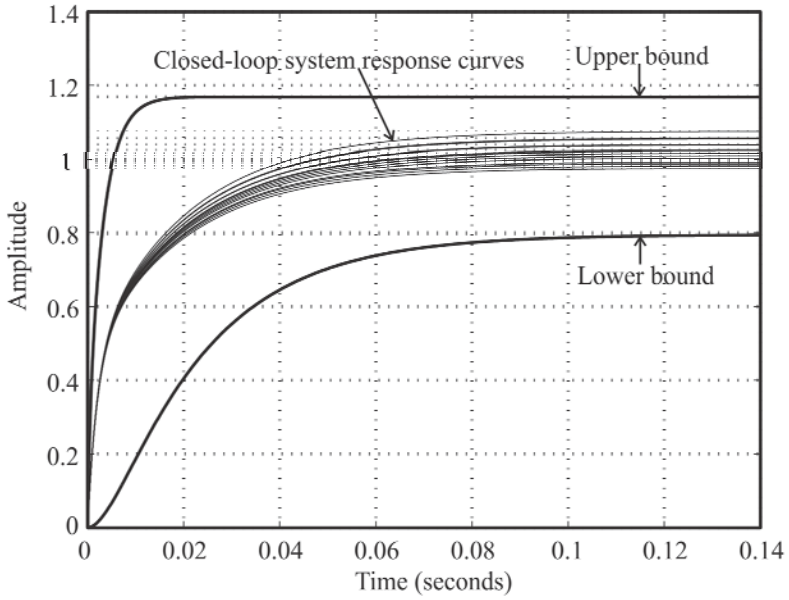

Figure 4.23 Step responses of the closed-loop system with uncertainties

Figure 4.23 shows a plot of the step responses of the closed-loop system with uncertainties. The plots shows that the time-domain system response curves are in the upper and lower bounds. Therefore, the design goals are achieved. The experiment validation with the QFT/ H_∞ design is postponed to Chapter 5.

4.7. AFC-enhanced QFT/H_∞ Controller Design

In the previous section, a QFT/ H_∞ method was designed to guarantee the performance robustness of the maglev system. This section proposes a method to embed the AFC into the QFT/ H_∞. The derived AFC-enhanced QFT/ H_∞ method not only guarantees the stability and performance robustness, but also provides a disturbance attenuation feature to the maglev system. The desired characteristics of a maglev system (as discussed in Section 4.4.1) are achieved with this single controller. To the best of the author's knowledge, the AFC-enhanced QFT/ H_∞ controller has never been reported previously.

The design of this controller starts with plant with uncertainty and a disturbance, as shown in Figure 4.24.

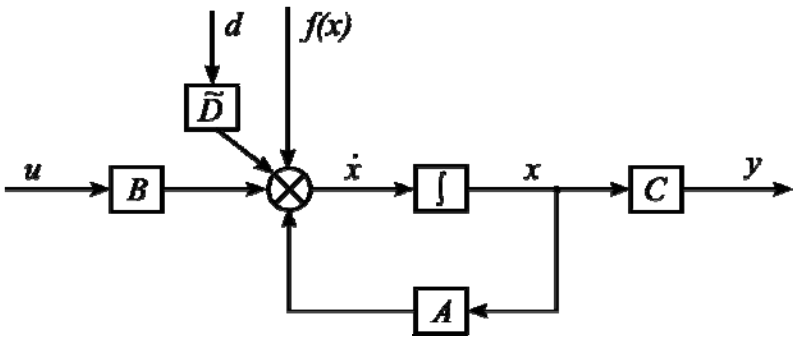

Figure 4.24 A plant with uncertainty and a disturbance

This system can be modeled using the following equations:

$$\begin{aligned} \dot{x} &= Ax + Bu + f(x) + \tilde{D}d \\ y &= Cx \end{aligned} \tag{4.50}$$

where $f(x)$ is an uncertainty term, d is the external disturbance, u is the input signal, y is the system output, A, B, C, and $\tilde{D}$ are constant matrices. A QFT/ H_∞ controller can be

designed for this system using the techniques discussed previously. The QFT portion of the controller deals with the uncertainty term $f(x)$, and the H_∞ portion of the controller stabilizes the following system,

$$\begin{aligned} \dot{x} &= Ax + Bu + \tilde{D}d \\ y &= Cx \end{aligned} \tag{4.51}$$

4.7.1. Controller Design with Known Disturbance ***d***

If the disturbance d is a known signal (such as one measured from an accelerometer), Eq. (4.51) can be written as:

$$\begin{aligned} \begin{bmatrix} \dot{x} \\ \ddot{x} \end{bmatrix} &= \begin{bmatrix} 0 & 1 \\ k_x & 0 \end{bmatrix} \begin{bmatrix} x \\ \dot{x} \end{bmatrix} + \begin{bmatrix} 0 \\ -k_x \end{bmatrix} i + \begin{bmatrix} 0 \\ 1 \end{bmatrix} d \\ y &= \begin{bmatrix} 1 & 0 \end{bmatrix} \begin{bmatrix} x \\ \dot{x} \end{bmatrix} \end{aligned} \tag{4.52}$$

where $A = \begin{bmatrix} 0 & 1 \\ k_x & 0 \end{bmatrix}$, $B = \begin{bmatrix} 0 \\ -k_x \end{bmatrix}$, $\tilde{D} = \begin{bmatrix} 0 \\ 1 \end{bmatrix}$, and $C = \begin{bmatrix} 1 & 0 \end{bmatrix}$.

The H_∞ portion of the controller takes the form of $i = Kx = \begin{bmatrix} k_1 & k_2 \end{bmatrix} \begin{bmatrix} x \\ \dot{x} \end{bmatrix}$.

Therefore Eq. (4.52) can be written as:

$$\begin{aligned} \begin{bmatrix} \dot{x} \\ \ddot{x} \end{bmatrix} &= \begin{bmatrix} 0 & 1 \\ k_x - k_1 k_i & -k_2 k_i \end{bmatrix} \begin{bmatrix} x \\ \dot{x} \end{bmatrix} + \begin{bmatrix} 0 \\ 1 \end{bmatrix} d \\ y &= \begin{bmatrix} 1 & 0 \end{bmatrix} \begin{bmatrix} x \\ \dot{x} \end{bmatrix} \end{aligned} \tag{4.53}$$

Eq. (4.53) shows that the disturbance d is not explicitly addressed with a feedback signal $i = Kx$. This research proposes the following design to directly attenuate the disturbance d. Assuming signal $i = Kx + v$ is the feedback signal, it can be written as

$$i = \begin{bmatrix} k_1 & k_2 \end{bmatrix} \begin{bmatrix} x \\ \dot{x} \end{bmatrix} + \begin{bmatrix} 0 \\ 1 \end{bmatrix} v \tag{4.54}$$

Subtituting Eq. (4.54) into Eq. (4.52)

$$\begin{bmatrix} \dot{x} \\ \ddot{x} \end{bmatrix} = \begin{bmatrix} 0 & 1 \\ k_x - k_1 k_i & -k_2 k_x \end{bmatrix} \begin{bmatrix} x \\ \dot{x} \end{bmatrix} + \begin{bmatrix} 0 \\ -k_i v + d \end{bmatrix}. \tag{4.55}$$

Eq. (4.55) shows if signal v is chosen to be $v = \frac{d}{k_i}$, the disturbance signal d will be attenuated.

4.7.2. Controller Design with Unknown Disturbance d

If the disturbance d is unknown, it is impossible to calculate v directly. In this research, an AFC is proposed to attenuate the disturbance d, and the loop gain is recovered using the previously discussed QFT/ H_∞ method. The system transfer function of a maglev plant with a disturbance d can be derived from its state-space form in Eq. (4.52):

$$\ddot{x} = k_x x - k_i i + d \tag{4.56}$$

Introducing an AFC as being described in Figure 3.13 and Eq. (3.44), Eq. (4.56) becomes

$$\ddot{x} = k_x x - k_i (i + k_{AFB} \ddot{x}) + d \tag{4.57}$$

Rearrange Eq. (4.57) to get the system equation

$$\ddot{x} = \frac{k_x x}{1 + k_{AFB}} - \frac{k_i i}{1 + k_{AFB}} + \frac{d}{1 + k_{AFB}} \tag{4.58}$$

The third term in Eq.(4.58) shows that the disturbance d is attenuated by a gain of $1 + k_{AFB}$. However, the loop gain from $I(s)$ to $X(s)$ is also attenuated by $1 + k_{AFB}$. The loop gain can be recovered with a QFT/ H_∞ controller to recover the loop gain.

The transfer function from $I(s)$ to $X(s)$ is:

$$\frac{X(s)}{I(s)} = \frac{-k_i}{(1 + k_{AFB}) s^2 - k_x} \tag{4.59}$$

Comparing Eq. (4.59) to Eq. (3.16), it is found the coefficient of s^2 term becomes $1 + k_{AFB}$. The system uncertainties can be updates using this new transfer function, as is shown in

Table 4.5. To simplify the design, this research assumes k_{AFB} is a constant. However, a QFT/ H_∞ controller can also be designed to a variable k_{AFB} by treating it as another uncertainty in the system transfer function.

The updated uncertainty ranges are:

$$k_i \in [29.37,\ 48.25]\ \frac{\text{m}}{\text{A-s}^2} \tag{4.60}$$

and

$$k_x \in \left[2.07\times10^3,\ 3.64\times10^3\right]\ \frac{\text{m}}{\text{s}^3} \tag{4.61}$$

Comparing the uncertainty ranges in Eqs. (4.60) and (4.61) to the original uncertainty range in Eqs. (4.11) and (4.12), it is found the uncertainties in the system with an AFC have smaller variation ranges. In other word, the gain $1+k_{AFB}$ also attenuates the uncertainties.

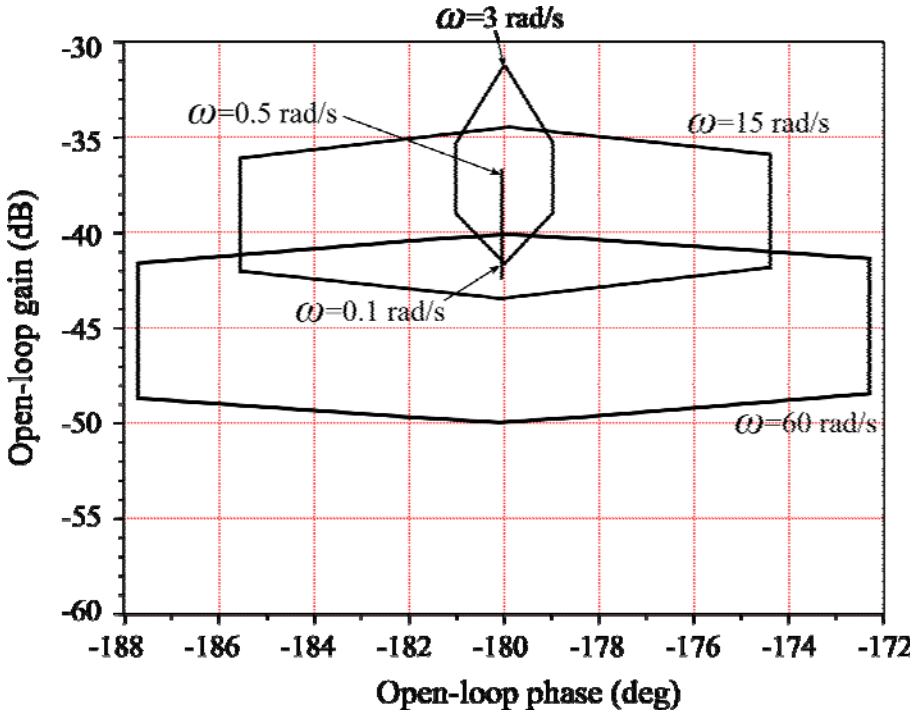

Figure 4.25 Updated plant templates

Figure 4.25 shows the updated plant templates. The four template corner transfer functions are:

$$G_1 = \frac{-48.25}{s^2 - 53.86} \tag{4.62}$$

$$G_2 = \frac{-41.86}{s^2 - 45.54^2} \tag{4.63}$$

$$G_3 = \frac{-29.37}{s^2 - 50.20^2} \tag{4.64}$$

$$G_4 = \frac{-34.99}{s^2 - 60.37^2} \tag{4.65}$$

The QFT/H_∞ controller design process has be discussed in Section 4.6, and will not be repeated here. The designed controller is given below. The controller transfer function is:

$$\left.\begin{aligned} \dot{x}_c &= \begin{bmatrix} -115 & 1 & 0 & -90 \\ -65\text{E}3 & -300 & 83\text{E}4 & 15\text{E}4 \\ 0 & 0 & -2.1\text{E}-2 & 0 \\ 30 & 0 & 0 & -10\text{E}2 \end{bmatrix} x_c + \begin{bmatrix} -120 \\ 31\text{E}3 \\ 10 \\ -4.4 \end{bmatrix} y \\ u &= \begin{bmatrix} 85\text{E}1 & 4.6 & -10\text{E}3 & -20\text{E}2 \end{bmatrix} x_c + \begin{bmatrix} -550 \end{bmatrix} y \end{aligned}\right\} \tag{4.66}$$

and the prefilter is

$$F(s) = \frac{1.65\left(\frac{s}{73}+1\right)}{\left(\frac{s}{58}+1\right)\left(\frac{s}{745}+1\right)} \tag{4.67}$$

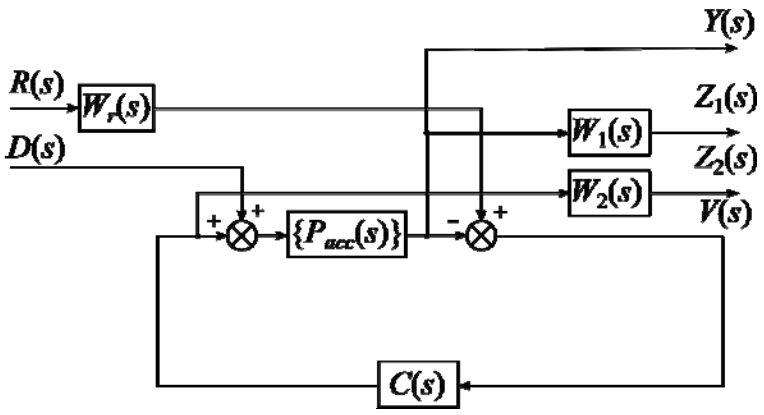

Figure 4.26 Block diagram of a system with an AFC-enhanced QFT/H_∞ controller

Figure 4.26 shows a block diagram of the system with an AFC-enhanced QFT H_∞ controller. Experiments to test this controller are discussed in Chapter 5.

Table 4.5 Maglev plant transfer functions with acceleration feedback

$P_{acc}(s)$	m = 8 g	m = 12 g	m = 16 g	m = 20 g	m = 24 g
x_0 = 3.5 mm	$\frac{-48.25}{s^2 - 53.86^2}$	$\frac{-43.22}{s^2 - 56.42^2}$	$\frac{-39.73}{s^2 - 58.12^2}$	$\frac{-37.09}{s^2 - 59.38^2}$	$\frac{-34.99}{s^2 - 60.37^2}$
x_0 = 4.5 mm	$\frac{-44.57}{s^2 - 49.16^2}$	$\frac{-39.64}{s^2 - 51.30^2}$	$\frac{-36.25}{s^2 - 52.72^2}$	$\frac{-33.71}{s^2 - 53.76^2}$	$\frac{-31.71}{s^2 - 54.57^2}$
x_0 = 5.5 mm	$\frac{-41.86}{s^2 - 45.54^2}$	$\frac{-37.03}{s^2 - 47.40^2}$	$\frac{-33.74}{s^2 - 48.62^2}$	$\frac{-31.29}{s^2 - 49.51^2}$	$\frac{-29.37}{s^2 - 50.20^2}$

4.8. Chapter Summary

This chapter discusses the robust controller design for a maglev system. The discussion begins with a review of the system robustness with classical controls. The robustness of a maglev system with a PD, PID, and lead type control are studied. These conventional controllers guarantee the system robustness using gain and phase margins. These two values indicate how much tolerance a system has toward feedforward loop gain changes, but only at the crossover frequencies. For the steady-state operation of the maglev system, gain and phase margins are effective to evaluate the system performance. However, to guarantee the system transient performance, gain and phase margins are not sufficient.

This chapter studied robust controller designs using the QFT and H_∞ methods. With these two design approaches, the transient response of the system is guaranteed even with system uncertainties. This is achieved by using the sensitivity function and complimentary sensitivity functions to evaluate controllers. The system performance robustness is guaranteed across the frequency spectrum.

This chapter proposed a QFT/H_∞ method and an AFC-enhanced QFT/H_∞ design method for control of the maglev system. The QFT design approach provides a quantitative evaluation of system uncertainties. The H_∞ approach mathematically guarantees the signal norm stays within predefined bounds. Their combination, the QFT/H_∞ method, offers advantages of both methods. It takes into consideration the system uncertainties, and results in a controller which is mathematically proved to be able to guarantee the system performance. This chapter also discussed how to add an AFC loop in the system and then design a QFT/H_∞ controller, which results in an AFC-enhanced QFT/H_∞ controller. This

novel controller provides the system with a disturbance attenuation feature along with guaranteed system robustness.

Chapter 5. Simulations and Experimentations

5.1. Chapter Outline

Chapters 3 and 4 discussed how to design controllers for the maglev system. Chapter 5 discusses how to evaluate the designs through simulations and experiments. Sections 2 and 3 of this chapter give a brief introduction of simulation and experimentation in control engineering, and how the simulation studies in this research are set up, followed by an introduction to the experimental platform. In this study, multiple hardware platforms were used during controller tests. A TI® TMS320 DSP platform was used to implement the designed controllers. A brief introduction of the TI® TMS320 DSP board is included in Appendix E. Section 4 discusses the experiments to validate that the control design goals are met. Simulations and experimental results prove that stable levitation can be achieved using the following controllers: PD, PID, lead, MRC, LQG, and AFC-enhanced QFT/ H_∞ (AQH). Experiments show that the noise in the maglev system is attenuated with an acceleration feedback controller (AFC) and system robustness is guaranteed with the proposed AQH controller. Section 5 summarizes the experiments and presents a conclusion.

5.2. Simulation versus Experimentation

In Chapters 3 and 4, multiple controllers were designed. Conventionally, the controller designs are evaluated via software simulation before implementation. In deriving the controllers, both the maglev system and the controllers are modeled as linear ordinary differential equations (LODEs). Therefore, they are deterministic systems, and hence the system responses to different inputs can be simulated by solving the LODEs with different

initial conditions.

After the simulations, experiments are conducted with the closed-loop system. This chapter evaluates the controller designs using both simulation and experiments. Simulations serve two purposes: (1) they are theoretical validations of the designs, and (2) they can identify potential issues and solve them through iteration on the design process before the controllers are implemented.

During the simulation, the system model is converted from differential equations to difference equations so that the simulation can be performed with digital computers. The details on conversion between differential equations and difference equations are not discussed here. However, the conversion introduces differences between simulation and experimental results, which will be discussed later.

There are many publicly available software packages for controller simulation. For example, Maplesim®, VisSim®, MATLAB®, and LabVIEW® all provide software environments to test and verify controller designs. In this research, MATLAB® is chosen to run the simulations since: (1) it provides a user interface which allows user-defined scripts and block diagrams and is intuitive for controller design, and (2) MATLAB® has an interface library that can transfer scripts and block diagrams directly into lower level computer languages (executable codes), and the latter can be downloaded to either microcontrollers or DSP units for experimentation. These two features help to reduce the time needed for the design-verification-modification cycle in this project.

5.3. Controller Platform

The controllers are implemented with a DSP platform. During the study, several

platforms have been investigated. Most of them work directly with MATLAB® through software-hardware interface libraries.

Table 5.1 Comparison among different platforms

Platform	Control Unit	Development Environment	User Interface	Cost
dSpace®	DSP	MATLAB	SIMULINK	Very expensive
RT-CON®	PIC	MATLAB	SIMULINK	Medium
NI® FlexRIO	FPGA	LABVIEW	LABVIEW	Expensive
TI® TMS320	DSP	MATLAB	SIMULINK	Inexpensive

Table 5.1 lists four platforms, the dSpace® controller design suit, the RT-CON® system, the NI® FlexRIO suit, and the TI® TMS320 DSP system. All the above platforms have been tested with controllers designed in this research. Both the dSpace® and NI® FlexRIO platforms provide powerful data processing units, high performance input buffers, and high resolution 16 bit A/D and D/A converters. However, these two platforms are cost prohibitive. The RT-CON® platform lacks the power to process the large amount of real-time data generated by the advanced control algorithms. The TI® TMS320 DSP platform was chosen to implement the controllers in this research. Its DSP unit can handle a relatively large amount of calculations and its price is reasonable. The DSP board has four 12-bit A/D and D/A converters. TI® TMS320 DSP provides a comprehensive, cost-effective, and adaptable platform to test the closed loop systems. More details on the TI® TMS320 DSP board are included in Appendix E.

5.4. Simulation Studies and Experiments

This section discusses the simulations and experimental studies for the controller designs. This discussion includes one group of simulations and three groups of experiments. (1) System stability simulations. Controllers are simulated with a nonlinear maglev model. The system responses to a finite energy reference signal ($Ae^{(-t)}, A > 0, t \geq 0$) and an infinite energy reference signal ($u(t) = 1, t \geq 0$) are simulated. (2) System stability and robustness experiments. The goal of this group of experiments is to find if system robustness is achieved with the designed controllers. First different masses are tested to find if stable levitation can be achieved. Then experiments are conducted on the stable systems to find their responses to a finite energy reference signal ($Ae^{(-t)}, A > 0, t \geq 0$) and an infinite energy reference signal ($u(t) = 1, t \geq 0$). (3) Disturbance attenuation experiments. The goal of these experiments is to find if acceleration feedback control is feasible on a maglev system. Experiments are conducted on a maglev system with an AFC to find if a disturbance signal (sine signal) can be attenuated in the response. (4) Disturbance attenuation experiments with an AQH controller. Experiments are conducted to find if disturbances at different frequencies (sine signal with different frequencies) can be attenuated with an AQH controller.

5.4.1. System Stability Simulation

This section discusses simulations of different controllers to investigate the system stability.

Table 5.2 Controllers to simulate and their transfer functions

Controller Type	Controller Transfer Function
PD controller	$G_c = 606 + 6s$
PID controller	$G_c(s) = 284.5 + \frac{4511}{s} + 5.3s$
Lead controller	$G_c = \frac{1.6\text{E}3(s+46.2)}{s+197}$
MRC controller	Not available
LQG controller	Not available
AQH controller	Eqs. (4.66) and (4.67)

Table 5.2 lists the controller transfer functions. A nonlinear Simulink® model of the maglev plant is built for the simulations, as shown in Figure 5.1. Figure 5.2 shows a block diagram of the closed-loop maglev system.

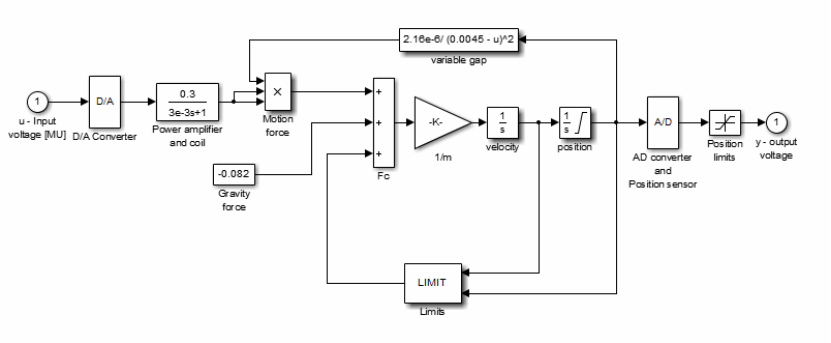

Figure 5.1 Simulink® model for the maglev plant

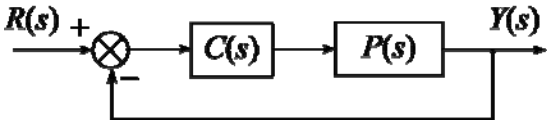

Figure 5.2 Block diagram of the closed-loop maglev system

5.4.1.1. Case 1: system response to a finite energy reference signal

In this simulation case, the reference signal is a finite energy signal with the transfer function:

$$R(s) = \frac{0.001}{s+1} \tag{5.1}$$

The mass and initial conditions for this simulation are: $m = 16$ gram , $x_0 = 4.5$ mm , $\dot{x}_0 = 0$, $i_0 = 0.345$ A .

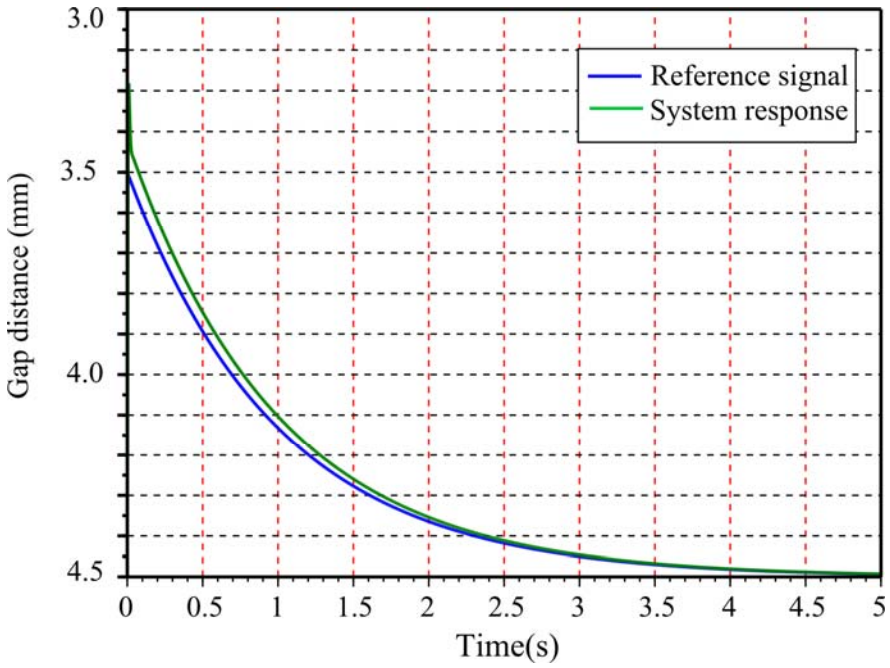

Figure 5.3 Simulation result of a system with PD controller responses to $R(s)$

Figure 5.3 shows a plot of the response of a system with PD controller to the reference signal $R(s)$. In the simulation, the reference signal $R(s)$ commands the gap distance to change from 4.5 mm to 3.5 mm.The plot shows a rapid position change near $t = 0$, then the system response closely follows the reference signal. The simulation result indicates that the system with a PD controller restores equilibrium after it is disturbed by a

signal $R(s)$. In other words, a PD controller guarantees system stability.

Table 5.3 shows the simulation results of case 1. All the controllers discussed in this research are able to guarantee stability when the maglev system is subjected to a finite energy position command.

Table 5.3 Stability simulations with a finite energy reference signal

$R(s)$	Controller	PD	PID	Lead	MRC	LQG	AQH
$\frac{0.001}{s+1}$	Maglev system (m=16 g)	stable	stable	stable	stable	stable	stable

5.4.1.2.Case 2: system response to an infinite energy reference signal

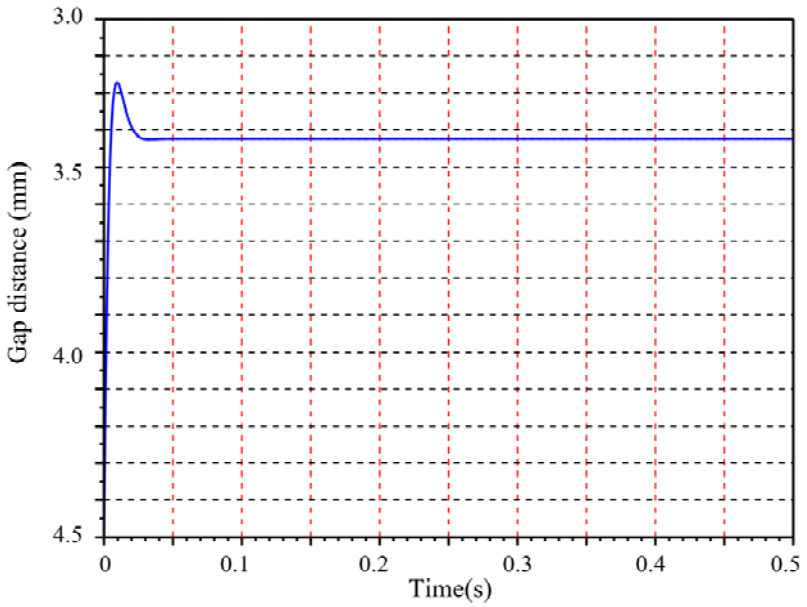

Figure 5.4 Step response of a maglev system with PD controller

In this simulation group, the reference signal is an infinite energy signal with the transfer function:

$$R(s) = \frac{0.001}{s} \tag{5.2}$$

$R(s)$ is a step position command in this case. The mass and initial conditions are the same as those in Case 1: $m = 16$ gram, $x_0 = 4.5$ mm, $\dot{x}_0 = 0$, $i_0 = 0.345$ A. Figure 5.4 shows the step response simulation result. The plot shows that the system is stable after the step position command is executed. The rest of the simulation results are summarized in Table 5.4.

Table 5.4 Step response simulation result

$R(s)$	Controller	PD	PID	Lead	MRC	LQG	AQH
$\frac{0.001}{s}$	Maglev system (m=16 g)	stable	stable	stable	stable	stable	stable

Simulation results indicate all the controllers guarantee system stability.

5.4.2.Stability and Robustness Experiments

5.4.2.1.Stability and Stability Robustness Experiments

This group of experiments checks if stability is achieved with the designed controllers, and further, if the system is robust against system uncertainties when stability is achieved. In these experiments, different masses are placed at an initial position with a gap distance $x_0 = 4.5$ mm, and then the support is removed to test if levitation can be achieved.

Table 5.5 shows the results of the stability and robustness experiments. The results show that all the controllers can guarantee system stability when *m* is 16 gram and 20 gram. This indicates (1) system stability is achieved with the designed controllers, and (2) all the controllers guarantee system robustness against system variation. However, the results also

show that system stability is achieved with an AQH controller for all the tested masses. Besides the AQH controller, the MRC and Lead controllers guarantee system stability for four out of five tested masses. With a PD controller, the system only levitates two masses. In conclusion, among all the discussed controllers, AQH controller exhibits the best stability robustness, while PD controller shows the poorest stability robustness.

Table 5.5 Results of stability and robustness experiments

Controller	mass				
	8 g	12 g	16 g	20 g	24 g
PD	unstable	unstable	stable	stable	unstable
PID	unstable	stable	stable	stable	unstable
Lead	stable	stable	stable	stable	unstable
MRC	stable	stable	stable	stable	unstable
LQG	unstable	unstable	stable	stable	stable
AQH	stable	stable	stable	stable	stable

5.4.2.2.Performance Robustness Experiments

This group of experiments checks the system performance robustness. The system configurations for this group of experiments are shown in Figure 5.5 and Figure 5.6.

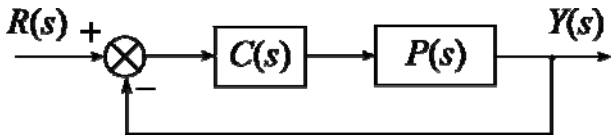

Figure 5.5 Experiment configuration for PD, PID, lead, MRC, and LQG controllers

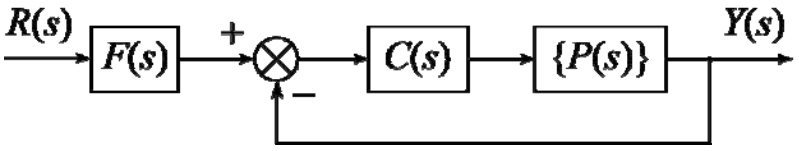

Figure 5.6 Experiment configuration for the AQH controller

Table 5.6 Performance robustness experiment cases

	Referenc signal	Initial gap distance
Case 1	$R(s)=\frac{0.002}{s+1}$	$x_0 = 5.5$ mm
Case 2	$R(s)=\frac{0.001}{s}$	$x_0 = 5.5$ mm
Case 3	$R(s)=\frac{0.001}{s}$	$x_0 = 4.5$ mm
Case 4	$R(s)=\frac{0.002}{s}$	$x_0 = 5.5$ mm

This group of experiments uses four different reference signals $R(s)$ with different initial conditions. The four experiment cases are listed in Table 5.6. Three indices are calculated from the experimental results to assess the system performance. They are the integral of the absolute magnitude of the error (IAE) index, which is

$$\text{IAE} = \int_0^\infty |\varepsilon(t)| dt , \tag{5.3}$$

the integral of the square of the error (ISE) index, which is

$$\text{ISE} = \int_0^\infty \varepsilon^2(t) dt , \tag{5.4}$$

and the integral of time weighted absolute value of error (ITAE) index, which is given by

$$\text{ITAE} = \int_0^\infty t|\varepsilon(t)| dt \tag{5.5}$$

where $\varepsilon(t)$ is the error between the reference and the system response.

The three indices assess the system performance from different perspectives [363]. IAE integrates the absolute error over time. It gives an evaluation of how close the response

follows the reference. ISE integrates the square of the error over time, which penalizes larger errors. ITAE integrates the absolute error multiplied by the time over time. It weights errors which exist after a long time. The indices for the four cases are presented below, followed by an assessment of the system performance using these indices.

Case 1 results:

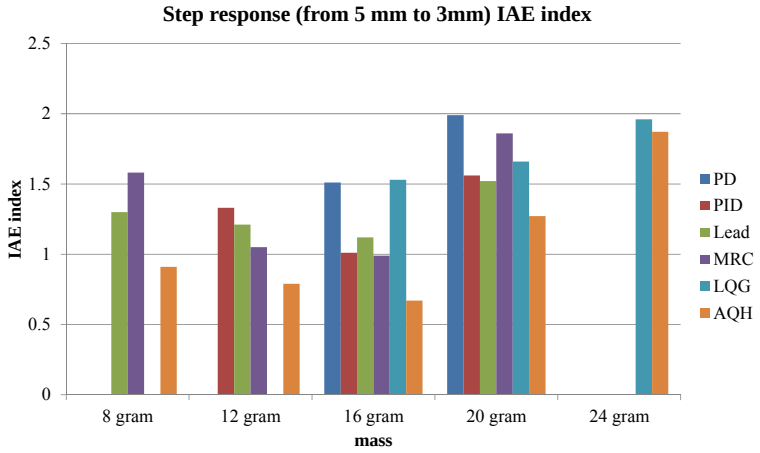

Figure 5.7 Maglev system step response (from 5 mm to 3mm) IAE index

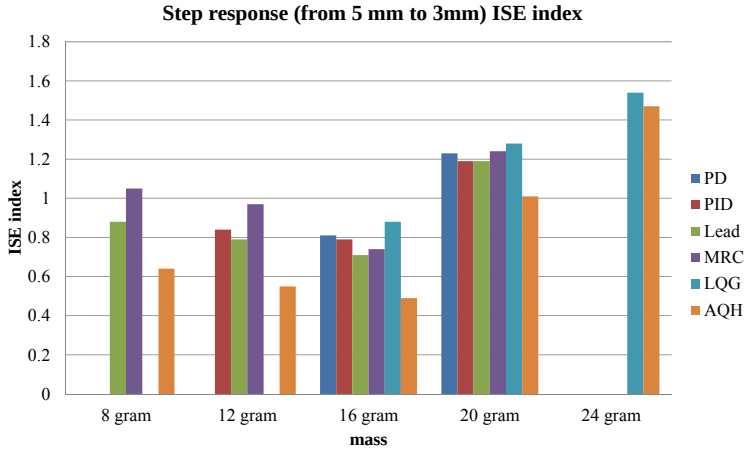

Figure 5.8 Maglev system step response (from 5 mm to 3mm) ISE index

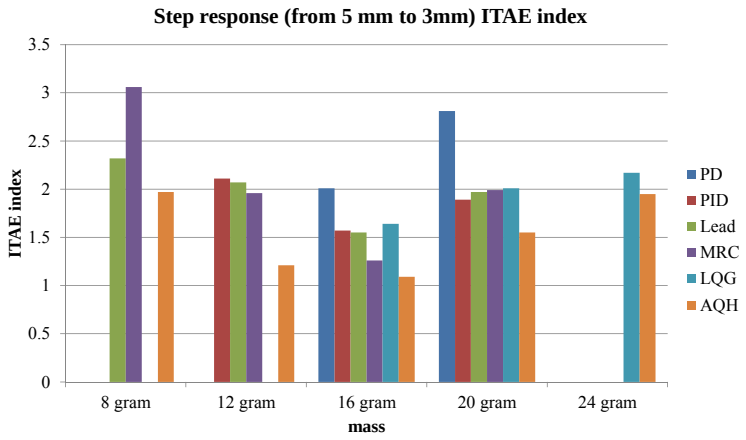

Figure 5.9 Maglev system step response (from 5 mm to 3mm) ITAE index

Case 2 results:

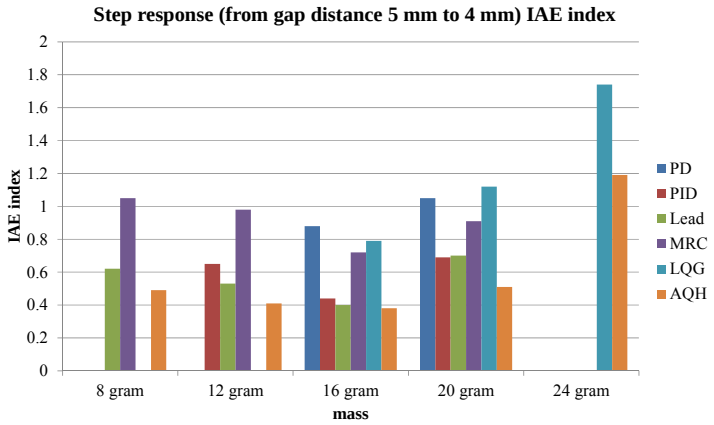

Figure 5.10 Maglev system step response (from 5 mm to 4mm) IAE index

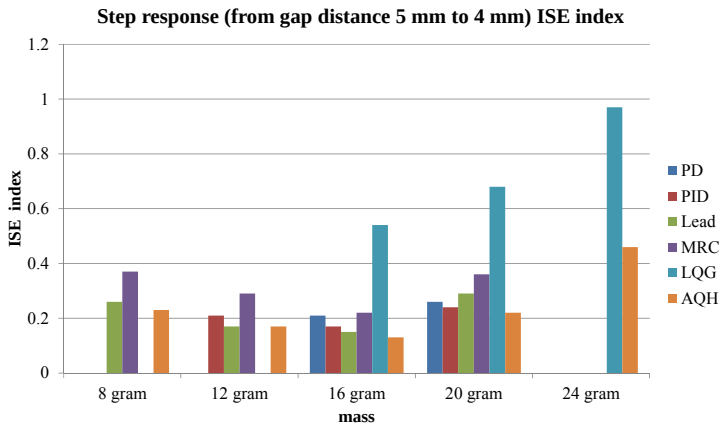

Figure 5.11 Maglev system step response (from 5 mm to 4 mm) ISE index

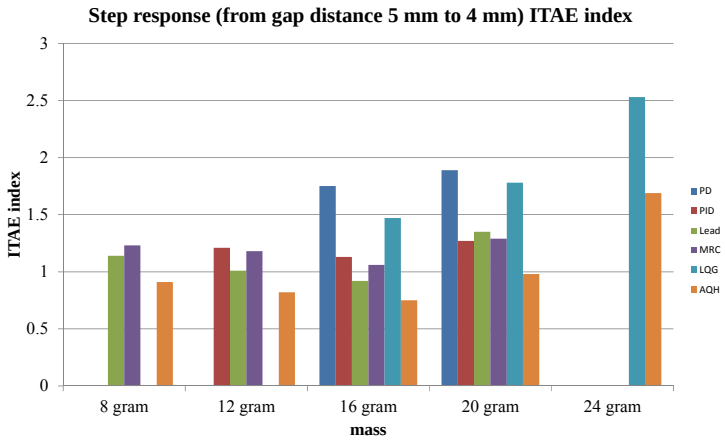

Figure 5.12 Maglev system step response (from 5 mm to 4 mm) ITAE index

Case 3 results:

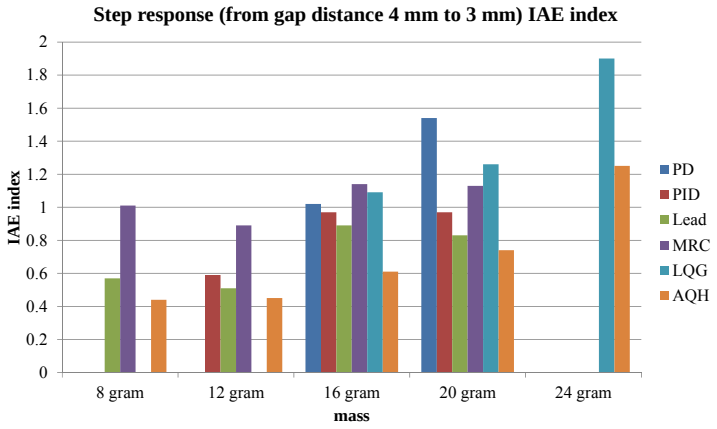

Figure 5.13 Maglev system step response (from 4 mm to 3 mm) IAE index

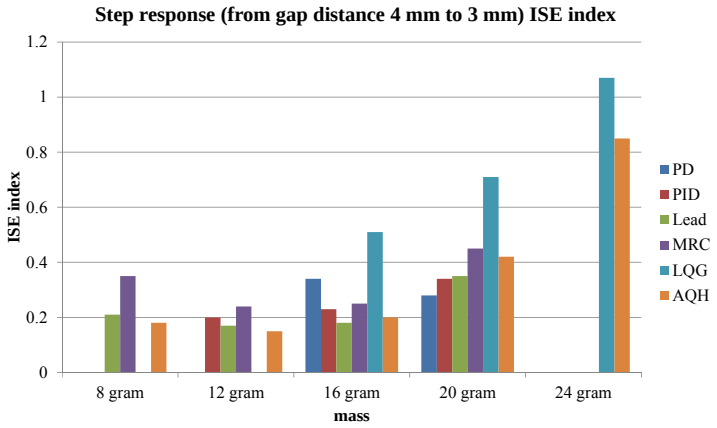

Figure 5.14 Maglev system step response (from 4 mm to 3 mm) ISE index

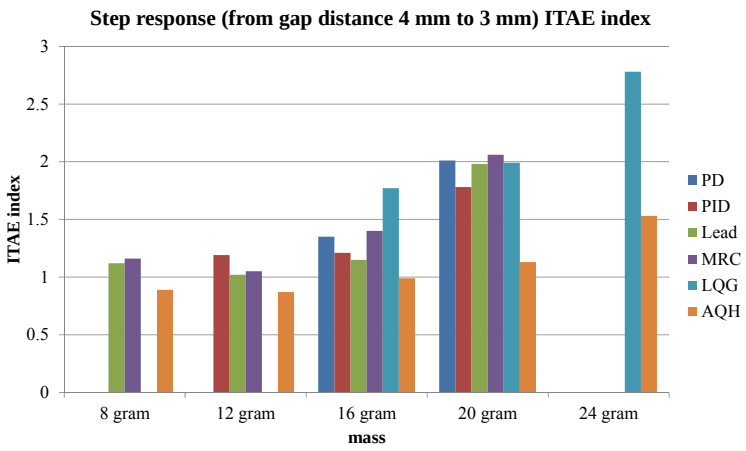

Figure 5.15 Maglev system step response (from 4 mm to 3 mm) ITAE index

Case 4 results:

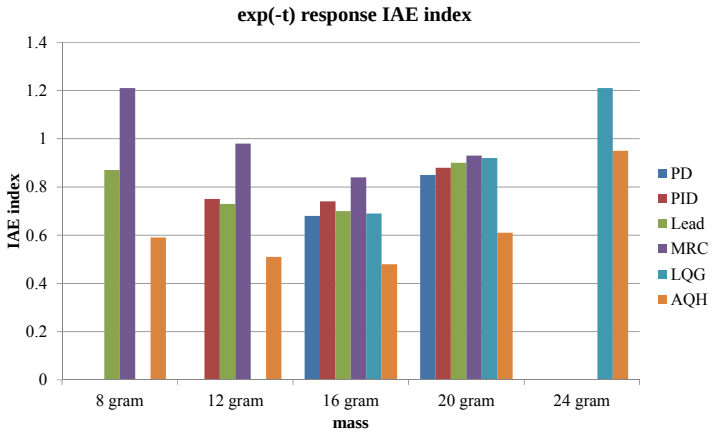

Figure 5.16 Exp(-t) response IAE index

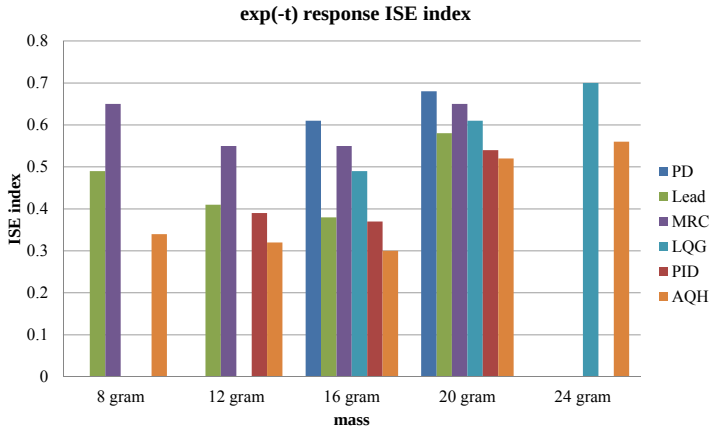

Figure 5.17 Exp(-t) response ISE index

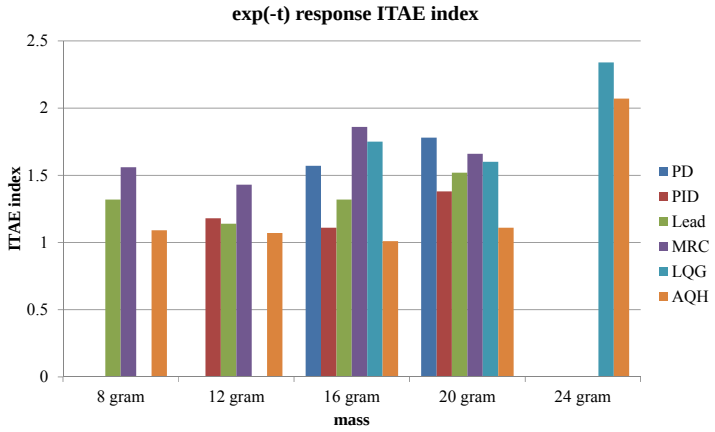

Figure 5.18 Exp(-t) response ITAE index

In cases 1 through 3, the levitated masses were following a step reference signal. The initial gap distances were 5.5 mm and 4.5 mm. The magnitudes of the step reference signal are 1 mm and 2 mm. In case 4, the levitated masses were following an exponential signal e^{-t}. The initial gap distance was 5.5 mm.

Four conclusions can be drawn from the calculated indices:

(1) The error indices are smallest when the levitated mass is 16 gram. As the mass changes, the error indices begin to increase. This is because all the controllers are

designed for the system model with a 16 gram mass.

(2) In all the cases, the error indices of the AQH controller have smaller variations compared to those of the other controllers. In other words, the system with an AQH controller exhibits better performance robustness.

(3) In cases 2 and 3, where the magnitude of the step reference signal is 1 mm, the IAE, ISE, and ITAE indices show little differences between cases. Therefore, system robustness has been achieved between gap distances of 5.5 mm and 3.5 mm. The indices in case 1 are larger than those in cases 2 and 3. This is due to the 2 mm magnitude of the step reference in case 1. Larger position changes resulted in larger error indices.

(4) In case 4, the IAE, ISE, and ITAE indices are more uniform compared to the other three cases, which means the system responses are more uniform when the reference signal is a finite energy signal. In other words, the maglev system exhibits better performance robustness with finite energy reference signals.

5.4.3. Disturbance Attenuation with AFC

This section discusses experiments to validate effective noise attenuation with AFC. For the maglev system discussed in this research, the position signal is available for measurement, and the control current is assumed known (which is the output of the controller). Eq. (3.14) gives the mathematical expression of the acceleration signal based on the position feedback signal and control current. Figure 5.19 shows the block diagram of a maglev system with an acceleration feedback loop, in which the acceleration signal is calculated from the measured position signal and control current. Note that there is also a

position feedback loop to achieve stable levitation.

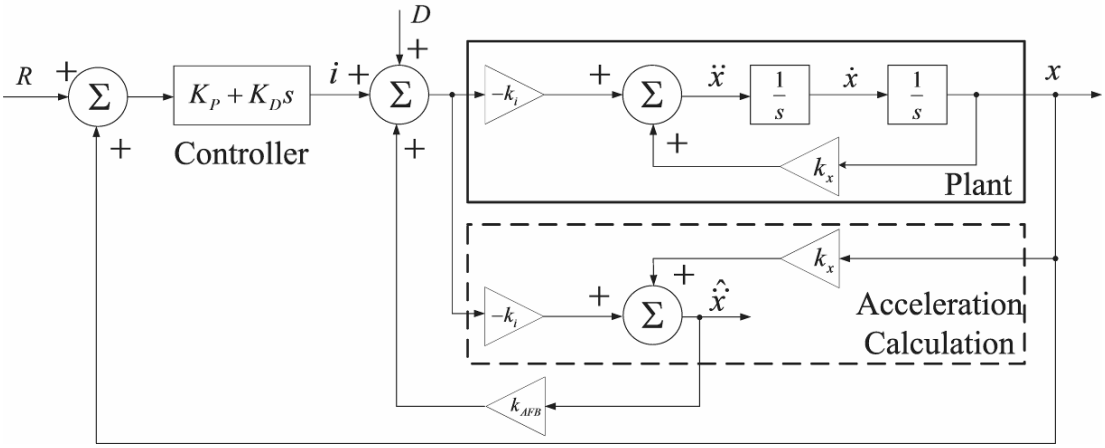

Figure 5.19 Block diagram of a maglev system with an acceleration feedback control

Table 5.7 Input signals of the two experiments

	$R(s)$	$D(s)$
Experiment 1	$\frac{1\mathrm{E}(-3)k}{s^2+k^2}, k \in \{0.1, 0.2, 0.5, 1, 2, 5\}$	0
Experiment 2	0	$\frac{1\mathrm{E}(-4)k}{s^2+k^2}, k \in \{0.2, 0.5, 1, 2, 5\}$

Two experiments are conducted to prove that disturbances can be attenuated by AFC. The first experiment compares the responses of the maglev system with and without acceleration feedback to a sinusoidal reference signal. The second compares the responses of the maglev system with and without acceleration feedback to a sinusoidal disturbance signal. The configurations of the systems for these two experiments are shown in Figure 5.20 and Figure 5.21. Input signals are listed in Table 5.7.

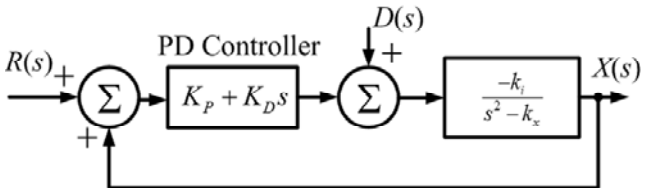

Figure 5.20 Configuration of a system without AFC

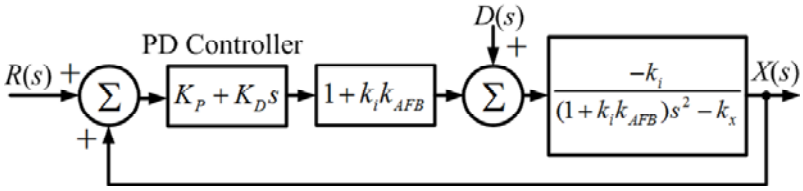

Figure 5.21 Configuration f a system with AFC

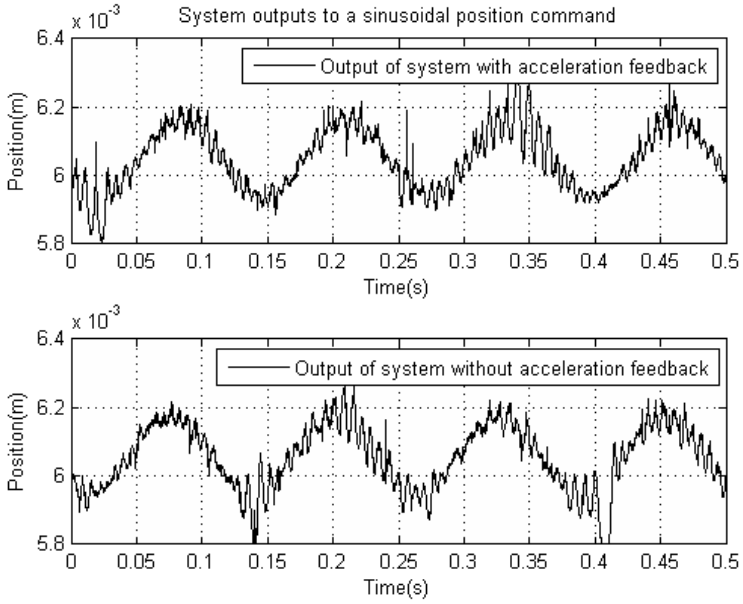

Figure 5.22 System outputs of a maglev system tracking a sine command signal

Figure 5.22 shows the result of the first experiment. It can be seen that the maglev system responds almost the same whether the acceleration feedback is used or not. The experiment was repeated for reference sinusoidal signals with frequencies from 0.1 Hz to 10 Hz. Experimental results show that the system can track a reference signal up to about 9

Hz. If the reference signal has a frequency larger than 10 Hz, the system fails to track the signal or loses stability. (This is because the linearized system does not take into consideration the nonlinear character of the components at high frequencies.)

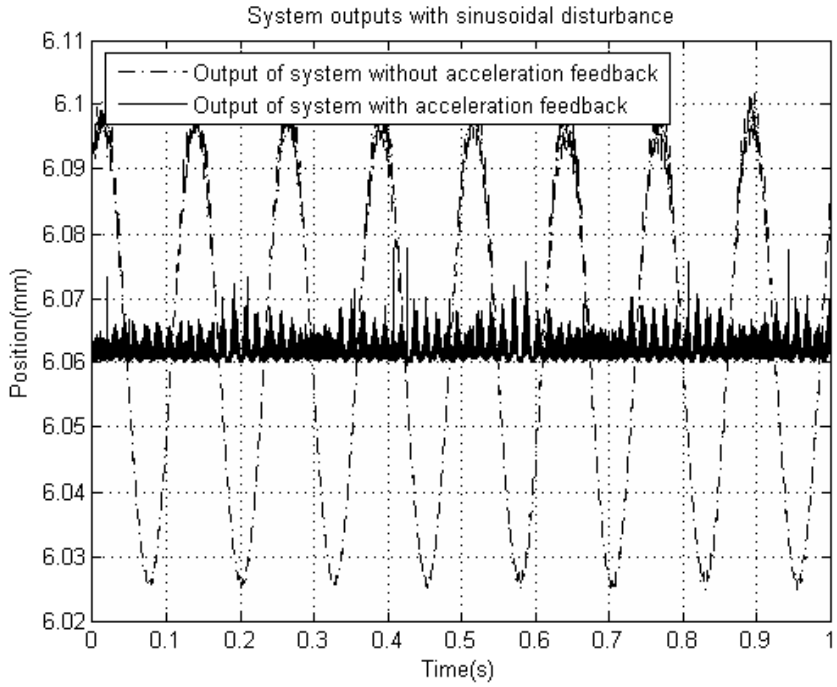

Figure 5.23 System outputs of a maglev system subject to a sine disturbance

Figure 5.23 shows the comparison between the system outputs with and without the acceleration feedback loop. The disturbance is greatly attenuated in the system with the acceleration feedback loop. Figure 3.15 shows the magnitude ratio of the disturbance signal is about 60 dB smaller in the system with an acceleration feedback loop. The amplitude of the system with acceleration feedback is five times smaller than that of the system without it. (The signal becomes noisy when the amplitude of the system output becomes small.) The experiment proves that an acceleration feedback loop in the system successfully

attenuates the disturbance.

5.4.4. Disturbance Attenuation with AQH

This group of experiments verifies that disturbance attenuation is achieved with the proposed AQH controller. The response of the maglev system with an AQH controller is compared to those with PD, PID, Lead, MRC, and LQG. To further investigate the noise attenuation feature of a robust AQH controller, the experiments are conducted with different masses. The error index is calculated to assess the controllers. The configurations of the systems are shown in Figure 5.24 and Figure 5.25.

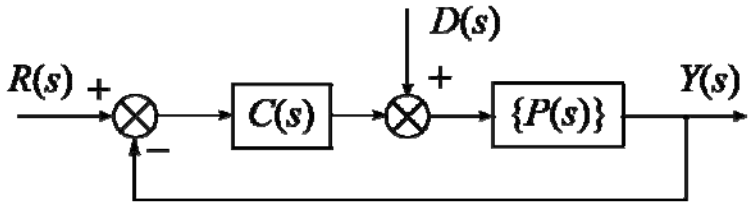

Figure 5.24 Block diagram of system with PD, PID, Lead, MRC, and LQG controllers

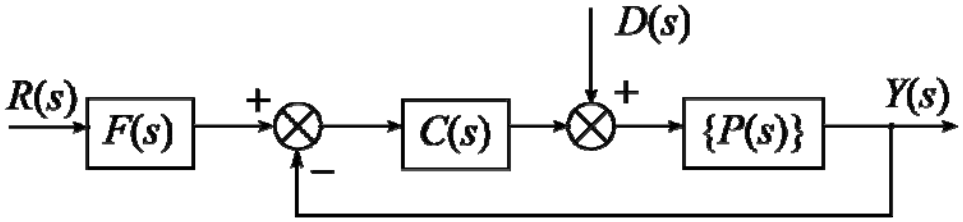

Figure 5.25 Block diagram of system with an AQH controller

Table 5.8 Signals used in the experiments

Signal	$R(s)$	$D(s)$
Transfer function	$\frac{5}{s^2+5^2}$	$\frac{k/10}{s^2+k^2}, k \in \{10,15,30\}$

This group of experiments tests a disturbance signal at three different frequencies. The signals used in the experiments are list in Table 5.8

The integral of the absolute magnitude of the error (IAE) indices are calculated from the experimental data. The error between a system response with a disturbance and one without a disturbance are integrated over time, as is shown in Figure 5.26.

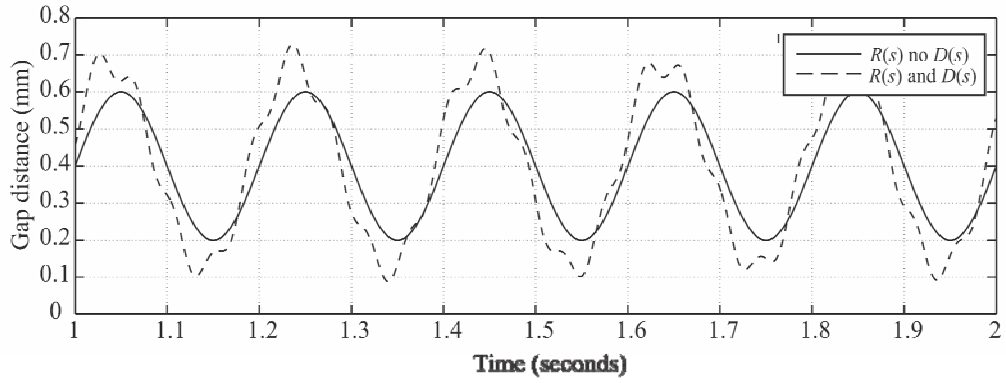

Figure 5.26 System responses to calculate IAE

The experimental results are shown in Figure 5.27 through Figure 5.29.

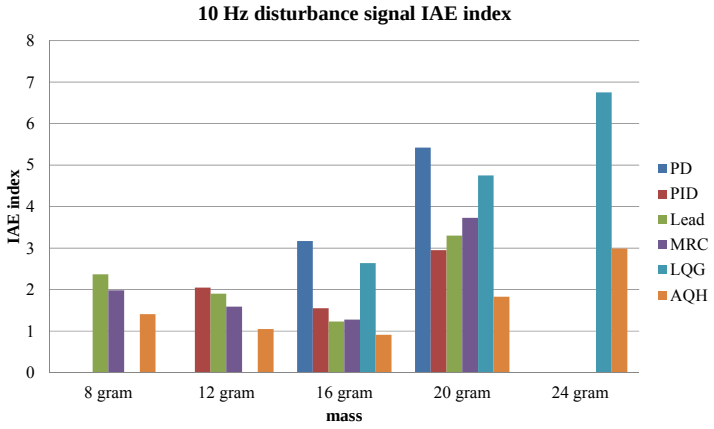

Figure 5.27 IAE index of 10 Hz disturbance

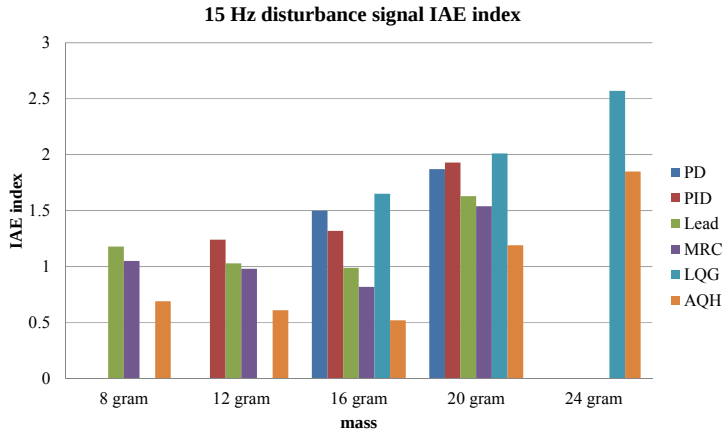

Figure 5.28 IAE index of 10 Hz disturbance

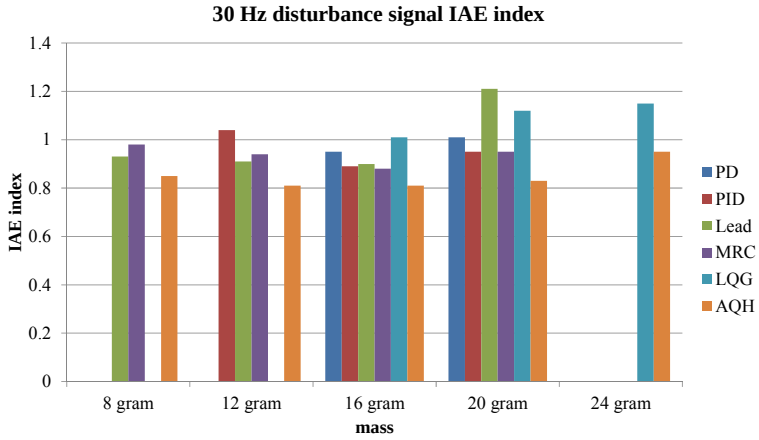

Figure 5.29 IAE index of 10 Hz disturbance

The following conclusions can be drawn from the experimental results shown in Figure 5.27 through Figure 5.29:

(1) The IAE indices of the AQH controller are smaller than those of other controllers. In other words, the AQH controller successfully attenuates the disturbance signals, so the system outputs are close to the reference signal.

(2) The IAE indices are smallest when the levitated mass is 16 gram. As the mass changes, the IAE indice increases. This indicates the disturbance attenuation is influenced by

system uncertainties. A system with large uncertainties may encounter poor disturbance attenuation when system parameters change.

(3) At low frequencies, the IAE indices are larger, and have a larger range of variation. As the disturbance signal frequency increases, the IAE indices decrease. This is due to the mass in the maglev system filters high frequency disturbances.

To sum up the experiments in this section, an AQH controller guarantees the maglev system stability robustness, and the system performance robustness. In addition, the AQH controller provides a disturbance attenuation feature. Therefore, design goals of guaranteed system robustness and disturbance attenuation can be achieved in a single AQH controller design.

5.5. Summary

This chapter discusses the software simulation and experimental validation of the controller designs. The simulation and experiment platforms are introduced at the beginning of this chapter. Validation experiments are presented. Both simulation and experimentation proved:

(1) The control designs to achieve maglev system stability are successful. All the controllers studied in this research, i.e., PD, PID, Lead, MRC, LQG, and AQH, can guarantee stable levitation.

(2) Disturbance attenuation is observed with the implementation of an AFC. The feedback loop gain is increased with an AFC so the disturbance signal is attenuated.

(3) System robustness and disturbance attenuation can be achieved with a single AQH controller.

Chapter 6. Summary and Future Work

Maglev technology is used in frictionless bearings, high-speed trains, and high-precision machines. This technology balances two basic forces: the electromagnetic force and the gravity. There are multiple methods to achieve this balance, but there is only one that has found its way to industrial applications — maglev with feedback control.

Technically, using feedback control to balance these two forces means: (1) finding an equilibrium point where the magnitudes of the two forces are equal and their directions are opposite, and (2) providing a restoring force that is always pointing towards the equilibrium point if the balance between the two forces is compromised.

Achieving a balance between the electromagnetic force and gravity is challenging. When no feedback is provided, these two forces cannot be balanced because of the nonlinear nature of the electromagnetic force. Although this force can be approximated by a parabolic function near the magnetic source, it is impossible to find a local minimal for the error between the two force functions. In other words, the difference between these two forces diverges, and to make things worse, their difference diverges in a nonlinear fashion. In control engineering terms, this case is referred to as open-loop unstable.

To design a feedback loop to stabilize the open-loop unstable system is not a simple task. In addition, when a maglev system is designed for industrial applications, there are at least two issues that need to be considered during the design process: (1) The mathematical model of the electromagnetic force is only an approximation at a certain location near the magnetic source. If the balance is broken, and the nominal model is still used to calculate the electromagnetic force, there is a model mismatch. How to compensate for this modeling

error needs to be considered. (2) In the harsh industrial working environment, the system experiences unexpected disturbances and noise. Some of these disturbances and noise can be modeled mathematically, others may just be unpredictable. How to design a controller that guarantees the system performance is another issue to be addressed.

Multiple methods have been proposed for the design of feedback controllers for the maglev system. Some of them are intended to achieve stable levitation with a certain amount of tolerance in the loop gain change, such as the classic PID type controller and lead-lag controller, while some of them are designed to accommodate the nonlinearity in the system model, such as the gain-scheduling controller, feedback-linearization controller, sliding-model controller, etc. With these controllers, stable magnetic levitation can be achieved. However, there are issues that previous research failed to investigate: (1) the system performance robustness is neglected in most designs, (2) using a controller to realize noise/disturbance attenuation is not discussed.

In this research, these issues are addressed by developing and experimentally implementing multiple control design techniques. Particularly, this research introduces AFC to achieve disturbance attenuation and three robust control design approaches: the QFT method, the H_∞ method, and the QFT/H_∞ control design method. This research then proposes a novel AQH controller, which can obtain system stability, system robustness, and disturbance attenuation in one single design.

This research has provided the mathematical model of the maglev plant. The classic Newtonian dynamic plus Maxwell equations are used to develop the system model. With the system model, multiple control design methods are discussed. With a linearized version

of the nonlinear model, PD, PID, and lead controllers are designed to achieve stable magnetic levitation while guaranteeing the stability robustness of the system. The system performance with these three different types of controllers is compared through simulation and experiments.

To accommodate the nonlinearity in the system, a model reference adaptive controller (MRC) is proposed. This controller is derived based on the linearized model but provided a switch mechanism to deal with the unmodeled nonlinearity. Experimental results proved that the system with MRC exhibits excessive overshoot in a step response. However, the MRC controller requires a fair amount of difference between the system output and model output because the control effort is adaptively determined by the amount of error.

Next an optimal LQR controller was designed for the maglev system. One advantage with the optimal LQR design approach is that the derived system is inherently robust to a certain degree. However, in order to estimate the unavailable system state, an observer is introduced to form an LQR/LQG controller and the robustness is lost. Techniques that can partially recover the system robustness are introduced but the optimal estimator is sacrificed. Experimental results show that a system with the LQR/LQG control has a certain amount of steady-state error in the existence of uncertainties. However, the LQR/LQG controller provides a method of balancing the transient response and the control effort.

Besides addressing the system stability, this research investigated how to guarantee the system response robustness. The stability robustness of the system with linear

controllers is investigated first. Then the performance robustness issue is discussed and the QFT, H_∞, and QFT/H_∞ controllers are derived. Further, an AFC-enhanced QFT/H_∞ (AQH) controller is proposed to address disturbance attenuation and robustness issues in one controller design.

The QFT method provides a design strategy that quantitatively defines the system uncertainty, and then derives a controller that satisfies the conventional stability criteria. The controller can be tuned to avoid over-complexity. The H_∞ method provides a mathematically oriented design approach in which the magnitude of the response to noise and disturbance is constrained. The QFT/H_∞ method combines the advantages of these two methods, and develops a controller that is tuned to the exactly amount of system uncertainty. Then an acceleration feedback loop is added into the QFT/H_∞ controller to obtain an AQH, which not only attenuates disturbance and noise but guarantees system robustness.

All of the controllers are implemented with a DSP platform, and tested with a maglev apparatus that controls the vertical position of five steel balls with different masses. The controllers are compared using the system response data. In particular, this research compared the error indices calculated from the systems responses with the designed controllers, and focused on how the system robustness is guaranteed. Experiments found that all of the designed controllers guarantee stable magnetic levitation. For the disturbance rejection experiment, the controller with acceleration feedback loop exhibits better disturbance attenuation ability than conventional linear controllers.

When comparing the transient response with system uncertainty, a maglev system

with an AQH controller exhibits better robust performance than system with conventional controllers. Systems with an AQH controller have advantages compared to AFC, QFT, and H_∞ controllers. The QFT controller quantitatively defines the system uncertainty while the H_∞ controller assumes a generalized uncertainty model. Therefore, the system with the QFT controller shows better robustness and the system with the H_∞ controller guarantees the magnitude of disturbance-triggered-response be confined within a certain range. The QFT/ H_∞ controller combines the design approaches of the above two controllers and provides a system whose uncertainty is quantitatively defined. Then an acceleration feedback loop is added to the QFT/ H_∞ controller for disturbance and noise attenuation purposes. With the proposed AFC-enhanced QFT/ H_∞ controller, system stability, robustness, and disturbance attenuation are all achieved.

The development, simulation, and experimentation proved that with the novel AFC and AQH design strategies, the performance of the maglev system has been improved in terms of stability, noise attenuation, and performance robustness. However, the maglev system discussed in this study is a prototype for conceptual purposes. The next logical step would be to implement these novel control strategies on an industrial system. An active magnetic bearing (AMB), for example, would be the ideal candidate platform to test all the controllers discussed in this research. AMB requires the position of its shaft to be controlled accurately despite disturbance and noise during operation. The robust controllers discussed in this research can guarantee these requirements to be met. In addition, AMB controls 5 DOF of a bearing shaft. Although the controllers discussed in this research are designed for SISO systems, the QFT and H_∞ controllers can be

transferred to MIMO controllers with minimal effort. In the past, linear controllers were developed to control multiple electromagnets in a “loop-around” fashion. With the novel controllers suggested in this research, it is possible to control multiple electromagnets simultaneously.

In closing, this research offers a sound foundation for future advances in designing robust controllers for maglev systems. The control design methods discussed in this research can be applied to other open-loop unstable systems. It has been proved with the maglev system that the novel control design approaches discussed in this research provide satisfactory system performance in terms of stability, noise attenuation, and significant improvement in system robustness.

Appendix A. Electromagnetic Force Calculation

The design of the maglev testbed is described by Green [112] and is shown in the photograph of Figure A.1. Green [112] also derived the equation for the electromagnetic force of the testbed using the Maxwell equations.

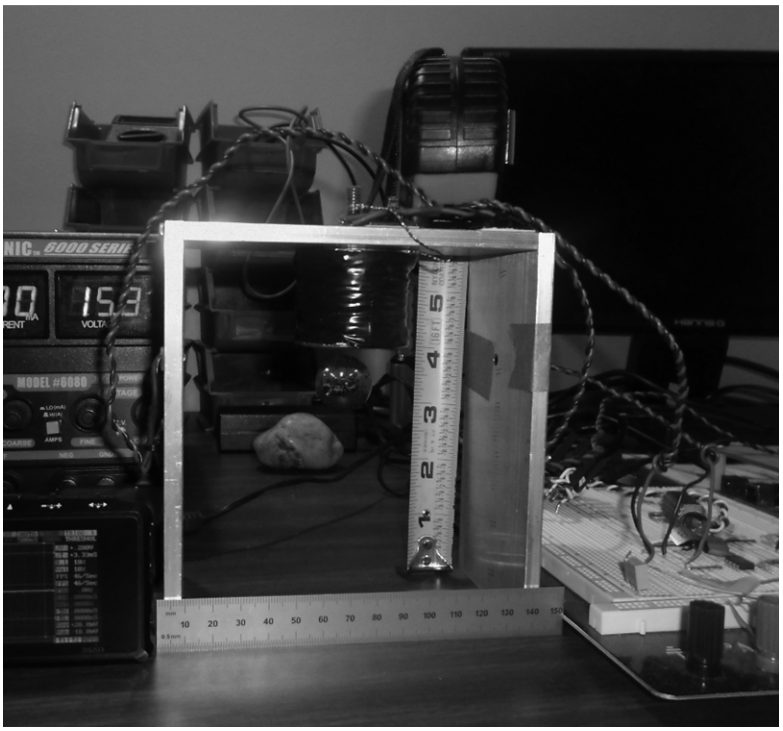

Figure A.1 Maglev testbed

The electromagnet, as documented by Green [112], has a core made of a standard one quarter inch alloy 20 (nickel-chromium-molybdenum) stainless steel screw. Approximately 3000 turns of 26 gauge copper wire are wound around the core.

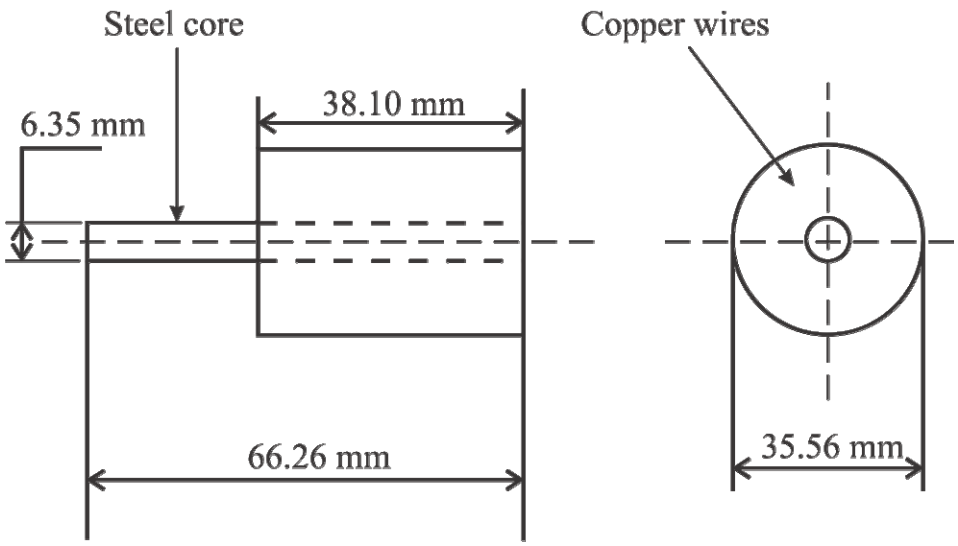

Figure A.2 Dimensions of the electromagnet (in the units of mm)

Figure .2 shows a schematic of the electromagnet with dimensions. The electromagnet was originally designed to operate below a voltage of 15 V. The measured resistance of the copper wire is 31 Ω, and as such the maximum current during operation is 0.48 A. Table 3.1 shows the measured current when a 8 gram levitated object is at the desired position is 0.289 A, which is about 60% of the maximum value.

In this study, the levitating force is an attractive force between the electromagnet and the steel ball. The magnitude of the force can be derived using Ampere's circuit law and Farady's inductive law. Both laws are included in the Maxwell equations.

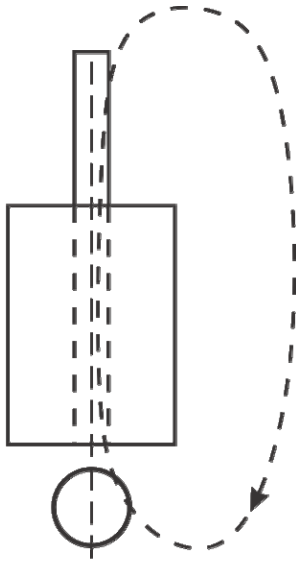

Figure A.3 One magnetic flux path

Figure A.3 shows a schematic of one of the magnetic flux paths. To simplify the calculation, flux leakage is assumed to be zero. This study briefly reviews two methods of calculating the electromagnetic force. They have been discussed by Corson and Lorrain [364] and Woodson and Melcher [108], respectively.

$$\oint \vec{H} d\vec{l} = i \tag{A.1}$$

Eq. (A.1) is the integral form of Ampere's circuit law, where $\vec{H}$ is the magnetic field intensity, $\vec{l}$ is the flux path length, and i is the current. In the electromagnet, the flux travels through the stainless steel core, then through the air gap, continues through ferrous ball, and returns to the stainless steel core to close the path. The integral in Eq. (A.1) gives:

$$\sum_{k=1}^{4} H_k l_k = N i_c \tag{A.2}$$

where $k = 1,2,3,4$ represents the flux path in the stainless steel core, air gap, ferrous ball, and ambient air, respectively, N is the total turns of the coil, and i_c represents the current

through the coil.

Since the flux leakage is neglected, the flux through the magnetic circuit is a constant. The magnetic flux density B is a constant through the cross-sectional area of the magnetic circuit. Therefore,

$$B_1 A_1 = B_2 A_2 = B_3 A_3 = B_4 A_4 \tag{A.3}$$

where the subscripts 1, 2, 3, and 4 represent the stainless steel core, air gap, ferrous ball, and ambient air, respectively.

The magnetic flux density and the magnetic field intensity are related through the permeability, i.e.,

$$B = \mu_0 \mu_r H \tag{A.4}$$

where μ_0 is the permeability of free space, and μ_r is the relative permeability.

Substituting Eqs. (A.3) and (A.4) into (A.2), the flux density B_2 in the air gap can be solved as:

$$B_2 = \frac{N i_c \mu_0}{A_2 \left(\frac{l_1}{\mu_r A_1} + \frac{x}{A_2} + \frac{l_3}{\mu_r A_3} + \frac{l_4}{A_4} \right)} = \frac{N i_c \mu_0}{\mu_0 A_2 \sum_{j=1}^{3} R_j + x} \tag{A.5}$$

where x is the gap distance, and $R_j = \frac{l_j}{\mu_0 \mu_r A_j}$ is the magnetic reluctance in the magnetic circuit. Eq. (A.5) gives the flux density in an ideal case, where the flux leakage is assumed to be zero.

There are two methods of deriving the attractive magnetic force acting on the ferrous ball. One is to calculate the force from the magnetic pressure from the magnetic field, as suggested by Corson and Lorrain [364]. The magnetic force F is written as:

$$F = -\frac{B_2^2 A_2}{2\mu_0} \tag{A.6}$$

The second method is based on the Faraday induction law of

$$\oint_C \vec{E} d\vec{l} = -\frac{d\lambda}{dt} \tag{A.7}$$

In Eq. (A.7) shows the electromotive force is equal to the rate of magnetic flux change in the magnetic circuit.

Assuming the flux leakage is zero, the flux linkage is calculated as:

$$\lambda = \oint_S \vec{B}_C \vec{n} da = NB_2 A_2 \tag{A.8}$$

The total energy W stored in the air gap can be calculated using:

$$W = \int_0^{i_c} \lambda di = \frac{\mu_0 A_2 N^2 i_c^2}{2\left(\mu_0 A_2 \sum_{j=1}^{3} R_j + x\right)} \tag{A.9}$$

The magnetic force F can be derived by taking the derivative of W with respect to the gap distance x:

$$F = \frac{\partial W}{\partial x} = -\frac{\mu_0 A_2 N^2 i_c^2}{2\left(\mu_0 A_2 \sum_{j=1}^{3} R_j + x\right)^2} = -\frac{B_2^2 A_2}{2\mu_0} \tag{A.10}$$

Substituting Eq. (A.5) into (A.10), the electromagnetic force can be written as:

$$F = -\frac{\mu_0 A_2 N^2}{2}\left(\frac{i_c}{\mu_0 A_2 \sum_{j=1}^{3} R_j + x}\right)^2 = -K_1\left(\frac{i_c}{K_2 + x}\right)^2 \tag{A.11}$$

Eq. (A.11) gives the attractive electromagnetic force F as a function of coil current i_c and gap distance x. K_1 and K_2 are two constants determined by the physical structure of the electromagnet.

Appendix B. Electromagnetic Force FEA

This appendix describes how to use finite element analysis (FEA) to calculate the electromagnetic force. Two cases are studied: case 1 calculates the electromagnetic force when the ball is levitated at the equilibrium point, and case 2 calculates the electromagnetic force assuming the coil current in case 1 reaches its maximum value.

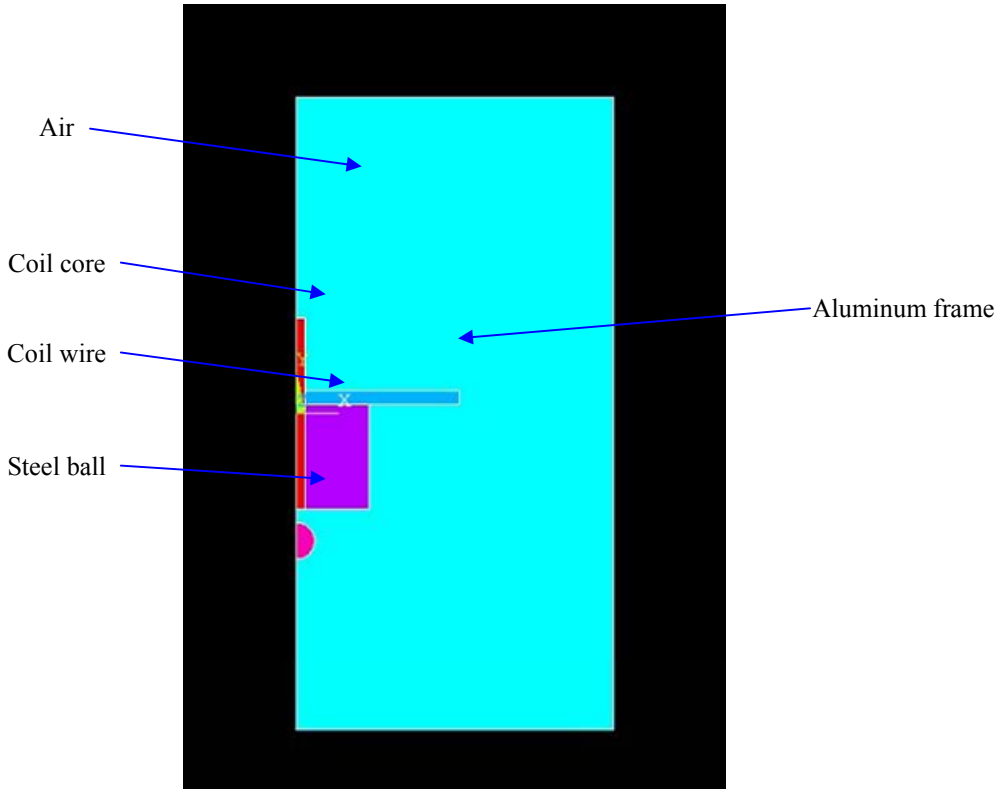

Figure B.1 FEA model of the electromagnet and steel ball

Figure B.1 shows the FEA model. Because the electromagnet and the steel ball are axially symmetric, the calculation can be simplified by running a simulation with a model of the cross-sectional area. In this analysis, the number of turns of wires is assumed to be 3384 [112].

Table B.1Material properties for the FEA

Geometry	Material	Permeability $\left(\frac{\mathrm{H}}{\mathrm{m}}\right)$
Air	Air	1.26×10^{-6}
Coil core	Alloy 20 stainless steel	4.61×10^{-4}
Steel ball	304 stainless steel	1.24×10^{-4}
Aluminum frame	Aluminum	1.26×10^{-6}
Coil wire	Copper	1.26×10^{-6}

Table B.1 lists the material properties used in the FEA. The permeability of air, aluminum, and copper are the same. The permeability of the coil core and steel ball are larger than those of air, aluminum, and copper. Therefore, the magnetic flux density has a larger value in the coil core and steel ball.

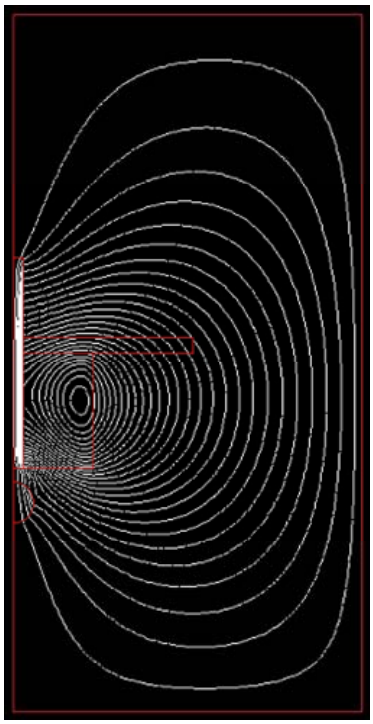

Figure B.2 Magnetic flux lines when steel ball is levitated

Figure B.2 shows simulation results of the magnetic flux lines when the steel ball is levitated at its equilibrium position. The figure also shows that the magnetic flux density is higher in the coil core and the steel ball. The FEA simulation results are summarized in the following table:

Table B.2 Summary of the FEA simulation results

FEA simulation results	
Maximum magnetic flux density is 1.7 T	Saturation happens at about 2 T
Electromagnetic force calculated at equilibrium state is 0.081 N	Electromagnetic force found by FEA is 0.08 N (tensor integration) / 0.079 N (virtual work)
The magnetic flux density at nominal current is 0.9 T	Force at maximum current is 0.35 N

Appendix C. Measuring the System Parameter

In this research, the system parameters of the maglev plant are measured using the experiment setup shown in Figure C.1. It includes an aluminum cantilever beam, an electromagnet, and a steel ball. The frame to support the electromagnet is not shown in the picture. This experiment uses the cantilever beam to measure the displacement of the ball, and thus calculate the electromagnetic force.

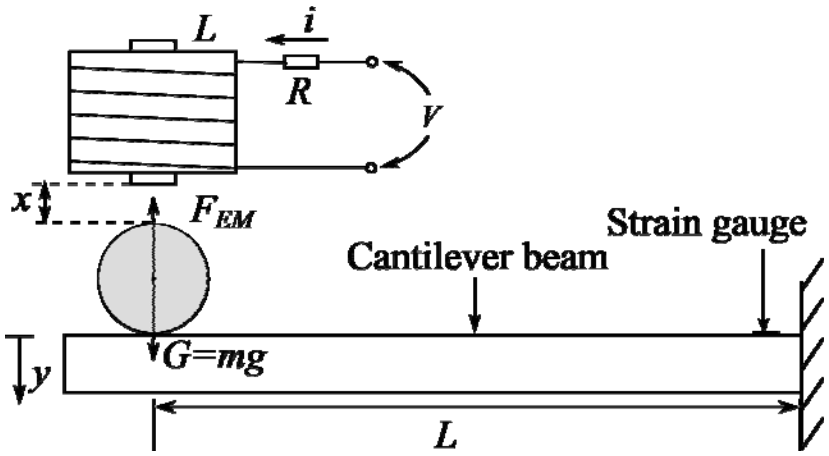

Figure C.1 Experiment to measure the system parameters

Parameters K_1 and K_2 in Table 3.1 can be calculated using the following steps:

(1) First place the steel ball underneath the electromagnet, then adjust the current i so the strain of the cantilever beam is zero (strain gauge reading is zero). This is one equilibrium point.

(2) Measure the gap distance x with a micrometer, and record the current i.

(3) Repeat steps 1 and 2 to find a second equilibrium point and get another group of x and i values.

(4) With two groups of x and i values, K_1 and K_2 can be calculated using Eq.

(3.12)

k_x and k_i can be calculated using K_1 and K_2 (using Eq. (3.13)). They also can be experimentally measured using the following steps:

(1) Adjust the current i to get a small beam deflection y. Record the current i, gap distance x and deflection y values.

(2) Repeat step 1 to get a second group of i, x, and y values.

(3) For each step, the force acting on the cantilever beam can be calculated using $F = \frac{3yEI}{L^3}$. This is also the force acting on the steel ball. Multiplying steel ball mass m through Eq. (3.14) to get a force equation:

$$m\ddot{x} = mk_x x - mk_i i = F$$

Then k_x and k_i can be calculated using two groups of x, i, and F values.

Appendix D. Crossover Frequency Selection

This appendix discusses how the crossover frequency of about 700 Hz is chosen. In Chapter 3, the plant transfer function is derived as:

$$\frac{X(s)}{I(s)} = \frac{-78.48}{s^2 - 66.03^2}$$

The pole at 66.03 rad/s makes the plant unstable.

Chapter 3 also derives the plant transfer function in terms of gap distance and the bias current, i.e.,

$$\frac{X(s)}{I(\mathrm{s})} = \frac{-k_i}{s^2 - k_x}$$

where $k_x = \frac{K_1}{m}\left(\frac{2i_{eq}^2}{(K_2 + x_0)^3}\right)$ and $k_i = \frac{K_1}{m}\left(\frac{2i_{eq}}{(K_2 + x_0)^2}\right)$. The unstable pole is located at $\omega = \sqrt{\frac{K_1}{m}\left(\frac{2i_{eq}^2}{(K_2 + x_0)^3}\right)}$. Assuming m, K_1, and K_2 are constants, the unstable pole ω is a function of bias current i_{eq} and gap distance x_0. If the equilibrium point is made closer to the electromagnet, x_0 will decrease and i_{eq} will increase. Hence, the unstable pole ω will increase, i.e., the positive pole will move right into the RHP. This indicates that there is a trade-off between the equilibrium position and the loop gain. In this study, excessively large positive ω is undesirable. Figure 3.14 shows that as a pole moves into the RHP, the unstable dynamics increase rapidly in the system response.

In testing the maglev testbed, it is found that the position sensor gives a linear output when the gap distance is around 4.5 mm. Therefore, a gap distance of 4.5 mm is chosen as the equilibrium point for the maglev system design, and ω is calculated to be 66.03 rad/s (10.05 Hz). The sampling rate of the DSP controller is about 20 kHz. From the

Nyquist's Theorem, the system bandwidth should be designed below 10 kHz. Murray *et al*. [365] suggested the following equation for systems with digital controllers:

$$\frac{\omega_c}{f} \approx 0.15 \text{ to } 0.5$$

where ω_c is the gain crossover frequency in rad/s and f is the sampling rate of the digital controller in Hz. The crossover frequency of the system is determined using $\frac{\omega_c}{f} = 0.45$, which is roughly 700 Hz.

Appendix E. TI® TMS320C6713 DSP Board

This appendix briefly introduces the DSP board, the Texas Instrument TMS320C6713 DSP board, used in this research. The TMS320C6x series are special purpose microprocessors with specialized architecture targeted for intensive numerical calculations. Applications include image processing, communications, and automation, such as cellular phones, printers, digital cameras, and MP3 players.

The 6713 DSK board includes following hardware:

(1) A C6713 DSP operating at 225 MHz

(2) 4 Kbytes memory for L1D data cache

(3) 4 Kbytes memory for L1P program cache

(4) 256 Kbytes memory for L2 memory

(5) 8 Mbytes of onboard SDRAM (Synchronous Dynamic RAM)

(6) 512 Kbytes of flash memory

(7) 16-bit stereo codec AIC23 with sampling frequency of 8 KHz to 96 KHz

A Code Composer Studio (CCS) software tool can be downloaded from the TI® website. It generates TMS320C6x executable files. CCS includes the assembler, linker, compiler, and simulator and debugger utilities. CCS also provides a software interface library to transfer MATLAB code into executable files for TMS320C6x.

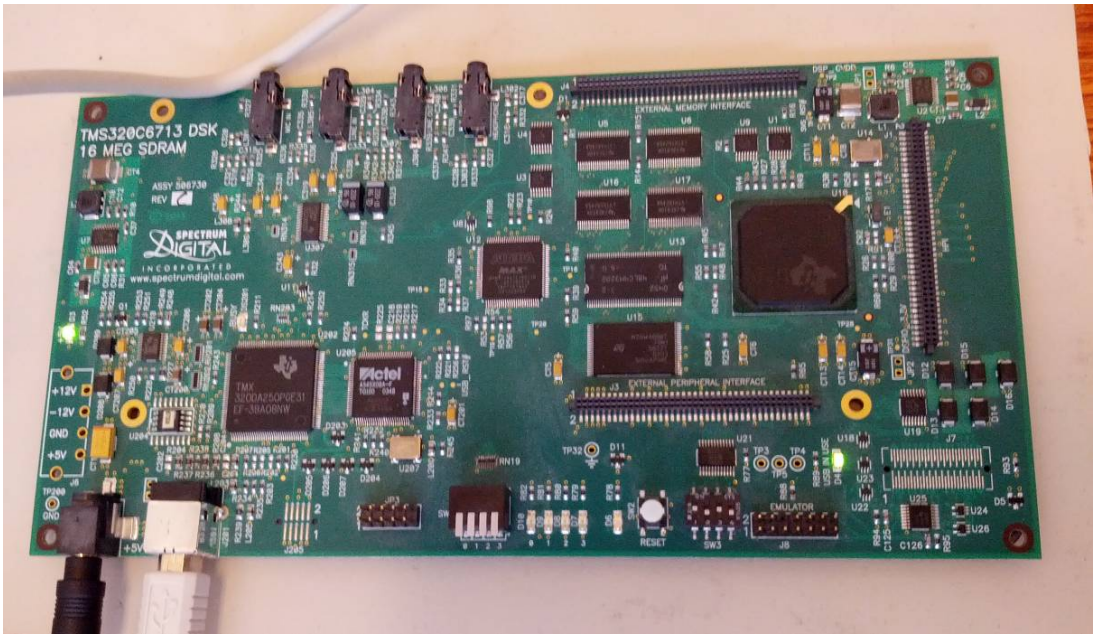

Figure E.1 TMS320C6713 DSP board

Figure E.1 shows a picture of the TMS320C6713 DSP board. In order to process a signal in real time, an Evaluation Module (EVM) is used.

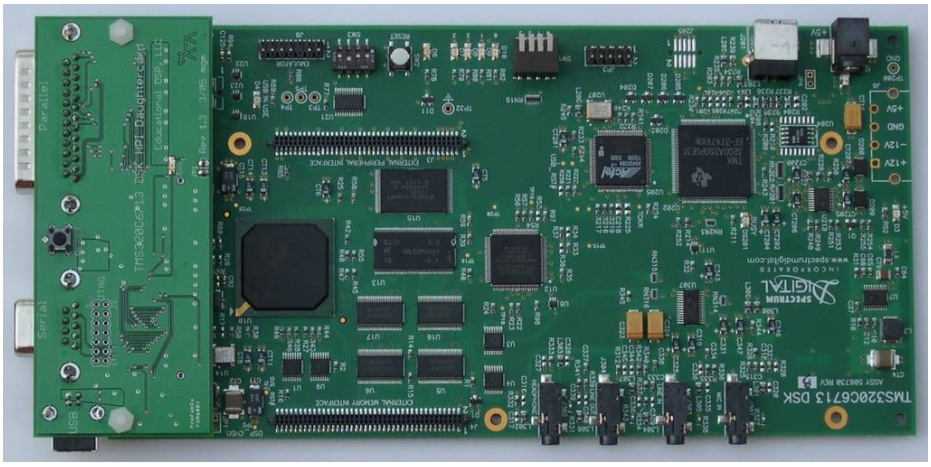

Figure E.2 TMS320C6713 DSP board with a daughter card

Figure E.2 shows a picture of the TMS320C6713 DSP board with a daughter card for signal interfacing. This DSP board is used in this study to implement the controllers.

BIBLIOGRAPHY

[1] J. Alvarez-Ramrez, R. Garrido, and R. Femat, "Control of systems with friction," *Physical Review E*, vol. 51, no. 6, pp. 6235–6238, 1995.

[2] K. J. Åström, "Control of systems with friction," Lund Institute of Technology, Tech. Rep., 1998.

[3] C. Canudas de Wit, H. Olsson, K. J. Åström, and P. Lischinsky, "A new model for control of systems with friction," *IEEE Transactions on Automatic Control*, vol. 40, no. 3, pp. 419–425, 1995.

[4] R. Hirschorn and G. Miller, "Control of nonlinear systems with friction," *IEEE Transactions on Control Systems Technology*, vol. 7, no. 5, pp. 588–595, 1999.

[5] B. C. Kuo and M. F. Golnaraghi, *Automatic control systems*, 4th ed. John Wiley & Sons, 2003.

[6] T. Carbino, M. Gassman, J. Glass, and M. Rashid, "A brief history and theory behind AC, DC and maglev trains and subways," in *Proceedings of the 37th Annual North American Power Symposium*, Ames, IA, 2005, pp. 165–171.

[7] "Magnemotion maglev M^3: The M^3 urban transportation system," Submitted to the Federal Transit Administration as part of FTA project MA-26-7077, MagneMotion Inc., Jan 2003, MagneMotion Document UM-1, Version 1.

[8] C. P. Britcher, J. M. Wells, B. Renaud, and T. Buvat, "Aerodynamics of urban maglev vehicles," *Proceedings of the Institution of Mechanical Engineers, Part F: Journal of Rail and Rapid Transit*, vol. 226, no. 6, pp. 561–567, 2012.

[9] R. Thornton, "Efficient and affordable maglev opportunities in the United States," *Proceedings of the IEEE*, vol. 97, no. 11, pp. 1901–1921, 2009.

[10] J. Beams, "Magnetically supported rotating bodies," U.S. Patent 2,691,306, 1954.

[11] ——, "Magnetic bearings," in *Automotive Engineering Conference*, Detroit, Michigan, Jan 1964, pp. 810–815.

[12] H. Bleuler, M. Cole, P. Keogh, R. Larsonneur, E. Maslen, Y. Okada, G. Schweitzer, A. Traxler, G. Schweitzer, E. Maslen *et al.*, *Magnetic bearings: theory, design and application to rotating machinery*, G. Schweitzer and E. H. Maslen, Eds. Springer-Verlag, 2009.

[13] P. K. Budig, "Magnetic bearings with DC bias: Design and optimum material choice," in *International Symposium on Power Electronics, Electrical Drives, Automation and Motion*, Ischia, Italy, Jun 2008, pp. 1346 –1350.

[14] T. Sato and Y. Tanno, "Magnetic bearing having PID controller and discontinuous controller," in *Proceedings of the International Conference on Industrial Electronics, Control, and Instrumentation*, Maui, HI, 1993, pp. 2121–2125.

[15] B. Shafai, S. Beale, P. Larocca, and E. Cusson, "Magnetic bearing control systems and adaptive forced balancing," *IEEE Control Systems*, vol. 14, no. 2, pp. 4–13, 1994.

[16] P. Studer, "A practical magnetic bearing," *IEEE Transactions on Magnetics*, vol. 13, no. 5, pp. 1155–1157, Sep 1977.

[17] M. Timmes, "An analysis of magnetic bearings," Master's thesis, Rensselaer Polytechnic Institute, New York, 1994.

[18] J. C. Weaver, "Constant Current magnetic bearing," *Review of Scientific Instruments*, vol. 42, no. 2, pp. 275–276, 1971.

[19] A. Eastham and W. Hayes, "Maglev systems development status," *IEEE Aerospace and Electronic Systems Magazine*, vol. 3, no. 1, pp. 21–30, Jan 1988.

[20] M. Fujino, M. Takahashi, M. Tanaka, and H. Nagano, "High speed surface transport system: Nagoya Est Hillside line and the operational testing for 3-car vehicle prototype," in *The 17th International Conference on Magnetically Levitated Systems and Linear Drives*, Lausanne, Switzerland, 2002.

[21] E. Gotizein, R. Meismger, and L. Miller, "The 'Magnetic Wheel' in the suspension of high-speed ground transportation vehicles," *IEEE Transactions on Vehicular Technology*, vol. 29, no. 1, pp. 17–28, Feb 1980.

[22] E. Grossert, "TRANSRAPID SHANGHAI – demonstration line German high technology with Chinese boundary conditions," in *The 17th International Conference on Magnetically Levitated Systems and Linear Drives*, Lausanne, Switzerland, 2002.

[23] H. Lee, K. Kim, and J. Lee, "Review of maglev train technologies," *IEEE Transactions on Magnetics*, vol. 42, no. 7, pp. 1917–1925, Jul 2006.

[24] G. Shu, R. Meisinger, and G. Shen, "Modeling and simulation of Shanghai maglev train Transrapid with random track irregularities," *Sonderdruck Schriftenreihe der Georg-Simon-Ohm-Fachhochschule Nürnberg*, vol. 39, pp. 3–14, 2007.

[25] M. Wackers, "Transrapid super speed maglev technology," in *The 17th International Conference on Magnetically Levitated Systems and Linear Drives*, Lausanne, Switzerland, 2002.

[26] L. Yan, "On the development strategy of the high-speed maglev in china," in *The 17th International Conference on Magnetically Levitated Systems and Linear*

Drives, Lausanne, Switzerland, 2002.

[27] ——, "Progress of the maglev transportation in China," *IEEE Transaction on Applied Superconductivity*, vol. 16, no. 2, pp. 1138–1141, Jun 2006.

[28] J. Choi and Y. Baek, "Magnetically-levitated steel-plate conveyance system using electromagnets and a linear induction motor," *IEEE Transactions on Magnetics*, vol. 44, no. 11, pp. 4171–4174, 2008.

[29] T. Hu and W. Kim, "Extended range six-DOF high-precision positioner for wafer processing," *IEEE/ASME Transactions on Mechatronics*, vol. 11, no. 6, pp. 682–689, 2006.

[30] K. Park, K. Ahn, S. Kim, and Y. Kwak, "Wafer distribution system for a clean room using a novel magnetic suspension technique," *IEEE/ASME Transactions on Mechatronics*, vol. 3, no. 1, pp. 73–78, 1998.

[31] J. B. Wronosky, T. G. Smith, M. J. Craig, B. R. Sturgis, J. R. Darnold, D. K. Werling, M. A. Kincy, D. A. Tichenor, M. E. Williams, and P. M. Bischoff, "Wafer and reticle positioning system for the extreme ultraviolet lithography engineering test stand," in *Microlithography 2000*, ser. Society of Photo-Optical Instrumentation Engineers (SPIE) Conference Series, vol. 3997. International Society for Optics and Photonics, Jul 2000, pp. 829–839.

[32] J. Jeon, M. Caraiani, D. Hwang, J. Lee, D. Kang, Y. Kim, and S. Kim, "High-precision positioning control of magnetic levitation system," in *The 32nd Annual Conference on IEEE Industrial Electronics*, Paris, France, Nov 2006, pp. 5221–5226.

[33] R. Owen, M. Maggiore, and J. Apkarian, "Nonlinear control design for a high-precision contactless positioning system using magnetic levitation," in *Proceedings of the 2005 IEEE Conference on Control Applications*, Toronto, ON, Aug 2005, pp. 481–486.

[34] X. Shan, S. Kuo, J. Zhang, and C. Menq, "Ultra precision motion control of a multiple degree of freedom magnetic suspension stage," *IEEE/ASME Transactions on Mechatronics*, vol. 7, no. 1, pp. 67–78, 2002.

[35] D. L. Trumper, "Magnetic suspension techniques for precision motion control," Ph.D. dissertation, Massachusetts Institute of Technology, Cambridge, MA, 1990.

[36] Y. Ueda and H. Ohsaki, "Six-degree-of-freedom motion analysis of a planar actuator with a magnetically levitated mover by six-phase current controls," *IEEE Transactions on Magnetics*, vol. 44, no. 11, pp. 4301–4304, 2008.

[37] T. Mizuno, M. Takasaki, H. Suzuki, and Y. Ishino, "Development of a three-axis active vibration isolation system using zero-power magnetic suspension," in

Proceedings of the 42nd IEEE Conference on Decision and Control, vol. 5, Maui, HI, Dec 2003, pp. 4493–4498.

[38] T. Mizuno, M. Takasaki, D. Kishita, and K. Hirakawa, "Vibration isolation system combining zero-power magnetic suspension with springs," *Control Engineering Practice*, vol. 15, no. 2, pp. 187–196, 2007.

[39] K. Nagaya and M. Ishikawa, "A noncontact permanent magnet levitation table with electromagnetic control and its vibration isolation method using direct disturbance cancellation combining optimal regulators," *IEEE Transactions on Magnetics*, vol. 31, no. 1, pp. 885–896, 1995.

[40] D. L. Trumper, M. Weng, and R. J. Ritter, "Magnetic suspension and vibration control of beams for non-contact processing," in *Proceedings of the 1999 IEEE International Conference on Control Applications*, Kohala Coast, HI, Aug 1999, pp. 551–557.

[41] K. Watanabe, S. Hara, Y. Kanemitsu, T. Haga, K. Yano, T. Mizuno, and R. Katamura, "Combination of H_∞ and PI control for an electromagnetically levitated vibration isolation system," in *Proceedings of the 35th IEEE Conference on Decision and Control*, vol. 2, Kobe, Japan, Dec 1996, pp. 1223 –1228.

[42] J. Antaki, B. Paden, G. Burgreen, and N. Groom, "Blood pump having a magnetically suspended rotor," Jun 2001, US Patent 6,244,835.

[43] H. Hoshi, K. Katakoa, K. Ohuchi, J. Asama, T. Shinshi, A. Shimokohbe, and S. Takatani, "Magnetically suspended centrifugal blood pump with a radial magnetic driver," *ASAIO journal*, vol. 51, no. 1, pp. 60–64, 2005.

[44] H. Hoshi, T. Shinshi, and S. Takatani, "Third-generation blood pumps with mechanical noncontact magnetic bearings," *Artificial organs*, vol. 30, no. 5, pp. 324–338, 2006.

[45] H. Loree, K. Bourque, D. Gernes, J. Richardson, V. Poirier, N. Barletta, A. Fleischli, G. Foiera, T. Gempp, R. Schoeb *et al.*, "The Heartmate III: design and in vivo studies of a maglev centrifugal left ventricular assist device," *Artificial Organs*, vol. 25, no. 5, pp. 386–391, 2002.

[46] B. Paden, "Magnetically-suspended centrifugal blood pump," May 2001, US Patent 6,227,817.

[47] R. Wampler, "Sealless rotary blood pump," Nov 1998, US Patent 5,840,070.

[48] B. Antkowiak and F. Nelson, "Rotodynamic modeling of an actively controlled magnetic bearing gas turbine engine," *Journal of Engineering for Gas Turbines and Power*, vol. 120, no. CONF-970604–, pp. 621–625, 1998.

[49] S. Haramura, P. Birch, M. Norton, M. Raine, and G. Reynolds, "Gas turbine engine," Nov 1998, US Patent 5,836,739.

[50] A. Newton and J. Sharp, "Gas turbine engine system," Feb 1999, US Patent 5,867,979.

[51] A. Storace, D. Sood, J. Lyons, and M. Preston, "Integration of magnetic bearings in the design of advanced gas turbine engines," *Journal of engineering for gas turbines and power*, vol. 117, no. CONF-940626–, pp. 435–449, 1995.

[52] S. Auchet, P. Chevrier, M. Lacour, and P. Lipinski, "A new method of cutting force measurement based on command voltages of active electro-magnetic bearings," *International Journal of Machine Tools and Manufacture*, vol. 44, no. 14, pp. 1441–1449, 2004.

[53] C. Fouche, "Workpiece-carrier spindle assembly having magnetic bearings, and a device implementing such an assembly for a very high precision machine tool," Dec 1990, US Patent 4,976,177.

[54] C. R. Knospe, "Active magnetic bearings for machining applications," *Control Engineering Practice*, vol. 15, no. 3, pp. 307–313, 2007.

[55] M. Rahman, A. Chiba, and T. Fukao, "Super high speed electrical machines-summary," in *IEEE Power Engineering Society General Meeting*. Denver, CO: IEEE, 2004, pp. 1272–1275.

[56] H. Ueyama and M. Taniguchi, "Magnetic bearing spindle device for machine tools," Jul 1998, US Patent 5,783,887.

[57] M. Ahrens, L. Kucera, and R. Larsonneur, "Performance of a magnetically suspended flywheel energy storage device," *IEEE Transactions on Control Systems Technology*, vol. 4, no. 5, pp. 494–502, 1996.

[58] T. Coombs, A. Campbell, R. Storey, and R. Weller, "Superconducting magnetic bearings for energy storage flywheels," *IEEE Transactions on Applied Superconductivity*, vol. 9, no. 2, pp. 968–971, 1999.

[59] J. Hull, T. Mulcahp, K. Uherka, R. Erck, and R. Abboud, "Flywheel energy storage using superconducting magnetic bearings," *Applied superconductivity*, vol. 2, no. 7, pp. 449–455, 1994.

[60] T. Ichihara, K. Matsunaga, M. Kita, I. Hirabayashi, M. Isono, M. Hirose, K. Yoshii, K. Kurihara, O. Saito, S. Saito *et al.*, "Application of superconducting magnetic bearings to a 10 kwh-class flywheel energy storage system," *IEEE Transactions on Applied Superconductivity*, vol. 15, no. 2, pp. 2245–2248, 2005.

[61] Y. Miyagawa, H. Kameno, R. Takahata, and H. Ueyama, "A 0.5 kwh flywheel

energy storage system using a high-T_c superconducting magnetic bearing," *IEEE Transactions on Applied Superconductivity*, vol. 9, no. 2, pp. 996–999, 1999.

[62] S. Nagaya, N. Kashima, M. Minami, H. Kawashima, and S. Unisuga, "Study on high temperature superconducting magnetic bearing for 10 kwh flywheel energy storage system," *IEEE Transactions on Applied Superconductivity*, vol. 11, no. 1, pp. 1649–1652, 2001.

[63] P. Ribeiro, B. Johnson, M. Crow, A. Arsoy, and Y. Liu, "Energy storage systems for advanced power applications," *Proceedings of the IEEE*, vol. 89, no. 12, pp. 1744–1756, 2001.

[64] B. Weinberger, L. Lynds Jr, and J. Hull, "Flywheel energy storage with superconductor magnetic bearings," Jun 1993, US Patent 5,214,981.

[65] Z. Xia, Q. Chen, K. Ma, C. McMichael, M. Lamb, R. Cooley, P. Fowler, and W. Chu, "Design of superconducting magnetic bearings with high levitating force for flywheel energy storage systems," *IEEE Transactions on Applied Superconductivity*, vol. 5, no. 2, pp. 622–625, 1995.

[66] P. Imoberdorf, C. Zwyssig, S. Round, and J. Kolar, "Combined radial-axial magnetic bearing for a 1 kW, 500,000 rpm permanent magnet machine," in *The 22nd Annual IEEE Applied Power Electronics Conference*, Anaheim, CA, 2007, pp. 1434–1440.

[67] K. Kemper, "Overhead suspension railway with wheel-less vehicles employing magnetic suspension from iron rails," German Patent 643316 and 644302, 1937.

[68] J. Meins, L. Miller, and W. Mayer, "The high speed maglev transport system TRANSRAPID," *IEEE Transactions on Magnetics*, vol. 24, no. 2, pp. 808–811, Mar 1988.

[69] D. Tum, D. Huhn, and D. Harbeke, "Design and development of the Transrapid TR09," in *Proceedings of the 19th international conference on magnetically levitated systems and linear drives*, Dresden, Germany, 2006.

[70] P. Holmer, "Faster than a speeding bullet train," *IEEE Spectrum*, vol. 40, no. 8, pp. 30–34, 2003.

[71] S. Miyamoto, Y. Osada, K. Yamazumi, and T. Furuki, "The status of the running tests of JR-Maglev," in *The 18th International Conference on Magnetically Levitated Systems and Linear Drives*, San Diego, CA, 2004, pp. 60–64.

[72] R. Thornton, "Flying low with maglev," *IEEE Spectrum*, vol. 10, no. X-73-043, pp. 47–54, 1973.

[73] V. Vuchic and J. Casello, "An evaluation of maglev technology and its comparison with high speed rail," *Transportation Quarterly*, vol. 56, no. 2, pp. 33–50, 2002.

[74] C. M. Osburn, “Reassessing contamination control requirements as dram capacities reach 16 Mb,” *Microcontamination*, vol. 9, no. 7, pp. 19–27, 1991.

[75] T. Azukizawa, M. Morishita, S. Kanda, N. Tamura, and T. Yokoyama, “A linear induction motor control system for magnetically levitated carrier system,” *IEEE Transactions on Vehicular Technology*, vol. 38, no. 2, pp. 102–108, May 1989.

[76] K. Aik-siong, R. Ford, and T. Seshadri, “Wafer handling with levitation,” *Journal of Electronics Manufacturing*, vol. 2, no. 03, pp. 101–107, 1992.

[77] R. Owen, M. Maggiore, and J. Apkarian, “A high-precision, magnetically levitated positioning stage: Toward contactless actuation for industrial manufacturing,” *IEEE Control Systems*, vol. 26, no. 3, pp. 82–95, 2006.

[78] W. Kim and D. L. Trumper, “High-precision magnetic levitation stage for photolithography,” *Precision Engineering*, vol. 22, no. 2, pp. 66–77, 1998.

[79] M. E. Williams, D. L. Trumper, and R. Hocken, “Magnetic bearing stage for photolithography,” *CIRP Annals-Manufacturing Technology*, vol. 42, no. 1, pp. 607–610, 1993.

[80] M. Holmes, R. Hocken, and D. Trumper, “The long-range scanning stage: a novel platform for scanned-probe microscopy,” *Precision engineering*, vol. 24, no. 3, pp. 191–209, 2000.

[81] K. Craig, “Is anything really new in mechatronics education?” *IEEE Robotics & Automation Magazine*, vol. 8, no. 2, pp. 12–19, 2001.

[82] K. Craig and F. Stolfi, “Teaching control system design through mechatronics: academic and industrial perspectives,” *Mechatronics*, vol. 12, no. 2, pp. 371–381, 2002.

[83] K. Craig, T. Kurfess, and M. Nagurka, “Magnetic levitation testbed for controls education,” in *Proceedings of the ASME Dynamic Systems and Control Division*, vol. 64, 1998, pp. 15–20.

[84] K. C. Craig and J. A. de Marchi, “Mechatronic system design at Rensselaer,” *Computer Applications in Engineering Education*, vol. 4, no. 1, pp. 67–78, 1996.

[85] K. C. Craig and F. R. Stolfi, *Introduction to mechatronic system design with applications: Course Book*. American Society of Mechanical Engineers, 1994.

[86] J. R. Brauer, *Magnetic Actuator and Sensors*. Wiley-IEEE Press, 2006.

[87] F. Di Puccio, A. Musolino, R. Rizzo, and E. Tripodi, “A self-controlled maglev system,” *Progress In Electromagnetics Research M*, vol. 26, pp. 187–203, 2012.

[88] M. Janic, “Multicriteria evaluation of high-speed rail, transrapid maglev and air

passenger transport in europe," *Transportation Planning and Technology*, vol. 26, no. 6, pp. 491–512, 2003.

[89] M. Ono, S. Koga, and H. Ohtsuki, "Japan's superconducting maglev train," *IEEE Instrumentation Measurement Magazine*, vol. 5, no. 1, pp. 9–15, Mar 2002.

[90] J. Powell and G. Danby, "Maglev vehicles-raising transportation advances of the ground," *IEEE Potentials*, vol. 15, no. 4, pp. 7–12, Nov 1996.

[91] D. Eaton, J. Rama, and S. Singhal, "Magnetic bearing applications & economics," in *The 57th Annual Petroleum and Chemical Industry Conference (PCIC)*. Duncanville, TX: IEEE, 2010, pp. 1–9.

[92] M. L. Long, J. Carroll, and R. Mukundan, "Adaptive control of active magnetic bearings under unknown static load change and unbalance," in *Proceedings of the 1996 IEEE International Conference on Control Applications*, Dearborn, MI, 1996, pp. 876–881.

[93] J. D. Yau, "Vibration control of maglev vehicles traveling over a flexible guideway," *Journal of Sound and Vibration*, vol. 321, no. 1–2, pp. 184–200, 2009.

[94] I. Horowitz, "Quantitative feedback theory," in *IEEE Proceedings on Control Theory and Applications*, vol. 129, no. 6. IET, 1982, pp. 215–226.

[95] ——, "Invited paper survey of quantitative feedback theory (QFT)," *International Journal of Control*, vol. 53, no. 2, pp. 255–291, 1991.

[96] A. Binnie, "Using the history of electricity and magnetism to enhance teaching," *Science & Education*, vol. 10, no. 4, pp. 379–389, 2001.

[97] M. Fowler, "Historical beginnings of theories of electricity and magnetism," 1995, Summer Lectures on History of Theories of Electricity and Magnetism, Physics Department, University of Virginia.

[98] S. Earnshaw, "On the nature of the molecular forces which regulate the constitution of the luminferous ether," *Trans. Camb. Phil. Soc.*, vol. 7, pp. 97–112, 1842.

[99] M. V. Berry and M. V. Berry, "The Levitron^{TM}: an adiabatic trap for spins," *Proceedings of the Royal Society of London. Series A: Mathematical, Physical and Engineering Sciences*, vol. 452, no. 1948, pp. 1207–1220, 1996.

[100] T. B. Jones, M. Washizu, and R. Gans, "Simple theory for the Levitron," *Journal of Applied Physics*, vol. 82, no. 2, pp. 883–888, Jul 1997.

[101] R. E. Pelrine, "Diamagnetic lévitationà," *American Scientist*, vol. 92, no. 5, pp. 428–437, 2004.

[102] M. N. O. Sadiku and C. M. Akujuobi, "Magnetic levitation," *IEEE Potentials*,

vol. 25, no. 2, pp. 41–42, Mar 2006.

[103] A. Gonzalez, R. Diaz, and E. Cabal, "Mathematical model of a levitation system based on eddy currents," in *International Conference on Industrial Electronics and Control Applications*, Quito, May 2005, pp. 5–15.

[104] R. Rabinovici, V. Berdichevsky, and M. Shvartsas, "Eddy-currents levitation system," in *The IEEE 27th Convention of Electrical Electronics Engineers in Israel (IEEEI)*, Eilat, Israel, Nov 2012, pp. 1–4.

[105] M. Thompson, "Eddy current magnetic levitation: Models and experiments," *IEEE Potentials*, vol. 19, no. 1, pp. 40–44, Feb 2000.

[106] W. Braunbeck, "Free suspension of bodies in electric and magnetic fields," *Zeitschrift für Physik*, vol. 112, no. 11, pp. 753–763, 1939.

[107] B. V. Jayawant, *Electromagnetic Levitation and Suspension Systems*. Edward Arnold, 1981.

[108] H. H. Woodson and J. R. Melcher, *Electromechanical Dynamics*. John Wiley & Sons Inc., 1968.

[109] F. T. Holmes, "Axial magnetic suspension," *Rev. Sci. Instrum.*, vol. 8, pp. 444–448, 1937.

[110] J. Beams, "Apparatus for rotating freely suspended bodies," U.S. Patent 3,041,482, 1962.

[111] N. Kinichi, T. Masaaki, and M. Ichiro, "Linear motor drive system for the normal conductivity maglev vehicle HSST-05," *IEEE Transactions on Industry Applications*, vol. 110, no. 1, pp. 23–31, 1990.

[112] S. A. Green, "Robust nonlinear control of magnetic-levitation systems," Ph.D. dissertation, Rensselaer Polytechnic Institute, Troy, New York, 1997.

[113] W. Wang, M. Lamb, and I. Busch-Vishniac, "An automated loading and unloading system for a maglev wafer transport path," *IEEE Transactions on Semiconductor Manufacturing*, vol. 6, no. 3, pp. 276–279, Aug 1993.

[114] K. Miller, "Wafer transport device," U.S. Patent 5,417,537, May, 1995.

[115] H. Lan, Y. Ding, H. Liu, and B. Lu, "Review of the wafer stage for nanoimprint lithography," *Microelectronic Engineering*, vol. 84, no. 4, pp. 684–688, 2007.

[116] S. Mittal and C. Menq, "Precision motion control of a magnetic suspension actuator using a robust nonlinear compensation scheme," *IEEE/ASME Transactions on Mechatronics*, vol. 2, no. 4, pp. 268–280, 1997.

[117] M. Chen, C. Jou, and Z. Guo, “Adaptive sliding mode controller applied to a high-precision positioning platform,” in *The 27th Chinese Control Conference*, 2008, pp. 624–628.

[118] L. Guang, Z. Yu, Z. Ming, D. Guanghong, and M. Tomizuka, “Six-DOF maglev nano precision microstage development,” in *2010 International Conference on Mechanic Automation and Control Engineering (MACE)*, Jun 2010, pp. 938 –941.

[119] J. Beams, “Suspension of rotatable bodies,” U.S. Patent 2,256,937, 1941.

[120] ——, “Magnetic suspension system,” U.S. Patent 3,196,694, Jul., 1965.

[121] H. White and H. Weltin, “Electromagnetic levitator,” *American Journal of Physics Teachers*, vol. 31, pp. 925–929, 1963.

[122] H. Gutberlet, “The German magnetic transportation program,” *IEEE Transactions on Magnetics*, vol. 10, no. 3, pp. 417–420, Sep 1974.

[123] G. Schweitzer and R. Lunge, “Characteristics of a magnetic rotor bearing for active vibration control,” in *Proc. of First International Conference on Vibration in Rotating Machinery*, Cambridge, 1976, pp. 1–6.

[124] H. Habermann and G. Liard, “Practical magnetic bearings,” *IEEE Spectrum*, vol. 16, no. 9, pp. 26–30, 1979.

[125] ——, “An active magnetic bearing system,” *Tribology international*, vol. 13, no. 2, pp. 85–87, 1980.

[126] E. H. Maslen, “Self-sensing for active magnetic bearings: overview and status,” in *Proc. of the 10th Int. Symp. on Magnetic Bearings, Martigny, Switzerland*, 2006.

[127] J. P. Yonnet, “Passive magnetic bearings with permanent magnets,” *IEEE Transactions on Magnetics*, vol. 14, no. 5, pp. 803–805, 1978.

[128] R. K. Wampler, “Sealless rotary blood pump with passive magnetic radial bearings and blood immersed axial bearings,” U.S. Patent 5,695,471, Dec, 1997.

[129] A. V. Filatov and E. Maslen, “A passive magnetic bearing,” in *Proceedings of the 7th International Symposium on Magnetic Bearings*, Zurich, Switzerland, 2000.

[130] A. V. Filatov and E. H. Maslen, “Passive magnetic bearing for flywheel energy storage systems,” *IEEE Transactions on Magnetics*, vol. 37, no. 6, pp. 3913–3924, 2001.

[131] A. Hamler, V. Gorican, B. Štumberger, M. Jesenik, and M. Trlep, “Passive magnetic bearing,” *Journal of magnetism and magnetic materials*, vol. 272, pp. 2379–2380, 2004.

[132] S. McCarthy, S. Flanagan, A. Simpson, and M. Sorin, "Passive magnetic bearing," U.S. Patent 20,110,001,379, Jul., 2010.

[133] *MBC 500 Magnetic Bearing System Operation Instructions*, Magnetic Moments, LLC, 5735 Hollister Ave., Suite B Goleta, CA 93117, Oct 2004, http://www.mmsb.com.

[134] C. Chen, B. Paden, J. Antaki, J. Ludlow, D. Paden, R. Crowson, and G. Bearnson, "A magnetic suspension theory and its application to the HeartQuest ventricular assist device," *Artificial organs*, vol. 26, no. 11, pp. 947–951, 2002.

[135] B. Paden, N. Groom, and J. F. Antaki, "Design formulas for permanent magnet bearings," *Journal of Mechanical Design*, vol. 125, pp. 734–739, 2003.

[136] K. Chu, Y. Wang, J. Wilson, C. Y. Lin, and T. C. Tsao, "Modeling and control of a magnetic bearing system," in *American Control Conference*, 2010, pp. 2206–2211.

[137] H. Chang and T. C. Tsao, "Repetitive control of a levitated shaft – FPGA implementation based on powell-chau filters," in *Proc. Int. Symp. Flex. Autom*, 2010, pp. 1–8.

[138] H. L. Chang and T. C. Tsao, "High-sampling rate dynamic inversion–filter realization and applications in digital control," *IEEE/ASME Transactions on Mechatronics*, vol. 2, no. 99, pp. 1–11, 2012.

[139] H. Bleuler, M. Cole, P. Keogh, R. Larsonneur, E. Maslen, Y. Okada, G. Schweitzer, A. Traxler, G. Schweitzer, E. Maslen *et al.*, *Magnetic bearings - theory, design and application to rotating machinery*, G. Schweitzer and E. H. Maslen, Eds. Springer-Verlag, 2009.

[140] P. K. Sinha, *Electromagnetic suspension dynamics and control*. Peter Peregrinus Ltd., 1987.

[141] M. L. Nagurka, "EMS maglev vehicle-guideway-controller model," in *1995 Proceedings of the American Control Conference*, vol. 2. IEEE, 1995, pp. 1167–1168.

[142] R. M. Goodall, "Generalised design models for EMS maglev," in *Proceedings of MAGLEV 2008 – The 20th International Conference on Magnetically Levitated Systems and Linear Drives*, 2008, pp. 15–18.

[143] S. Joo and J. Seo, "Design and analysis of the nonlinear feedback linearizing control for an electromagnetic suspension system," *IEEE Transactions on Control Systems Technology*, vol. 5, no. 1, pp. 135–144, 1997.

[144] B. V. Jayawant, "Electromagnetic suspension and levitation," *IEE Proceedings A Physical Science, Measurement and Instrumentation, Management and Education,*

Reviews, vol. 129, no. 8, pp. 549–581, 1982.

[145] V. A. Dzenzerskii, A. A. Zevin, and L. A. Filonenko, "Stability of vertical oscillations in an electrodynamic suspension system with a discrete guideway structure," *International applied mechanics*, vol. 31, no. 7, pp. 587–591, 1995.

[146] S. B. Kuznetsov, "Method and apparatus for combined levitation and guidance along guideway curvature in electrodynamic magnetically levitated high speed vehicle," U.S. Patent 5,628,252, May, 1997.

[147] D. M. Rote and Y. Cai, "Review of dynamic stability of repulsive-force maglev suspension systems," *IEEE Transactions on Magnetics*, vol. 38, no. 2, pp. 1383–1390, 2002.

[148] P. K. Sinha and A. N. Pechev, "Nonlinear H_∞ controllers for electromagnetic suspension systems," *IEEE Transactions on Automatic Control*, vol. 49, no. 4, pp. 563–568, 2004.

[149] R. F. Post, *Inductrack demonstration model*. Lawrence Livermore National Laboratory, 1998.

[150] R. F. Post and D. D. Ryutov, "The inductrack: a simpler approach to magnetic levitation," *IEEE Transactions on Applied Superconductivity*, vol. 10, no. 1, pp. 901–904, 2000.

[151] R. Post and S. Gurol, "The inductrack approach to electromagnetic launching and maglev trains," in *6th International Symposium on Magnetic Levitation Technology*, Turin, Italy, 2001.

[152] L. S. Tung, R. F. Post, and J. Martinez-Frias, "Final progress report for the NASA inductrack model rocket launcher at the lawrence livermore national laboratory," NASA Livermore National Laboratory, Tech. Rep., June 2001.

[153] R. F. Post, "Inductrack magnet configuration," U.S. Patent 6,664,880, Dec., 2003.

[154] T. Murai and H. Hasegawa, "Electromagnetic analysis of inductrack magnetic levitation," *Electrical Engineering in Japan*, vol. 142, no. 1, pp. 67–74, 2003.

[155] R. F. Post, "Laminated track design for inductrack maglev systems," U.S. Patent 6,758,146, Jul., 2004.

[156] K. Sawada, "Magnetic levitation (maglev) technologies," *Japan Railway & Transport Review*, vol. 12, no. 25, pp. 58–61, 2005.

[157] Y. Yasuda, M. Fujino, M. Tanaka, and S. Ishimoto, "The first HSST maglev commercial train in japan," in *Proceedings of the 18th International Conference on Magnetically Levitated Systems and Linear Drives (MAGLEV 2004)*, 2004, pp.

76–85.

[158] S. Aoki, “3-dimensional magnetic field calculation of the levitation magnet for hsst by the finite element method,” *IEEE Transactions on Magnetics*, vol. 16, no. 5, pp. 725–727, 1980.

[159] E. Masada, M. Kitamoto, J. Kato, and M. Kawashima, “Present status of maglev development in japan and hsst-03 project,” in *International Conference on Maglev Transport: Now and for the Future*, 1984.

[160] S. Suzuki, M. Kawashima, Y. Hosoda, and T. Tanida, “HSST-03 system,” *IEEE Transactions on Magnetics*, vol. 20, no. 5, pp. 1675–1677, 1984.

[161] K. Fujisaki and E. Masada, “Dynamic behaviour of a magnetic wheel,” *IEEE Transactions on Magnetics*, vol. 20, no. 5, pp. 1678–1680, 1984.

[162] Y. Hosoda, M. Kawashima, M. Iwaya, and Y. Hikasa, “Curvature running test results of hsst vehicle,” *IEEE Transactions on Magnetics*, vol. 23, no. 5, pp. 2344–2346, 1987.

[163] Y. Nozaki, T. Koseki, and E. Masada, “Analysis of linear induction motors for HSST and linear metro using finite difference method,” *Proc. LDIA*, pp. 168–171, 2005.

[164] M. Takahashi, G. Kwok, and K. Kubota, “Marketing strategy of the HSST system,” *Proceeding of Maglev2006,*, vol. 1, pp. 53–57, 2006.

[165] Educational Control Products, “Model 730 Maglev apparatus fact sheets,” www.ecpsystems.com.

[166] Feedback Instruments, “Magnetic levitation system 33-006-PCI,” www.feedback-instruments.com.

[167] K. Lundberg, K. Lilienkamp, and G. Marsden, “Low-cost magnetic levitation project kits,” *IEEE Control Systems*, vol. 24, no. 5, pp. 65–69, 2004.

[168] A. A. Awelewa, I. A. Samuel, A. Ademola, and S. O. Iyiola, “An undergraduate control tutorial on root locus-based magnetic levitation system stabilization,” *International Journal of Engineering & Computer Science*, vol. 13, no. 1, pp. 14–22, Feb 2013.

[169] S. A. Green, R. S. Hirsch, and K. C. Craig, “Magnetic levitation device as teaching aid for mechatronics at rensselaer,” in *Proceedings of ASME IMECE Dynamic Systems and Control*, Nov 1997.

[170] S. A. Green and K. C. Craig, “Robust, digital, nonlinear control of magnetic-levitation systems,” *Journal of Dynamic Systems, Measurement, and*

Control, vol. 120, no. 4, pp. 488–495, 1998.

[171] K. Craig, "Mechatronics at rensselaer: a two-course senior-elective sequence in mechanical engineering," in *IEEE/ASME International Conference on Advanced Intelligent Mechatronics*. IEEE, 1999, pp. 452–458.

[172] B. V. Jayawant, "Electromagnetic suspension and levitation," *Rep. Prog. Phys.*, vol. 44, pp. 411–472, 1981.

[173] T. Wong, "Design of a magnetic levitation system—an undergraduate project," *IEEE Transaction on Education*, vol. 29, pp. 196–200, 1986.

[174] P. K. Sinha, *Electromagnetic Suspension, Dynamics and Control*. Peter Perginus Ltd., 1987.

[175] E. E. Covert, "Magnetic suspension and balance systems," *IEEE AES Magazine*, vol. 3, pp. 14–22, May 1988.

[176] W. Barie and J. Chiasson, "Linear and nonlinear state-space controllers for magnetic levitation," *International Journal of System Science*, vol. 27, no. 11, pp. 1153–1163, 1996.

[177] M. B. Scudiere, R. A. Willems, and G. T. Gillies, "Digital controller for a magnetic suspension system," *Rev. Sci. Instrum.*, vol. 57, no. 8, pp. 1616–1626, 1986.

[178] R. Williams, F. Keith, and P. Allaire, "Digital control of active magnetic bearings," *IEEE Transactions on Industrial Electronics*, vol. 37, no. 1, pp. 19–27, 1990.

[179] W. Hurley, M. Hynes, and W. Wolfle, "PWM control of a magnetic suspension system," *IEEE Transactions on Education*, vol. 47, no. 2, pp. 165–173, 2004.

[180] C. Zhu and Z. Mao, "A PWM based switching power amplifier for active magnetic bearings," in *Proceedings of the 8th International Conference on Electrical Machines and Systems*, vol. 2, 2005, pp. 1563–1568.

[181] R. Marino and P. Tomei, *Nonlinear control design: geometric, adaptive and robust*. Prentice Hall International (UK) Ltd., 1996.

[182] H. K. Khalil and J. W. Grizzle, *Nonlinear systems*. Prentice Hall Upper Saddle River, 2002, vol. 3.

[183] M. A. Henson and D. E. Seborg, "Input-output linearization of general nonlinear processes," *AIChE Journal*, vol. 36, no. 11, pp. 1753–1757, 1990.

[184] J. J. E. Slotine and J. KARL HEDRICK, "Robust input-output feedback linearization," *International Journal of control*, vol. 57, no. 5, pp. 1133–1139, 1993.

[185] J. Hung, "Nonlinear control of a magnetic levitation system," in *The International*

Conference on Industrial Electronics, Control and Instrumentation, 1991, pp. 268–273 vol.1.

[186] M. Filho and C. Munaro, "A design methodology of tracking controllers for magnetic levitation systems," in *Proceedings of the 2001 IEEE International Conference on Control Applications*, 2001, pp. 47–51.

[187] Z. J. Yang and M. Tateishi, "Adaptive robust nonlinear control of a magnetic levitation system," *Automatica*, vol. 37, no. 7, pp. 1125–1131, 2001.

[188] J. Lindlau and C. Knospe, "Feedback linearization of an active magnetic bearing with voltage control," *IEEE Transactions on Control Systems Technology*, vol. 10, no. 1, pp. 21–31, 2002.

[189] T. Mizutani, H. Katayama, and A. Ichikawa, "Tracking control of a magnetic levitation system by feedback linearization," in *SICE 2004 Annual Conference*, vol. 1, 2004, pp. 121–126 vol. 1.

[190] M. Chen and C. Knospe, "Feedback linearization of active magnetic bearings: current-mode implementation," *IEEE/ASME Transactions on Mechatronics*, vol. 10, no. 6, pp. 632–639, 2005.

[191] Y. Lin and E. D. Sontag, "A universal formula for stabilization with bounded controls," *Systems & Control Letters*, vol. 16, no. 6, pp. 393–397, 1991.

[192] E. D. Sontag, "A universal construction of artstein's theorem on nonlinear stabilization," *Systems & control letters*, vol. 13, no. 2, pp. 117–123, 1989.

[193] F. Blanchini and S. Carabelli, "Robust stabilization via computer-generated Lyapunov functions: an application to a magnetic levitation system," in *Proceedings of the 33rd IEEE Conference on Decision and Control*, vol. 2, 1994, pp. 1105–1106.

[194] A. Polanski, "On absolute stability analysis by polyhedral lyapunov functions," *Áutomatica*, vol. 36, no. 4, pp. 573–578, 2000.

[195] H. K. Chiang, C. A. Chen, and M. Y. Li, "Integral variable-structure grey control for magnetic levitation system," *IEE Proceedings on Electric Power Applications*, vol. 153, no. 6, pp. 809–814, 2006.

[196] F. J. Lin and S. Y. Chen, "Intelligent integral backstepping sliding mode control using recurrent neural network for magnetic levitation system," in *The 2010 International Joint Conference on Neural Networks (IJCNN)*, 2010, pp. 1–7.

[197] M. De Queiroz and D. Dawson, "Nonlinear control of active magnetic bearings: a backstepping approach," *IEEE Transactions on Control Systems Technology*, vol. 4, no. 5, pp. 545–552, 1996.

[198] P. Pranayanuntana and R. Vanchai, “Nonlinear backstepping control design applied to magnetic ball control,” in *Proceedings of TENCON*, vol. 3. IEEE, 2000, pp. 304–307.

[199] F. J. Lin, L. T. Teng, and P. H. Shieh, “Intelligent adaptive backstepping control system for magnetic levitation apparatus,” *IEEE Transactions on Magnetics*, vol. 43, no. 5, pp. 2009–2018, 2007.

[200] R. J. Wai and K. Chuang, “Design of backstepping particle-swarmoptimisation control for maglev transportation system,” *IET Control Theory Applications*, vol. 4, no. 4, pp. 625–645, 2010.

[201] B. Draženovic, “The invariance conditions in variable structure systems,” *Áutomatica*, vol. 5, no. 3, pp. 287–295, 1969.

[202] S. Emelyanov, V. Utkin, V. Taran, N. Kostyleva, A. Shubladze, and V. Ezerov, “Theory of variable structure systems,” *Moscowz Nauka (en ruso)*, vol. 7, pp. 191–199, 1970.

[203] K. K. D. Young, “Controller design for a manipulator using theory of variable structure systems,” *IEEE Transactions on Systems, Man and Cybernetics*, vol. 8, no. 2, pp. 101–109, 1978.

[204] V. Utkin, “Variable structure systems with sliding modes,” *IEEE Transactions on Automatic Control*, vol. 22, no. 2, pp. 212–222, 1977.

[205] V. I. Utkin, *Sliding modes and their application in variable structure systems*. Mir Publishers, 1978.

[206] V. Utkin, “Variable structure systems - present and future,” *Automation and Remote Control*, vol. 44, no. 9, pp. 1105–1120, 1984.

[207] J.-J. E. Slotine, W. Li *et al.*, *Applied nonlinear control*. Prentice Hall New Jersey, 1991.

[208] D. Cho, Y. Kato, and D. Spilman, “Sliding mode and classical controllers in magnetic levitation systems,” *IEEE Control Systems*, vol. 13, pp. 42–48, 1993.

[209] A. El-Hajjaji and M. Ouladsine, “Modeling and nonlinear control of magnetic levitation systems,” *IEEE Transactions on Industrial Electronics*, vol. 48, no. 4, pp. 831–838, 2001.

[210] N. Al-Muthairi and M. Zribi, “Sliding mode control of a magnetic levitation system,” *Mathematical Problems in Engineering*, vol. 2004, no. 2, pp. 93–107, 2004.

[211] N. Tsai, C. Chiang, and C. H. Kuo, “Robust sliding mode control for axial AMB

systems," in *The 5th Asian Control Conference*, vol. 1, 2004, pp. 64–69 Vol.1.

[212] E. Alvarez-Sanchez, J. Alvarez-Gallegos, and R. Castro-Linares, "Dynamical sliding mode control of a maglev system with 3 DOFs: Experimental results," in *The 4th International Conference onElectrical and Electronics Engineering*, 2007, pp. 270–273.

[213] Y. Kim and K. Kim, "Gain scheduled control of magnetic suspension system," in *American Control Conference*, vol. 3. IEEE, 1994, pp. 3127–3131.

[214] C. Knospe and C. Yang, "Gain-scheduled control of a magnetic bearing with low bias flux," in *Proceedings of the 36th IEEE Conference on Decision and Control*, vol. 1, 1997, pp. 418–423.

[215] F. Betschon and C. Knospe, "Reducing magnetic bearing currents via gain scheduled adaptive control," *IEEE/ASME Transactions on Mechatronics*, vol. 6, no. 4, pp. 437–443, 2001.

[216] K. J. Åström and B. Wittenmark, *Adaptive control*. Dover Publications, 2008.

[217] R. Bellman and R. E. Kalaba, *Dynamic programming and modern control theory*. Academic Press New York, 1965.

[218] Y. Z. Tsypkin and S. Nikolic, *Adaptation and learning in automatic systems*. Academic Press, Inc., 1971.

[219] I. Z. Tsypkin, *Foundations of the theory of learning systems*. Academic Press, 1973, vol. 101.

[220] B. T. Poljak and J. Z. Tsypkin, "Robust identification," *Automatica*, vol. 16, no. 1, pp. 53–63, 1980.

[221] H. Unbehauen, "Review and future of adaptive control systems," in *Analysis and Control of Industrial Processes*. Springer, 1991, pp. 3–22.

[222] W. D. Meadow Jr, W. D. Meadow, P. J. Berkelman *et al.*, "Adaptive magnetic levitation apparatus and method," U.S. Patent 7,224,252, may, 2007.

[223] Z. J. Yang, K. Kunitoshi, S. Kanae, and K. Wada, "Adaptive robust output-feedback control of a magnetic levitation system by k-filter approach," *IEEE Transactions on Industrial Electronics*, vol. 55, no. 1, pp. 390–399, 2008.

[224] A. C. Huang, Y. M. Lin, and C. Y. Kai, "Adaptive control of horizontal magnetic levitation system subject to external disturbances," in *The 7th IEEE Conference on Industrial Electronics and Applications (ICIEA)*, 2012, pp. 467–471.

[225] P. J. Werbos, "Neural networks for control and system identification," in *Proceedings of the 28th IEEE Conference on Decision and Control*. IEEE, 1989, pp.

260–265.

[226] K. S. Narendra and K. Parthasarathy, “Identification and control of dynamical systems using neural networks,” *IEEE Transactions on Neural Networks*, vol. 1, no. 1, pp. 4–27, 1990.

[227] M. Kutz, *Mechanical engineers’ handbook, energy and power*. Wiley, Hoboken, NJ (United States), 2005.

[228] M. Lairi and G. Bloch, “A neural network with minimal structure for maglev system modeling and control,” in *Proceedings of the 1999 IEEE International Symposium on Intelligent Control/Intelligent Systems and Semiotics*. IEEE, 1999, pp. 40–45.

[229] P. Shiakolas, S. Van Schenck, D. Piyabongkarn, and I. Frangeskou, “Magnetic levitation hardware-in-the-loop and matlab-based experiments for reinforcement of neural network control concepts,” *IEEE Transactions on Education*, vol. 47, no. 1, pp. 33–41, 2004.

[230] M. Aliasghary, A. Jalilvand, M. Teshnehlab, and M. Shoorehdeli, “Sliding mode control of magnetic levitation system using radial basis function neural networks,” in *2008 IEEE Conference on Robotics, Automation and Mechatronics*, 2008, pp. 467–470.

[231] M. Aliasghary, M. Shoorehdeli, A. Jalilvand, and M. Teshnehlab, “Magnetic levitation control based-on neural network and feedback error learning approach,” in *IEEE The 2nd International Power and Energy Conference*, 2008, pp. 1426–1430.

[232] B. Friedland, *Advanced control system design*. Prentice Hall, Inc., 1995.

[233] O. Yaniv, *Quantitative Feedback Design of Linear and Nonlinear Control Systems*. Springer, 1999.

[234] J. C. Doyle, B. A. Francis, and A. R. Tannenbaum, *Feedback control theory*. Courier Dover Publications, 2013.

[235] J. D. Jackson, *Classical electrodynamics*. Wiley-VCH, 1998, vol. 1.

[236] L. El Ghaoui, F. Oustry, and M. AitRami, “A cone complementarity linearization algorithm for static output-feedback and related problems,” *IEEE Transactions on Automatic Control*, vol. 42, no. 8, pp. 1171–1176, 1997.

[237] D. Xue, Y. Chen, and D. P. Atherton, *Linear feedback control: analysis and design with MATLAB*. Society for Industrial and Applied Mathematics, 2007.

[238] B. Ramaswami and K. Ramar, “Stability of systems with rhp pole-zero

cancellations," *International Journal of Control*, vol. 11, no. 2, pp. 241–244, 1970.

[239] X. Shan and C. H. Menq, "Robust disturbance rejection for improved dynamic stiffness of a magnetic suspension stage," *IEEE/ASME Transactions on Mechatronics*, vol. 7, no. 3, pp. 289–295, 2002.

[240] Y. Fang, M. Feemster, and D. Dawson, "Nonlinear disturbance rejection for magnetic levitation systems," in *The 2003 IEEE International Symposium on Intelligent Control*. IEEE, 2003, pp. 58–62.

[241] J. H. She, X. Xin, and T. Yamaura, "Analysis and design of control system with equivalent-input-disturbance estimation," in *Proceeedings of the 2006 IEEE International Conference on Control Applications*, Munich, 2006, pp. 1463–1469.

[242] P. B. Schmidt and R. D. Lorenz, "Design principles and implementation of acceleration feedback to improve performance of dc drives," *IEEE Transactions on Industry Applications*, vol. 28, no. 3, pp. 594–599, 1992.

[243] Y. Hori, "Disturbance suppression on an acceleration control type DC servo system," in *The 19th Annual IEEE Power Electronics Specialists Conference*, 1988, pp. 222–229.

[244] R. E. Christenson, B. Spencer Jr, N. Hori, and K. Seto, "Coupled building control using acceleration feedback," *Computer-Aided Civil and Infrastructure Engineering*, vol. 18, no. 1, pp. 4–18, 2003.

[245] Y. Hori, "Position and mechanical impedance control method of robot actuators based on the acceleration control," in *The 20th Annual IEEE Power Electronics Specialists Conference*, 1989, pp. 423–430.

[246] Y. I. Neimark, "D-partition and robust stability," *Computational Mathematics and Modeling*, vol. 9, no. 2, pp. 160–166, 1998.

[247] ——, "Structure of the D-partition of the space of polynomials and the diagram of Vishnegradskii and Nyquist," in *Dokl Akad Nauk SSSR*, vol. 59, 1948, p. 853.

[248] ——, "Robust stability and D-partition," *Automation and Remote Control*, vol. 53, no. 7, pp. 957–965, 1992.

[249] P. C. Parks, "A new proof of the Routh-Hurwitz stability criterion using the second method of Lyapunov," in *Proc. Cambridge Philos. Soc*, vol. 58, no. 4. Cambridge Univ Press, 1962, pp. 694–702.

[250] E. X. DeJesus and C. Kaufman, "Routh-Hurwitz criterion in the examination of eigenvalues of a system of nonlinear ordinary differential equations," *Physical Review A*, vol. 35, no. 12, pp. 52–88, 1987.

[251] E. A. Faulkner, *Introduction to the theory of linear systems*. Chapman and Hall, 1969.

[252] D. Levišauskas and T. Tekorius, "Investigation of P and PD controllers performance in control systems with steady-state error compensation," *Elektronika ir Elektrotechnika*, vol. 121, pp. 63–68, 2012.

[253] P. C. Parks, "Lyapunov redesign of model reference adaptive control systems," *IEEE Transactions on Automatic Control*, vol. 11, pp. 362–367, March 1966.

[254] C. C. Hang and P. C. Parks, "Comparative studies of model reference adaptive control systems," *IEEE Transactions on Automatic Control*, vol. 18, no. 5, pp. 419–428, 1973.

[255] G. Lightbody and G. Irwin, "Direct neural model reference adaptive control," *IEE Proceedings-Control Theory and Applications*, vol. 142, no. 1, pp. 31–43, 1995.

[256] B. Vinagre, I. Petráš, I. Podlubny, and Y. Chen, "Using fractional order adjustment rules and fractional order reference models in model-reference adaptive control," *Nonlinear Dynamics*, vol. 29, no. 1-4, pp. 269–279, 2002.

[257] P. Swarnkar, S. Jain, and R. Nema, "Effect of adaptation gain on system performance for model reference adaptive control scheme using mit rule," *World Academy of science, engineering and technology*, vol. 70, pp. 621–626, 2010.

[258] I. Landau, "A survey of model reference adaptive techniques¡ªtheory and applications," *Automatica*, vol. 10, no. 4, pp. 353–379, 1974.

[259] L. Hsu and R. R. Costa, "Variable structure model reference adaptive control using only input and output measurements: Part 1," *International Journal of Control*, vol. 49, no. 2, pp. 399–416, 1989.

[260] C. H. Chou and C. C. Cheng, "A decentralized model reference adaptive variable structure controller for large-scale time-varying delay systems," *IEEE Transactions on Automatic Control*, vol. 48, no. 7, pp. 1213–1217, 2003.

[261] Y. Yang, C. Zhou, and J. Ren, "Model reference adaptive robust fuzzy control for ship steering autopilot with uncertain nonlinear systems," *Applied Soft Computing*, vol. 3, no. 4, pp. 305–316, 2003.

[262] R. V. Monopoli, "Model reference adaptive control with an augmented error signal," *IEEE Transactions on Automatic Control*, vol. 19, no. 5, pp. 474–484, 1974.

[263] T. Ionescu and R. Monopoli, "Discrete model reference adaptive control with an augmented error signal," *Automatica*, vol. 13, no. 5, pp. 507–517, 1977.

[264] S. S. Sastry and A. Isidori, "Adaptive control of linearizable systems," *IEEE Transactions on Automatic Control*, vol. 34, no. 11, pp. 1123–1131, 1989.

[265] H. Kaufman, I. Barkana, and K. Sobel, *Direct adaptive control algorithms: theory and applications*. Springer, 1998.

[266] C. A. Winsor and R. J. Roy, "Design of model reference adaptive control systems by Lyapunov second method," *IEEE Transactions on Automatic Control*, vol. 13, pp. 204–204, Feb 1968.

[267] B. Shackcloth and R. L. Butchart, "Synthesis of model reference adaptive systems by Lyapunov's second method," in *Theory of Self Adaptive Control Systems*. Springer, 1966, pp. 145–152.

[268] P. V. Osburn, *New developments in the design of model reference adaptive control systems*. Institute of the Aerospace Sciences, 1961.

[269] M. I. Weinstein, "Lyapunov stability of ground states of nonlinear dispersive evolution equations," *Communications on Pure and Applied Mathematics*, vol. 39, no. 1, pp. 51–67, 1986.

[270] L. S. Pontryagin, *Mathematical theory of optimal processes*. CRC Press, 1987.

[271] ——, *Topologische Gruppen*. Teubner, 1957.

[272] L. Pontryagin, "Optimal control processes," *Usp. Mat. Nauk*, vol. 14, no. 3, 1959.

[273] I. M. Ross, *A primer on pontryagin's principle in optimal control*. Collegiate Publ., 2009.

[274] J. L. Speyer and D. H. Jacobson, *Primer on optimal control theory*. SIAM, 2010, vol. 20.

[275] H. J. Pesch, "A practical guide to the solution of real-life optimal control problems," *Control and Cybernetics*, vol. 23, no. 1/2, pp. 7–60, 1994.

[276] S. M. Shinners and S. Adelman, "Modern control system theory and application," *IEEE Transactions on Systems, Man and Cybernetics,*, vol. 9, no. 6, pp. 365–366, 1979.

[277] O. von Stryk and R. Bulirsch, "Direct and indirect methods for trajectory optimization," *Annals of operations research*, vol. 37, no. 1, pp. 357–373, 1992.

[278] A. E. Bryson Jr, "Optimal control: 1950 to 1985," *IEEE Control Systems*, vol. 16, no. 3, pp. 26–33, 1996.

[279] R. F. Stengel, "Flight dynamics," *Aircraft Engineering and Aerospace Technology*, vol. 77, no. 3, pp. 223–244, 2005.

[280] D. Grass, J. P. Caulkins, G. Feichtinger, G. Tragler, and D. A. Behrens, *Optimal control of nonlinear processes: with applications in drugs, corruption, and terror*. Springer, 2008.

[281] J. Sokolowski and J.-P. Zolésio, *Introduction to shape optimization*. Springer, 1992.

[282] F. Da Lio, "On the Bellman equation for infinite horizon problems with unbounded cost functional," *Applied Mathematics and Optimization*, vol. 41, no. 2, pp. 171–197, 2000.

[283] D. E. Kirk, *Optimal control theory: an introduction*. Courier Dover Publications, 2012.

[284] F. L. Lewis, D. Vrabie, and V. L. Syrmos, *Optimal control*. John Wiley & Sons, 2012.

[285] K. Zhou, J. C. Doyle, K. Glover *et al.*, *Robust and optimal control*. New Jersey: Prentice Hall, 1996, vol. 40.

[286] D. Magill, "Optimal adaptive estimation of sampled stochastic processes," *IEEE Transactions on Automatic Control*, vol. 10, no. 4, pp. 434–439, 1965.

[287] D. Jacobson, "Optimal stochastic linear systems with exponential performance criteria and their relation to deterministic differential games," *IEEE Transactions on Automatic Control*, vol. 18, no. 2, pp. 124–131, 1973.

[288] T. Kailath, *Linear systems*. Prentice Hall Englewood Cliffs, NJ, 1980, vol. 1.

[289] E. Todorov, "Stochastic optimal control and estimation methods adapted to the noise characteristics of the sensorimotor system," *Neural computation*, vol. 17, no. 5, pp. 1084–1108, 2005.

[290] J. S. Meditch and E. Tacker, "Stochastic optimal linear estimation and control," *IEEE Transactions on Systems, Man and Cybernetics*, vol. 2, no. 3, pp. 128–135, 1972.

[291] R. E. Kalman, "Linear stochastic filtering theory - Reappraisal and outlook (linear stochastic filtering theory assessing Kalman-Bucy filter and equivalence with Kolmogorov-Wiener problem)," in *PROCEEDINGS OF THE SYMPOSIUM Proceedings of the symposium on system theory*, New York, 1965, pp. 197–205.

[292] K. Brammer and G. Siffling, *Kalman-Bucy-Filter: Deterministische Beobachtung und stochastische Filterung*. Oldenbourg, 1975.

[293] A. MacFarlane, "Return-difference matrix properties for optimal stationary Kalman-Bucy filter," in *Proceedings of the Institution of Electrical Engineers*, vol.

118, no. 2. IET, 1971, pp. 373–376.

[294] J. H. Davis, “Kalman-bucy filters,” in *Foundations of Deterministic and Stochastic Control*. Springer, 2002, pp. 185–200.

[295] H. Kwakernaak and R. Sivan, *Linear optimal control systems*. Wiley-interscience New York, 1972, vol. 1.

[296] D. Hyland and D. Bernstein, “The optimal projection equations for fixed-order dynamic compensation,” *IEEE Transactions on Automatic Control*, vol. 29, no. 11, pp. 1034–1037, 1984.

[297] C. E. De Souza, “On stabilizing properties of solutions of the riccati difference equation,” *IEEE Transactions on Automatic Control*, vol. 34, no. 12, pp. 1313–1316, 1989.

[298] R. S. Liptser, A. N. Shiri,,1,,2a,,1,,3ev, and A. N. Shiryaev, *Statistics of Random Processes II: II. Applications*. Springer, 2001, vol. 2.

[299] B. R. Barmish and E. Jury, “New tools for robustness of linear systems,” *IEEE Transactions on Automatic Control*, vol. 39, no. 12, pp. 2525–2525, 1994.

[300] M. Krstic, I. Kanellakopoulos, and P. V. Kokotovic, *Nonlinear and adaptive control design*. Wiley, 1995.

[301] J. Ackermann, A. Bartlett, D. Kaesbauer, W. Sienel, and R. Steinhauser, *Robust control*. Berlin: Springer, 1993.

[302] K. Zhou and J. C. Doyle, *Essentials of robust control*. Upper Saddle River, NJ: Prentice Hall, 1998, vol. 104.

[303] R. Matušu, *Robust Control of Systems with Parametric Uncertainty: An Algebraic Approach*. Tomas Bata University in Zln, 2008.

[304] K. Glover, R. F. Curtain, and J. R. Partington, “Realisation and approximation of linear infinite-dimensional systems with error bounds,” *SIAM Journal on Control and Optimization*, vol. 26, no. 4, pp. 863–898, 1988.

[305] G. Gu, P. P. Khargonekar, and E. B. Lee, “Approximation of infinite-dimensional systems,” *IEEE Transactions on Automatic Control*, vol. 34, no. 6, pp. 610–618, 1989.

[306] G. Gu and P. P. Khargonekar, “Linear and nonlinear algorithms for identification in h_∞ with error bounds,” *IEEE Transactions on Automatic Control*, vol. 37, no. 7, pp. 953–963, 1992.

[307] H. Akcay, G. Gu, and P. P. Khargonekar, “A class of algorithms for identification in

H_∞: continuous-time case," *IEEE Transactions on Automatic Control*, vol. 38, no. 2, pp. 289–294, 1993.

[308] P. M. Mäkilä, "Worst-case input-output identification," *International Journal of Control*, vol. 56, no. 3, pp. 673–689, 1992.

[309] A. J. Helmicki, C. A. Jacobson, and C. N. Nett, "Control oriented system identification: a worst-case/deterministic approach in H_∞," *IEEE Transactions on Automatic Control*, vol. 36, no. 10, pp. 1163–1176, 1991.

[310] L. Ljung, "System identification: theory for the user," *Prentice Hall Inf and System Sciences Series*, vol. 7632, pp. 1–35, 1987.

[311] T. Söderström and P. Stoica, *System identification*. Prentice-Hall, Inc., 1988.

[312] L. Ljung, *System identification*. Springer, 1998.

[313] B. Peeters and G. De Roeck, "Stochastic system identification for operational modal analysis: a review," *Journal of Dynamic Systems, Measurement, and Control*, vol. 123, no. 4, pp. 659–667, 2001.

[314] V. Kucera, "Robustní regulátory (robust controllers)," *Automa*, vol. 7, no. 6, pp. 43–45, 2001.

[315] R. S. Sanchez-Pena and M. Sznaier, *Robust systems theory and applications*. John Wiley & Sons, Inc., 1998.

[316] N. Tan and D. P. Atherton, "Some results on control systems with mixed perturbations," in *Preprints of 15th World Congress, Barcelona, Spain*, 2002.

[317] S. P. Bhattacharyya, H. Chapellat, and L. H. Keel, *Robust control*. Englewood Cliffs, New Jersey, USA: Prentice Hall, 1995.

[318] B. Barmish, "New tools for robustness analysis," in *Proceedings of the 27th IEEE Conference on Decision and Control*. IEEE, 1988, pp. 1–6.

[319] V. L. Kharitonov, "Asymptotic stability of an equilibrium position of a family of systems of linear differential equations," *Differential Equations*, vol. 14, pp. 1483–1485, 1978.

[320] H. Chapellat and S. Bhattacharyya, "A generalization of kharitonov's theorem; robust stability of interval plants," *IEEE Transactions on Automatic Control*, vol. 34, no. 3, pp. 306–311, March 1989.

[321] A. C. Bartlett, C. V. Hollot, and H. Lin, "Root locations of an entire polytope of polynomials: It suffices to check the edges," in *American Control Conference*, June 1987, pp. 1611–1616.

[322] W. H. Chen, D. J. Ballance, and Y. Li, "Automatic loop-shaping in QFT using genetic algorithms," in *Proceedings of 3rd Asia-Pacific Conference on Control and Measurement*. Citeseer, 1998, pp. 63–67.

[323] J. Ziegler and N. Nichols, "Optimum settings for automatic controllers," *ASME Transactions*, vol. 64, no. 11, 1942.

[324] P. Meshram and R. G. Kanojiya, "Tuning of PID controller using Ziegler-Nichols method for speed control of DC motor," in *2012 International Conference on Advances in Engineering, Science and Management (ICAESM)*. IEEE, 2012, pp. 117–122.

[325] C. C. Hang, K. J. Åström, and W. K. Ho, "Refinements of the ziegler–nichols tuning formula," in *IEE Proceedings D (Control Theory and Applications)*, vol. 138, no. 2. IET, 1991, pp. 111–118.

[326] P. Naslin, *The dynamics of linear and non-linear systems*. Gordon and Breach, 1965.

[327] J. Miller, A. Lopez, C. Smith, P. Murrill *et al.*, "A comparison of controller tuning techniques," *Control Engineering*, vol. 14, no. 12, p. 72, 1967.

[328] A. Arora, Y. V. Hote, and M. Rastogi, "Design of PID controller for unstable system," in *Control, Computation and Information Systems*. Springer, 2011, pp. 19–26.

[329] L. Donghai, J. Yinghuang, L. Mingda, and L. Jinggong, "PID controller design for a class of distributed parameter systems," in *2011 30th Chinese Control Conference (CCC)*, July 2011, pp. 1021–1026.

[330] G. Kreisselmeier and B. D. Anderson, "Robust model reference adaptive control," *IEEE Transactions on Automatic Control*, vol. 31, no. 2, pp. 127–133, 1986.

[331] G. C. Goodwin and D. Q. Mayne, "A parameter estimation perspective of continuous time model reference adaptive control," *Automatica*, vol. 23, no. 1, pp. 57–70, 1987.

[332] J. P. Hespanha, *Linear systems theory*. Princeton university press, 2009.

[333] D. S. Bernstein and M. Haddad, "Robust stability and performance analysis for linear dynamic systems," *IEEE Transactions on Automatic Control,*, vol. 34, no. 7, pp. 751–758, 1989.

[334] J. C. Doyle, J. E. Wall, and G. Stein, "Performance and robustness analysis for structured uncertainty," in *The 21st IEEE Conference on Decision and Control*. IEEE, 1982, pp. 629–636.

[335] S. Skogestad and I. Postlethwaite, *Multivariable feedback control: analysis and design*. Wiley New York, 2007, vol. 2.

[336] Z. Yang, S. Hara, S. Kanae, and K. Wada, "Robust output feedback control of a class of nonlinear systems using a disturbance observer," *IEEE Transaction on Control System Technology*, vol. 19, pp. 256–268, Mar 2011.

[337] M. Vagia and A. Tzes, "Robust PID control design for an electrostatic micromechanical actuator with structured uncertainty," *IET Control Theory Appl.*, vol. 2, pp. 365–373, 2008.

[338] X. Shan and C. Menq, "Robust disturbance rejection for improved dynamic stiffness of a magnetic suspension stage," *IEEE/ASME Transactions on Mechatronics*, vol. 7, pp. 289–295, 2002.

[339] Y. Satoh, H. Nakamura, N. Nakamura, H. Katayama, and H. Nishitani, "Robust adaptive control of nonlinear systems with convex input constraints: Case study on the magnetic levitation system," in *ICROS-SICE International Joint Conference 2009*, 2009, pp. 4411–4416.

[340] O. Yaniv and M. Nagurka, "Automatic loop shaping of structured controllers satisfying QFT performance," *Journal of Dynamic Systems, Measurement and Control*, vol. 127, pp. 472–477, 2005.

[341] I. M. Horowitz, *Quantitative Feedback Design Theory (QFT)*. QFT Publications, 1993.

[342] K. Ogata, *Modern control engineering*. Prentice Hall, 2001.

[343] F. Tian, K. Craig, and M. Nagurka, "Disturbance attenuation in a magnetic levitation system with acceleration feedback," in *2011 IEEE International Conference on Industrial Technology (ICIT)*, 2011.

[344] G. Zames, "Feedback and optimal sensitivity: Model reference transformations, multiplicative seminorms, and approximate inverses," *IEEE Transactions on Automatic Control*, vol. 26, no. 2, pp. 301–320, 1981.

[345] G. Zames and B. Francis, "Feedback, minimax sensitivity, and optimal robustness," *IEEE Transactions on Automatic Control*, vol. 28, no. 5, pp. 585–601, 1983.

[346] B. Francis and G. Zames, "On H_∞ optimal sensitivity theory for SISO feedback systems," *IEEE Transactions on Automatic Control*, vol. 29, no. 1, pp. 9–16, 1984.

[347] L. A. Sievers and A. H. Von Flotow, "Comparison of two LQG-based methods for disturbance rejection," in *Proceedings of the 28th IEEE Conference on Decision and Control*. IEEE, 1989, pp. 483–485.

[348] D. McFarlane and K. Glover, "A loop-shaping design procedure using H_∞ synthesis," *IEEE Transactions on Automatic Control*, vol. 37, no. 6, pp. 759–769, 1992.

[349] J. B. Burl, *Linear Optimal Control: H_2 and H_∞ Methods*. Addison-Wesley Longman Publishing Co., Inc., 1998.

[350] I. Petersen, V. A. Ugrinovskii, and A. V. Savkin, *Robust Control Design Using H_∞ Methods*. Springer, 2000.

[351] T. Basar and P. Bernhard, *H_∞ optimal control and related minimax design problems: a dynamic game approach*. Springer, 2008.

[352] K. Glover and J. C. Doyle, "State-space formulae for all stabilizing controllers that satisfy an H_∞ norm bound and relations to relations to risk sensitivity," *Systems & Control Letters*, vol. 11, no. 3, pp. 167–172, 1988.

[353] J. Doyle, K. Glover, P. Khargonekar, and B. Francis, "State–space solutions to standard H_2 and H_∞," *IEEE Trans. Automata Control*, vol. 34, pp. 831–847, 1989.

[354] J. C. Doyle, "Quantitative feedback theory (qft) and robust control," in *American Control Conference*, 1986, pp. 1691–1698.

[355] O. Yaniv and I. Horowitz, "Quantitative feedback theory – reply to Doyle's criticisms," in *American Control Conference*, June 1987, pp. 622–627.

[356] M. Sidi, "Feedback synthesis with plant ignorance, nonminimum-phase, and time-domain tolerances," *Automatica*, vol. 12, no. 3, pp. 265–271, 1976.

[357] I. Horowitz and M. Sidi, "Optimum synthesis of non-minimum phase feedback systems with plant uncertainty," *International Journal of Control*, vol. 27, no. 3, pp. 361–386, 1978.

[358] M. J. Sidi, *Spacecraft dynamics and control: a practical engineering approach*. Cambridge university press, 1997, vol. 7.

[359] ——, *Design of Robust Control Systems: From classical to modern practical approaches*. Krieger Publishing Company, 2001.

[360] ——, "A combined QFT/H_∞ design technique for TDOF uncertain feedback systems," *International Journal of Control*, vol. 75, no. 7, pp. 475–489, 2002.

[361] I. Horowitz and M. Sidi, "Synthesis of cascaded multiple-loop feedback systems with large plant parameter ignorance," *Automatica*, vol. 9, no. 5, pp. 589–600, 1973.

[362] H. W. Bode, *Network analysis and feedback amplifier design*. New York: Van Nostrand-Reinhold, 1945, vol. 11.

[363] S. M. Shinners, *Modern control system theory and design*. John Wiley & Sons, 1998.

[364] D. R. Corson and P. Lorrain, *Electromagnetic fields and waves*. WH Freeman, 1970.

[365] R. M. Murray, Z. Li, S. S. Sastry, and S. S. Sastry, *A mathematical introduction to robotic manipulation*. CRC press, 1994.